

Improvement of fuel injection and atomization in the HCCI engine

Victor Akimov

A thesis submitted for the degree of
Doctor of Philosophy



Bauman Moscow State Technical University
Moscow - 2015

CONTENTS

NOMENCLATURE	III
INTRODUCTION	1
CHAPTER 1. ORGANIZATION OF FUEL INJECTION, ATOMIZATION AND MIXTURE FORMATION IN THE DIESEL AND HCCI ENGINES	7
1.1. Substantiation of necessity to improve exhaust gases toxicity indicators of internal combustion engines	7
1.2. The phenomena and factors influencing quality metrics of fuel injection, atomization and mixture formation	14
1.3. Objective of work and research tasks	40
CHAPTER 2. NUMERICAL INVESTIGATIONS OF PROCESSES OF FUEL INJECTION, ATOMIZATION AND MIXTURE FORMATION OF THE DIESEL AND HCCI ENGINE	43
2.1. Problems of the organization of homogeneous mixture formation in the cylinder	43
2.2. Software packages for simulation of fuel outflow and atomization. Finite volume method	52
2.3. Constitutive equations of mathematical models	60
2.4. Simulation of a fuel flow in a nozzle hole of an injector	84
2.5. Simulation of break-up and evaporation of the jets produced by nozzle holes of injectors	88
2.6. Simulation of a fuel flow in a pintle nozzle	102
2.7. Simulation of the hollow cone spray	110
2.8. Simulation of evaporation of single droplet	113
2.9. Two-stage method of analysis of fuel injection atomization and evaporation by a nozzle with nonconventional geometry	115
2.10. Search of methods for limiting of spray tip penetration	117
2.11. Problems of simulation of jet primary break-up	122
2.12. Chapter 2 summary	126
CHAPTER 3. NUMERICAL INVESTIGATIONS OF OPERATION CHARACTERISTICS OF THE DIESEL AND HCCI ENGINE. Z-ENGINE	129
3.1. Substantiation of necessity of development and deployment of new types of internal combustion engines. <i>Z-engine</i>	129
3.2. Software packages for simulation of internal combustion engines operation	135
3.3. Numerical investigations of operation of the diesel and <i>Z-engine</i>	151

3.4. Chapter 3 summary	163
CHAPTER 4. EXPERIMENTAL STUDIES OF OPERATION CHARACTERISTICS OF THE Z-ENGINE	165
4.1. Substantiation of necessity of experimental studies of the <i>Z-engine</i>	165
4.2. Experimental studies of the <i>Z-engine</i>	166
4.3. Comparative analysis of experimental and calculation data of the <i>Z-engine</i>	176
4.4. Chapter 4 summary	178
THE MAIN RESULTS AND CONCLUSIONS OF THE THESIS	179
REFERENCES	182
APPENDIX	201

NOMENCLATURE

BMSTU - Bauman Moscow State Technical University

HP – high pressure;

D/S – cylinder bore Diameter / piston Stroke;

TDC, BDC - top dead center, bottom dead center;

FLC - full-load curve;

ICE - internal combustion engine;

DF - diesel fuel;

CC - combustion chamber;

EG - exhaust gases;

IDP - ignition delay period;

SP - software package;

CA - crank angle;

CA deg. - crank angle degrees;

SOI - start of injection (injection timing);

PM - particulate matter;

TC - turbocharger;

CFD - Computational Fluid Dynamics;

EGR - Exhaust Gas Recirculation;

HCCI - Homogeneous Charge Compression Ignition;

SA HCCI - Spark Assisted Homogeneous Charge Compression Ignition;

NO_x, CO, a HC - nitrogen oxides, carbon monoxide, hydrocarbons;

e_{NO_x} - specific emission of nitrogen oxides;

g_i, g_e - indicated and brake specific fuel consumption (ISFC and BSFC);

η_e - engine efficiency;

d_{32} - Sauter mean diameter (SMD);

n - engine speed;

p_e - break mean effective pressure (BMEP);

p_c - cylinder pressure;

p_z - maximum cycle pressure;

$p_{inj\ max}$ - maximum injection pressure;

p_v - saturated vapor pressure;

ϕ_{inj}, p_{inj} - duration of injection and injection pressure;

α - air-fuel equivalence ratio;

CN - cavitation number;

W_e - Weber number;

M - Mach number;

Oh - Ohnesorge number;

Re - Reynolds number.

INTRODUCTION

Perfection of processes of fuel injection, atomization and mixture formation substantially predetermines power and effective characteristics of transport diesels as well as characteristics of exhaust gases toxicity. Thus, at the present stage of development of engines the most priority task is a minimization of pollutant emissions. Providing required characteristics of toxicity of EG is impossible without implementation of high-quality process of the mixture formation that predetermines nature of the subsequent combustion process and emission of toxic components.

Nature of denoted processes in internal combustion engines is influenced by a design of fuel supply system. Main element of this system is the injector nozzle, which predetermines characteristics of fuel injection and atomization. Design of the injector nozzle determines parameters of fuel flow inside the nozzle flowing channels, performance characteristics of this flow, geometrical characteristics of jets of the atomized fuel, structure of fuel spray, a fuel atomization fineness, a number of other parameters of fuel supply and mixture formation.

For organization of these processes in the downsized internal combustion engines it is necessary to provide: concordance between maximal spray tip penetration and size of combustion chamber, uniform distribution of fuel in volume of combustion chamber, required characteristics of a fineness of atomization of fuel. It is also important to prevent hit of fuel on cylinder walls. These targets may be reached, first of all, by the choice of a design of injector nozzles, implementation of the constructive actions improving fuel atomization.

Fuel flow inside the nozzle flowing channels, the subsequent development of jets in cylinder volume, jets break-up into droplets, further evaporation of droplets are is the complex physical processes including a great number of different physical effects. Research of these processes by experimental methods represents a complex technical challenge. In these conditions computational methods will be more preferable. Thereby there is a problem of development of the complex mathematical model capable of describing all specified processes.

Also the serious problem is the choice of the ways of the organization of operation of the engine providing the best characteristics of fuel efficiency and toxicity of EG. One of such ways is the organization of combustion of a homogeneous air-fuel mixture called *HCCI (Homogeneous Charge Compression Ignition)*. Implementation of HCCI means uniform distribution of fuel in cylinder volume and creation of a homogeneous air-fuel mixture with the absence of the locally rich zones (zones with low values of an air-fuel equivalence ratio). As a result formation of nitrogen oxides, particle matters and unburnt combustibles considerably decreases. Besides due to the mixture leaning, recirculation and cooling of EG, the level of temperatures in combustion zone remains rather low. It also promotes minimization of pollutant emissions.

Requirements to the fuel injection, atomization and mixture formation at the organization of HCCI become stricter in comparison with conventional diesel combustion. By the beginning of ignition of a fuel-air charge it is desirable to provide the maximum uniformity of fuel droplets distribution in cylinder volume, their evaporation, the most uniform field of an air-fuel equivalence ratio in cylinder volume. Thereby it is necessary a comprehensive study of complex physical processes of injection, atomization of fuel and mixture formation in the HCCI engine with the use of the whole complex of mathematical models of these processes.

The thesis is devoted to problems of improvement of fuel injection and atomization in the HCCI engine.

In the thesis the methods of analysis of fuel injection, atomization and evaporation are developed for the nozzles in the conditions of cavitation. Using of these methods makes it possible to obtain characteristics of a fuel flow, fuel jets and mixture formation, quality metrics of atomization and evaporation for any geometry of a nozzle. Numerical investigations of influence of cavitation on a fuel flow in a nozzle hole and on the characteristics of fuel atomization and jets break-up were conducted. There were performed numerical investigations of the factors influencing spray tip penetration, intensity of jet break-up and evaporation of

droplets in the conditions of the low gases density in the cylinder. There were determined the ways of limitation of spray tip penetration and improvement of quality metrics of atomization in the conditions of the low gases density in the cylinder. It was developed the concept of mixture formation in the *HCCI* engine providing full evaporation of droplets and preventing hit of fuel on cylinder walls. It was developed the concept of the *Z-engine* with *HCCI* providing reduce of nitrogen oxides and smoke emissions. Comparative numerical investigations of the *Z-engine* operation with conventional diesel combustion and with *HCCI* were conducted. Experimental studies of single-cylinder *Z-engine* prototype operation have been conducted. Comparative analysis of computational results of engine operation with the known and obtained experimental data has been carried out.

Relevance of a thesis is caused by necessity of satisfaction of modern strict requirements to characteristics of fuel efficiency and toxicity of exhaust gases of internal combustion engines. These characteristics substantially depend on fuel injection, atomization and mixture formation, which, in turn are defined by a design of fuel supply system and especially by a design of injectors and their nozzles.

The problem of ensuring required parameters of fuel injection, atomization and mixture formation is especially actual for engines in which combustion of a homogeneous air-fuel mixture is implemented (*HCCI*). In these engines it is necessary to organize the mixture formation providing uniform distribution of the evaporated fuel in the cylinder volume and the perfect combustion with the greatest efficiency of the operating cycle. So, it is required carrying out the whole complex of the numerical and experimental studies directed to improvement of fuel injection and atomization in the *HCCI* engines. At the organization of *HCCI* due to homogeneity of a fuel-air charge, rather high values of an air-fuel equivalence ratio and low values of local temperatures it is possible minimization of pollutant emissions.

Objective: improvement of fuel injection and atomization in the *HCCI* engine.

Methods of investigations. The objective of the work is achieved by a combination of theoretical and experimental methods. By means of theoretical methods it was conducted numerical investigations of parameters of fuel injection, atomization and mixture formation, characteristics of fuel efficiency and toxicity of exhaust gases, influence of geometry of the flowing channels of different injector nozzles on characteristics of fuel flow and parameters of fuel atomization. The experimental part of work was concentrated on determination of characteristics of the engine operation.

Scientific novelty of work:

- the two-stage method of analysis of fuel injection atomization and evaporation have been developed which is applicable for any geometry of a nozzle;
- the method of sharing the software packages *Ansys Fluent*, INJECT and DIESEL-RK for simulation of *HCCI* with multistage fuel injection by a nozzle with nonconventional geometry was implemented;
- it was proposed the concept of the *Z-engine* representing the two-stroke diesel engine with the valve-controlled gas exchange and compression separated into two parts - preliminary in external units and final in the engine cylinder;
- multistage strategy of injection by the pintle nozzle with small effective flow section was offered to prevent hit of fuel on cylinder walls in the conditions of low gas density.

Reliability and validity of scientific provisions are defined by following factors:

- use of modern methods of computation of engine operation parameters, characteristics of fuel injection, atomization and mixture formation;
- coincidence of results of the numerical and experimental studies obtained by the engine tests.

Practical value:

- at numerical investigations of internal nozzle fuel flow and in-cylinder spray behavior it was shown the influence of cavitation and air entrainment on

characteristics of a fuel flow in nozzles with different geometry and on characteristics of a spray;

- by use of experimental data it was carried out the choice and adjustment of mathematical models of fuel injection, atomization and evaporation for nozzles with nonconventional geometry of a flowing channel in the conditions of cavitation;

- influence of different factors on characteristics of fuel atomization and evaporation was investigated; ways of limitation of spray tip penetration and improvement of quality metrics of atomization in the conditions of low gas density in the cylinder were offered;

- it was presented an expediency of implementation of *HCCI* and its kind called *SA HCCI* in the *Z-engine* for decreasing emissions of nitrogen oxides and smoke of EG;

- results of the conducted experimental studies have confirmed operability of the developed *Z-engine* and its efficiency for decreasing emissions of nitrogen oxides and smoke of EG.

Implementation of the work results. Work was carried out according to plans of the state budget, government contracts and grants for departments of piston engines and thermophysics of Bauman Moscow State Technical University and laboratory of Research Institute of Power Engineering under Bauman Moscow State Technical University. Results of researches are implemented in Russian State Agrarian University - Timiryazev Moscow Agricultural Academy and in Forant-Service Ltd. (Noginsk city).

Work approbation:

The thesis have been heard and approved at the meeting of piston engines department of Bauman Moscow State Technical University in 2015. According to the main sections of a thesis following reports have been made:

- at the meeting of piston engines department of Bauman Moscow State Technical University (Moscow, 2013, 2015);

- at school-seminar of young scientists and specialists under supervision of Professor A.I. Leontiev, academician of the Russian academy of sciences, (Orehovo-Zuyevo, Russia, 2013);
- at the international science and technology conference “The 6th Lukanin’s readings” (Moscow, 2013);
- at the international science and technology conference “The 7th Lukanin’s readings” (Moscow, 2015);
- at the All-Russian Scientific and Technical Seminar named after Prof. V.I. Krutov on Automatic Control and Regulation of Thermal Power Engineering Plants under Bauman Moscow State Technical University (Moscow, 2011-2014).

Publications. According to the substance of a thesis 15 works are published, all of them in the science journals from the list of State Commission for Academic Degrees and Titles [4, 6, 8, 35, 36, 73, 74, 77, 79, 81, 91-93, 95, 112]. Also 9 publications in conferences proceedings [1, 45, 46, 78, 83, 88, 94, 114, 147].

Structure and the scope of work. The thesis consists of introduction, four chapters, the main results and conclusions, the references and the appendix. The total volume of work is 218 pages, including 181 pages of the body text containing 137 drawings, 15 tables. The references include 181 names on 19 pages. The appendix on 18 pages includes listings of results of numerical investigations and user-defined functions for CFD simulations.

CHAPTER 1. ORGANIZATION OF FUEL INJECTION, ATOMIZATION AND MIXTURE FORMATION IN THE DIESEL AND HCCI ENGINES

1.1. Substantiation of necessity to improve exhaust gases toxicity indicators of internal combustion engines

Operation of the internal combustion engines (ICE) is determined by the whole complex of operational and technical characteristics: specific power and mass-dimensional characteristics, fuel efficiency, toxicity of the exhaust gases (EG), dynamic qualities, etc. [34]. The most important of them are toxicity characteristics of EG, i.e. amount of the pollutant emissions which are exhausted by the engine [20]. It is caused both by deterioration of ecology and toughening of requirements imposed to ICE by emissions standards.

ICEs are applied practically in all types of transport facilities and remain the main type of mobile heat engines, due to the autonomy, efficiency and reliability. As the main source of energy for the different power plants ICEs are also the main consumer of fuels. During combustion of fuel the pollutant emissions are produced and released into the atmosphere. In Table 1.1 it is presented the data over the Russian Federation for the end of the 20th century characterizing the fuel consumption by different types of transport and emissions of EG as a result of fuel combustion. The greatest contribution to pollution of the atmosphere by EG is made by automobile engines [75].

At present days automobile transport in Russia annually releases 13-15 million tons of carbon oxides and 1,2-1,5 million tons of nitrogen oxides into the atmosphere. At the same time up to 22% of all emissions of carbon dioxide, about 50% of the substances causing acidity of the atmosphere, and 60-90% of smog produced by transport facilities. Especially, heavy ecological conditions developed in the large cities. For example, in Moscow annual total pollutant emissions produced by automobile transport is over 1,7 million tons [75].

Table 1.1.

Consumption of motor fuels and pollutant emissions to the atmosphere by internal combustion engines

Type of transport	Total power, %	Fuel consumption		Emissions of EG to the atmosphere	
		%	million tons	%	million tons
Automobile	50	56,5	65,0	71,3	21,7
Agricultural and timber industry machinery	20	23,5	27,0	17,8	5,4
Railway	16	11,0	12,6	6,3	1,9
River craft	8	5,6	6,8	2,6	0,8
Road-building machines	4	1,9	2,2	1,3	0,4
Aircraft	2	1,2	1,4	0,7	0,2
Total	100	100	115,0	100	30,4

Characteristic feature of the present stage of development of automotive industry and engine building is the sharp growth of number of cars. At the beginning of 2001 the world automobile fleet contained nearly 700 million cars with average annual growth rate of their number of 2-3%. If it were about 120 cars per 1000 people in the world in 2005, then by 2025 this number will increase up to 160 units. There were 700 cars per 1000 people in the USA in 2001, in Great Britain - 410, in Japan - 340. Only for the last 20 years (from 1990 to 2010) the automobile fleet in Moscow has increased from 800 thousands to 3600 thousands cars, i.e. approximately by 4,5 times. In turn, growth of number of cars inevitably leads to increase of pollutant emissions to atmosphere and deterioration of ecological conditions in the large cities.

Ecological safety of vehicles substantially defined by structure and level of concentration of pollutant emissions of EG of automobile engines. Data presented on Fig. 1.1. confirm growth rates of world vehicle fleet which has increased from 650 million units in 2000 to 785 million units in 2008. But at the same time amount of total pollutant emissions after 1991 tends to its decrease caused by introduction of continuously toughening requirements of emissions standards.

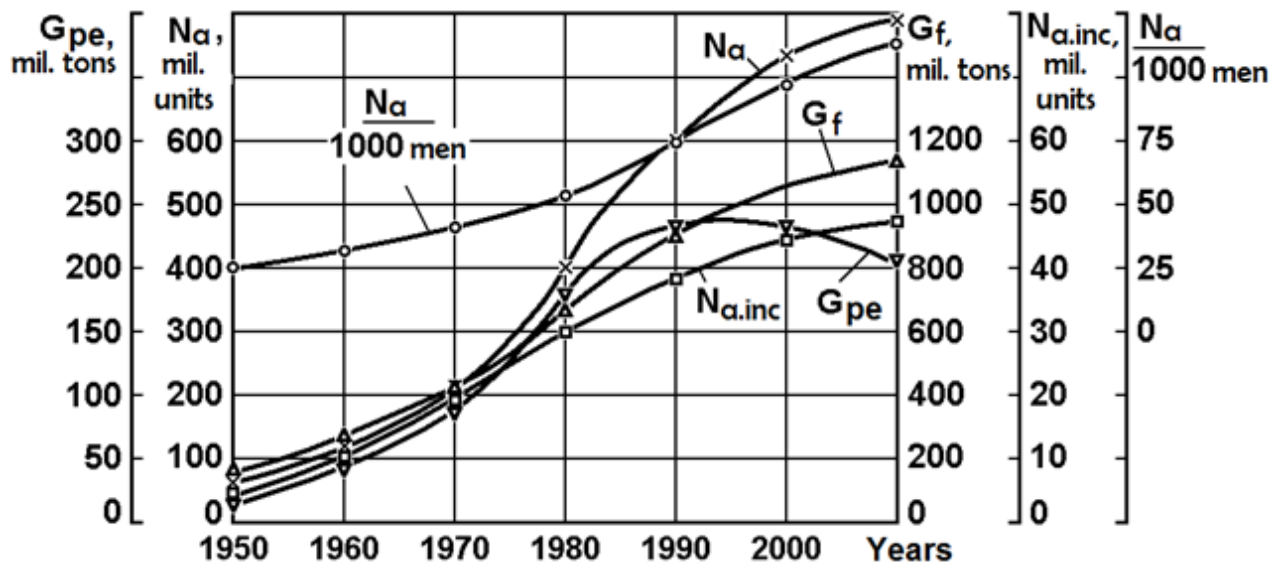


Fig. 1.1. A time history of a world automobile fleet size (number of automobiles N_a), the number of cars per 1000 men ($N_a/1000$ men), annual increase of world automobile fleet $N_{a.inc}$, world consumption of the motor fuels G_f , pollutant emissions from the combustion of motor fuels G_{pe}

Regulations and standards for pollutant emissions are differ depending on type of engines and transport facilities. For diesel passenger cars dynamic of European emission standards is shown in Fig. 1.2 and requirements in Fig. 1.3 [20]. The main EGs toxic components of diesels are nitrogen oxides NO_x and soot (the carbon C or particle matters containing not only carbon, but also some other components - sulfates, metal oxides, etc.). Besides, 60-90% of equivalent toxicity produced by nitrogen oxides. But also particle matters constitute serious human health hazard as they adsorb on themselves the cancerogenic polycyclic aromatic hydrocarbons (PAH) [75]. It should be noted also that a serious problem of reducing EG toxicity of diesels is opposite influence of overwhelming majority of methods on emission of these two main EGs toxic components (nitrogen oxides and particle matters): decrease in emission of one of them is usually followed by increase in emission of another [75].



Fig. 1.2. Dynamics of introduction of toughening requirements of European emission standards for diesel passenger cars

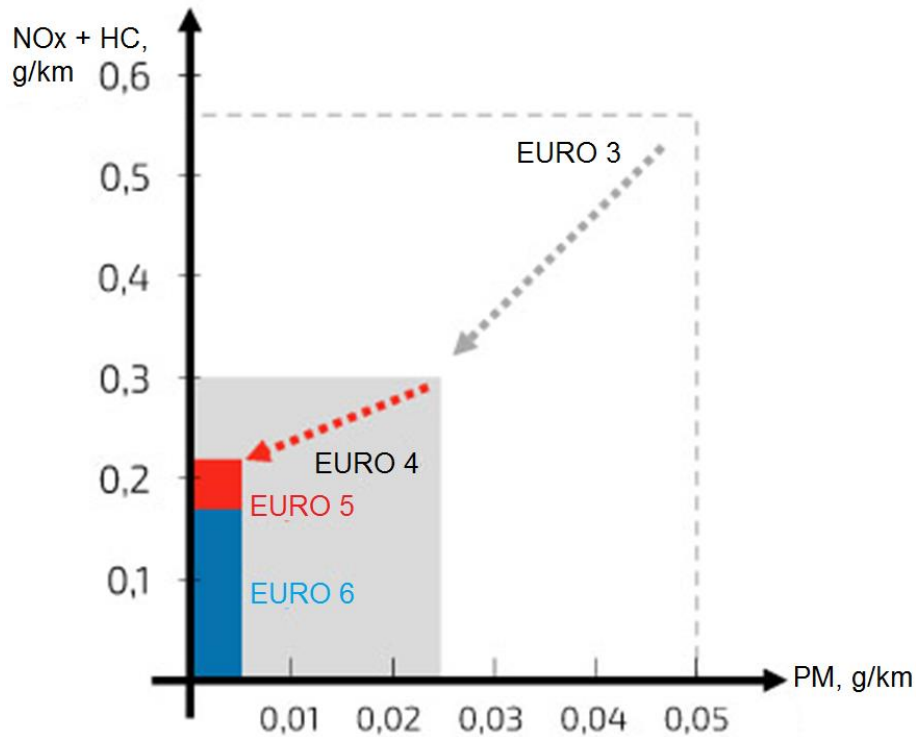


Fig. 1.3. Requirements of European emission standards for diesel passenger cars (PM - particulate matter, NO_x + HC – total emissions of nitrogen oxides and light unburned hydrocarbons)

Given data confirm necessity of implementation in engine building of the means and methods for decrease the EG toxicity. Actions for EG toxicity reduction can be developed in the following main directions (Fig. 1.4) [18, 66, 75]: improvement of engine construction, accounting of operational factors, and use of alternative fuels.

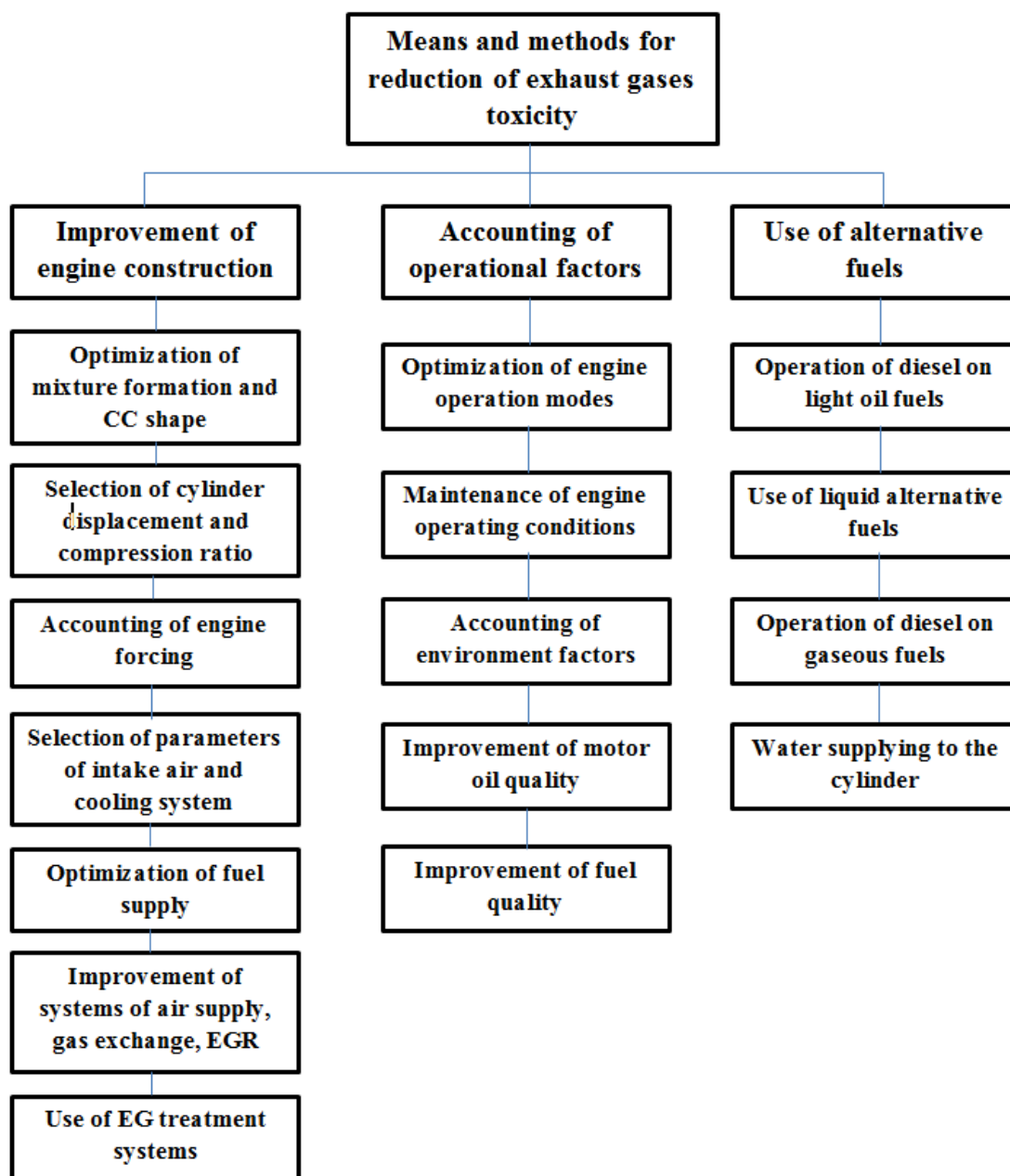


Fig. 1.4. Scheme of basic means and methods for reduction of EG toxicity

Engine construction substantially predetermines toxicity of its EG. The most significant design factors are type of combustion chamber (CC) and type of mixture formation, cylinder capacity and compression ratio, level of forcing of the engine, parameters of an air charge and cooling system, a design of fuel supply systems, air supply, gas distribution, an EGR, existence of devices of EG treatment. Also a significant factor influencing on ecological characteristics of diesels are the control laws over their parameters (cyclic fuel supply, injection

timing, injection profile, injection pressure, air charge pressure, intake and exhaust timings, EGR, etc.). These control laws produced by the systems of the engine listed above.

By optimization of the listed design factors and the control laws it may be provided improvement of engine behavior on the wide range of operating modes and improvement of ecological characteristics. Decrease of EG toxicity of diesels is reached also by the installation in exhaust system of the additional components providing physicochemical treatment of exhaust gases. Use of different exhaust converters and filters belongs to this direction of decrease of EG toxicity. The specified method of decrease of EG toxicity consists in cleaning of diesels EG from already formed toxic components. By means of these devices it is possible to reduce considerably emissions of unburnt combustibles of fuel: monoxide of carbon, unburned hydrocarbons, particle matters (soot). Reducing and catalytic converters are effective in cleaning of EG from the most significant EGs toxic components - nitrogen oxides.

Improvement of ecological characteristics of diesels by improvement of their design is possible only at a stage of creation of new engines. An essential reserve of improvement of the called characteristics is also accounting of operational factors. Among these factors it may be to noted engine behavior, technical condition of the diesel and environmental factors, quality of motor oil and its burning, quality of the applied fuel. This accounting can be also provided by use different automatic control systems over engine parameters. In this case application of automatic control systems allows to improve significantly ecological characteristics of diesels by ensuring their work on optimum regimes, diagnostics of technical condition of the engine, a correcting of the control laws depending on parameters of an ambient air and properties of the applied fuel.

Decrease of EG toxicity could be reached also by using different nonconventional types of fuels (the lightweight oil fuels and alternative non-oil fuels, gas fuels) and also by water delivery in engine cylinders. Some of the specified directions of decrease of EG toxicity of diesels will be described in more

details bellow.

The simplest and most effective remedy to impact on diesel operation for the purpose of improvement of its ecological characteristics is improvement of process of fuel supply [20, 32, 57, 76, 134]. It is due to the processes of fuel supply, atomization and mixture formation substantially predetermine a history of the subsequent combustion process. Besides, the main part of toxic components of EG represents fuel combustion products. Basically for the solution of a problem of decrease of EG toxicity it is necessary to provide best value of an air-fuel equivalence ratio on a given mode of engine operation and high injection pressure. Injection of fuel under HP in the combustion chamber allows to increase quality of fuel atomization. Besides, it is necessary to implement the control over SOI allowing to establish required injection timing on a number of the modes. It is desirable the organization of control over injection profile by change of fuel flow rate through a nozzle, implementation of pilot injection, etc. Each of these actions has the advantages and disadvantages (Fig. 1.5) [18, 63, 66, 75]. However, at the same time it is possible finding of compromise solutions at joint implementation of these actions and use of some other technical decisions (the organizations of EGR, control over the air supply parameters, etc.).

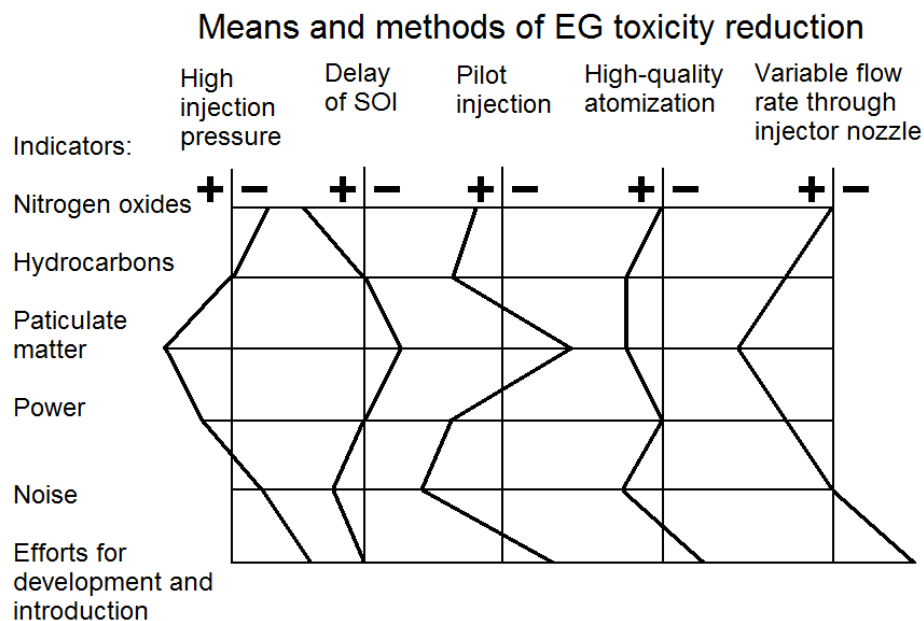


Fig. 1.5. Influence of different technical solutions on diesel characteristics: "+" - positive influence; "-" - negative influence

The data presented on Fig. 1.5 once again confirm a conclusion that achievement of modern efficiency and ecological characteristics of diesels is possible only by further improvement of fuel injection, atomization and mixture formation. These processes exert the determining influence on completeness and perfection of combustion and predetermine characteristics of fuel efficiency and EG toxicity.

1.2. The phenomena and factors influencing quality metrics of fuel injection, atomization and mixture formation

Quality of fuel injection, atomization and mixture formation in many respects depends on design features of a fuel supply system [20, 59, 70, 76]. One of the main parts of fuel systems of diesels are injector nozzles. Different types of injector nozzles are known: pintle, multi-hole, outward opening etc. But even nozzles of one type differ by geometry features of a flowing channels: by design of a clamping cone and a needle tip, in pintle nozzles by design of the pintle channel and a pin [20, 133, 138], in multi hole injectors by arrangement and condition of inlet edges of the holes, their number and effective flow area, by length of the holes [64, 76, 86, 107]. Further we will consider the major factors influencing quality of mixture formation in diesels.

Injection pressure

One of the directions of improvement of diesels operation for providing of required efficiency and toxicity characteristics is the increase of efficiency of mixture formation by an intensification of a fuel supply [20, 76, 109]. Injection pressure exerts impact on such characteristics of process of a fuel supply as spray tip penetration (length L), its width B , a spray cone angle β , atomization fineness. Length of a spray and its volume substantially directly influence on mixture

formation process. Dispersion of atomization determines also fuel evaporation rate and therefore inflammability and heat release rate. Parameters L , B and β determine order of covering of cylinder volume by spray, evaporation rate and finally quality of mixture formation. Increase of injection pressure allows to increase the volume of a spray and to provide fuller coverage of cylinder volume by fuel jets. But at the same time it may lead to hit of part of fuel on rather cold walls of the cylinder, its incomplete combustion and deterioration in characteristics of engine operation. In certain cases, for example at the organization of *HCCI*, hit of fuel on cylinder walls is inadmissible.

Increase of injection pressure is followed by increase of fuel velocity inside the nozzle holes and rate of propagation of fuel jets in the cylinder, break-up of fuel jets begins directly near the hole of the injector nozzle. These factors lead to improvement of quality of fuel atomization. The aggregate view of atomization fineness may be presented by cumulative curves of atomization representing dependences of the sum of relative volumes or mass ΣQ of droplets (which diameters d_p do not exceed the current value) versus d_p (Fig. 1.6) [64, 76]. Curves $\Sigma Q=f(d_p)$ may be drawn using four points: $(d_{p_min}; 0)$, $(d_{p_mean}; 50\%)$, $(d_{p1}; \Sigma Q_1)$, $(d_{p_max}; 100\%)$, where point $(d_{p1}; \Sigma Q_1)$ is transition point from the first curve piece (with larger curve slope) to the second piece (with smaller curve slope). Data on Fig. 1.6 obtained for the high-speed forced diesel with nondivided CC. It demonstrates that with increase of maximum injection pressure p_{inj_max} cumulative curves of atomization are displaced to the region of the best atomization. With a growth of p_{inj_max} from 30 to 68,5 MPa the minimum diameter of droplets d_{p_min} decreases by 2 microns, the average diameter d_{p_mean} - by 12 microns, d_{p1} - by 13 microns, the maximum diameter d_{p_max} - by 40 microns. With increase of pressure p_{inj_max} to 96 MPa d_{p_min} , d_{p_mean} and d_{p1} decrease twice, and d_{p_max} - by 25% in comparison with $p_{inj_max}=30$ MPa.

Improvement of the specified characteristics of atomization leads to more uniform fuel distribution over the cylinder volume. The increase of injection

pressure provided by increase in rate of fuel supply by injection pump plunger is followed also by reduction of injection duration (φ_{inj}) at the fixed cyclic delivery. In particular, in the six-cylinder diesel with $D/S = 130\text{mm}/140\text{mm}$ increase of maximum injection p_{inj_max} from 50 to 200 MPa lead to reduce injection duration from 18 to 10 CA deg. (Fig. 1.7) [76]. Increase of injection pressure to such values leads to growth of fuel spray angle β and to increase of spray tip penetration during IDP $L\tau_i$ and, as a result, to improvement of quality of mixture formation. In particular, it is observed reduction of droplets diameters after jets break-up (for example, the mean droplet diameter d_{p_mean}). It means improvement of atomization fineness, better coverage of cylinder volume by fuel spray, alignment of air-fuel equivalence ratio over cylinder volume, improvement of characteristics of the diesel.

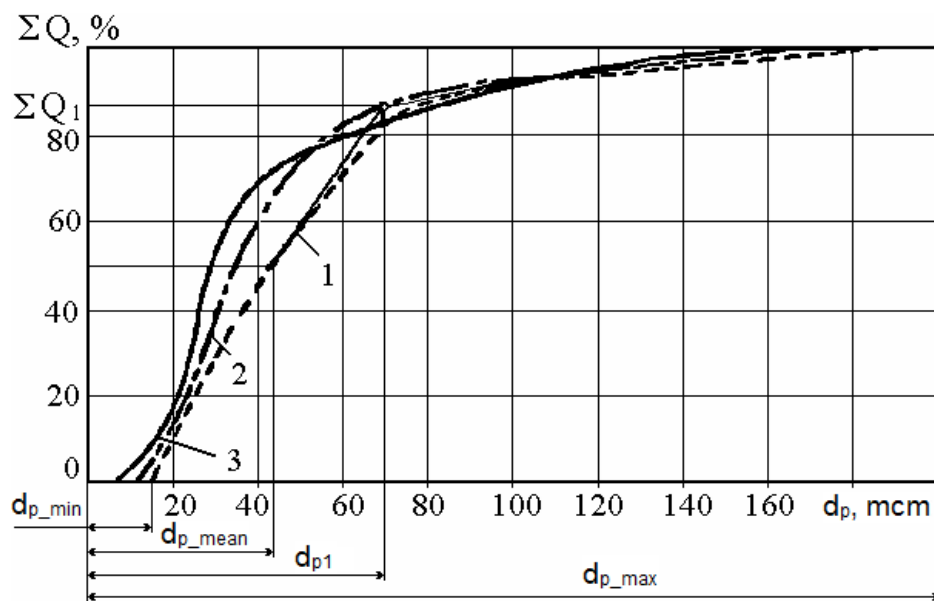


Fig. 1.6. Cumulative curves of fuel atomization with different maximum injection pressures p_{inj_max} , MPa: 1 - 30; 2 - 68,5; 3 - 96

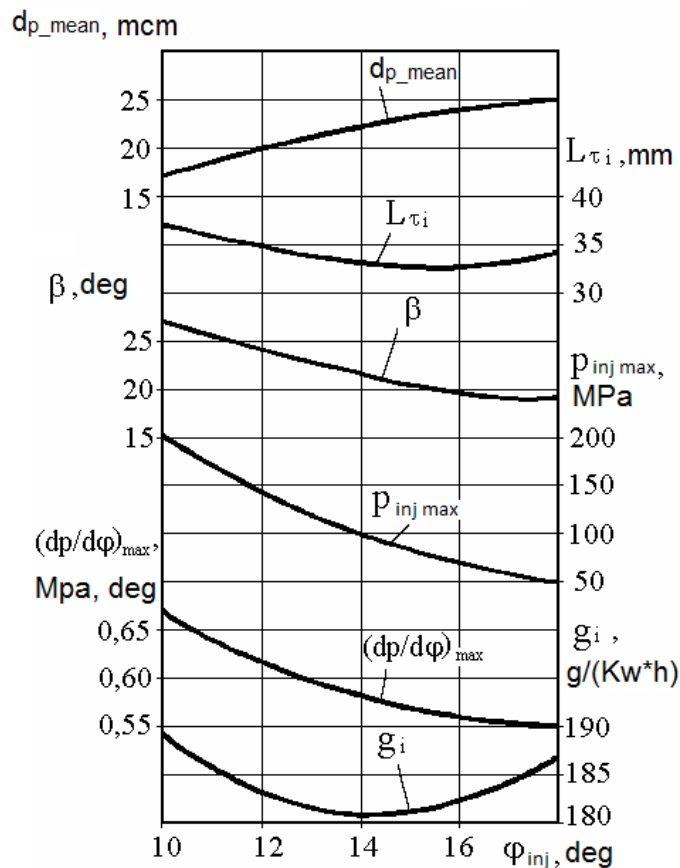


Fig. 1.7. Characteristics of a fuel supply, maximum rate of pressure rise and specific indicated fuel consumption versus injection duration for six-cylinder four-stroke diesel with $D/S = 130\text{mm}/140\text{mm}$ on nominal capacity mode at $n=1750$ rpm (effective area of nozzle holes $\mu f = 0,3 \text{ mm}^2$, their number $i=4$)

As can be seen from Fig. 1.7, the minimum of specific indicated fuel consumption g_i of the diesel occurs at injection duration $\phi_{inj}=14$ CA deg. and injection pressure $p_{inj_max}=100$ MPa. Increase of g_i at $\phi_{inj} < 14$ CA deg. caused by necessity of considerable reduction of injection timing for ensuring allowable maximum pressure of combustion p_z which is not exceeding 15 MPa. As a result combustion is delayed on an expansion stroke that reduces efficiency of heat usage. Therefore while choosing of injection duration it is necessary to consider possible limitation of p_z .

Main objective of injection pressure increase is improvement of atomization fineness. However, at the reached level of injection pressures the mean droplet diameter slightly depends on fuel supply intensity. Therefore, efficiency of a further increase of injection pressure is small. At the same time the hydraulic

efficiency of a fuel supply significantly worsens and the required power input to drive the injection pump increases [76]. Besides, growth of injection pressures is limited by permissible fuel combustion rate (by the level of maximum combustion pressure p_z and by intensity of pressure rise during combustion $dp/d\phi$), by possible increase in emission of NO_x and also by a possibility of hit of fuel on rather cold cylinder walls that leads to incomplete combustion and hydrocarbon emission.

In works [119,124,137] influence of fuel injection pressure in multi-hole injectors on spray penetration is investigated. According to these works during injection pressure increment up to 80 MPa a jet length considerably increases and during further increase of injection pressure penetration vary slightly. In work [124] it is shown that at fuel injection with injection pressure of 100 MPa during $t=1,2$ ms to the medium with atmospheric pressure jet length is about 140 mm (Fig. 1.8). With injection pressure of 25 MPa the fuel jet extends to the same distance during $t=2,0$ ms.

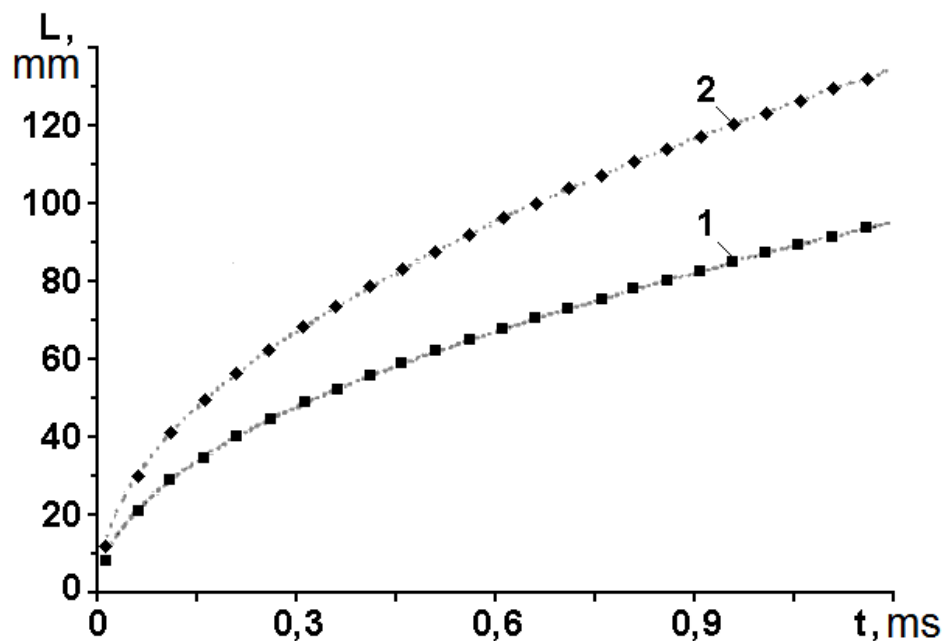


Fig. 1.8. Fuel jet length (spray penetration) at injection by multi-hole injectors to the medium with atmospheric pressure: 1 - injection pressure 25 MPa; 2 - injection pressure 100 MPa

In works of Professor L.V. Grekhov it is shown that with rail pressures over 260 MPa fuel significantly heats during outflow and fuel velocity reaches sound

speed in heated liquid. In other words, flow becomes choked. At further increment of injection pressure, the fuel velocity begins to fall in accordance with sound speed. It demonstrates that the reserve of improvement of atomization quality by method of an increase of injection pressure can be exhausted soon. On the other hand, for the organization of high-quality mixture formation it is necessary to provide uniform distribution of fuel over whole cylinder volume with the absence of hit of fuel on cylinder walls. An example of such mixture formation is *HCCI*. Usually, for organization of *HCCI*, injection performs in the conditions of lower backpressure in comparison with conventional diesels. In these conditions injection under HP is inexpedient therefore for the organization of *HCCI* resort to injection with low pressure by means of the injectors providing lower spray penetration in conditions of low cylinder gases density. Also uses different adaptive strategy of injection. All these factors force engine manufacturers to look for ways of improvement of quality of fuel supply and mixture formation without significant increase of injection pressure. A noticeable reserve of improvement of these processes is influence on internal fuel flow in the nozzles by optimization of flowing channels geometry and flow regimes.

Flow in channels of the injector nozzle

Geometrical parameters of a flowing channel of injector nozzles substantially define quality of a fuel atomization. It is due to features of internal fuel flow in the injector nozzle and its outflow through nozzle holes. In conventional fuel systems fuel supplied by injection pump comes to injector and lifts a needle 1 (Fig. 1.9, *a*) and flows through the annular gap 3 formed between a needle 1 and the body 2 and comes to a cavity 4 under a needle 1 where injection pressure p_{inj} is established. Under this pressure fuel comes to a nozzle hole 5.

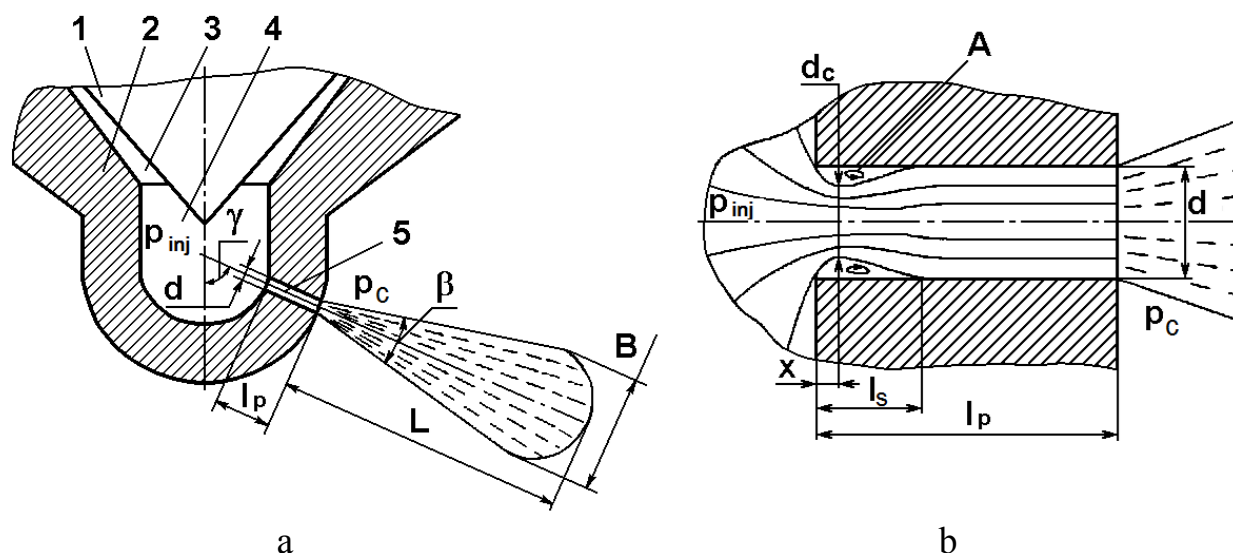


Fig. 1.9. The scheme of injector nozzle with geometrical characteristics of atomized fuel jet (a) and the scheme of a fuel flow inside a nozzle hole (b)

Streamlines are curving just before an entrance to a nozzle hole (Fig. 1.9, b) and their curvature increases from a hole axis to its periphery. These factors lead to appearance of nonuniform pressure and velocity distributions. At the same time minimum pressures (and local high velocities) are reached in peripheral flow areas where local pressure can drop lower saturated vapor pressure. It is typical that once behind hole inlet edge the fuel flow is contracted and there is a vortex fuel flow (zone A of separation on Fig. 1.9, b). Here the ring vortexes are arising and growing up and then partially breaking up and flowing away with the fuel [64, 76, 108]. In this transient flow there are pulsations of pressure and velocities in separation zone extending to all fuel flow in a nozzle hole. Thus, the vortexes which have arisen at an inlet edge of a nozzle hole lead to the growing of fuel jet instability and to subsequent jet break-up.

The difficult flow pattern is supplemented by heat effects and phases transition. Process of formation of gas voids in a liquid due to a sudden pressure p_l drop lower than the critical level p_{cr} (Fig. 1.10) called cavitation [122]. As a critical pressure level at which phases transition begin usually use the saturated vapor pressure $p_{cr} = p_v$. It is caused by the fact that in comparison with the reached injection pressure level the difference between p_{cr} and p_v is negligible. The equation of a static equilibrium of bubble containing the emitted gas (for example

air) with vapor and surrounded by liquid:

$$p_B = p_l + \frac{2 \cdot \sigma}{R}, p_B = p_v + p_g, \quad (1.1)$$

where p_B - pressure in a bubble, p_v , p_g - partial pressures of vapor and the emitted gas respectively, R - bubble radius, σ - surface tension. In details equilibrium of a bubble is described in chapter 2.

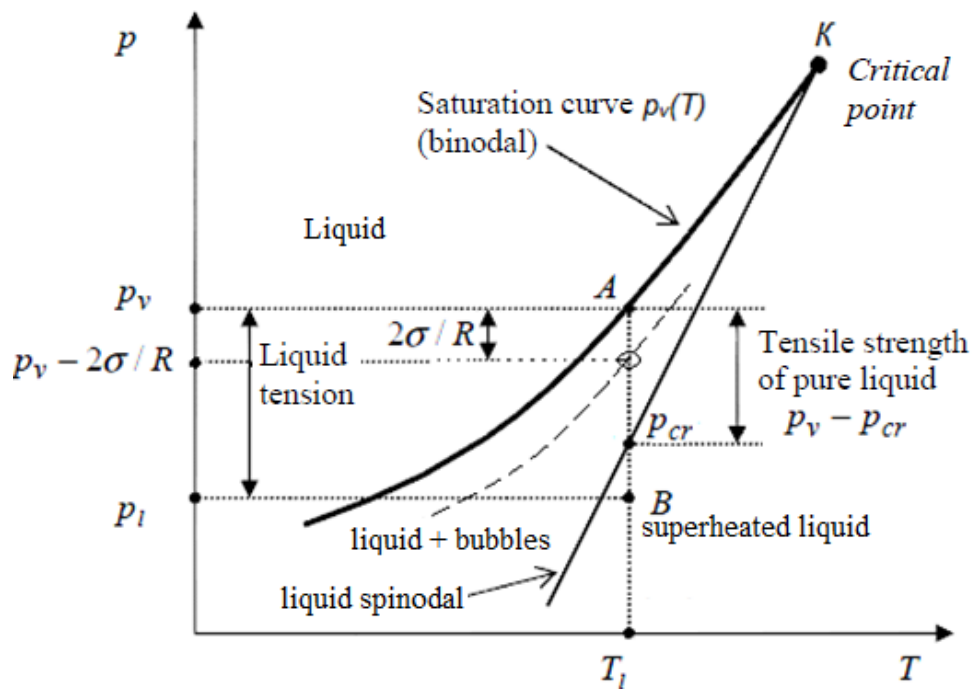


Fig. 1.10. p - T constitution diagram

In relation to fuel supply systems of diesels there are two mechanisms of cavitation: dynamically induced and geometry induced [173]. In the first case cavitation occurs in the regions with low pressure produced by the movement of pressure waves (expansion wave). Unlike to the dynamically induced mechanism which exists only in transient flows the geometry induced mechanism exists both in transient and in the steady flows. In this case the prime cause of emergence of cavitation are features of a flowing channel geometry, for example its sudden change (Fig. 1.11) [172].

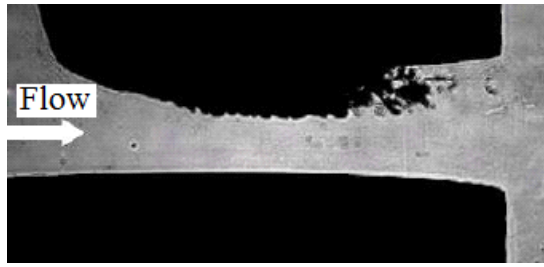


Fig. 1.11. The cavitation caused by geometrical features of a flowing channel

At sudden change of geometry of a flowing channel (for example sudden area contraction on an entrance to a nozzle hole) (Fig. 1.9.) there is a boundary layer separation (Fig. 1.12) and locally high velocities of liquid in a recirculation zone may lead to pressure drop below level p_{cr} and to emergence of cavitation [154,173].

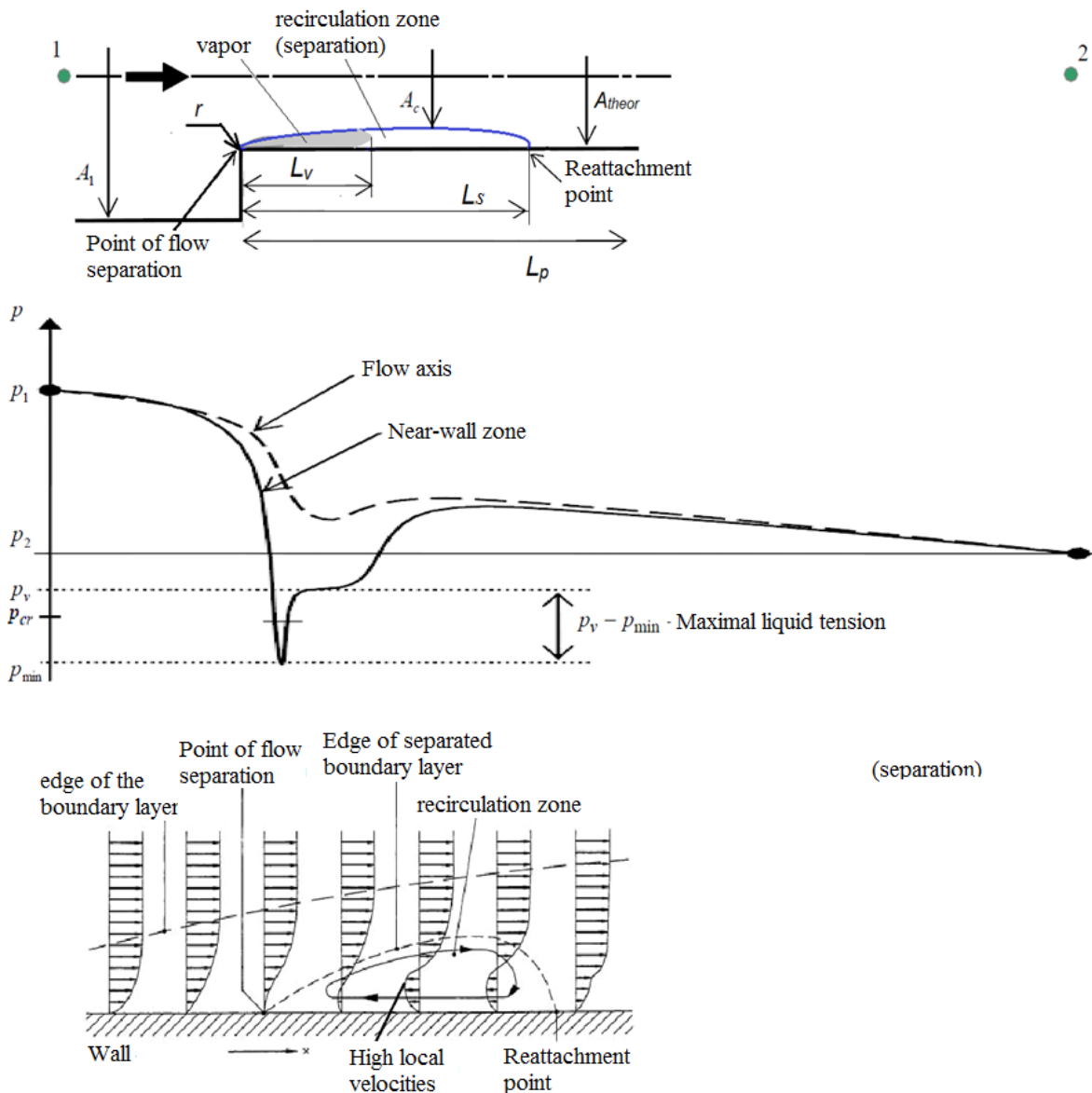


Fig. 1.12. The scheme of boundary layer separation and formation of cavitation in a fluid flow

The vapor bubbles which are formed in separation zones depending on intensity of a flow could collapse soon after formation or may be carried away by flow to zone with higher pressure. Zone occupied with vapor (L_v , Fig. 1.12) may extend to all length of geometrical object and the collapse of bubbles occurs beyond its limits (Fig. 1.13). This phenomenon is called supercavitation [144]. Cavitation intensity is usually evaluated by some kind of characteristic number. There are different determinations for a cavitation number. In this work are used two the most widely used from them [121,159]:

$$CN = \frac{p_1 - p_2}{p_2 - p_v} = \frac{p_{inj} - p_c}{p_c - p_v} \quad K = \frac{p_1 - p_v}{p_1 - p_2} = \frac{p_{inj} - p_v}{p_{inj} - p_c} = 1 + \frac{1}{CN} \quad (1.2)$$

It is also convenient to use CN^{-1} that is inverse of CN . Classification of cavitation and flow regimes depending on length of zone occupied by vapor L_v [154] is presented on Fig. 1.14.

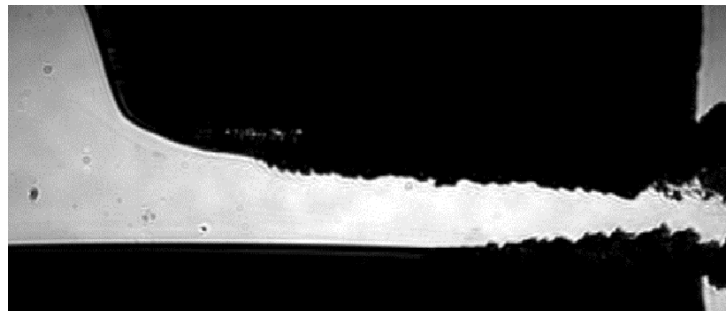


Fig. 1.13. Visualization of supercavitation

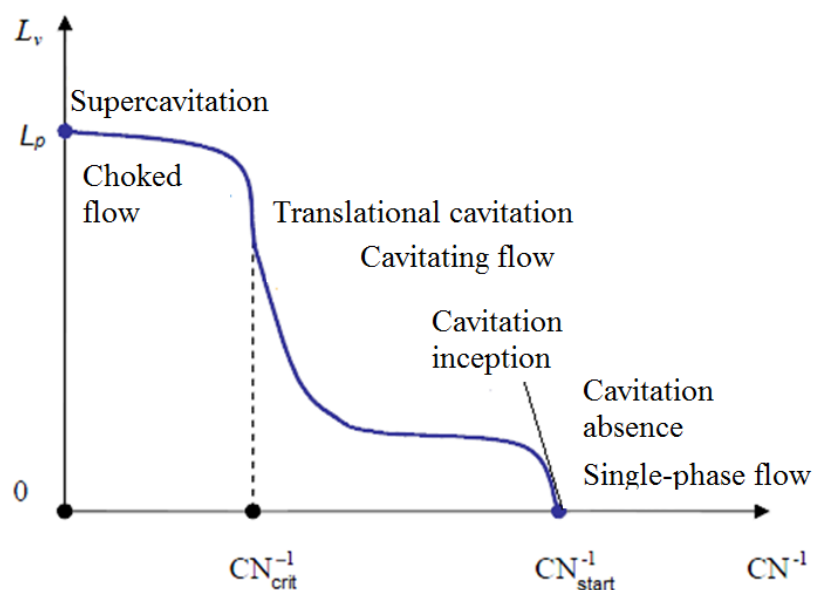


Fig. 1.14. Classification of flow and cavitation regimes [154]

In work [179] fuel flow inside submerged nozzle hole is investigated at different cavitation numbers. It was shown that with constant inlet pressure reduction of backpressure below a certain level lead to flow rate independence from pressure drop (Fig. 1.15). It occurs because at value of a cavitation number $CN(\Delta P)=CN_{crit}$ all cross-section of the hole is filled with two-phase mixture (Fig. 1.16) and flow velocity reaches sound speed in two-phase medium $a_{liq-gas}$ [179].

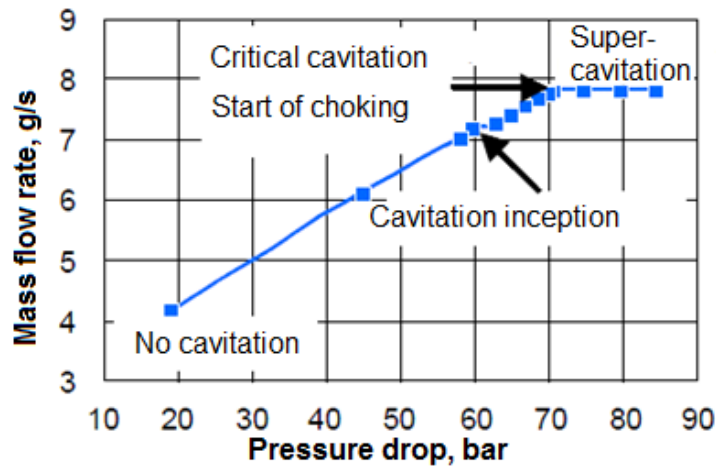


Fig. 1.15. Dependence of fuel mass flow rate from pressure drop

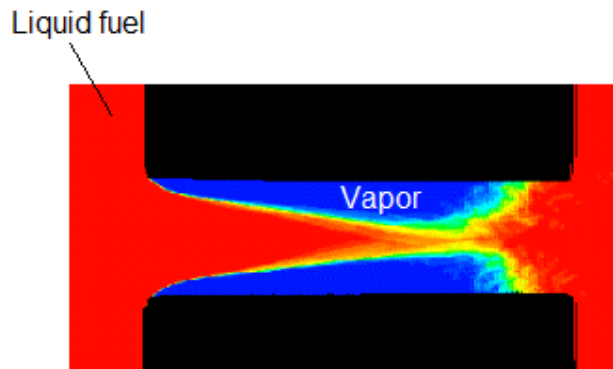


Fig. 1.16. Visualization of phases distribution in a flow at $CN= CN_{crit}$

On Fig. 1.17 it is shown that sound speed in a two-phase medium is much lower, than in a pure liquid or gas, therefore this value may be easily achieved in real flows. When in whole cross-section velocity have values exceeding sound speed in a two-phase medium (in other words Mach number $M = \frac{v}{a_{liq-gas}} \geq 1$), the expansion wave caused by outlet pressure reduction cannot pass through this

section any more. Therefore the flow rate becomes independent of this factor [149]

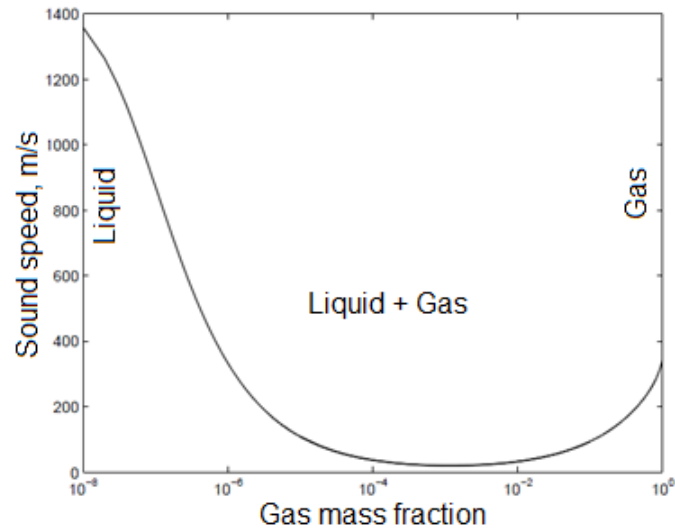


Fig. 1.17. Sound speed in a two-phase medium

In work [173] it is shown that for outflowing into gas there is one more flow regime named hydraulic flip (Fig. 1.18). For nozzle channels it may occur total hydraulic flip (Fig. 1.18, *d*), and partial hydraulic flip (Fig. 1.19)

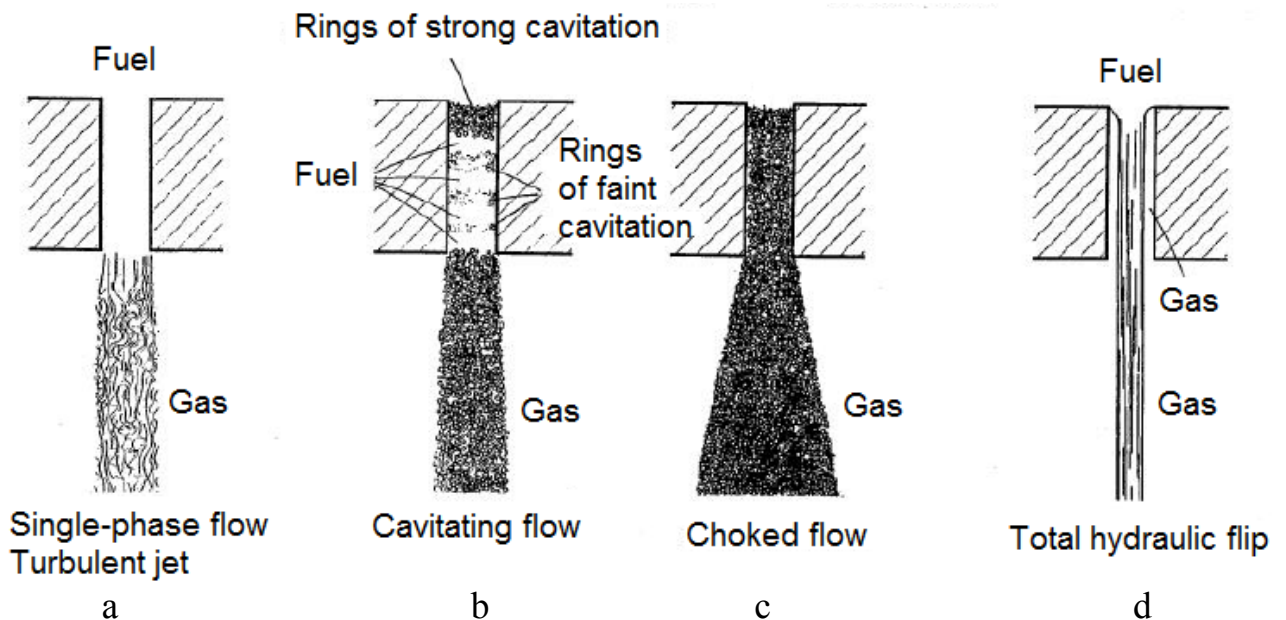


Fig. 1.18. Flow regimes in injector nozzle holes at outflow of fuel into gas

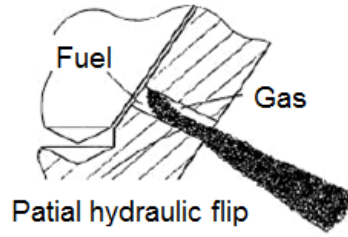


Fig. 1.19. Partial hydraulic flip

As it noted above, increase of injection pressure higher than 250 MPa may lead to significant fuel warming during compression in the hole and choking and therefore sonic speed in liquid fuel considerably decreases (below 800m/s) and becomes achievable. Outflow of fuel with velocities higher than local sound speed in liquid is impossible. Thereby, at further injection, pressure increase flow rate decreases in proportion to sound speed in liquid $a_{liq}(p,T)$. Generalizing data of works [159,173] it can be defined the field of possible fuel flow regimes in a nozzle hole at increase in a cavitation number due to injection pressure increment p_{inj} (Fig. 1.20).

For choked flow a volumetric flow rate V can be calculated both through a conventional coefficient of discharge μ , and through its critical value which is constant of a flowing channel geometry $\mu_{crit}=C_c=const$:

$$V = \mu \cdot A_{theor} \sqrt{\frac{2(p_{inj} - p_c)}{\rho_l}}$$

$$\Downarrow$$

$$V = \mu_{crit} \cdot A_{theor} \sqrt{\frac{2(p_{inj} - p_v)}{\rho_l}} \Rightarrow \mu = \mu_{crit} \sqrt{\frac{p_{inj} - p_v}{p_{inj} - p_c}} = \mu_{crit} \sqrt{K} = C_c \sqrt{K} = C_c \sqrt{1 + \frac{1}{CN}} \quad (1.3)$$

where $C_c=A_c/A_{theor}$ - contraction coefficient, A_c , A_{theor} - the area of real cross-section in most contracted place and the area of geometrical cross-section of a hole (Fig. 1.12). Contraction coefficient usually have values from 0,61 to 0,70 depending on geometrical features, first of all from the ratio of hole inlet edge radius to hole diameter r/d (to Fig. 1.12) and the K -factor described below (see Fig. 1.21 and explanations to it).

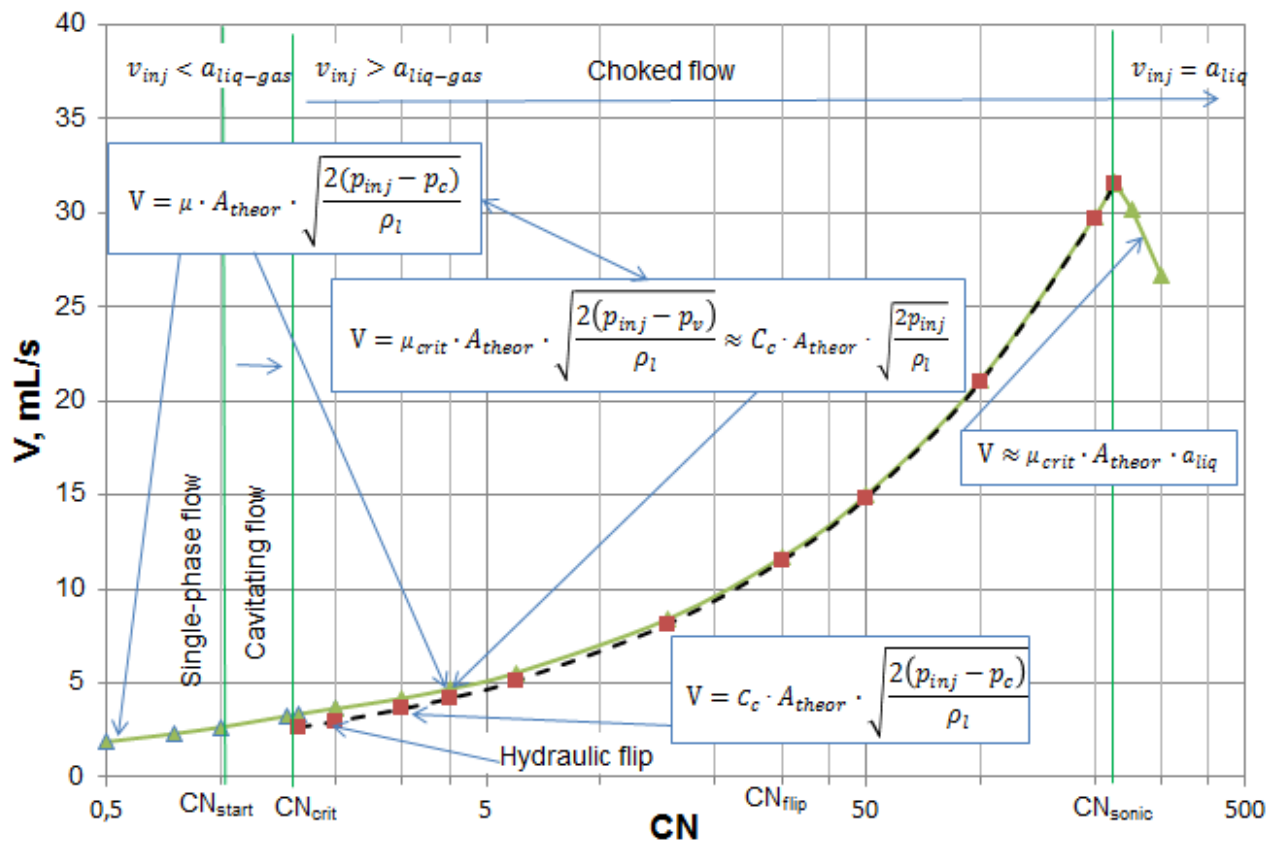
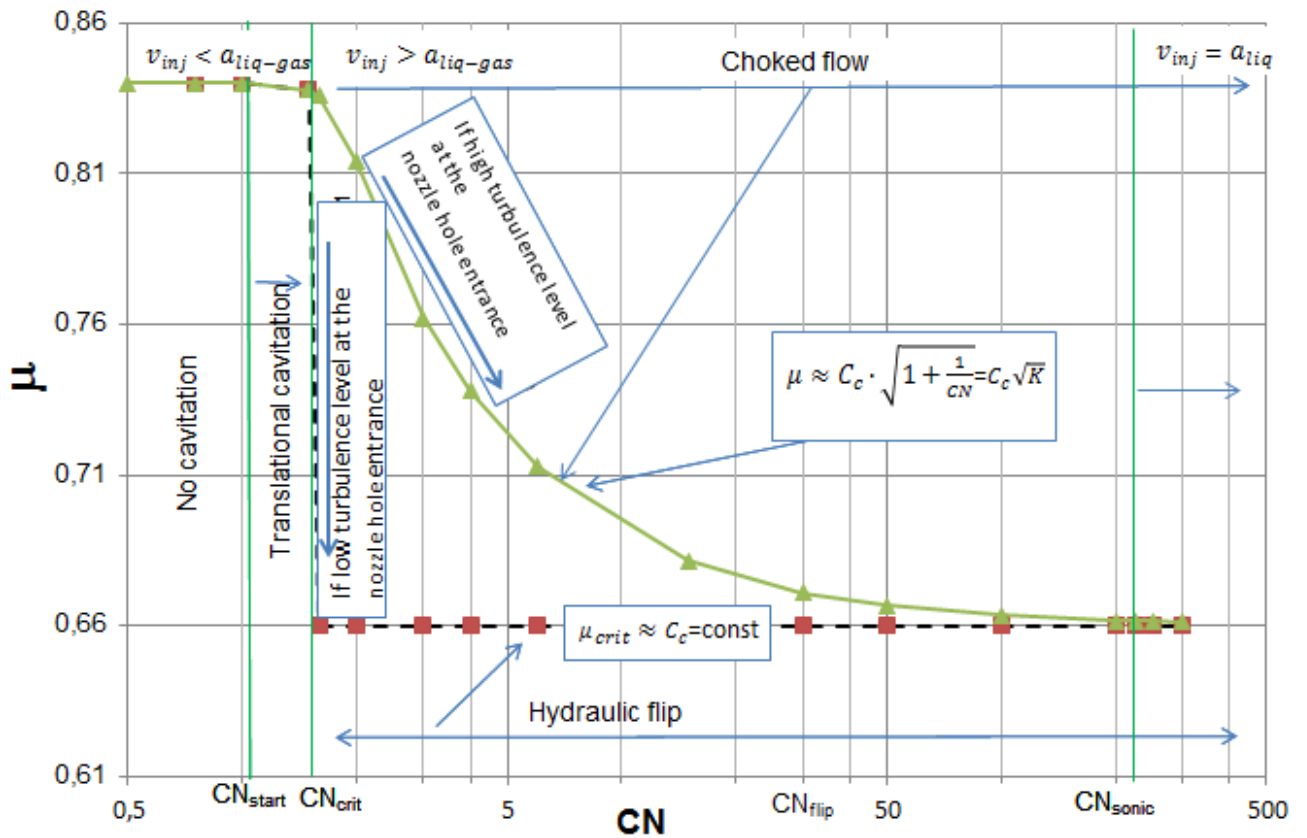


Fig. 1.20. The field of flow regimes in a nozzle hole (the values on axes is estimations for hole diameter of 0.275 mm)

It is necessary to distinguish contraction coefficient C_c and area coefficient

$C_a = \frac{\rho \cdot A}{\rho_{theor} \cdot A_{theor}}$ which multiplied on velocity coefficient $C_v = \frac{u}{u_{theor}}$ is equal to a coefficient of discharge:

$$\mu = C_a \cdot C_v = \left(\frac{\rho \cdot A}{\rho_{theor} \cdot A_{theor}} \right) \cdot \left(\frac{u}{u_{theor}} \right) = \frac{Q}{Q_{theor}}, \quad (1.4)$$

where Q and Q_{theor} - respectively the real and theoretical mass flow rate. Value $CN = CN_{flip}$ on Fig. 1.20 corresponds to value of a cavitation number CN at which there are no any more significant differences in flow rate characteristics between the choked flow and hydraulic flip.

The best quality of a fuel atomization is reached at a choked flow at which break-up of a jet begins inside nozzle hole. Further break-up of droplets also happens more intensively, the spray angle increases (this process is displayed below on Fig. 1.27, *b, c*). According to [173] outflow at partial hydraulic flip (Fig. 1.19) is also followed by high quality of atomization (see Fig. 1.28*a* given below). But total hydraulic flip lead to smooth uniform outflow (Fig. 1.18, *d*) and intensity of a jet break-up decreases, despite great values of velocities, the spray angle has the minimum values (Fig. 1.28, *b*). Whether there will be full substitution of the vapor zones by gas from the cylinder and the subsequent forming of hydraulic flip depends generally on features of geometry and prehistory of a flow. If turbulence level at the nozzle hole entrance is insignificant then streamlines have smooth nature and it promotes that the reattachment point of a boundary layer (Fig. 1.12) may be located behind nozzle hole outlet. In this case gases from the cylinder entraining to the zone with low pressure and replace the vapor and lead to formation of total hydraulic flip. Such flow is typical for injectors with single nozzle hole especially if hole inlet located in the sac and far from needle sock. Besides, significant influence has the geometry features of a nozzle hole - the ratio r/d and L_p/d . The increased turbulence level, curved streamlines on an entrance to a nozzle hole promote the shift of a reattachment point of a boundary layer towards the hole inlet and gases from the cylinder cannot get into the zone occupied with vapor.

Thus, on structure of a fuel jet at the nozzle exit exerts impact fuel flow pattern inside a nozzle hole and also the fuel flow disturbances arising at its flowing in a ring channel between the body and a nozzle needle (i.e. in an annular gap 3 on Fig. 1.9, *a*). Due to the specified factors in Russia and other countries the numerous researches directed to improvement of injector nozzles design for diesels of different function [56,76,118,119,162] are conducted.

In work [119] it is presented results of optical researches of fuel jets injected using *Common-Rail* system to the chamber with the atmospheric pressure and pressure typical for diesel engine. There were examined injector nozzles with different diameters and the conicity of nozzle holes. Conicity may be determined by the K-factor (Fig. 1.21):

$$K = (d_{in} - d_{out}) / 10. \quad (1.5)$$

It were investigated injector nozzles with the inlet edges of nozzle holes located in cavity under a needle - in a sac of the injector nozzle (*SAC* nozzle, Fig. 1.22, *a*) and on a clamping cone of the injector nozzle (*VCO* nozzle, Fig. 1.22, *b*).

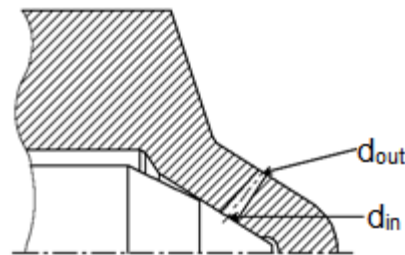


Fig. 1.21. Injector nozzle with conical nozzle holes

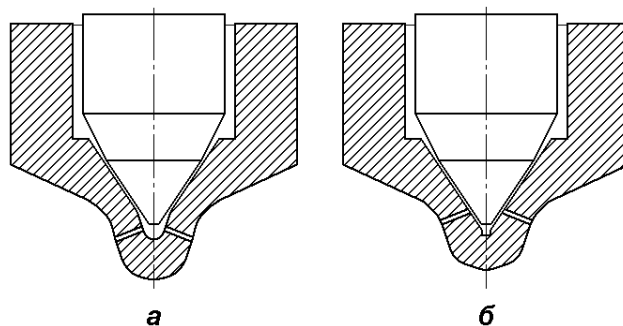


Fig. 1.22. Injector nozzles *SAC* type (*a*) and *VCO* type (*b*)

Characteristics of fuel sprays have been investigated in the chamber filled with nitrogen under pressure. Chamber had optical access for video filming. For

obtaining frontal images atomized fuel jets were highlighted by the argon laser and for obtaining side images of jets the spark source of light was used. The view of the fuel jets produced by the *VCO* nozzle is presented on Fig. 1.23.

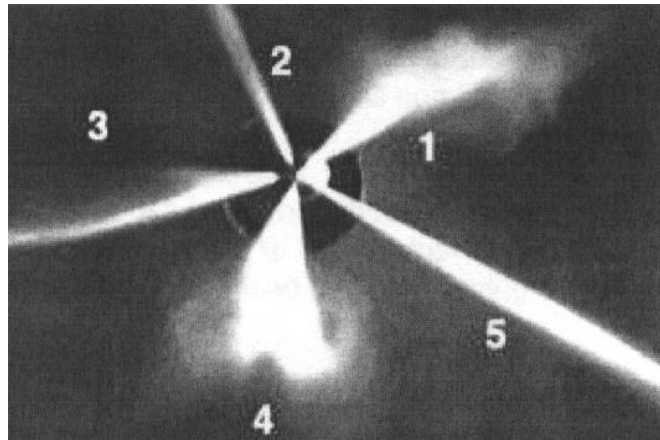


Fig. 1.23. A view of the fuel jets produced by the *VCO* nozzle at injection to atmospheric condition at 0,1 ms after SOI

In the mentioned work [119] there were conducted researches of influence of different design factors and parameters of injection: location of nozzle holes (*SAC* and *VCO* nozzles), conicity of nozzle holes (*K factor* equal 0; 1,5; 2,0), injection pressures (from 25 to 120 MPa). It was noted that great values of the *K factor* reduce spray tip penetration (length L) at injection in atmospheric condition. Reduction of length of jets L with growth of the *K factor* is due to finer atomization with reduction of total jet impulse. With reduction of injection pressure influence of *K factor* on length L decreases. By results of researches the following features of a fuel injection and atomization are noted. When using the *VCO* nozzles with a needle without additional guide irregularity of a fuel supply is noted (Fig. 1.23) and poor repeatability of jets from injection to injection at small needle lift. When using double-guided injector nozzles improving needle centering, the geometry of fuel jets was stable. Length of jets L , their width B and a spray angle β substantially depend on the injection pressure and backpressure. Big conicity of nozzle holes (great value of the *K factor*) leads to reduction of jet length L and the angle of their dispersion β , especially noticeable at injection in the atmosphere. With an injection pressure of 25 MPa time of the beginning of a jet break-up was

about 0,1 ms from SOI. Increase of injection pressure to 120 MPa lead to the fact that break-up of a jet began almost at the same time with SOI. Increase of injection pressure also leads to reduction of average diameter of droplets and more homogeneous structure of a jet.

Primary jet break-up

It has been noted above that the most important effects influencing jet break-up are turbulence and cavitation. Outside of the injector nozzle one more is added - aerodynamic interaction. The scheme of a jet break-up offered in work [126] is presented on Fig. 1.24.

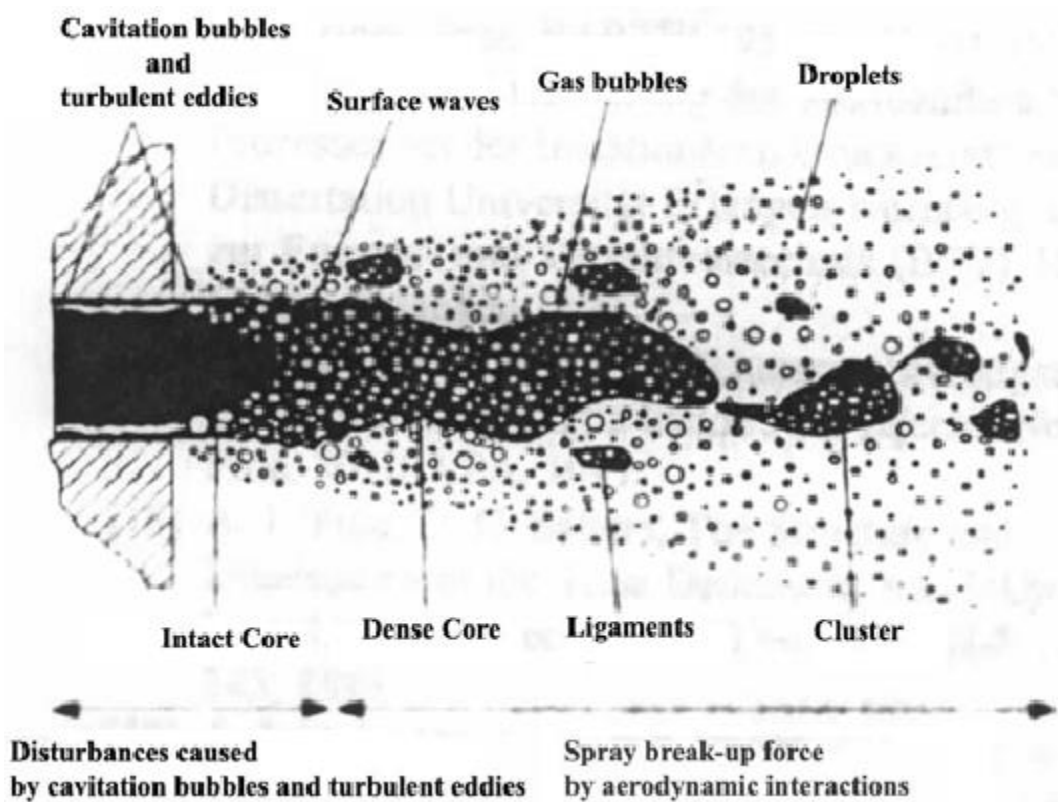


Fig. 1.24. The scheme of fuel jet break-up after outflow from the injector nozzle

Process of formation of ligaments, clusters and the first droplets is referred to primary jet break-up, further decay of droplets in the cylinder is called secondary break-up. There is mutual action of forces of different nature on liquid surface when fuel outflows from the nozzle. This action leads to disturbances on jet

surface, break of its integrity and subsequent decay. The mentioned forces are: inertial forces, surface tension, aerodynamic forces and forces of viscous friction. The characteristic numbers Reynolds, Weber and the Ohnesorge are used for estimation of the ratios between these forces:

$$Re = \frac{u \cdot d \cdot \rho}{\mu} \quad We = \frac{d \cdot \rho \cdot u^2}{\sigma} \quad Oh = \frac{\mu}{\sqrt{\sigma \cdot d \cdot \rho}} = \frac{\sqrt{We}}{Re} \quad (1.6)$$

Classification of modes of primary jet break-up according to works [160, 167] is given in Fig. 1.25. The points corresponding to experiments in work [171] of injection by outward-opening injector at different values of pressure drop ($p_{inj}-p_c$) and the maximum lift of a pin (valve) h_{pin} are marked on the chart. The provided data demonstrate that for the considered injectors a typical mode is the atomization. Other modes usually take place only at the initial and closing stages of injection.

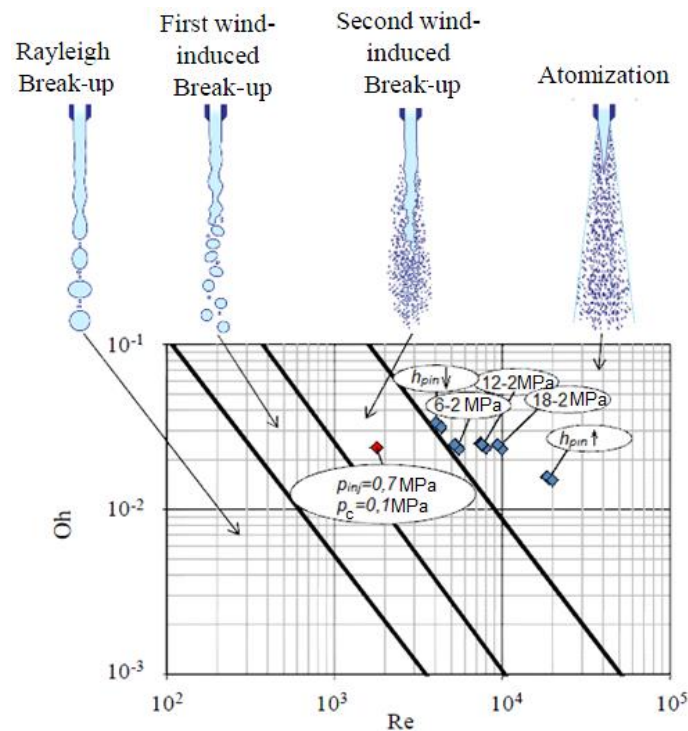


Fig. 1.25. Classification of jet primary break-up modes

In the experimental picture presented on Fig. 1.26 it may be seen that together with outflowing liquid there are vapor bubbles on jet periphery which intensify primary jet break-up [132]. It has been noted above that depending on a cavitation number and a turbulence intensity the different regimes of outflow are possible

(Fig. 1.18). In particular it is possible the beginning of a jet break-up inside a nozzle hole (choked flow). Experimental pictures of jet break-up at the different regimes of outflow from different type of injector nozzles [132] are presented on Fig. 1.27.

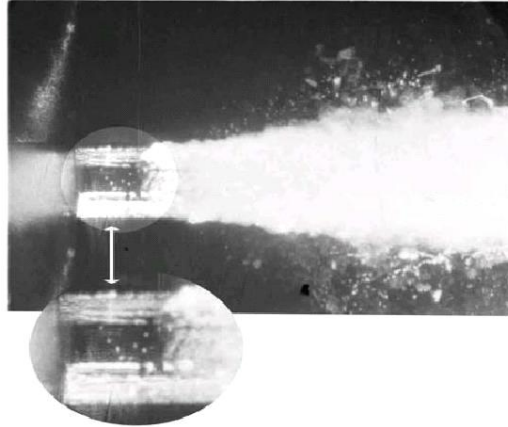


Fig. 1.26. A primary jet break-up at the cavitating outflow

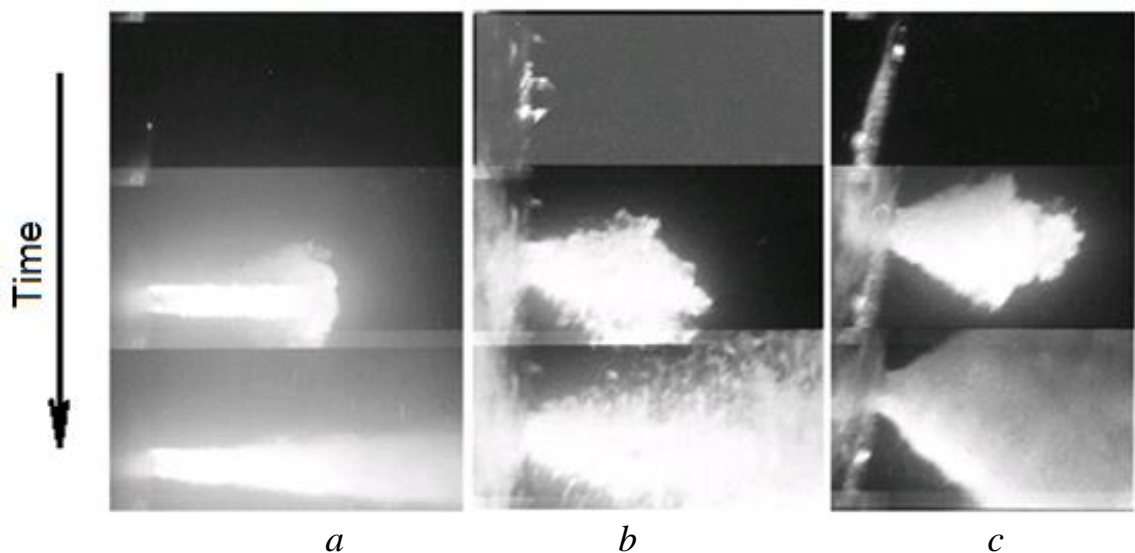


Fig. 1.27. A jet break-up at the different regimes of outflow from different types of injector nozzles: *a* - cavitating flow, single-hole VCO nozzle with $d=0,18$ mm; *b* - choked flow, multi-hole SAC nozzle, $d=0,124$ mm; *c* - choked flow, multi-hole VCO nozzle, $d=0,146$ mm

This data confirm that the best quality of a fuel atomization is provided at a choked flow (Fig. 1.27,*b,c*) and at a partial hydraulic flip (Fig. 1.28, *a*).

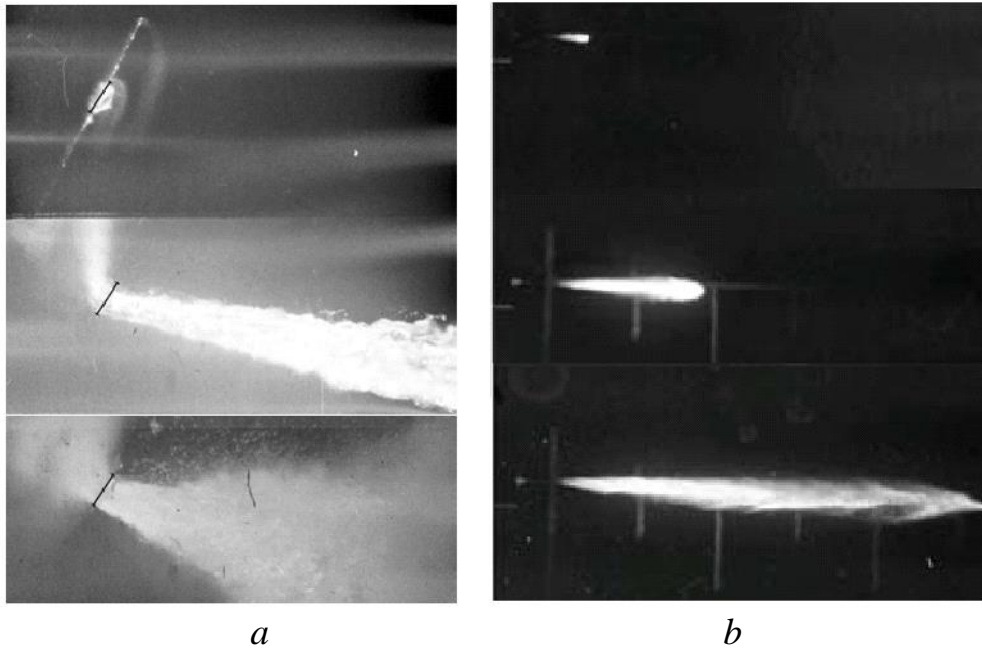


Fig. 1.28. Outflow of fuel at hydraulic flip: *a* - partial hydraulic flip (the multi-hole VCO nozzle), *b* - total hydraulic flip (the coaxial single-hole injector nozzle)

The phenomena of cavitation and gas entrainment from the cylinder to the nozzle [120,152] are also typical for the injectors producing conical shape of a spray (pintle and outward-opening injectors) (Fig. 1.29). The gas entrainment in pintle nozzles may occur both in cavitating, and in not cavitating flows. In the first case gases also can get into the zones occupied with vapor, substitute it and promote hydraulic flip (usually partial). In the first and second case the gases entraining from the cylinder cause a break-up of the liquid hollow cone on strings (Fig. 1.29, *b*). Such effect is explained by action on a liquid surface of aerodynamic forces, a surface tension force and the mass conservation law. It is obvious that cavitation, turbulence and gas entrainment are the determinative effects influencing a jet break-up.

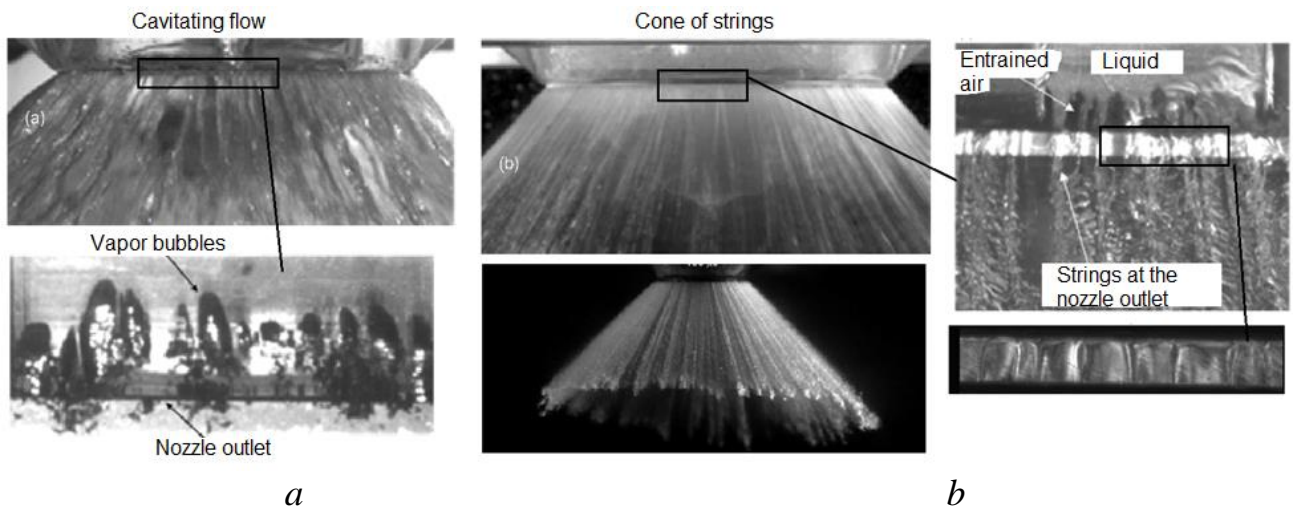


Fig. 1.29. Outflow of fuel from the injector producing conical shape of a spray: *a* - cavitating flow; *b* – strings formation

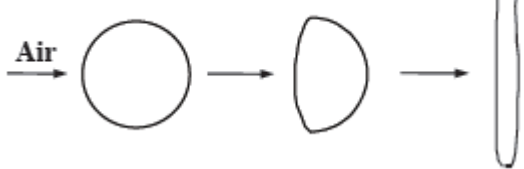
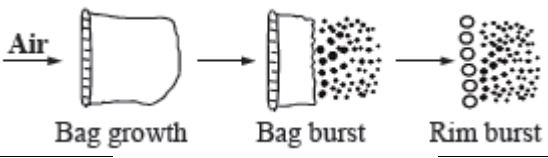
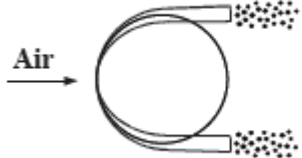
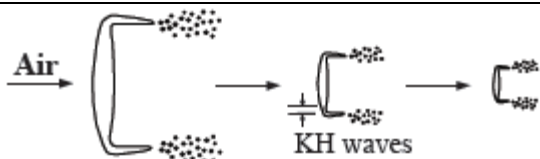
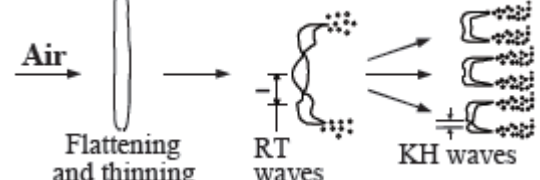
Secondary break-up of droplets

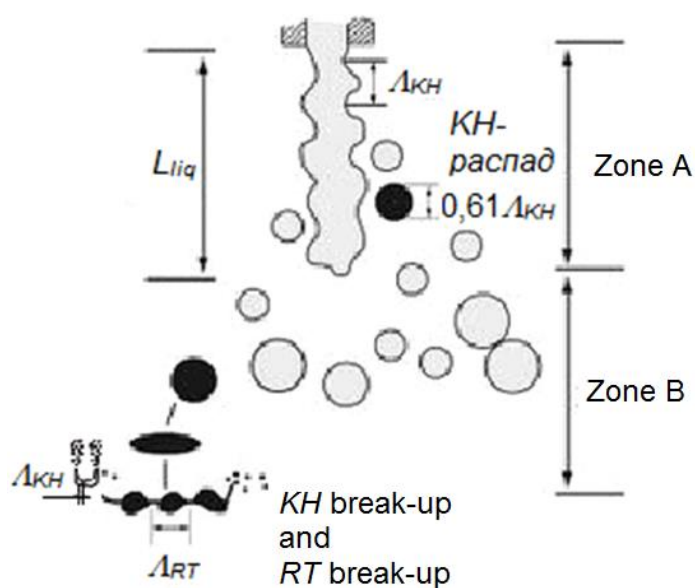
The great influence on a jet break-up is exerted by surface tension of fuel. From the data presented on Fig. 1.25 it is possible to see that at Ohnesorge number $Oh < 0,1$ influence of viscous effects are insignificant therefore the modes of break-up of droplets can be classified depending on a Weber number. Classification of modes of droplets secondary break-up according to [125, 164, 167] is given in Table 1.2.

At Weber numbers $We > 100$ action of aerodynamic forces lead to growth of the Kelvin-Helmholtz instability causing formation of waves (*KH*-waves) on the droplet periphery. This mechanism occurs due to difference of droplet velocity and velocity of surrounding gas. This relative velocity leads to emergence on the droplet periphery of shear stresses, to appearance of shear forces and, as a result, *KH*-waves. Length of Kelvin-Helmholtz waves and rate of their growth determine a droplet break-up time and radius of child droplets (Fig. 1.30) [168].

Table 1.2.

Modes of droplet break-up

Break-up stage	Deformation type or break-up mode	Scheme	Weber number value
First stage	Deformation and flattening		$We < 12$
Second stage	Bag Break-up		$12 < We < 100$
	Break-up due to shear forces		$We < 80$
	Break-up due to stretching and thinning		$100 < We < 350$
	Catastrophic break-up		$We > 350$

Fig. 1.30. Scheme of a jet break-up under *KH-RT* mechanism

For a jet break-up at $We > 350$ Rayleigh-Taylor instability becomes also considerable mechanism destroying a droplet. It arises on an interface of phases, having different density. While interphase boundary remains smooth the surface of a droplet is stable, but the slightest perturbation causes growth of waves (*RT*-waves) leading to further droplet break-up. The frequency of the fastest growing wave and the corresponding wave number determine a droplet break-up time and radius of child droplets.

One of the most widely used models of droplets break-up is so-called *KH-RT* model based on the corresponding mechanisms. The scheme of this model is presented on Fig. 1.30. This model also includes the theory offered by V. G. Levich for length of the liquid core of a jet [150]. It is assumed that within L_{liq} (Fig. 1.30) only the *KH* mechanism operates. Model is stated in details in section 2.3 of chapter 2.

Thus, intensity of secondary droplets break-up depends generally on fuel properties, the relative velocity of droplets and density of a medium in which injection is made. On Fig. 1.31 characteristics of a jet depending on a fuel type and gas density are given [177]. These data show that larger gas density promotes reduction of spray penetration and increase of spray angle that means more intensive jet break-up.

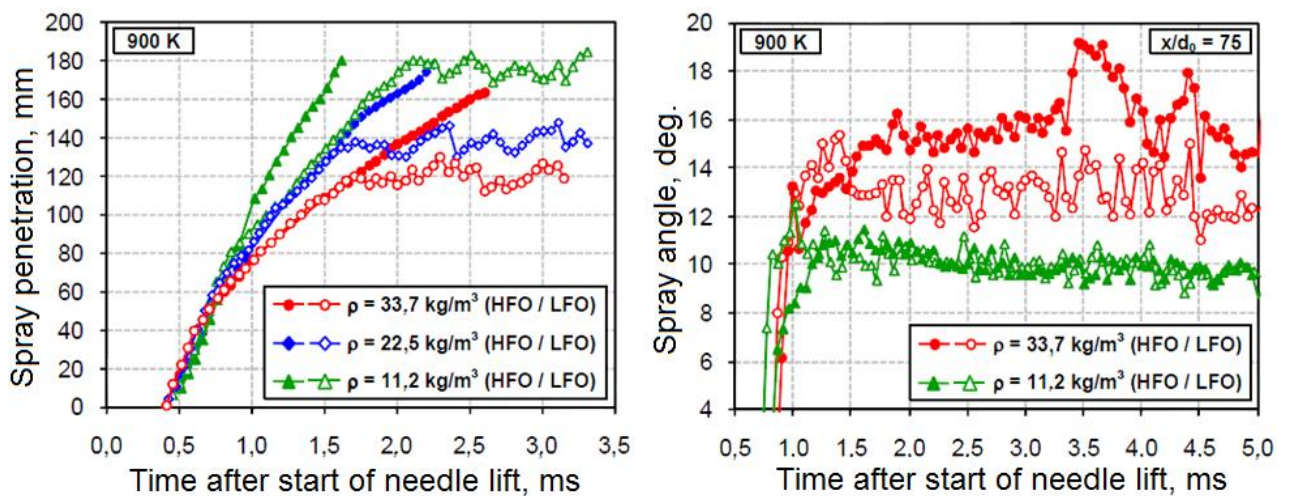


Fig. 1.31. Dependences of spray penetration and spray angle versus time for different fuel types at the different gas density ρ (*LFO* - light fuel oil: $\rho_l=851,4 \text{ kg/m}^3$, *HFO* - heavy fuel oil: $\rho_l=1001,0 \text{ kg/m}^3$)

Droplets evaporation

Evaporation rate of droplets in cylinder volume in many respects depends on quality metrics of atomization: fineness of atomized droplets and their distribution on volume [20, 55, 76]. It causes more and more high requirements to quality of the organization of injection and atomization. In addition to these factors it is also important behavior of convective-diffusion processes on a droplet surface. In turn behavior of these processes depends on gas parameters in the cylinder: temperatures and pressure and, somewhat, from the relative velocity of droplets [48]. Process of transformation of a droplet of liquid fuel to vapor is usually subdivided into two periods: heating and evaporation. Proceeding from the equation of droplet heat balance during heating stage, heating time of droplet with a diameter d_{p0} up to the temperature of equilibrium vaporization (saturation temperature) T_s may be determined as follows:

$$\tau = \frac{d_{p0}^3}{12} C_f \cdot \rho_f \int_{T_{p0}}^{T_s} \frac{dT_p}{\alpha(T_\infty - T_p)} \quad (1.7)$$

Thus, the heating rate depends on fuel properties, medium temperature T_∞ , intensity of heat transfer α and saturation temperature T_s . In general, droplet heating time is much less than time of its evaporation and often it is neglected. But for the better accuracy, especially in case of evaporation of rather big droplets in a medium with big pressure and very slow droplets it is better to take into account droplets warm-up period.

Fuel droplet evaporation occur in the conditions of convective heat exchange and molecular diffusion. Radiation heat exchange in the course of evaporation usually is not considered because the overwhelming majority of fuel droplets evaporates prior to combustion (especially in *the HCCI engines*) and generally the heat radiation of combustion products and hot walls is rather small. Evaporation occurs at almost constant droplet temperature which is temperature of its equilibrium vaporization T_s . This parameter first of all depends from cylinder pressure and temperature and can be found from the heat balance equation offered

by professor D. N. Vyruvov [9,12]:

$$\lambda_{\infty}(T_{\infty} - T_s) = D_p p_s \left[C_f (T_s - T_{p_0}) + h_{bp} + C_{fv} \frac{T_{\infty} - T_s}{2} \right], \quad (1.8)$$

where $\lambda_{gas} = f(p, T_{\infty})$ - heat conductivity of the gas surrounding of a droplet, $D_p(p, T_s)$ - baro-diffusion coefficient, $p_s = f(T_s)$ - the saturated vapor pressure of fuel, $C_f = f(T_s)$ - heat capacity of liquid fuel, h_{bp} - vaporization latent heat of fuel at boiling point, $C_{fv} = f(T_s)$ - heat capacity of vapors of fuel.

Usually heat balance of the evaporating droplet (see formulas 2.44-2.46 in chapter 2) is solving jointly with the evaporation model [117,170]. In this coupled calculations temperature of equilibrium vaporization T_s is determined. It should be noted that at all variety of evaporation models, all of them include direct dependence on coefficient of molecular diffusion and saturated vapor pressure

$\frac{dm_p}{dt} = f(D, p_s, \dots)$. Thus, evaporation rate depends on saturated vapor pressure $p_s = f(T_s)$ at a saturation temperature and on a diffusion coefficient $D(p, T_{film})$ at a pressure of the gas surrounding a droplet and average temperature $T_{film} = T_s + a(T_{gas} - T_s)$ where $a = 0..0,5$ averaging coefficient depending on evaporation model. The diffusion coefficient depends on temperature and pressure and is determined as follows:

$$D = D_0 \left(\frac{T}{T_0} \right)^{1.7} \cdot \frac{p_0}{p}, \quad (1.9)$$

where D_0, T_0, p_0 - values under normal conditions. Generalizing it is possible to make a conclusion that droplet evaporation rate is maximum at high temperatures and low pressures. Results of droplet evaporation experiments at different temperatures and pressures of surrounding gas and numerical simulation using different droplet evaporation models for *n-heptane* droplet with diameter 0,3 mm are presented on Fig. 1.32[170].

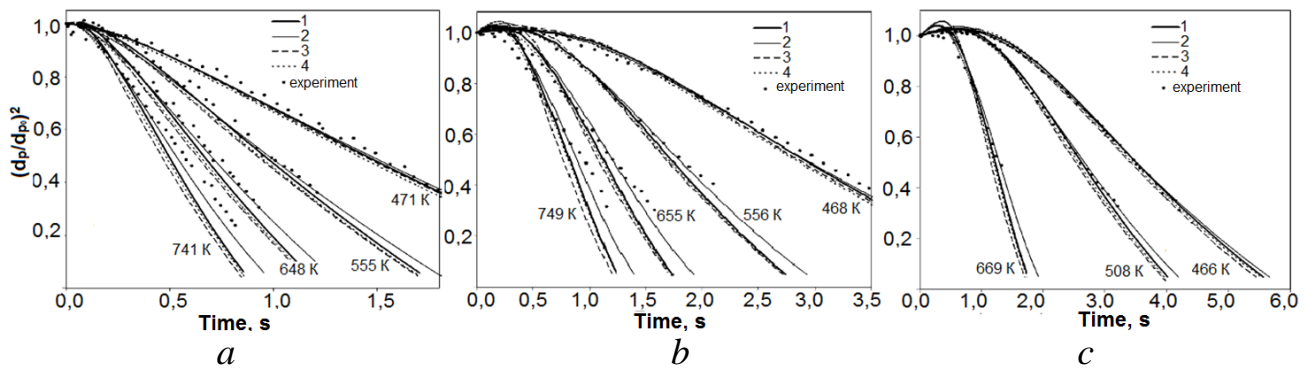


Fig. 1.32. Evaporation rates of *n-heptane* at different temperatures and pressures of surrounding gas: *a* - $p = 1$ bar, *b* - $p = 5$ bar, *c* - $p = 10$ bar, 1-4 - different droplet evaporation models

1.3. Objective of work and research tasks

The conducted analysis of the organization features of a fuel injection, atomization and mixture formation in diesels and *the HCCI engines*, analysis of the phenomena and factors influencing quality metrics of these processes confirm complexity of the phenomena that occurs in injectors flowing channels and during outflow of fuel from nozzle holes. Works of I.V. Astakhov [87, 107], D. N. Vyubov [2, 9-12], L.N. Golubkov [14-17], L.V. Grekhov [19-24], S. N. Devyanin [37, 38], R. Z. Kavtaradze [47, 48], A.S. Kuleshov [60, 148], A.S. Lyshevsky [69-71], V. I. Malchuk [68, 72], R. V. Rusinov [97, 98], Yu.B. Sviridov [101, 102], V. I. Trusov [108], B. N. Faynleyb [110] and some other scientists are devoted to problems of improvement of processes of a fuel supply, a fuel atomization and mixture formation in diesels. The experimental and theoretical works devoted to research of structure of jets of atomized diesel fuel are known [13, 49, 50, 119, 136]. Analytical models of fuel jets formation and break-up are developed [5, 25, 65, 85, 129]. Influence of diesel injectors flowing channels geometry on characteristics of injection and atomization is investigated [128, 130, 142, 153, 176]. Features of these processes in *the HCCI engines* are investigated in works of L.V. Grekhov [20, 22], S. V. Gusakov [27-31], R. Z. Kavtaradze [48], A.S. Kuleshov [61, 62], V. G. Kamaltdinov [51-54], E.A. Fedyanov [111], etc. There are much theses defended on this subject matter [30, 40, 54, 58, 80, 82, 100, 105]. A number of the researches conducted in BMSTU is devoted to problems of the

organization of mixture formation in *the HCCI engines* [52, 100, 146], RUDN University [27, 28, 29], South Ural State University (Chelyabinsk) [51, 52, 54], Volgograd State Technical University [111].

At the same time, questions regarding of the organization of a fuel injection, atomization and mixture formation in *the HCCI engines*, influences of cavitation on injection, atomization and mixture formation are insufficiently studied. It especially concerns injector nozzles with nonconventional geometry of flowing channels. Formation of a jet, its break-up during injection by pintle nozzles into cylinder with low gas density are also poorly explored. There are actual problems of the organization of full droplets evaporation in the engine cylinder without hit of fuel on walls within *HCCI* organization in an ICE. The solution of these questions will allow to increase considerably quality of fuel injection and atomization in the *HCCI* engine and improve characteristics of fuel efficiency and an EG toxicity of these engines.

The purpose of this work is improvement of fuel injection and atomization in the *HCCI* engine. To accomplish this purpose the following scientific and practical tasks have to be performed:

1. Development of methods of analysis of fuel injection, atomization and evaporation for injector nozzles. By use of these methods it could be possible to obtain characteristics of a fuel flow, fuel spray and mixture formation, quality metrics of atomization and evaporation for any geometry of the injector nozzle.

2. Numerical investigations of influence of cavitation on a fuel flow inside injector nozzles and on characteristics of a spray.

3. Numerical investigations of the factors influencing characteristics of a fuel spray, its atomization and evaporation in conditions of low gas density in the cylinder.

4. Search of ways of limitation of spray tip penetration and improvement of quality metrics of atomization in the conditions of low gas density in the cylinder.

5. Development of the mixture formation concept for the HCCI engine which provides full droplets evaporation and prevents hit of fuel on cylinder walls.
6. Development of the *Z-engine* concept with *HCCI* realization which allows to decrease emissions of nitrogen oxides and smoke.
7. Comparative numerical investigations of the *Z-engine* operation with realization of conventional diesel combustion and *HCCI*.
8. Experimental studies of operation of the single-cylinder *Z-engine* prototype.
9. Comparative analysis of results of numerical investigations of engine operation with the obtained experimental data.

CHAPTER 2. NUMERICAL INVESTIGATIONS OF PROCESSES OF FUEL INJECTION, ATOMIZATION AND MIXTURE FORMATION OF THE DIESEL AND *HCCI* ENGINE

2.1. Problems of the organization of homogeneous mixture formation in the cylinder

At the present stage of development of engine building the most important tasks are increase of fuel efficiency and decrease of pollutant emissions. One of effective methods of solution of these tasks is development of new ways of the organization of ICE operation process. One of such ways consists in the organization of combustion of a homogeneous air-fuel mixture. Such operation is called *HCCI* (*Homogeneous Charge Compression Ignition*) [115, 123, 131, 135, 140, 145, 151]. Organization of *HCCI* mean that fuel is injected, evaporated and evenly mixed up with air in the cylinder before ignition occurs. At the same time there is no locally enriched zones, both formation of nitrogen oxides and a PM at fuel combustion considerably decreases. If ignition of fuel happens almost instantly, then combustion covers whole cylinder volume. In this case the level of temperatures in a combustion zone remains rather low due to lean mixture, an EGR and EG cooling. Thus, at the organization of *HCCI* it is provided combustion of lean mixture at rather high local values of an air-fuel equivalence ratio and low values of local temperatures. The minimum values of pollutant emissions (Fig. 2.1) are as a result noted [143,174].

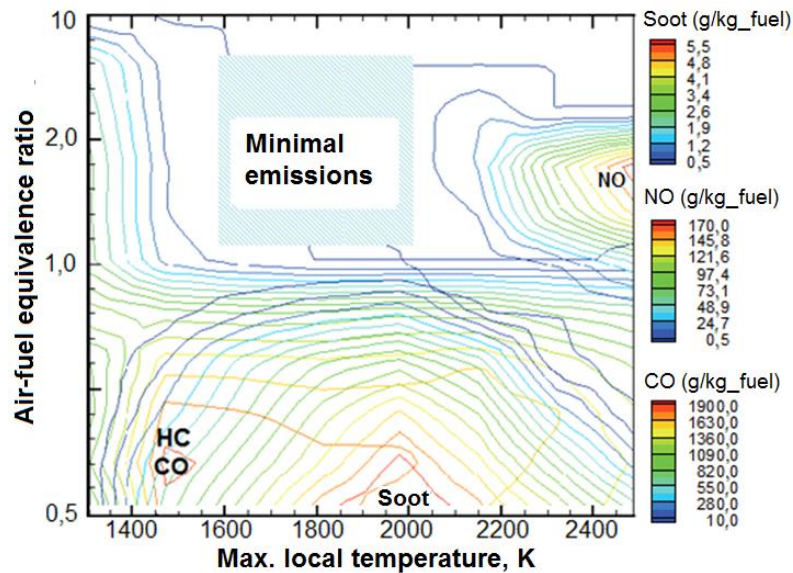


Fig. 2.1. Dependence of emission of the EG toxic components on values of local temperatures and air-fuel equivalence ratio

It should be noted that *HCCI* is an ideal case of the organization of homogeneous mixture formation at which mixture is considered absolutely homogeneous. In reality such organization of operation is hard to achieve, and there are number of different methods of approach to *HCCI*. They have different names and differ, first of all, by level of homogenization of mixture and by ways of its achievement, and also by aspects of the organization of combustion. The most widely known among them: *SA HCCI* (*Spark Assisted Homogeneous Charge Compression Ignition*), *PCCI* (*Premixed Charge Compression Ignition*), *PREDIC* (*Premixed Lean Diesel Combustion*), *SCCI* (*Stratified Charge Compression Ignition*), and *LTC* (*Low Temperature Combustion*). In this work the term *HCCI* is used as the generalizing type of engine operation included all methods of approach to an ideal *HCCI*.

One of implementation methods of *HCCI* is provided in work [143]. According to this method called *MK* (*Modulated Kinetics*) combustion, duration of injection should be shorter, than a combustion delay. In this work by means of a low compression ratio, considerable cooling of recycled gases and HP injection has allowed to shift ignition up to an expansion stroke. Low-temperature combustion of almost homogeneous mixture was provided as a result. The scheme of the

organization of this process is presented on Fig. 2.2, and comparison of curves of heat release rate and pictures of conventional diesel combustion and *MK* combustion - on Fig. 2.3. On Fig. 2.4 it is shown how different actions for the organization of engine operation influence efficiency of combustion and emissions of toxic components of EG. Data on Fig. 2.4 demonstrate that implementation of these actions considerable decrease emission of NO_x , HC and PM at preservation of combustion efficiency.

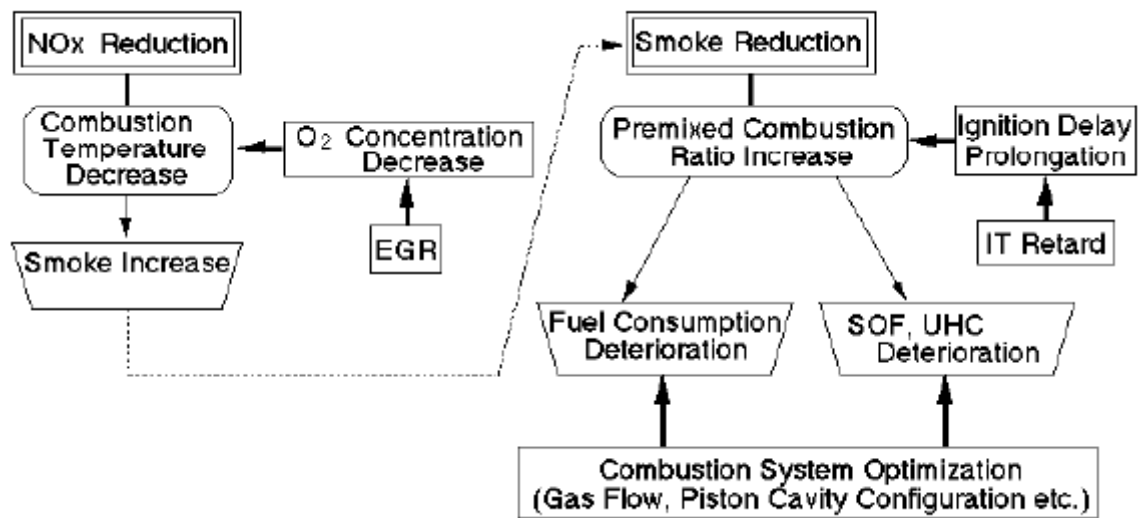


Fig. 2.2. Scheme of the MK combustion

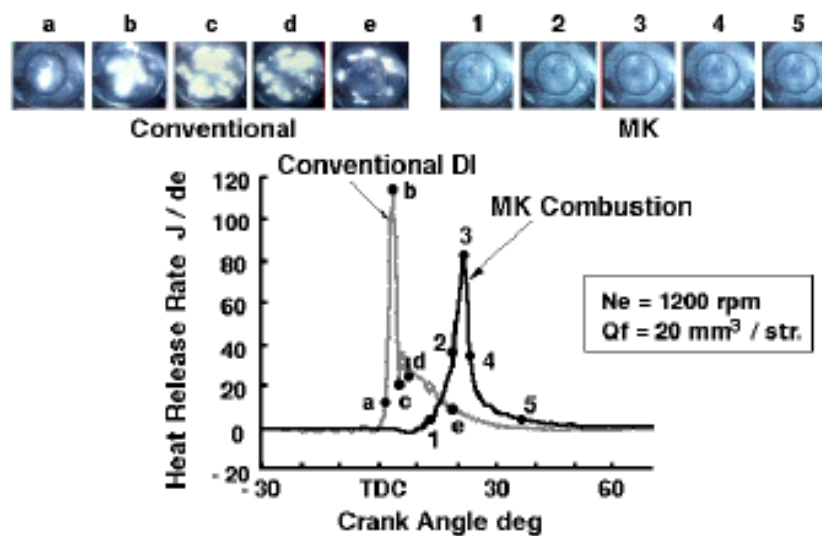


Fig. 2.3. Heat release rate and pictures of a conventional diesel combustion and *MK* combustion

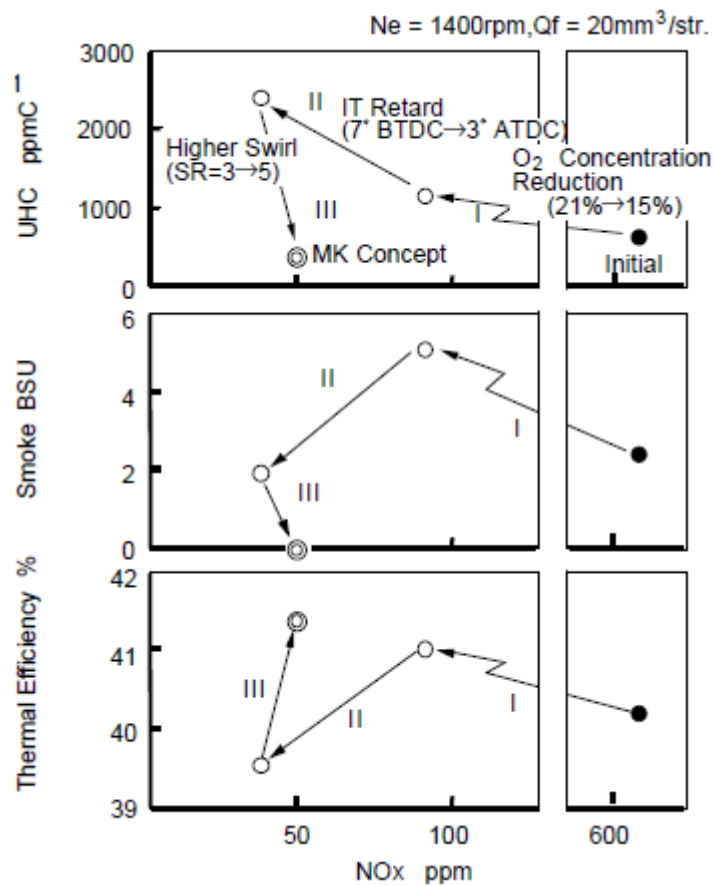


Fig. 2.4. Influence of different actions on emissions of toxic components of EG and efficiency

These data confirm efficiency of the organization of *HCCI* for simultaneous decrease in emissions of NOx and PM, however at implementation of this process a number of problems appears. Among them: uncontrollable self-ignition, high heat release rate, increase of emissions of HC and CO, hit of fuel on cylinder walls at early injection, a low evaporability of DF, complexity of extension of the field of operation modes with implemented *HCCI*. Complexity of the organization of engine operation on high load modes is confirmed by Fig. 2.5 from which follows that at implementation of *HCCI* the engine can operate with air-fuel equivalence ratio $\alpha=2,5-5,0$ (at low *EGR* typical of a high load modes) [26,165]. On high load modes and at low α uncontrollable self-ignition and inadmissible high rate of combustion pressure rise are possible.

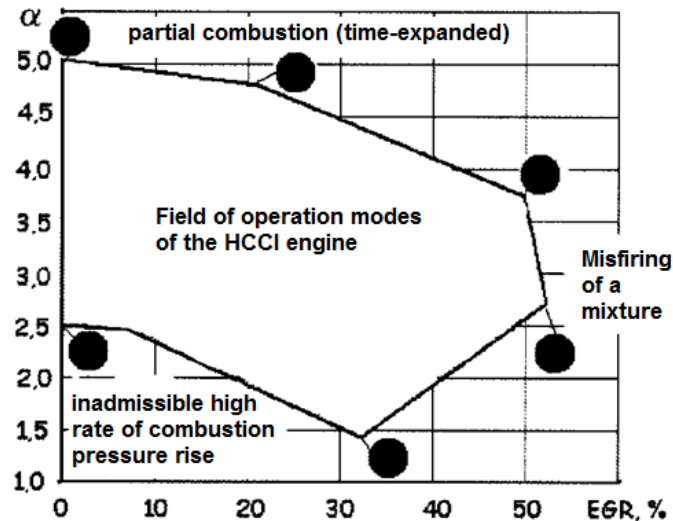


Fig. 2.5. Field of operation modes of the HCCI engine

For organization of *HCCI* different actions may be used. Among them there are: high level of EGR with considerable cooling, injection of fuel long before TDC (during intake or at the beginning of compression stroke), different strategies of injection. As it has been noted above at early injection (long before TDC) the low density of gases in the cylinder promotes decrease of jet break-up intensity. As a result injection under HP leads to increased spray tip penetration and, as a result, to hit of a considerable amount of fuel on cylinder walls. Hit of fuel on cylinder walls is followed by deterioration in characteristics of fuel efficiency and EG toxicity and can cause mixture preignition. In these conditions is reasonable to use of injector nozzles with great number of holes (up to 30) and small hole diameter (to 0,08 mm) [133], injector nozzles with the crossed axes of nozzle holes [44,72], the injector nozzles producing conical shape of a spray (swirl, pintle and outward-opening injectors) [133,138,139,174]. Multistage injection (to 5 stages) is used [135] and different adaptive strategies of injection are implemented [138,139,158,174].

In work [174] adaptive strategy of the injection consisting of two stages is offered: at an early stage injection is carried out under low pressure by swirl nozzle or by multi-hole injector producing narrow-angle spray and closer to a TDC injection is made by a conventional multi-hole injector under HP. Fig. 2.6. shows

the dependences of fuel fraction hitting walls and inhomogeneity factor (normalized standard deviation (NSD) of fuel-air equivalence ratio) from SOI for two types of injector nozzles. In work [174] it was made a conclusion that injector producing hollow cone spray has advantages for the SOI near to BDC in the conditions of gas density up to 3 kg/m^3 . At higher density use of a multi-hole injector is more reasonable.

It is also necessary to consider data presented on Fig. 2.7 showing evaporation curves of diesel fuel in the cylinder of the *HCCI engine*. Due to low evaporability of DF its active evaporation begins only at temperature in the cylinder higher than 450 K.

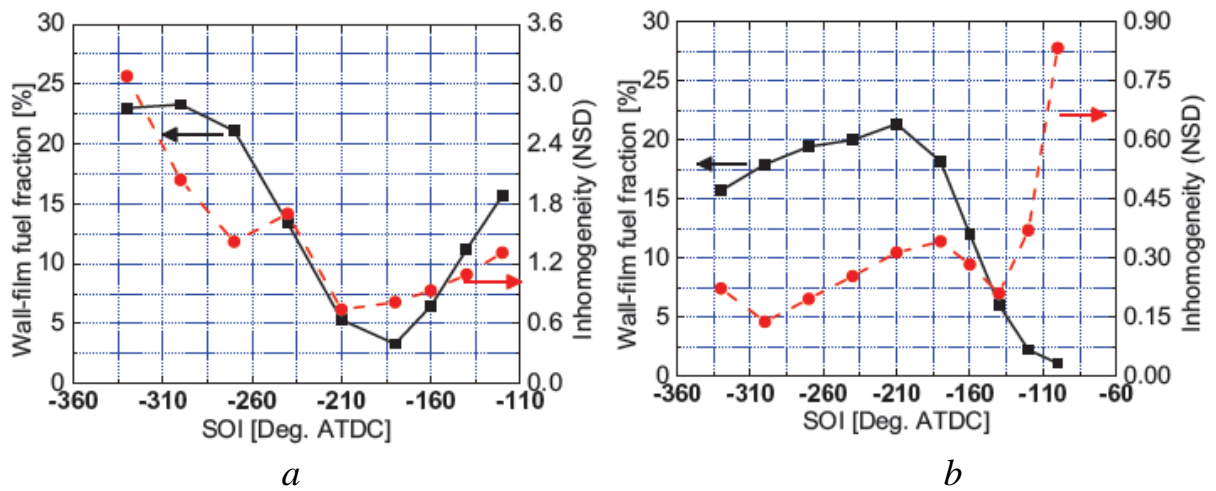


Fig. 2.6. Fuel fraction hitting walls and mixture inhomogeneity factor versus SOI: a - swirl nozzle; b - multi-hole injector producing narrow-angle spray

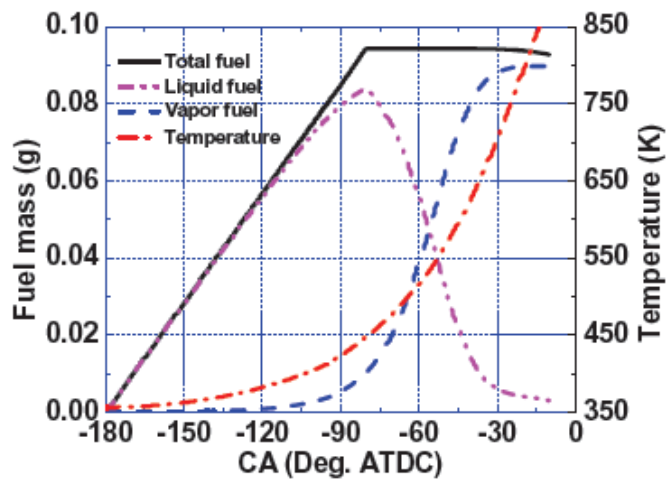


Fig. 2.7. Evaporation history of diesel fuel in the cylinder of the HCCI engine

In works [138,139] the adaptive strategy of injection is offered. The hybrid injector shown on Fig. 2.8 at early stages of injection, when cylinder pressure is insignificant, produces a hollow cone of fuel like pintle-type injector. Closer to a TDC the shape of a spray becomes the same as produced by conventional multi-hole injectors (Fig. 2.9). Injection in hollow cone mode lead to the lowest spray tip penetration, more uniform coverage of the cylinder volume by fuel droplets (Fig. 2.10) and good fineness of atomization ($d_{32}=10..15$ microns). Combination of such injection strategy with other actions make it possible to reduce NO_x emissions by 50-70%, emissions of PM - by 30-50% with preservation of CO and HC emissions level and decrease of fuel consumption by 5-12%.

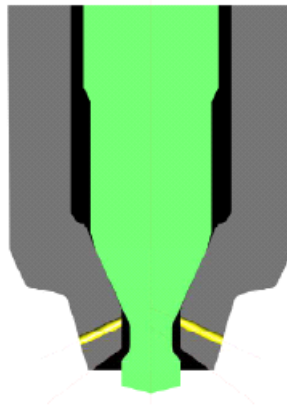


Fig. 2.8. Design concept of the hybrid injector nozzle

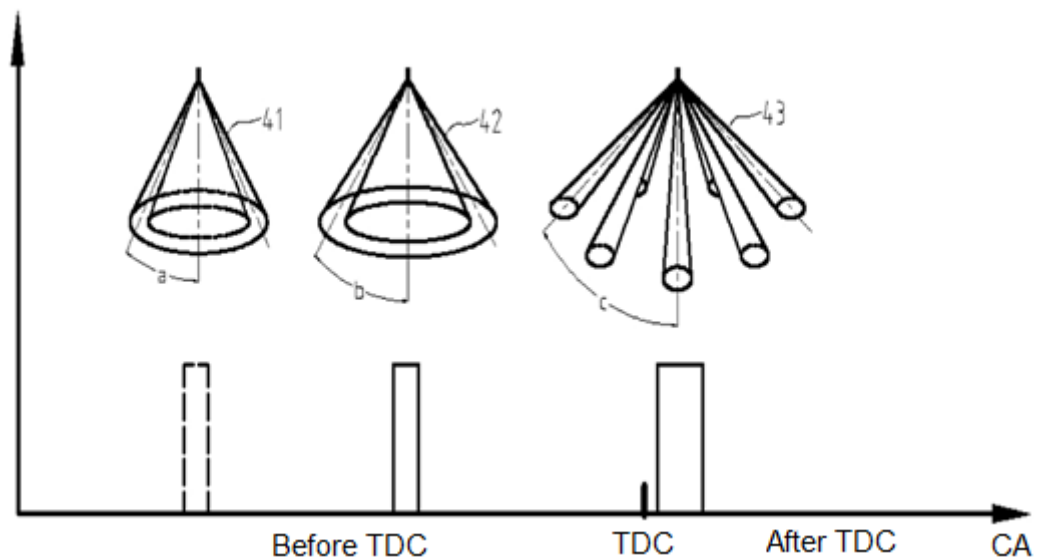


Fig. 2.9. Scheme of injection strategy using hybrid injector nozzle

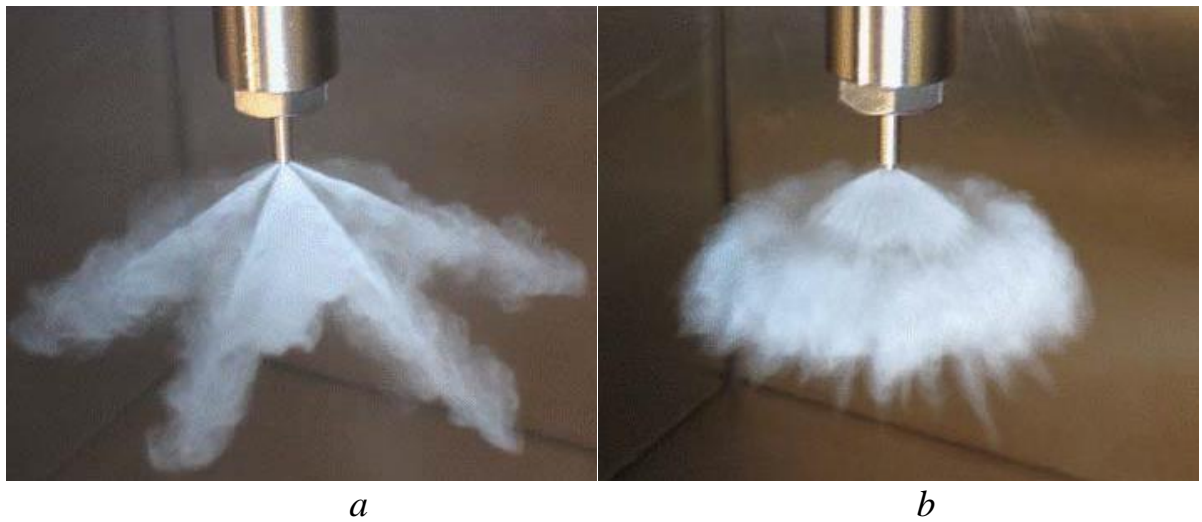


Fig. 2.10. Injection by hybrid injector in a different modes: *a* - the multi-hole mode; *b* - hollow cone mode

In work [133] it is conducted a comparison of characteristics of fuel spray produced by multi-hole injector having 30 holes with a diameter of 0,08 mm and spray produced by three designs of pintle nozzle (Fig. 2.11) for injections into a gas with pressure of 10 bars. Geometrical characteristics of the sprays produced by these injector nozzles are presented on Fig. 2.12. It is shown that only pintle nozzles provide uniform distribution of fuel over cylinder volume and prevent hit of fuel on cylinder walls and piston head. Pictures of the sprays produced by different type of injectors are presented on Fig. 2.13. It shows that fuel distribution over cylinder volume more uniform in case of a pintle nozzle. According to Fig. 2.12 and 2.13 the conclusion have made that pintle nozzles are more reasonable for a fuel injection in the conditions of low back pressure. In work [133] it is also shown that almost all characteristics of EG toxicity and fuel efficiency of the studied engine is better in case of usage of pintle nozzles.

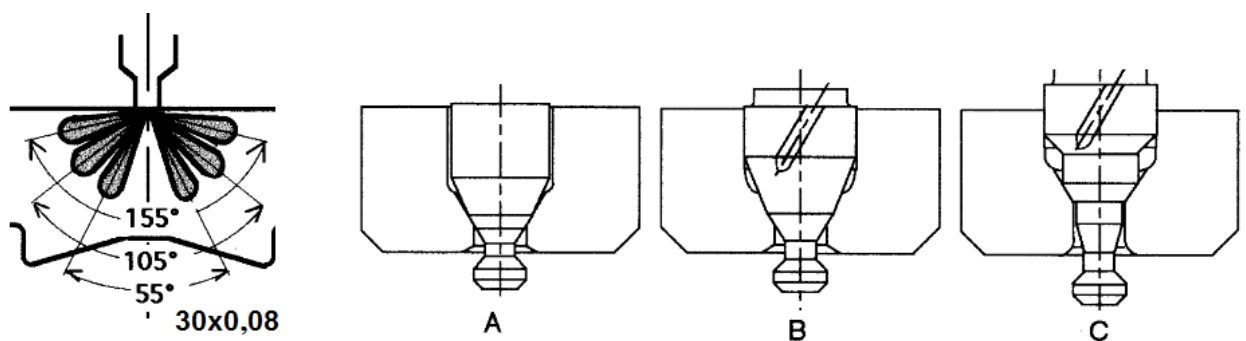


Fig. 2.11. Design concepts of the studied injector nozzles

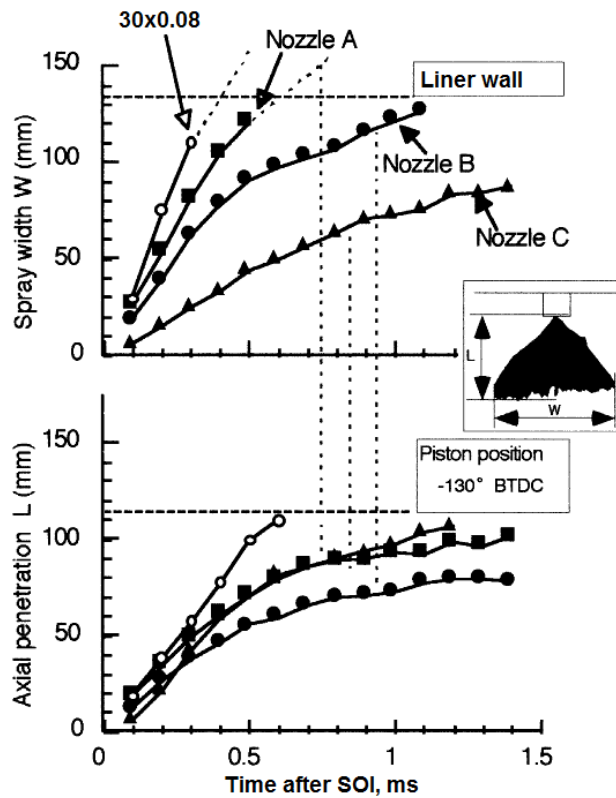


Fig. 2.12. Comparison of geometrical characteristics of the fuel sprays produced by the injector nozzles presented on Fig. 2.11

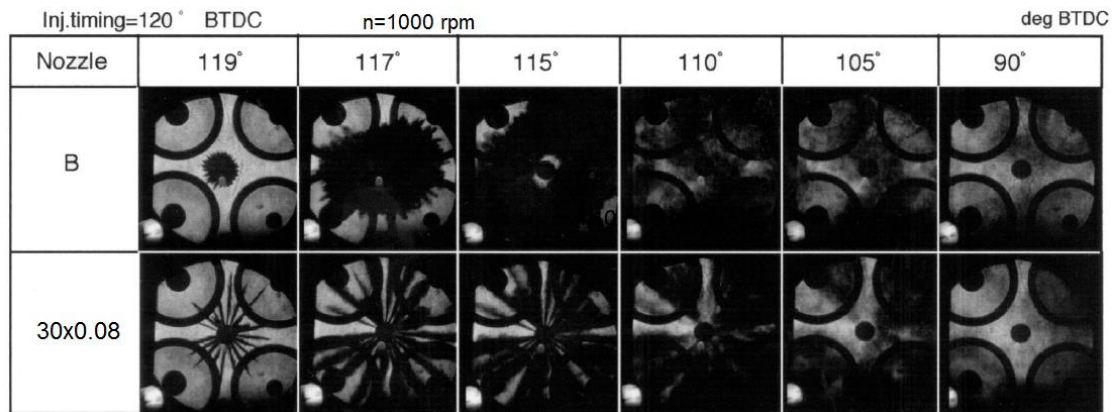


Fig. 2.13. Comparison of experimental pictures of the fuel sprays produced by different injectors

It has been noted above that hit of fuel on cylinder walls of the *HCCI engine* can lead to emergence of the local ignition centers. As result combustion on a surface of fuel film in the conditions of locally rich mixture and low temperature of walls happens. Such combustion is incomplete and is followed by considerable emission of soot. But hit of fuel on cylinder walls and piston head is not a single

problem of HCCI organization. The solution of these problems is reached by implementation of control by engine operation. The most widespread actions in this direction are control of valve timing, EGR level, boost pressure, extent of cooling of intake air and recirculated gas.

2.2. Software packages for simulation of fuel outflow and atomization. Finite volume method

Outflow of fuel from the injector nozzle with further jet formation is the difficult physical phenomenon including a set of the effects considered in chapter 1. The scheme of this process on the example of the pintle nozzle is presented on Fig. 2.14. According to it outflow and atomization of fuel can be conditionally separated into two stages: internal nozzle flow and in-cylinder spray behavior. Complexity of these physical processes predetermines effects which need to be considered at simulation. On the basis of the data provided in chapter 1 in Table 2.1 it is summarized the factors influencing processes of outflow, atomization and evaporation, and the effects which arise.

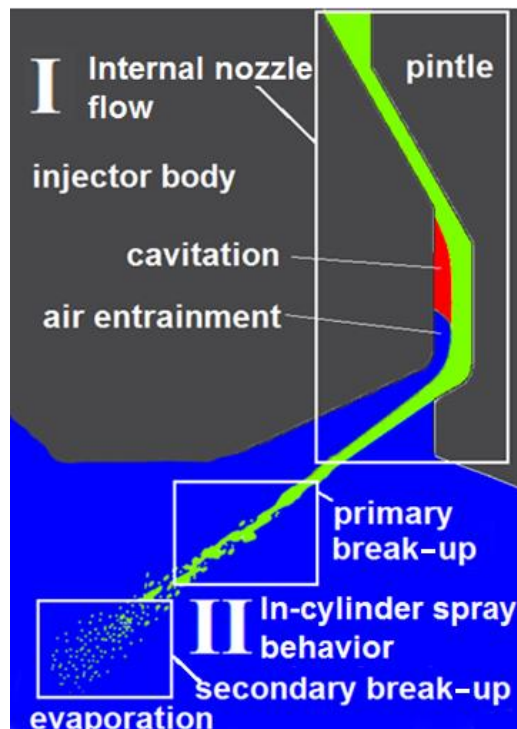


Fig. 2.14. Scheme of outflow and atomization of fuel

Table 2.1.

The factors and effects arising at outflow, atomization and fuel evaporation

Stage	I: Internal nozzle flow				II: In-cylinder spray behavior			
Zone	Internal channels of the injector nozzle		Transition zone from the injector nozzle to the cylinder		In-cylinder zone			
Process	Flow in internal channels		Primary break-up		Secondary break-up		Evaporation and mixture formation	
	The influencing factors	Effects	The influencing factors	Effects	The influencing factors	Effects	The influencing factors	Effects
	<ul style="list-style-type: none"> - Fuel properties - Flowing channel geometry - Quality of surfaces treatment - Injector inlet pressure - Cylinder pressure - Movement of a clamping element (needle, pintle, valve) 	<ul style="list-style-type: none"> - Turbulence - Cavitation - Fuel compressibility - Heating of fuel - Air entrainment 	<ul style="list-style-type: none"> - Fuel properties - Parameters of a flow on outlet of the injector nozzle - Magnitude and profile of velocity - Cavitation - Turbulence - Thickness of a liquid core - Air entrainment - Density and gas flow parameters in the cylinder 	<ul style="list-style-type: none"> - Waves on a free surface of liquid - Turbulent structures - Jet break-up on clusters, ligaments and initial droplets 	<ul style="list-style-type: none"> - Fuel properties - Size of initial droplets and their relative velocity - Density and gas flow parameters in the cylinder - Turbulence 	<ul style="list-style-type: none"> - Aerodynamic interactions between fuel droplets and gas - Deformations of droplets - Growth of stress on droplets surface and formation of waves - Droplets Break-up - Interactions between droplets (collision and coalescence) 	<ul style="list-style-type: none"> - Fuel properties - Distribution of droplets sizes over cylinder volume - Relative velocity of droplets - Flow parameters in the cylinder - Cylinder temperature and pressure - Turbulence 	<ul style="list-style-type: none"> - Heating of droplets at convective heat exchange - Radiation heat exchange - Droplets evaporation by convective-diffusion mechanism

The set of the effects given in Table 2.1 determines necessity of use of a big set of the mathematical models describing these processes. At the same time in a simulated phenomenon some effects can be absent or have insignificant influence (in particular, it has been shown above that for describing of droplets evaporation in the HCCI engine radiation heat exchange is not considered). Necessity of accounting of the specific phenomena at numerical simulation predetermines the choice of a software package.

For accounting of all necessary effects arising during fuel outflow and atomization it is reasonable to use of the program code based on methods of computational fluid dynamics [3, 67, 96, 113]. Such program code usually named *a CFD (Computational Fluid Dynamics)*. The different software products allowing to solve problems of fluid and gas dynamics exist and are successfully used. The

following software packages are most known: *Ansys CFX* [116], *Ansys Fluent* [117], *Open Foam*, *KIVA*, *Star-CCM*, the specialized SP of AVL company, a number of Russian software packages [41,42, 90] including *FlowVision* [127]. It is necessary to distinguish *the Ansys Fluent* [117] from these software products. This software product is chosen for carrying out numerical investigations. It includes models of turbulence, cavitation, a jet break-up, evaporation, has possibility of implementation of own submodels and tools, and its efficiency is confirmed with numerous numerical investigations.

For solving problems of fluid and gas dynamics in *the Ansys Fluent* the finite volume method (FVM) is used. It is convenient to describe fundamentals of FVM in consideration of "standard" balance equation of some parameter φ in control (finite) volume Ω , $S=\sum_k S_k$ bounded by a surface with an outer normal line n [104]:

$$\int_{\Omega} \frac{\partial \rho \varphi}{\partial t} d\Omega + \sum_k \int_{S_k} \vec{n} \cdot \vec{q} \cdot ds = \int_{\Omega} Q d\Omega \quad \vec{q} = \rho \vec{V} \varphi - \alpha \nabla \varphi \quad (2.1)$$

where \vec{q} - is a vector of flux density of parameter φ , including convective and diffusion components; Q - distribution density of volume sources; \vec{V} - velocity vector; ρ - density of the medium; α - diffusion coefficient. As parameter φ it may be used for example internal energy of medium, concentration of substance, turbulence kinetic energy. In a limit, when tightening volume in a point, on the basis of Ostrogradsky-Gauss's formula it is possible to rewrite this equation in a differential form:

$$\frac{\partial \rho \varphi}{\partial t} + \nabla \vec{q} = Q \quad (2.2)$$

Note, that the specified differential form of the equation due to more frequent usage in literature sometimes is considered primary, and the integral formulation of conservation law deduced from differential by volume integration. Such equations are written for the variables used in calculation.

When using MKO discretization of space for simulated problem is carried out by decomposition of computational domain into the small finite volumes shown on Fig. 2.15. For each of volumes the balance relationship writes down [104]. In each

control volume there is one (and only one) point of "binding" of the required solution. The majority of codes oriented to the solution of three-dimensional hydrodynamics problems for difficult geometries in the capacity of control volume used the cells of computational grid. Nodes of a grid are located in vertex of polyhedron (for the structured grids - vertex of hexahedron), grid lines go along his edges, and values of variables attributed to the geometrical center of a cell [41,104]. It can be alternatives for creation of control volume, for example, creation of this volume around a node of a grid or introduction of different control volumes for different variables. But such approach is used much rarer.

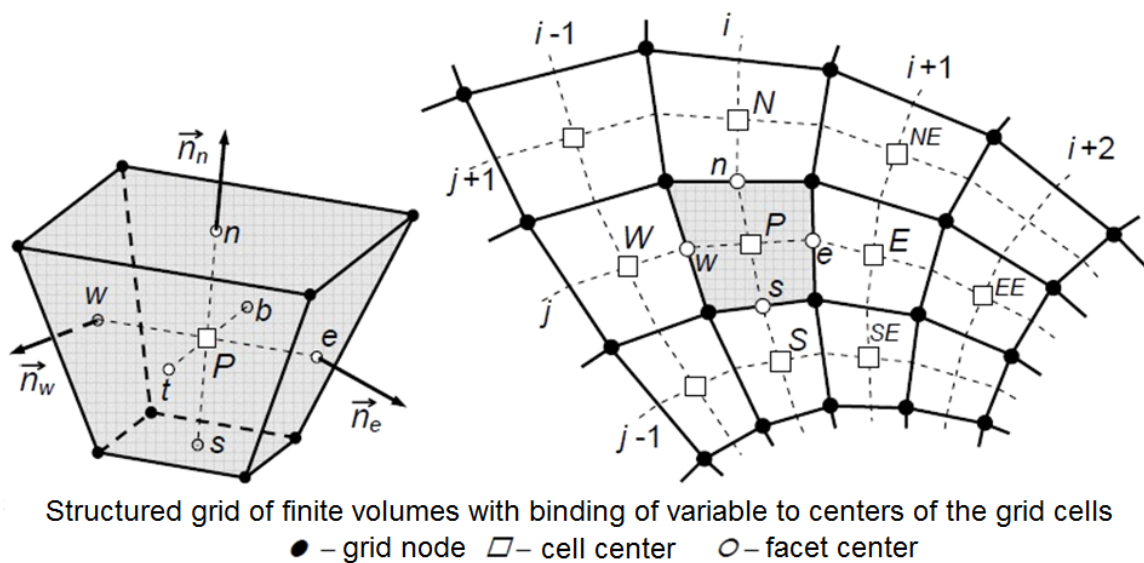


Fig. 2.15. Finite (control) volumes at decomposition of computational domain (e.g. nozzle flowing channel)

For obtaining discrete analog of the balance equation in the chosen cell it is necessary to calculate the integrals from expression (2.1), using any quadrature formulas. At the same time it is important to that for the contacting cells a surface integral on their common edge Sk was calculated identically. This requirement implemented during development of the computer program provides conservatism of the numerical scheme, i.e. exact (within the accepted way of calculation of integrals) observance of balance of parameter φ according to the equation (2.1) for whole flow domain. This FVM property profitable distinguishes it from the finite difference method (FDM) and the finite-element method (FEM) in which

implementation of strict conservatism of the scheme is rather an exception, than the rule [43,84,99,113].

The way of approximation of integrals influences such important properties of the numerical scheme as accuracy, stability, monotony, etc. Let's consider the most popular alternatives of approximation for the structured grids and using the "geographical" notation accepted in such cases (see Fig. 2.15): the center of the current control volume (i, j, k) is marked as P (*pole*), the centers of the volumes contacting to it marked as E (*east; i+1, j, k*), N (*north; i, j+1, k*), W (*west; i-1, j, k*), etc., the centers of their common edges - the corresponding lowercase letters ($e, n, w \dots$). As for all edges of a cell surface integrals in the equation (2.1) are calculated by the same rules, we will consider only "east" edge of S_e for an example. The simplest and most widely used in FVM quadrature formulas of the second order of accuracy directly follow from the mean value theorem:

$$\int_{S_e} \vec{n} \cdot \vec{q} \cdot ds \approx \vec{S}_e \cdot \vec{q}_e \qquad \int_{\Omega} Q d\Omega \approx Q_p \cdot \Omega \qquad (2.3)$$

where $\vec{S}_e \equiv S_e \cdot \vec{n}$ - the conditional vector of the edge area calculated as a cross product of its diagonals; \vec{q}_e - a flux density vector φ in the center of an edge. If value \vec{q}_e is calculated with the second order of accuracy, then formulas (2.3) provide the second order of approximation of the equation (2.1). Lowering of accuracy of calculation \vec{q}_e immediately affects order of accuracy of the whole numerical scheme. For providing an order of approximation strict above the second order it would be required not only to improve accuracy of calculation of \vec{q}_e , but also to use instead of (2.3) more precise quadrature formulae considering change \vec{q} along a surface (the same treats also calculation of volume integrals). It leads both to considerable complication of calculations and to expansion of approximation template. Therefore schemes of the higher order of accuracy do not wide used for practical application. Thus, within a FVM, unlike FDM, it is very difficult to construct the numerical scheme with order of accuracy strictly above the second. But this, usually, is not demanded for the majority of practical applications.

Therefore we will assume as a basis a quadrature formula (2.3) and we will address a question of calculation \bar{q}_e .

The convective component of a flux of φ is defined with the following reasons. As a rule for subsonic flows, liquid mass flow rate through an edge of a cell $g_e = \bar{S}_e \cdot (\rho \bar{V})_e$ is calculated at approximation of continuity equation, and then used for all other equations. At the known mass flow rate the question of calculation of a convective component of φ flux of through an edge is reduced to determination of φ_e . The adequate accuracy is provided by linear interpolation. Usually used the elementary quasionedimensional variant - interpolation along the grid line using two nodal values φ_P and φ_E considering distances Pe and eE . The numerical scheme obtained by such method is partially equivalent to the central differential scheme of FDM (for a case of a uniform Cartesian grid the schemes FVM and FDM match). Such scheme in the conditions of a small physical diffusion is unstable. The way to increase stability of the central differential scheme is known - it is approximation of convective derivatives one-sided differences "against a flow" (upwind). It can be treated as priority accounting of information about variables from the nodes located upstream from a current point along the grid line. In relation to a FVM the principle of a priority of information from upstream means that for a case $g_e > 0$ (liquid flows from P to E , see Fig. 2.15) at calculation φ_e it is necessary to use values φ_P and φ_W , and for a case $g_e < 0$ - values φ_E and φ_{EE} . Linear extrapolation on two nodes will provide the second order of approximation (an equivalent of the second order upwind scheme of the FDM), and simple transfer of value of φ downstream from the nearest node (P or E) on an edge corresponds to first order upwind FDM scheme. Information priority from upstream can be treated wider, providing at interpolation on an edge not exclusive and only preferential use of upstream nodal values along with downstream values. Such principle used in so-called *QUICK* Leonard's scheme in which for calculation φ_e square interpolation on three nodes (W, P and E at $g_e > 0$) is used. Because of the mentioned limitations of a quadrature formula (2.3),

Leonard's scheme provides only the second order of approximation. Use of high-accuracy interpolation make Leonard's scheme of one of the least dissipative among schemes of the second order. These options of interpolation can be considered as particular cases of the scheme with the adjustable (weighed) degree of upwind priority. In the simplified look (without accounting changes of cells size) the upwind scheme of the second order of accuracy can be described as follows:

$$\varphi_e \approx \bar{\varphi}_e - \varepsilon \cdot \delta_e \quad \delta_e = \begin{cases} \frac{\varphi_W - 2\varphi_P + \varphi_E}{2}, g_e > 0 \\ \frac{\varphi_P - 2\varphi_E + \varphi_{EE}}{2}, g_e < 0 \end{cases} \quad (2.4)$$

where $\bar{\varphi}_e$ - the "central" value obtained at linear interpolation; δ_e - the upwind correction implemented with an adjustable weight factor ε . At $\varepsilon=1$ we have completely upwind scheme, $\varepsilon=0,25$ corresponds to *QUICK* Leonard's scheme, $\varepsilon=0$ - the central differential scheme. The correction δ_e can consider change φ not only along the direction i , but also along the directions j and k , as in the generalized Leonard's scheme. To the family of the weighed first order upwind schemes corresponds the correction of the following look ($\varepsilon=1$ gives strict upwind scheme):

$$\delta_e = \begin{cases} \frac{\varphi_E - \varphi_P}{2}, g_e > 0 \\ \frac{\varphi_P - \varphi_E}{2}, g_e < 0 \end{cases}$$

The stabilizing correction δ_e may be not upwind, as, for example, in the scheme of artificial dissipation of the 4th order. It may be noted also that at implementation of second order schemes on an unstructured grid search of additional (upstream) nodes for interpolation is not a trivial task; additional complications are brought also by procedure of multipoint interpolation. Approximation of a diffusion component of a flow, unlike convective, does not demand any actions for ensuring stability of the scheme. Some complexity is represented only by calculation of a derivative $\bar{n}\nabla\varphi \equiv \partial\varphi/\partial n$ in the center of an edge. There are, at least, two opportunities. The first - to calculate values $\nabla\varphi$ in the

centers of cells, using integral representation of a gradient:

$$\int_{\Omega} \nabla \varphi d\Omega = \int_S \vec{n} \varphi ds \rightarrow (\nabla \varphi)_P \approx \frac{1}{\Omega} \sum_k \vec{S}_k \varphi_k \quad (2.5)$$

then to apply usual procedure of linear interpolation to calculation of value $\nabla \varphi$ on the edge of a cell. Other way is to approximate by finite differences a derivative $\partial \varphi / \partial n$ on the edge, passing as in case of FDM into local index coordinate system (actually, using formulas of transition to generalized curvilinear coordinates). The second approach demands less calculations and provides a smaller error of approximation on a uniform grid (within the second order of accuracy), but is applicable only for the structured grids.

The considered approaches to approximation of the scalar equation are applicable also to liquid motion equations. There is only one difference: during calculation of diffusion component of a flow impulse through an edge of a cell it is necessary to operate with a stress tensor, and the pressure gradient contribution to balance of an impulse is considered according to integral representation (2.5). Approximation of continuity equation, apparently, is even simpler - it is only necessary to summarize flow rates on all edges of a cell, using the elementary quadrature $g_e = \vec{S}_e \cdot (\rho \vec{V})_e$ in combination with one of the considered interpolation schemes for evaluation density and velocity in the center of an edge. However at the same time there can be so-called even-odd space oscillations of the pressure field that is especially typical of low-speed gas flows and incompressible flows (this is not about use of spaced grids with "binding" of velocity and pressure to different points). For suppression of these unphysical oscillations it is widely used the correcting procedure, introducing into flow rate expression g_e the special stabilizing correction factor. This correction can be presented in a little simplified form as follows:

$$g_e = \bar{g}_e - \frac{C}{A_e} \left[p_E - p_P - \frac{1}{2} \left(\frac{p_E - p_W}{2} + \frac{p_{EE} - p_P}{2} \right) \right] \quad (2.6)$$

where $C < 1$ - a weighting factor; A_e - the coefficient depending on geometry of

cells and on a way of approximation of motion equations. Let's note that the introduced correction (2.6) reacts to a deviation of a "index" derivative $(\partial p/\partial i)e = pE - pP$ from its mean value $[(\partial p/\partial i)P+(\partial p/\partial i)E]/2$, providing effective suppression of pulsations. In case of the smooth field this correction is proportional $\partial^3 p/\partial i^3$ and has the third order infinitesimal.

2.3. Constitutive equations of mathematical models

Software packages of a computational fluid dynamics are based on the solution of differential equations in partial derivatives: continuity equation, momentum conservation (Navier-Stokes equation) and energy equation. These equations are supplemented with diffusion equations, chemical kinetics and with additional models. These models are necessary to close system of differential equations after of appearance of additional members in the constitutive equations related taking into account any phenomenon or effect.

One of the constitutive equations implemented into any *CFD* code is continuity equation which describes the mass conservation law:

$$\frac{\partial \rho}{\partial t} + \nabla \cdot (\rho \vec{V}) = S_m, \quad (2.7)$$

where S_m - a source of the mass added to continuous medium, for example, at liquid droplets evaporation.

One more obligatory equation of all SP of computational fluid and gas dynamics is momentum conservation equation (Navier-Stokes equation). Generally, for inertial frames of reference in the *Ansys Fluent* the following look of this equation is used:

$$\frac{\partial}{\partial t}(\rho \vec{v}) + \nabla \cdot (\rho \vec{v} \vec{v}) = -\nabla p + \nabla \cdot (\vec{\tau}) + \rho \vec{g} + \vec{F} \quad \vec{\tau} = \mu \left[(\nabla \vec{v} + \nabla \vec{v}^T) - \frac{2}{3} \nabla \cdot \vec{v} I \right] \quad (2.8)$$

where $\rho \vec{g}$ - gravity force; \vec{F} - external impact on continuous medium (for example from dispersed droplets, from other medium or a phase); $\vec{\tau}$ - stress tensor; the first member of a tensor expresses a friction stress, the second member - is the effect of

volume dilation; I - unit tensor.

The system consisting of equations (2.7) and (2.8) is called system of equations of Navier-Stokes. For accounting of heat exchange it is also necessary to use the energy equation which in chosen SP written in the following look:

$$\frac{\partial}{\partial t}(\rho E) + \nabla \cdot (\bar{v}(\rho E + p)) = \nabla \cdot \left(k_{eff} \nabla T - \sum_j h_j \bar{J}_j + (\bar{\tau}_{eff} \cdot \bar{v}) \right) + S_h \quad E = h - \frac{p}{\rho} + \frac{v^2}{2} \quad (2.9)$$

where $k_{eff} = k + k_t$ - the effective heat conductivity which is the sum of molecular and turbulent heat conductivity; h - enthalpy of medium ; h_j - an enthalpy of components; \bar{J}_j - diffusion flux of a component with index j ; S_h - the volume heat source (for example from chemical reactions, radiation, etc.). Members in brackets in the right side of an equation (2.9) describe heattransfer by means of heat conductivity, diffusion and viscous dissipation.

At simulation of processes of components mixing in continuous medium (for example, mixing of vapors of fuel with air), and also at simulation of chemical reactions between components it is necessary to solve the equations, describing substance transport (the equation of a mass transfer or a mass exchange). In the *Ansys Fluent* it called species transport equations. The mass fraction of each component (species) Y_i of mixture is evaluated at the solution of convective-diffusion conservation equation for this component:

$$\frac{\partial}{\partial t}(\rho Y_i) + \nabla \cdot (\rho \bar{v} Y_i) = - \nabla \cdot \bar{J}_i + R_i + S_i \quad (2.10)$$

where R_i - a component generation rate by means of chemical reactions; S_i - a component generation rate from other sources of a mass transfer, for example fuel evaporation from a liquid droplet surface. The diffusion flow J_i is described by the Fick's law:

$$\bar{J}_i = - \left(\rho D_{i,m} + \frac{\mu_t}{Sc_t} \right) \nabla Y_i - D_{T,i} \frac{\nabla T}{T} \quad Sc_t = \frac{\mu_t}{\rho D_t} \quad (2.11)$$

where $D_{i,m}$ - coefficient of molecular diffusion of species i into mixture, μ_t - turbulent viscosity; Sc_t - a turbulent Schmidt number; D_t - coefficient of turbulent

diffusion; $D_{T,i}$ - thermal diffusion.

Three phase conditions of substance are known: solid, liquid and gas (sometimes plasma distinguished as forth), but from the point of view of numerical simulation the quantity of computational phases can be any. In computational methods the phase can be dedicated as set of substances and the modeled physical processes. The computational phase can have an individual response in the field of velocities and pressure, in a special way interacts with other flow. Usually computational phases dedicated for assign an individual set of the modeled physical processes, for implementation of transport processes between phases (phase transition), for describing interphase boundaries (interface). *Ansys Fluent* has a great amount of tools for simulation of multiphase flows. In this work are used model of multiphase flow *Volume of Fluid (VOF)* describing the phenomena of phases transitions and interphase boundaries, and also a model of dispersion medium *Discrete Phase Model (DPM)* modeling interactions of fuel droplets with a gaseous fluid.

The VOF model is used for the description of multiphase flows in which phases almost immiscible, but phases transitions are possible (at the same time interphase boundaries are precisely described). Within this model the momentum equation is common for all phases and volume fraction of each phase is evaluated individually in all computational domains. The mass conservation equation expressing transfer of volume fraction α_q of a phase q looks as follows:

$$\frac{\partial}{\partial t} (\alpha_q \rho_q) + \nabla \cdot (\alpha_q \rho_q \bar{v}_q) = S_{\alpha_q} + \sum_{p=1}^n (\dot{m}_{pq} - \dot{m}_{qp}) \quad (2.12)$$

where the member under summation symbol is a resulting mass flux due to a mass exchange of phase q with other phases (transfer of a phase); S_{α_q} - an additional source of a mass flux. For the description of process of phase transition of liquid in gas in areas with low pressure the cavitation model is used. Transfer of a phase at cavitation or, in other words, a mass transfer between phases (evaporation and condensation) is described by vapor transport equation:

$$\frac{\partial}{\partial t}(\alpha\rho_v) + \nabla \cdot (\alpha\rho_v\vec{V}_v) = R_e - R_c \quad (2.13)$$

where α - vapor volume fraction; the index v - indicates compliance of parameter to a gas phase (vapor); R_e , R_c - transfer rate at evaporation and condensation.

Balance of a vapor bubble is described by Rayleigh-Plesset equation:

$$\mathcal{R}_b \frac{D^2 \mathcal{R}_b}{Dt^2} + \frac{3}{2} \left(\frac{D\mathcal{R}_b}{Dt} \right)^2 = \left(\frac{P_b - P}{\rho_l} \right) - \frac{4v_l \dot{\mathcal{R}}_b}{\mathcal{R}_b} - \frac{2\sigma}{\rho_l \mathcal{R}_b} \quad (2.14)$$

where \mathcal{R}_b - the radius of a vapor bubble; P_b - bubble surface pressure, σ - surface tension.

In the *Ansys Fluent* there are three models of cavitation. The fullest of them - *Singhal full cavitation model* considers influence of dissolved gases amount in liquid, but demands big resources and it is number unstable and has considerable limitations on application. In particular, it is incompatible with model of multiphase flow *VOF* and moving objects. In this work the model of cavitation *Schnerr and Sauer* is used. Within this model the equation (2.13) has a form:

$$\frac{\partial}{\partial t}(\alpha\rho_v) + \nabla \cdot (\alpha\rho_v\vec{V}) = \frac{\rho_v\rho_l D\alpha}{\rho Dt} \quad \rho = \alpha\rho_v + (1-\alpha)\rho_l \quad (2.15)$$

Radius of a bubble is expressed by dependence on bubble density numbers n :

$$\mathcal{R}_B = \left(\frac{\alpha}{1-\alpha} \cdot \frac{3}{4\pi} \cdot \frac{1}{n} \right)^{1/3} \quad (2.16)$$

In the course of production of vapor (evaporation, growth of the bubbles size) at $P \leq P_v$ the right member of equation (2.15) takes a form:

$$R = \frac{\rho_v\rho_l d\alpha}{\rho dt} = R_e = \frac{\rho_v\rho_l}{\rho} \alpha(1-\alpha) \frac{3}{\mathcal{R}_B} \sqrt[3]{\frac{2(P_v - P)}{\rho_l}}, \quad (2.17)$$

and at $P \geq P_v$ in the course of reduction of the bubbles sizes, their collapse and condensation:

$$R = \frac{\rho_v\rho_l d\alpha}{\rho dt} = R_c = \frac{\rho_v\rho_l}{\rho} \alpha(1-\alpha) \frac{3}{\mathcal{R}_B} \sqrt[3]{\frac{2(P - P_v)}{\rho_l}} \quad (2.18)$$

Threshold pressure is determined with local values of turbulent fluctuations of

pressure:

$$P_v = P_{sat} + \frac{1}{2}(0.39\rho k),$$

where k - turbulence kinetic energy, P_{sat} - the predetermined saturation pressure. Value n is determined by experimental data and at its adjusting it is possible to compensate absence of direct accounting in model of amount of dissolved gases and surface tension. The surface tension, nevertheless, is considered as an origin of additional force on a interphase boundary which includes in the equation (2.8). On a phase boundary there is Laplace's pressure, then pressure drop on interface can be written down as:

$$P_2 - P_1 = \sigma \kappa \quad \kappa = \nabla \cdot \hat{n} \quad (2.19)$$

where k - interfacial curvature; \hat{n} - unit normal. At the same time force operating on a interphase boundary can be provided as the volume force which is the sum for all couples of phases contacting on a surface in this computational cell:

$$F_{vol} = \sum_{\substack{ij, i < j}} \sigma_{ij} \frac{\alpha_i \rho_i \kappa_j \nabla \alpha_j + \alpha_j \rho_j \kappa_i \nabla \alpha_i}{\frac{1}{2}(\rho_i + \rho_j)} \quad (2.20)$$

In the considered tasks turbulence of fuel flow inside the injector nozzle and turbulence of gases in the cylinder have great importance. Now it is possible to distinguish three main approaches to turbulence simulation: direct numerical simulation (*DNS*), large eddy simulation (*LES*) and Reynolds-averaged Navier-Stokes (*RANS*).

When performing calculations for a time span bigger than time of fluctuations (pulsations) in a turbulent flow, it is reasonable to use averaging approach. In this case a vector and scalars in a turbulent flow are considered as the sum of components - mean value and a turbulent (fluctuating) component:

$$u_i = \bar{u}_i + u'_i \quad \phi = \bar{\phi} + \phi' \quad (2.21)$$

This method is offered by O. Reynolds therefore in modern literature it is called also *RANS method (Reynolds-averaged Navier - Stokes)*, and the models which are based on this method - *RANS models*. At introduction to system of

differential equations of Navier-Stokes of variables in the form of (2.21) the new unknown quantities appears which are vectors of a higher order than basic variables. For example, momentum equation (2.8) in Cartesian coordinates after averaging according to Reynolds takes a form:

$$\frac{\partial}{\partial t}(\rho u_i) + \frac{\partial}{\partial x_j}(\rho u_i u_j) = -\frac{\partial p}{\partial x_i} + \frac{\partial}{\partial x_j} \left[\mu \left(\frac{\partial u_i}{\partial x_j} + \frac{\partial u_j}{\partial x_i} - \frac{2}{3} \delta_{ij} \frac{\partial u_l}{\partial x_l} \right) \right] + \frac{\partial}{\partial x_j} (-\rho \overline{u'_i u'_j}) \quad (2.22)$$

The system of equations obtained after averaging is called Reynolds system of equations. The last member in the right side of an equation (2.22) appears as a result of averaging and is called Reynolds stress. At the same time there is a problem of closure of a Reynolds system of equations, i.e. necessity to implement additional equations establishing relationships between unknown quantities.

The problem of closure of a Reynolds system of equations is one of the main problems of turbulence simulation and to solve this problem the different models called turbulence models are used. Let's note that Reynolds's approach remains the most effective until present time that causes creation of the different turbulence models used for numerical calculations. Thus, the turbulence models should be understood as a system of equations (algebraic or differential) which contain the unknown quantities from a Reynolds system of equations and allow to close this system. The most widespread *RANS models* of turbulence are subdivided into two basic groups [48]: the models based on a hypothesis of Boussinesq (models of turbulent viscosity) and Reynolds stress models (models with the equations for stress), in which the hypothesis of Boussinesq is not used. For engineering calculations so-called κ - ε model and its versions is most often used. The model belongs to the first group as it is based on a Boussinesq hypothesis according to which at a turbulent flow a tangential stress is defined by analogy with a laminar flow and Reynolds stress depend on mean velocity gradients:

$$-\rho \overline{u'_i u'_j} = \mu_t \left(\frac{\partial u_i}{\partial x_j} + \frac{\partial u_j}{\partial x_i} \right) - \frac{2}{3} \left(\rho k + \mu_t \frac{\partial u_k}{\partial x_k} \right) \delta_{ij} \quad (2.23)$$

Here μ_t - the coefficient of turbulent dynamic viscosity which is coefficient of a

turbulent exchange, but not a physical constant, and depending on distribution of mean velocity. Effective dynamic viscosity at the same time is defined as the sum: $\mu_{eff} = \mu + \mu_t$. In the forties last century A.N. Kolmogorov and L. Prandtl have suggested to accept as the typical turbulence velocity scale the square root from turbulence kinetic energy \sqrt{k} which represents specific kinetic energy of eddies in a turbulent flow and characterized by mean square of fluctuating velocity:

$$k = \frac{1}{2} \overline{u'_i u'_i} \quad (2.24)$$

As the turbulence length scale it was offered to use the Prandtl mixing length:

$$l = \kappa y \left[1 - \exp\left(-\frac{y^+}{A^*}\right) \right] \quad (2.25)$$

where κ – dimensionless Karman constant. According to experimental studies, numerical value of a constant: $\kappa = 0,41$. In this formula $A^* = 26$ - the damping constant, and expression in square brackets - the damping function which establishes connection between completely developed boundary layer where $l = \kappa \cdot y$ and the viscous sublayer where $l \rightarrow 0$. Parameter y^+ representing dimensionless distance from a wall surface:

$$y^+ = \frac{1}{v_w} \sqrt{\frac{|\tau_w|}{\rho_w}} \cdot y \quad (2.26)$$

A certain problem is evaluation of turbulent kinetic energy k . If for its calculation employed only one equation describing transport of energy k then such turbulent model belongs to one-equation models. This additional equation is usually obtained from Navier-Stokes equations. Thus, in models with one equation the length scale l is still specified by algebraic expression and depends only on local conditions. This quite important assumption because it is obvious that length scale in turbulent models should depend not only on local conditions, but also on a flow prehistory. For accounting of more difficult dependence of length scale l on a flow pattern it is necessary to introduce differential equation of transfer of l . We

will have in this case a turbulent model with two equations. One of the most widespread turbulent models with two equations is k - ε model. In k - ε -model first equation represents transport equation of turbulence kinetic energy k , and the second - transport equation of this energy dissipation rate ε . Communication between these parameters is defined by expression

$$\bar{\varepsilon} = \frac{\bar{k}}{l} = \frac{\bar{k}^{3/2}}{l}, \quad \left[\frac{\text{energy}}{\text{time}} \right] \quad (2.27)$$

Resistance to errors, profitability and adequate accuracy for the wide range of turbulent flows does k - ε model the most applicable in engineering tasks. It is necessary to note that this model demands to specify the coefficients obtained experimentally therefore it is also semi-empirical model. The so-called standard k - ε model for high Reynolds numbers in *the ANSYS FLUENT* have a form:

$$\frac{\partial}{\partial t}(\rho k) + \frac{\partial}{\partial x_i}(\rho k u_i) = \frac{\partial}{\partial x_j} \left[\left(\mu + \frac{\mu_t}{\sigma_k} \right) \frac{\partial k}{\partial x_j} \right] + G_k + G_b - \rho \varepsilon - Y_M + S_k \quad (2.28)$$

$$\frac{\partial}{\partial t}(\rho \varepsilon) + \frac{\partial}{\partial x_i}(\rho \varepsilon u_i) = \frac{\partial}{\partial x_j} \left[\left(\mu + \frac{\mu_t}{\sigma_\varepsilon} \right) \frac{\partial \varepsilon}{\partial x_j} \right] + C_{1\varepsilon} \frac{\varepsilon}{k} (G_k + C_{3\varepsilon} G_b) - C_{2\varepsilon} \rho \frac{\varepsilon^2}{k} + S_\varepsilon$$

$$G_k = -\rho \overline{u'_i u'_j} \frac{\partial u_j}{\partial x_i} = \mu_t S^2 = \mu_t 2S_{ij}S_{ij} \quad G_b = \beta g_i \frac{\mu_t}{Pr_t} \frac{\partial T}{\partial x_i} \quad \beta = -\frac{1}{\rho} \left(\frac{\partial \rho}{\partial T} \right)_p \quad Y_M = 2\rho \varepsilon M_t^2 \quad M_t = \sqrt{\frac{k}{a^2}}$$

Here G_k - the generation of turbulence kinetic energy due to the mean velocity gradients (strain rate); S - strain rate tensor; G_b - the generation of turbulence kinetic energy due to buoyancy; β - thermal expansion coefficient; g_i - the component of the gravitational vector; Y_M - the contribution of the fluctuating dilatation in compressible turbulence to the overall dissipation rate; M_t - turbulent Mach number; $C_{1\varepsilon}$, $C_{2\varepsilon}$, $C_{3\varepsilon}$, σ_k , σ_ε - empirical constants, S_k , S_ε - additional user-defined source terms. Turbulent viscosity at the same time is:

$$\mu_t = \rho C_\mu \frac{k^2}{\varepsilon}, \quad (2.29)$$

where C_μ - an empirical constant. The model equations for high Reynolds $Re = \sqrt{k} \ell / \nu$ number are applicable for areas located enough far from a wall surface

and in which influence of molecular viscosity is negligible in comparison with turbulent viscosity. It means for typical near-wall flows that $y^+ > 30$, i.e. the laminar and transitional (buffer) sublayer in which there is no logarithmic profile of velocity (Fig. 2.16) are excluded from consideration. Thereby high-Reynolds approach is almost not applicable to flows with high gradient of medium properties across a flow which occurs in boundary-layer flow. In such flows, for example in near-wall flows, the number $Re_t = \sqrt{k} \ell / \nu$ (it also called a turbulent Reynolds number) becomes small. It is obvious because velocity fluctuations u' and turbulence kinetic energy k respectively (as a result of damping action of a wall) and characteristic length $l = \delta_T$ (where δ_T is boundary layer thickness) significantly decrease regardless of their values outside a boundary layer. Thereby the stated above equations of k - ε model are equitable only for completely developed turbulent flows, i.e. far from the damping influence of a wall. Therefore much attention has so-called models for flows with low Reynolds numbers.

The main problem at simulation of the low Reynolds number flows is to avoid the viscous (laminar) and buffer sublayers adjoining a wall surface. Thereby development of a way of boundary conditions setting for k value is required. When using numerical methods it is necessary to set boundary conditions for k in the control volumes adjoining the wall. In *the ANSYS FLUENT* it performs by means of the so-called wall functions offered by B. Launder and B. Spalding. It is set of the semi-empirical functions obtained on the basis of experimental studies and a similarity theory. Velocity and temperature profiles in a turbulent boundary layer are set using dimensionless coordinates (y^+, u^+). Dimensionless velocity: $u^+ = u/u^*$, where

$$u^* \stackrel{\text{def}}{=} \sqrt{\frac{|\tau_w|}{\rho_w}} \quad (2.30)$$

is a so-called dynamic velocity (friction velocity).

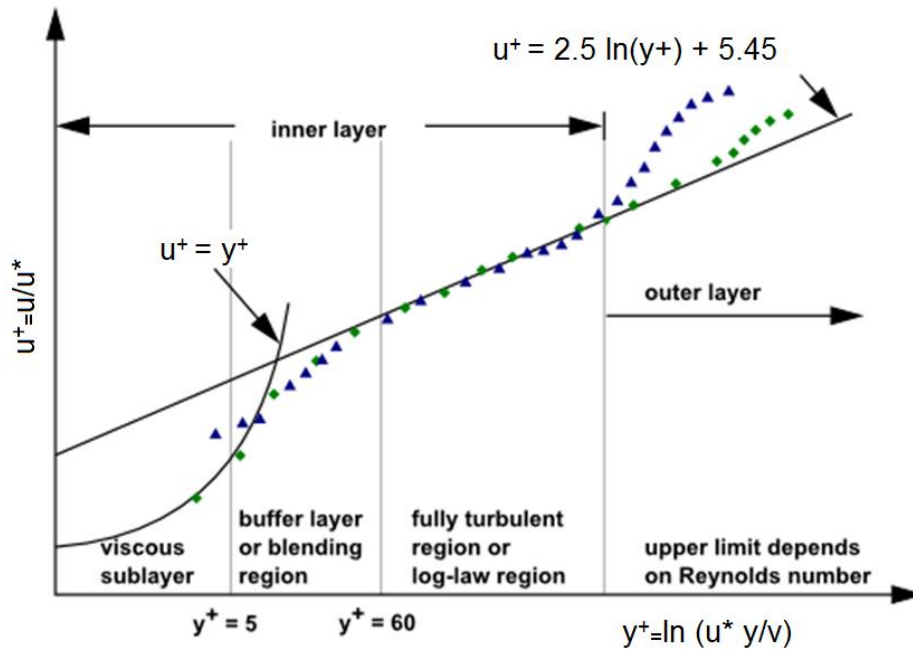


Fig. 2.16. Structure of a turbulent boundary layer for typical incompressible flow on a smooth plate

In engineering analyses is accepted that at $y^+ > 11,63$ inertial forces begin to prevail over friction forces therefore the logarithmic velocity profile exists, and in the laminar sublayer (at $y^+ < 11,63$) distribution of velocity has linear character, i.e.:

$$u^+ = y^+, \quad y^+ < 11,63 \quad (2.31)$$

$$u^+ = \frac{1}{\alpha} \ln(Ey^+), \quad y^+ > 11,63$$

Here $\alpha = 0,41$ - the Karman constant, $E = 9,0$ - constant of wall function. Therefore, the logarithmic velocity profile in this case differs from the classical universal distribution law of velocity:

$$u^+ = \frac{1}{\alpha} \ln y^+ + 5,5 \quad (2.32)$$

that was confirmed experimentally by Nikuradze for the wide range of Reynolds numbers ($4000 < Re < 3240000$). It is obvious that the classical logarithmic distribution law of velocity is modified for the purpose of accounting of decrease in turbulent friction depending on reduction of y^+ (i.e. come near to a wall). In

expressions the dimensionless velocity and dimensionless wall distance respectively:

$$u^+ = \tilde{u}^* = C_\mu^{1/4} \frac{\bar{k}_p^{1/2}}{u} u_p; \quad y^+ = y^* = C_\mu^{1/4} \frac{\rho \bar{k}_p^{1/2} y_p}{\mu} \quad (2.33)$$

Here the index p belongs to parameters in the central point of the control volume located directly at a wall surface. Viscosity near a wall can be replaced with the value defined from expression

$$\mu_w = \frac{y^+}{u^+} \mu \quad (2.34)$$

For first, nearest to a wall control volume the equation defining turbulence kinetic energy (k -equation) is solved just as for all other control volumes using condition of zero gradient (a zero flux of k). However the member describing turbulence generation evaluated by means of a velocity gradient from the logarithmic distribution law. At the same time shear stress is replaced with a wall shear stress and normal stress is neglected. Rate of turbulence kinetic energy dissipation can be evaluated, allowing a linear variation of length scale depending on distance from a wall surface:

$$\bar{\varepsilon}_p = C_\mu^{3/4} \frac{\bar{k}_p^{3/2}}{\alpha y_p} \quad (2.35)$$

It is possible to treat the separate components of ε equation as well as for k equation. In practice usually try to avoid the solution of ε equation in the first control volume located directly on a wall surface and to use for it the equation for ε_p . So-called standard wall functions for κ - ε -model may be employed when dimensionless wall distance $y^+ > 11$. In case of smaller value of y^+ , i.e. more dense computational grid leads to high errors. It can be a serious problem, in a case when the computational grid with small cells is necessary for simulation of other phenomena, for example an interphase boundary. Therefore in *ANSYS FLUENT* in addition to standard wall functions there are a number of alternatives, in particular,

so-called scalable wall functions. According to this approach for the best correspondence between the logarithmic law and wall function limitation is used:

$$\tilde{y}^* = \text{MAX}(y^*, y^* \text{ limit}) \quad (2.36)$$

where $y^* \text{ limit} = 11.225$, and y^* in expressions is replaced with result of (2.36). When characteristics in a near-wall zone are determinative (for example when determining heat release on friction, forces operating on a wall or heat exchange with a wall), often wall functions do not give adequate accuracy. In such cases it is necessary a resolution of a near-wall zone by computational grid up to $y^+ = 1$ and use of low-Reynolds modifications of turbulent models.

In the *ANSYS FLUENT* in addition to standard $\kappa\text{-}\varepsilon$ model there are other modifications, such as *RNG- $\kappa\text{-}\varepsilon$* and *Realizable- $\kappa\text{-}\varepsilon$* . *RNG- $\kappa\text{-}\varepsilon$* model is widely used for simulation of flows in the cylinder of the ICE and is obtained from Navier-Stokes equations using the *renormalization group theory*. The *RNG- $\kappa\text{-}\varepsilon$* model is similar to standard $\kappa\text{-}\varepsilon$ model, but has the following advantages:

1. The RNG model has an additional term in its ε equation that improves the accuracy for rapidly strained flows.
2. The RNG theory provides an analytical formula for turbulent Prandtl numbers, while the standard $\kappa\text{-}\varepsilon$ model uses user-specified, constant values.
3. There is an option of simulation of the rotating and swirling flows, if it is enabled the turbulent viscosity is evaluated accounting its dependence on swirl number.
4. While the standard $\kappa\text{-}\varepsilon$ model is a high-Reynolds number model, the RNG theory provides an analytically-derived differential formula for effective viscosity (2.37), that accounts for low-Reynolds number effects. Effective use of this feature does, however, depend on an appropriate treatment of the near-wall region.

$$d \left(\frac{\rho^2 k}{\sqrt{\varepsilon \mu}} \right) = 1.72 \frac{\hat{v}}{\sqrt{\hat{v}^3 - 1 + C_v}} d\hat{v} \quad \hat{v} = \frac{\mu_{eff}}{\mu} C_v \approx 100 \quad (2.37)$$

The main differences of *Realizable-k-ε* model are as follows:

1. The parameter C_μ in the equation (2.29) is not a constant, and represents function from flow strain rate, relative velocity at rotation and turbulent from parameters k and ε . Thus values of turbulent viscosity are corrected, and it is possible to avoid obtaining negative values in areas with high gradients.

2. A transport equation (2.28) for the dissipation rate ε has been derived in modified form from an exact equation for the transport of the mean-square vortices fluctuation.

The name Realizable indicates that the model imposes certain mathematical limitations for Reynolds stresses which take place in physics of real turbulent flows. It should be noted that due to a number of corrections and advantages this model shows the most exact, in comparison with other two-equation models, results at simulation of detached flows, in the conditions of cavitation, and also at simulation of jets [117]. Besides, it can be used as subgrid model for the description of near-wall zones in hybrid approach *Detached Eddy Simulation (DES)* which combines *LES* and *RANS* models and is stated below.

Models of κ - ε family possess a number of the shortcomings connected with the fact that the equation (2.28) for parameter ε is too simple to describe the real physical processes associated with dissipation of turbulent kinetic energy. It especially concerns low-Reynolds regions. Therefore different modifications of κ - ε model, such as κ - ω [178], *SST* [156], etc. have been offered.

The main advantage κ - ω model ($\omega = \varepsilon/k$ -the specific rate of dissipation) is better formulation of laws for near-wall region of low-Reynolds flows. The model does not include the difficult non-linear dependences considering the damping influence of a wall which is necessary in k - ε model and therefore it is more accurate and reliable for these flows. Low-Reynolds κ - ε model demands grid resolution near the wall $y^+ < 1$, while low-Reynolds κ - ω model - $y^+ < 2$. In the simulated flows even $y^+ < 2$ cannot be always provided therefore the new

description of near-wall zones for κ - ω model is developed. It allows to perform smooth transition from a low-Reynolds form of the equations to wall functions. Turbulent viscosity in this model is defined as:

$$\mu_t = \alpha^* \frac{\rho k}{\omega} \quad (2.38)$$

where α^* - correction coefficient for a low-Reynolds zone. In a high-Reynolds zone it has value equal to unit. The worse description of a high-Reynolds zone and high sensitivity to flow parameters outside a boundary layer are the main lack of this model.

F. Menter in the developed by him *SST* model (*Shear Stress Transport*) has combined k - ω and k - ε model. This model is based on the closed ω -equation for near-wall region which far from a wall is transformed to the ε -equation. At the same time ω -equation accepts unit value in a near-wall region to which k - ω model is applied, and is equal to zero far from a wall where k - ε model is applied. Constants of *SST* model differ from constants in initial models.

Thus, if low-Reynolds effects slightly influence required integral characteristics of a flow, then high-Reynolds models with wall functions are used. At the same time it is necessary to provide dimensionless distance from a wall to the center of the first cell of a computational grid $y^+ > 11$, and for achievement of the best accuracy - even $y^+ > 25$. If it is necessary to consider all effects in a viscous and buffer sublayer low-Reynolds models should be used. At the same time wall functions are not used, and the boundary layer is resolved by a computational grid with providing $y^+ < 2$, and in certain cases - $y^+ < 0,5$. It should be noted that at $2 < y^+ < 11$ "dead zone" is formed which is not good for both approaches. In engineering tasks often there is no opportunity to provide a computational grid with identical value y^+ near all walls. For this purpose in *ANSYS FLUENT* hybrid approach called *EWT* (*Enhanced Wall Treatment*) is implemented. According to it the computational domain is separated into two zones: a zone of influence of

viscosity and a zone of the developed turbulence. At the same time physically reasonable transition between zones is carried out. In a viscosity influence zone, depending on quality of the near-wall region grid resolution, it is implemented the description similar to low-Reynolds approaches or by means of wall functions of a special form. Thus, the accurate solution performed as in local regions where $y^+ < 2$ as in regions with transitional ($2 < y^+ < 11$) and even for rough near-wall grid ($y^+ > 11$). In the *ANSYS FLUENT* approach of *EWT* for models $\kappa\text{-}\omega$ and *SST* is used by default.

The fullest of *RANS models* is the model of Reynolds stresses *RSM (Reynolds Stress Model)* which considers in more strict way effects of streamlines curvature, the swirling flow, rotation flow, fast change of a strain rate of a flow. As it has been described above *RSM* do not use the Boussinesq hypothesis of isotropic turbulent viscosity and use the equations for transfer of turbulent stresses. Therefore the *RSM* is more universal and accurate due to of smaller quantity of assumptions. Use of this model is recommended for flows with Reynolds stress anisotropy: flows in cyclones, strongly swirled flows in a CC, secondary flows in channels caused by stresses. However application of this model is limited from the point of view of computational resources because five new equations in a two-dimensional case and seven - in three-dimensional case are added to system of equations. The model can be also used for examination of the solution obtained by means of simpler *RANS* models. It should be noted the quadratic *RSM* which is most precisely capable to consider sudden contractions and expansions at flows in axisymmetric channels.

As in basis of *RANS* approach exists averaging of equations, use of models of this group is capable to obtain adequate results of average and integral characteristics of a flow. But when the small-scale phenomena in interest, such as a jet break-up, the turbulent viscosity promotes "smoothing" of a solution picture. In such cases it is necessary to use more full approach, such as *DNS, LES or DES*. *Detached Eddy Simulation (DES)* is a hybrid approach according which in the zones far from walls simulation of large eddies (*LES*) is implemented, and in near-

wall zones a *RANS method* employed [117]. So, in a simulation of fuel outflow from an injector the near-wall flow can be described by the most suitable *Realizable-k-ε RANS* model and free jet described by means of *LES* approach. At the same time it is considered that sufficient grid resolution for resolving of the interesting droplets sizes will almost resolve turbulent structures of the most influencing scales.

For simulation of spray behavior in the cylinder, break-up and droplets evaporation the Euler-Lagrange approach is employed. According to it the continuous medium, for example gas in the cylinder, is calculated by use system of equations of Navier-Stokes, and components of dispersion medium (fuel droplet) are described in Lagrangian coordinates individually. At the same time the exchange equations (the moment, mass and energy) between phases (continuous and disperse) are solved. In *the ANSYS FLUENT* this approach is implemented within the *DPM (Discrete Phase Model)*. DPM predicts the trajectory of a discrete phase particle (or droplet or bubble) by integrating the force balance of the particle, which is written in a Lagrangian reference frame:

$$\frac{d\bar{u}_p}{dt} = F_D(\bar{u} - \bar{u}_p) + \frac{\bar{g}(\rho_p - \rho)}{\rho_p} + \bar{F} \quad F_D = \frac{18\mu C_D Re_D}{\rho_p d_p^2} \quad Re_D = \frac{\rho d_p |\bar{u}_p - \bar{u}|}{\mu} \quad (2.39)$$

where the index *p (particle)* belongs to dispersion particles (droplets); the first member of the right part - aerodynamic force, the second - gravitational; *F* - other forces; *C_D* - drag coefficient. The deviation of trajectories of particles due to turbulent fluctuations in a continuous phase (turbulent dispersion) is also considered by use of the additional model based on stochastic methods. Discretization and integration of the equation (2.39) performs by particle time step, different from a computational time step for a continuous phase. For drag coefficient *C_D* the different empirical laws considering a shape and velocity of particles are offered. The most acceptable is the so-called dynamic drag model accounts for the effects of droplet distortion, linearly varying the drag between that of a sphere and a value of 1.54 corresponding to a disk. The drag coefficient is

given by:

$$C_d = C_{d,sphere} (1 + 2.632y) \frac{d^2y}{dt^2} = \frac{C_F \rho_g u^2}{C_b \rho_l r^2} - \frac{C_k \sigma}{\rho_l r^3 y} - \frac{C_d \mu_l}{\rho_l r^2} \frac{dy}{dt} \quad (2.40)$$

where y - the droplet distortion ($y=1$ for a disk, $y=0$ - for the sphere); the drag coefficient for spherical shape at the same time as following:

$$C_{d,sphere} = \begin{cases} 0.424 & Re_D > 1000 \\ \frac{24}{Re_D} \left(1 + \frac{1}{6} Re_D^{2/3} \right) & Re_D \leq 1000 \end{cases} \quad (2.41)$$

During motion of disperse droplets in the environment of hot gases between them there is a heat exchange. In the engine cylinder a droplet heating by convective heat exchange:

$$m_p c_p \frac{dT_p}{dt} = \alpha A_p (T_{gas} - T_p) \quad (2.42)$$

where α – the heat transfer coefficient calculated by Ranz-Marshall equation:

$$Nu = \frac{\alpha \cdot d_p}{k_{gas}} = 2 + 0.6 Re_D^{1/2} Pr^{1/3} \quad Pr = \frac{c_p \mu}{k} \quad (2.43)$$

where the Re is defined for a droplet in the form of (2.39); the Pr is calculated for a gas phase. Radiation heat exchange in this work is not considered (in chapter 1 it is shown that such approach is justified, especially for HCCI). After heating of droplets up to the certain temperature process of their evaporation begins. The equation of a heat balance of the evaporating droplet looks as follows:

$$m_p c_p \frac{dT_p}{dt} = \alpha A_p (T_{gas} - T_p) - \frac{dm_p}{dt} \cdot h_{fg} \quad (2.44)$$

where heat of phase transition (latent vaporization heat) is defined in a form:

$$h_{fg} = - \int_{T_p}^{T_{bp}} c_{p,g} dT + h_{fg,bp} + \int_{T_p}^{T_{bp}} c_{p,p} dT \quad (2.45)$$

Here $h_{fg,bp}$ - latent vaporization heat in a boiling point, an index g belongs to a gas phase. The member $\frac{dm_p}{dt}$ in the equation (2.44) is the evaporation rate described by convective-diffusion model of evaporation [169,170]:

$$\frac{dm_p}{dt} = k_c A_p \rho_\infty \ln(1+B_m) B_m = \frac{Y_{i,s} - Y_{i,\infty}}{1 - Y_{i,s}} \quad (2.46)$$

$Y_{i,\infty}$, $Y_{i,s}$ - mass fractions of vapor in continuous medium and on a droplet surface, where:

$$Y_{i,s} = \left[1 + \left(\frac{p}{p_s} - 1 \right) \frac{M_g}{M_f} \right]^{-1}, \quad (2.47)$$

p_s - saturated vapor pressure; M_g , M_f - the molar mass of the gas surrounding a droplet and of fuel. k_c mass-transfer coefficient in the equation (2.46) is evaluated from the equation for a Sherwood number that is similar to the equation (2.43) :

$$Sh_{AB} = \frac{k_c d_p}{D_{i,m}} = 2.0 + 0.6 Re_d^{1/2} Sc^{1/3} \quad Sc = \frac{\mu}{\rho D_{i,m}} \quad (2.48)$$

Here Sc - a Schmidt number; $D_{i,m}$ - diffusion coefficient of vapor into surrounding gas. According to convective-diffusion model in the course of evaporation the equation (2.43) is transformed to a look:

$$Nu = \frac{\alpha d_p}{k_\infty} = \frac{\ln(1+B_T)}{B_T} (2 + 0.6 Re_d^{1/2} Pr^{1/3}) \quad B_T = B_m \quad (2.49)$$

Within this model is accepted that Spalding numbers for a mass exchange and heat exchange are equal (2.49).

In model of a disperse phase *DPM* break-up of droplets is calculated with the use of subgrid models of secondary break-up (*Secondary break-up models*). At the same time distribution of diameters and velocities of the initial droplets produced as a result of primary break-up needs to be set using experimental or computational data. This data may be obtained also by use of semi-empirical models or direct simulation of primary break-up of a jet.

For the single or multi-hole injector nozzle in *the Ansys Fluent* the semi-empirical model is implemented called *plain orifice atomizer* model. It allows to obtained necessary distribution of diameters and velocities without calculation of an internal nozzle flow. The model based on works [159,172,173,180] use the theory of different flow regimes inside the nozzle hole depending on value of a cavitation number:

$$K = \frac{p_1 - p_v}{p_1 - p_2} = \frac{p_{inj} - p_v}{p_{inj} - p_c} = 1 + \frac{1}{CN} \quad (2.50)$$

The flow in a nozzle hole may have one of three regimes: single-phase (Fig. 1.18, *a* chapter 1), cavitating (Fig. 1.18*b,c*) and total hydraulic flip (Fig. 1.18, *d*). Using the inserted boundary condition value of mass flow rate through a hole, the cavitation number K and a hydraulic Reynolds number is defined:

$$Re_h = \frac{d\rho_l}{\mu} \sqrt{\frac{2(p_1 - p_2)}{\rho_l}} \quad (2.51)$$

The current value of a cavitation number is compared to critical value for the exact nozzle hole geometry. Value $K_{start} = 1 + 1/CN_{start}$ at which cavitation occurs (see Fig. 1.14, 1.20):

$$K_{start} = 1.9 \left(1 - \frac{r}{d}\right)^2 - \frac{1000}{Re_h} \quad (2.52)$$

where r - the rounding radius of an inlet edge (Fig. 1.12.). Value $K_{flip} = 1 + 1/CN_{flip}$ (Fig. 1.20) at which hydraulic flip is formed:

$$K_{flip} = 1 + \frac{1}{\left(1 + \frac{L}{4d}\right) \left(1 + \frac{2000}{Re_h}\right) e^{70r/d}} \quad (2.53)$$

The flow regime is defined from a relation between K , K_{start} and K_{flip} according to Table 2.2. For each flow regime other characteristics may be evaluated using empirical formulas (Table 2.2) [159,172,180].

Table 2.2.

Characteristics of primary break-up of the jet produced by a nozzle hole depending on a flow regime (*plain orifice atomizer model*)

	Single-phase flow	The cavitating and choked flow	Total hydraulic flip
Cavitation number	$K > K_{start}, K \geq K_{flip}$	$K_{flip} \leq K \leq K_{start}$	$K < K_{flip}$
Coefficient of discharge	$\mu = \frac{1}{\frac{1}{C_{du}} + 20 \frac{(1+2.25L/d)}{Re_k}}$ $C_{du} = 0.827 - 0.0085 \frac{L}{d}$	$\mu = C_c \sqrt{K}$ $C_c = \frac{1}{\sqrt{\frac{1}{C_{ct}^2} - \frac{11.4r}{d}}}$ $C_{ct} = 0.611$	$\mu = C_{ct} = 0.611$
Injection velocity	$u = \frac{\dot{m}_{eff}}{\rho_l A}$	$u = \frac{2C_d p_1 - p_2 + (1-2C_d)p_v}{C_c \sqrt{2\rho_l(p_1 - p_v)}}$	$u = \frac{\dot{m}_{eff}}{\rho_l C_{ct} A}$
Semi-angle of initial jet dispersion	$\frac{\theta}{2} = \tan^{-1} \left[\frac{4\pi}{C_A} \sqrt{\frac{\rho_g}{\rho_l}} \frac{\sqrt{3}}{6} \right]$	$C_A = 3 + \frac{L}{3.6d}$	$\frac{\theta}{2} = 0.01$
Sauter mean diameter	$d_{32} = 133.0 \lambda We^{-0.74}$ $\lambda = d/8$ $We \equiv \frac{\rho_l u^2 \lambda}{\sigma}$	$d_{32} = 133.0 \lambda We^{-0.74}$ $\lambda = d_{eff}/8$ $d_{eff} = \sqrt{\frac{4\dot{m}_{eff}}{\pi \rho_l \mu}}$	—
Rosin-Rammler spread parameter	$s = 3,5$	$s = 1,5$	∞
The most probable diameter of primary droplets	$d_0 = 1.2726 d_{32} \left(1 - \frac{1}{s}\right)^{1/s}$		$d_0 = d \sqrt{C_{ct}}$

Parameter C_A can be set other than the correlation offered in Table 2.2. In reality for the cavitating flow it has a little smaller values, than for single-phase flows. Finally, from the given mass flow rate profile for exact geometry of a nozzle hole (d, L, r, C_A) at each moment it is defined a set of all necessary data for the description of primary break-up results. And further calculation of secondary break-up by subgrid *CFD* models may be performed.

The Ansys Fluent has several models of a droplets secondary break-up. For an analysis of diesel injectors the the most widely used the models of *WAVE* family

(the *WAVE* model and the *KH-RT* model) based on wave stability analysis of a viscous cylindrical jet [168]. The model of secondary break-up *WAVE* is developed for break-up of droplets at values $We > 100$ when the dominating mechanism of droplets destruction is Kelvin–Helmholtz instability (*KH waves*, see chapter 1). Within this model length Λ and the rate of maximum growth rate Ω for the most fast-growing wave can be calculated by the dependences:

$$\frac{\Lambda}{a} = 9.02 \frac{(1+0.45Oh^{0.5})(1+0.4Ta^{0.7})}{(1+0.87We_2^{1.67})^{0.6}} \quad \Omega \sqrt{\frac{\rho_1 a^3}{\sigma}} = \frac{0.34+0.38We_2^{1.5}}{(1+Oh)(1+1.4Ta^{0.6})} \quad (2.54)$$

$$We_1 = \rho_1 U^2 a / \sigma \quad We_2 = \rho_2 U^2 a / \sigma \quad Oh = \sqrt{We_1} / Re_1 \quad Ta = Oh \sqrt{We_2}$$

where a - the initial radius of a cylindrical jet; the index 1 belongs to a fluid disperse phase, index 2 - to a continuous gas phase. The size of the child droplets which are formed during jet break-up is proportional to the wavelength of the fastest-growing unstable surface wave on the parent droplet. Then the radius of child droplets and a break-up time:

$$r = B_0 \Lambda \quad \tau = \frac{3.726 B_1 a}{\Lambda \Omega} \quad (2.55)$$

where B_0, B_1 - the constants of the size and time which are adjusted according to experimental data. Value $B_0 = 0,61$ is offered authors of model [168].

The break-up model *KH-RT* includes also the description of droplets break-up under action of Rayleigh–Taylor instability (*RT waves*, see chapter 1). Within this model the theory offered by V. G. Levich for length of a liquid core of a jet is used [150]:

$$L_{liq} = const \cdot D_h \cdot \sqrt{\frac{\rho_p}{\rho_g}} \quad (2.56)$$

where D_h - hydraulic diameter. Is assumed that within L_{liq} (Fig. 1.30) only the *KH* mechanism acts and beyond this length - both mechanisms of break-up *KH* and *RT* operates. Frequency of the most fastest-growing unstable surface wave and the corresponding wave number are expressed as follows:

$$\Omega_{RT} = \sqrt{\frac{2(-g_t(\rho_p - \rho_g))^{3/2}}{3\sqrt{3\sigma}(\rho_p + \rho_g)}} \quad K_{RT} = \sqrt{\frac{-g_t(\rho_p - \rho_g)}{3\sigma}} \quad (2.57)$$

where g_t - acceleration of a droplet in moving direction. Then the radius of child droplets and a break-up time are defined in a look:

$$r_c = \frac{\pi C_{RT} \tau_{RT}}{K_{RT}} = \frac{C_\tau}{\Omega_{RT}} \quad (2.58)$$

where C_{RT} , C_τ - the constants of the size and time defined experimentally.

To obtain full description of necessary effects and adequate results it is important to set properties of substances correctly. For example, when calculating a flow in internal channels of the injector nozzle and accounting of the phenomena related with achievement by a fuel flow of sound speed in multiphase medium (throttling, supercavitation) compressibility should be considered. For it equation of state is implemented, describing substance density. And also dependence for determination of sonic speed is set. For gases such is in-cylinder air and vapor of fuel, density and sonic speed may be defined by ideal gas law with an adequate accuracy:

$$\rho_{gas} = \frac{p}{R_\mu T} \quad a_{gas} = \sqrt{\gamma R_\mu T} \quad (2.59)$$

For the description of liquid compressibility in *the Ansys Fluent* the Tait equation of state is implemented:

$$(\rho_l / \rho_0)^n = K / K_0 \quad K = K_0 + n\Delta p \quad \Delta p = p - p_0 \quad (2.60)$$

where K - a bulk modulus of liquid, n - an exponent. The index 0 corresponds to values at atmospheric or other "reference" conditions. Reference values and an exponent can be taken from handbook data. Sound speed at the same time can be calculated by a formula:

$$a_{liq} = \sqrt{K / \rho_l} \quad (2.61)$$

In a case when injection pressure is considerable (more than 1500 bars) it is desirable to consider that outflow is nonisothermal. The following dependences can be for this purpose used [20,39]:

$$\left(\frac{\rho_l}{\rho_{0t}}\right)^\chi = \frac{B+p}{B} \quad a_{liq} = \sqrt{\frac{\chi}{\rho_{20}} B^{\frac{1}{\chi}} (B+p)^{\frac{\chi-1}{\chi}}} \quad (2.62)$$

$$B = 10^6 [222,3 - 1,26(t - 20) + 0,62(\rho_{20} - 825)] \quad \chi = 7,49 + 0,0086 \cdot (t - 20)$$

Where t – temperature in Celsius, ρ_{20} - density under standard conditions, ρ_{0t} - dependence of density on temperature at atmospheric pressure. Let's note that the equations (2.60) and (2.62) have a similar appearance of pressure dependence therefore provide close results in the absence of a noticeable heating of fuel (Fig. 2.17). But use of a formula (2.62) has negative influence on stability of the numerical solution. Because in this work the pressure level does not exceed 1600 bars, dependences (2.60) and (2.61) are generally used.

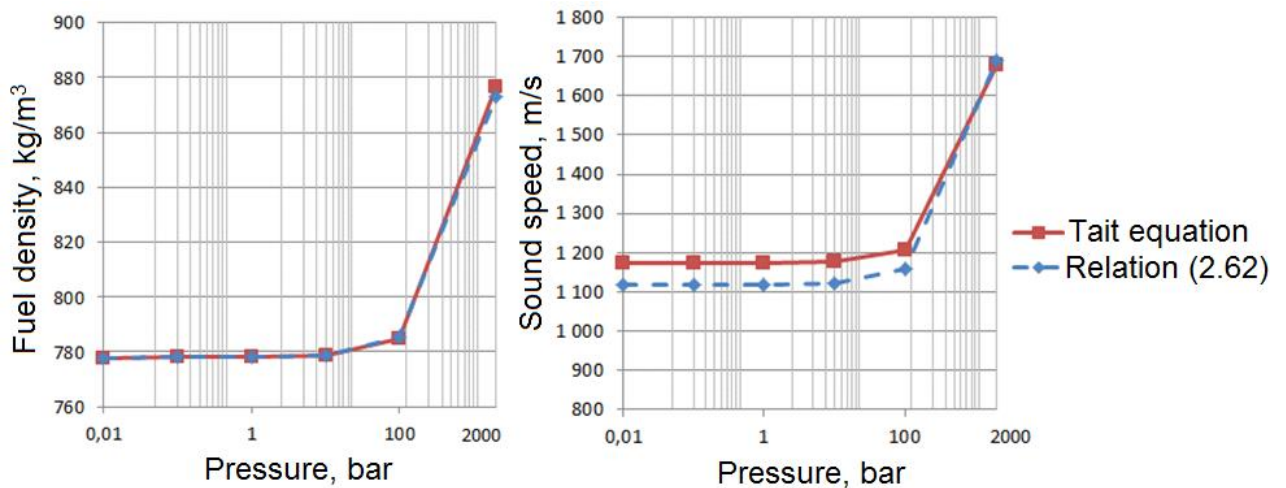


Fig. 2.17. Dependences of density and sound speed in diesel fuel from pressure obtained by the different equations at temperature of 373 K

In *the Ansys Fluent* there is rather wide database of substances properties which is based on reference data [117, 163]. In this work data from this base and from other sources are used. The main dependences used in this work are given in Table 2.3.

Table 2.3.

Properties of the substances used at simulation

	Heat capacity	Viscosity	Heat conductivity	Surface tension	Diffusion coefficient
Liquid DF	$c_p = 1848 + 4,9t$ $20 \leq t \leq 300^\circ C$ [48]	$\mu = ABe^C$ $A = 0,004881$ $B = \frac{1 - 0,001839t}{1 + 0,039991t}$ $C = \frac{0,001529p}{1 + 0,004423t}$ [48]	$k = 0,118 - 0,000105t$ $0 \leq t \leq 225^\circ C$ [48]	$\sigma = 0,032 - 0,000088t$ $0 \leq t \leq 300^\circ C$ $\sigma = 0,0179 - 0,000041t$ $300 \leq t \leq 437^\circ C$ [48, 163]	-
Vapor of DF	$c_p = 59,37374 + 5,332576T + 0,0005T^2 - 5,048318 \cdot 10^{-6}T^3 + 2,340991 \cdot 10^{-9} \cdot T^4$ $0 \leq T \leq 1000K$ [117]	$\mu = 10^{-7} (3 + 0,1368116T)$ [163]	$k = 0,000228T - 0,055$ [163]	-	$D_{i,m} = D_0 \left(\frac{T}{T_0}\right)^{1,7} \cdot \frac{p}{p_0}$ [48]
Air	[117]	$\mu = f(T)_{p=p_u}$ [163]	$k = f(T)_{p=p_u}$ [163]	-	$D_{i,m} = D_0 \left(\frac{T}{T_0}\right)^{1,7} \cdot \frac{p}{p_0}$ [48]

Saturated vapor pressure at a low fuel temperature (for cavitation simulation) was set according to Fig. 2.18 [110]. At the high temperature of DF for simulation of droplets evaporation the widely used relationship was employed [48]:

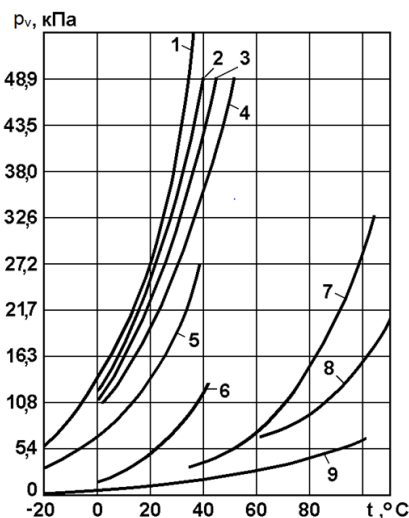


Fig. 2.18. Dependence of saturated vapor pressure of motor fuels and hydrocarbons on temperature: 1 - synthin; 2 - aviation gasoline; 3 - aviation gasoline from Baku; 4 - automobile cracked gasoline; 5 - aviation gasoline B-70 ; 6 - isooctane; 7 - jet fuel; 8 - kerosene from Baku; 9 - diesel fuel

$$p_s = 25200 \cdot 10^5 \exp\left(\frac{-5220}{T}\right) \quad (2.63)$$

Numerical investigations of flows in internal channels of injector nozzles, formation of jets, its penetration, break-up and evaporation in the cylinder are conducted using mathematical models presented above.

2.4. Simulation of a fuel flow in a nozzle hole of an injector

For correct statement of a computational task, the choice of necessary models and adjustment of empirical constants are necessary to carry out validation according to experimental data. For this purpose the researchers use the results of experimental studies which are similar to the given problem by a set of the physical phenomena and conditions. So, in work [179] experimental researches of a flow in the nozzle hole in the conditions of cavitation and supercavitation are conducted. The studied channel represents a cavity of a special shape in a steel sheet with a thickness of 0,3 mm. The computational scheme according to experiment and computational grid is presented on Fig. 2.19.

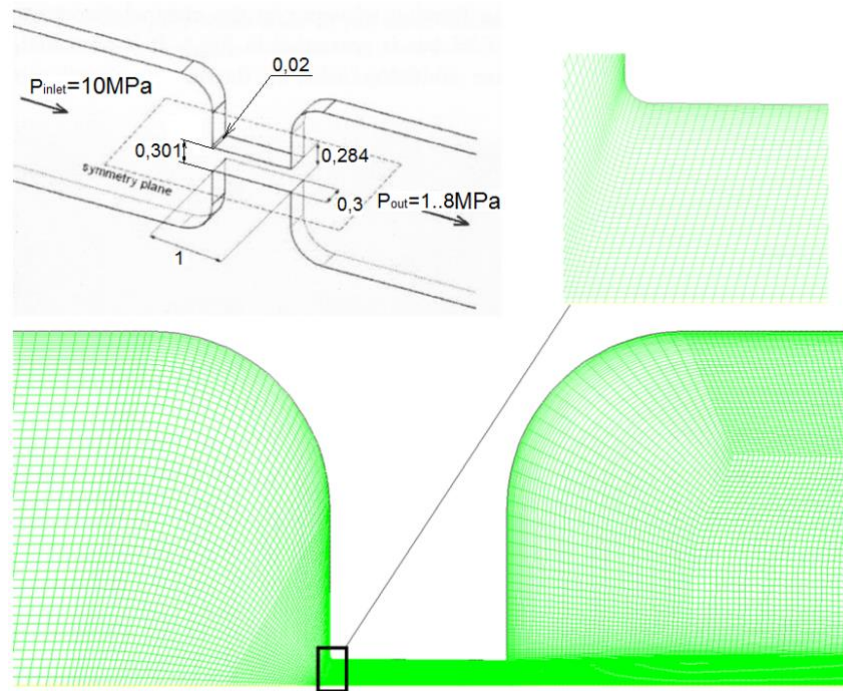


Fig. 2.19. Computational scheme and grid

At experimental studies [179] all channel has been submerged in diesel fuel. Thus, outflow of fuel through a hole happened in a liquid medium, inlet pressure has been fixed 10 MPa, and outlet pressure varied - step by step decreased from 8 MPa to 1 MPa. At the same time the important effect has been observed: after achievement of some critical pressure drop flow rate through a hole become independent from further decrease of outlet pressure, that is a supercavitation sign (see section 1.2 of chapter 1). Comparison of results obtained in this study with

experimental data of *Winklhofer* work [179] and computational data of *Ming Jia et al.* [140] is presented on Fig. 2.20.

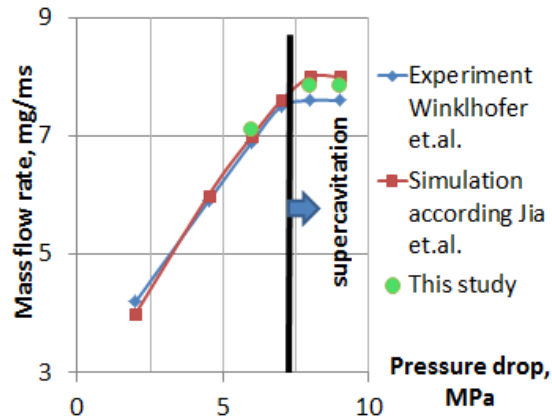


Fig. 2.20. Comparison of results of different simulations with experiment

Comparison of visualizations of phases distribution (liquid and vapor) in a flow obtained in experiment [179] and in this work is presented on Fig. 2.21. The values of a coefficient of discharge obtained at simulation also correspond well with experiment.

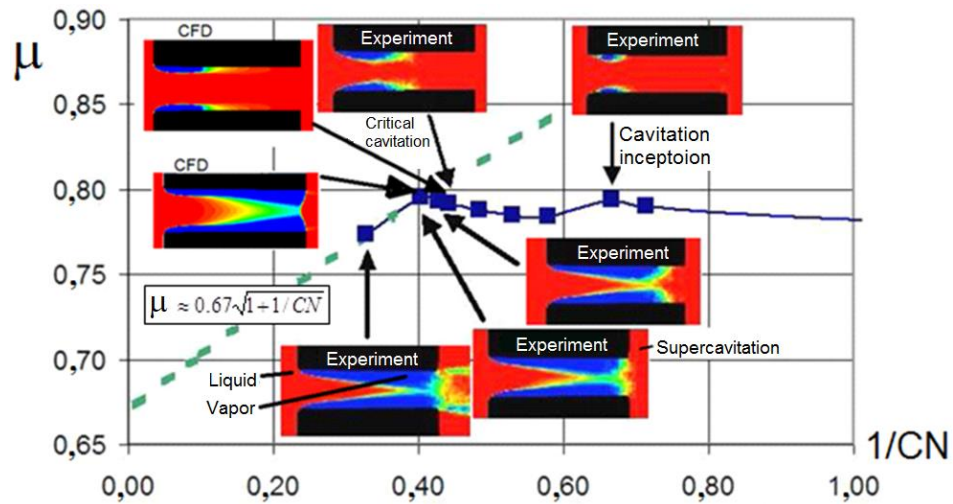


Fig. 2.21. Coefficient of discharge and visualization of a flow

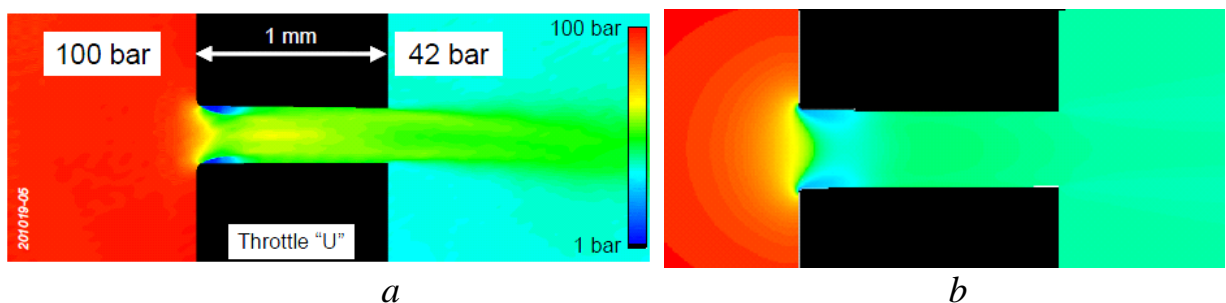


Fig. 2.22. Pressure distribution in a flow at the absence of cavitation: *a* - result of experiment [179]; *b* - result of simulation (this study)

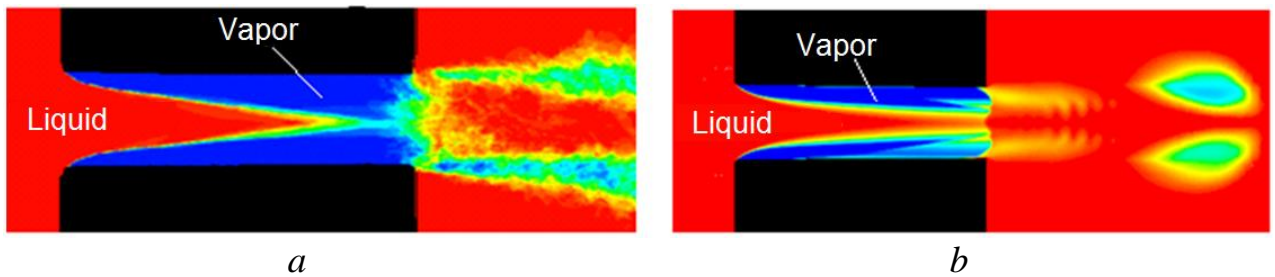


Fig. 2.23. Visualization of phases distribution in a flow at supercavitation: *a* - result of experiment [179], *b* - result of simulation in this work

Fig. 2.22 shows comparison of pressure distribution in a flow at the absence of cavitation and Fig. 2.23 shows visualization of phases distribution in a flow at supercavitation.

According to the data presented in chapter 1, fuel flow rate through a hole becomes independent of outlet pressure (Fig. 2.20) due to flow velocity reaches sound speed in a two-phase medium. It is confirmed by Fig. 2.24 on which

$$M = \frac{v}{a_{liq-gas}}$$

visualization of Mach number distribution is given in the section of the channel at critical value of a cavitation number. It may be seen there is a zone where in whole section Mach number exceeds unit, i.e. flow velocity have reached values of sound speed. At an outlet pressure decrease, the expansion wave does not pass through nozzle section any more, and the flow rate remains invariable.

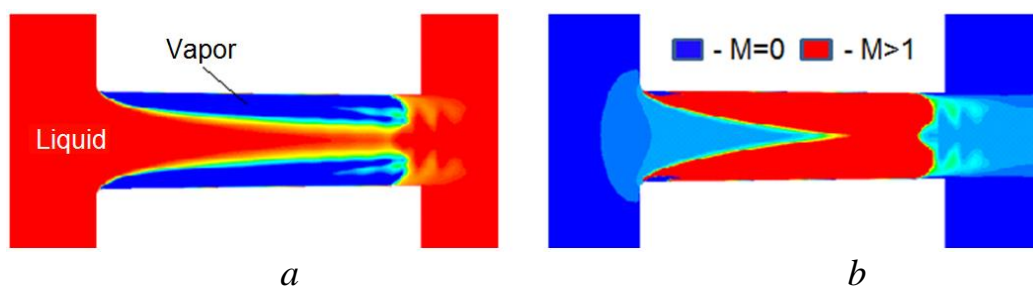


Fig. 2.24. Visualization of phases distribution in a flow (*a*), and *Mach number* (*b*) at critical cavitation

The presented results describe outflow of fuel through a hole into a liquid medium. In chapter 1 it has been noted that process of outflow of liquid in gaseous medium possesses a number of features, among which: entrainment of surrounding gas into the nozzle, substitution of vapor zones by this gas and further formation of

hydraulic flip (Fig. 1.18, *d*). The corresponding experiments were made in many works, including *Soteriou [173]* and *Nurick [159]*. One of experiments of *Soteriou* was carried out for a single cylindrical hole with uniform flow before an entrance to it. The scheme and computational grid for simulation of such flow is presented on Fig. 2.25. For accounting of gas entrainment into the nozzle at simulation three computational phases were used: liquid fuel, vapor of fuel and surrounding gas. As it has been shown in chapter 1, at such flow with low level of turbulence on the inlet of a nozzle hole it is typical the fast formation of total hydraulic flip. Comparison of results of coefficient of discharge depending on a cavitation number is presented on Fig. 2.26, and visualization of computational phases distribution in a flow is also shown. It may be seen that typical flow regimes are reproduced in numerical model. Differences are explained by the insufficient exact data about experiment statement (exact geometry of the channel before nozzle hole inlet, radius of an inlet edge of a hole, fuel properties).

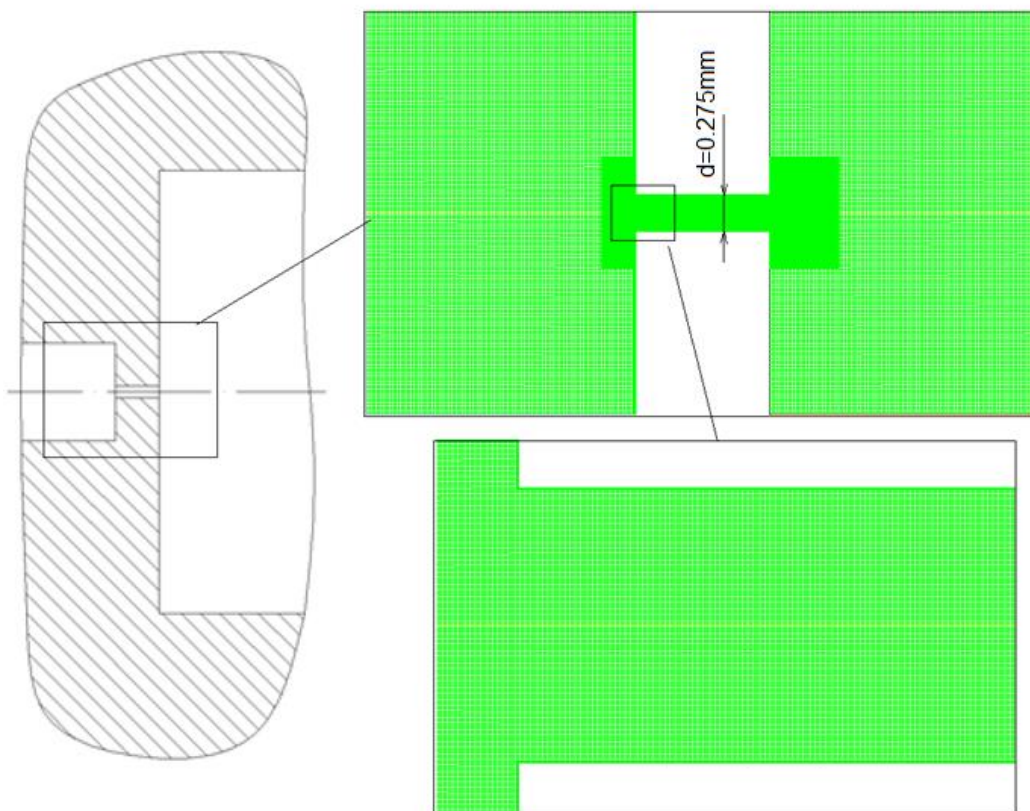


Fig. 2.25. Scheme and computational grid for simulation of outflow through a single nozzle hole

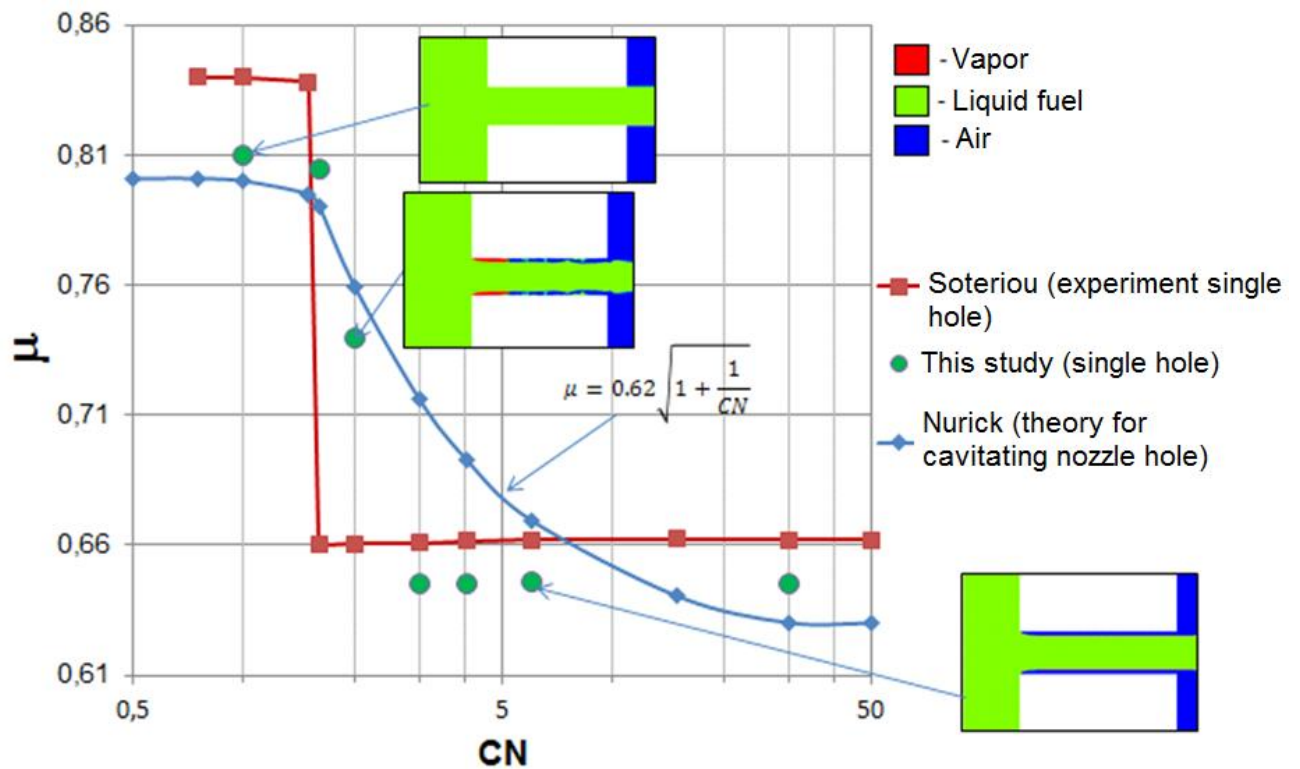


Fig. 2.26. Comparison of calculated values of discharge coefficient with the experimental and theory data and visualizations of a flow

2.5. Simulation of break-up and evaporation of the jets produced by nozzle holes of injectors

For simulation of a jet formation by the nozzle hole computational domain consists of in-cylinder zone. For conventional nozzle geometry, such as a nozzle hole, there is no necessity to simulate the flow in a nozzle hole because it may be described with an adequate accuracy by the semi-empirical models considered in section 2.3 (see Table 2.2). At simulation mass flow rate through the nozzle hole outlet is set as boundary condition. Proceeding from the current value of a flow rate the flow regime is defined and by means of semi-empirical formulas the coefficient of discharge is calculated. Then the velocity and the size of initial droplets are calculated. The transient profile of mass flow rate through the nozzle hole can be obtained from experimental data, or from fuel supply process computation. It is necessary to consider that curve of flow rate through the hole outlet differs from the conventional representation of fuel injection rate profile, especially at the initial stage. For estimation of these differences the simplified

simulation of nozzle hole filling by a fuel has been made. In work [177] results of experiments of fuel injection by nozzle with single hole with diameter of 0,875 mm are presented. According to data [177] fuel reaches outlet of a nozzle hole in 0,43 ms after the beginning of a needle lift. Initial and boundary conditions of an estimating computation are set according the fact that fuel has reached a nozzle hole inlet at the time of 0,4 ms when injection pressure (pressure in sac) was 100 bars (Fig. 2.27, 2.28). From the mass flow rate profile through the nozzle outlet obtained in this calculation (Fig. 2.28, 2.29) it is visible that the actual moment of the injection beginning has a delay and then almost instantly mass flow rate get the value corresponding to injection pressure of 105 bars. The mass flow rate profile of such form is represent actual fuel jet appearance in the cylinder and it have to be set as boundary condition. As it has been noted above, this profile at the initial stage considerably differs from the conventional injection rate profile (Fig. 2.28, Fig. 2.29).

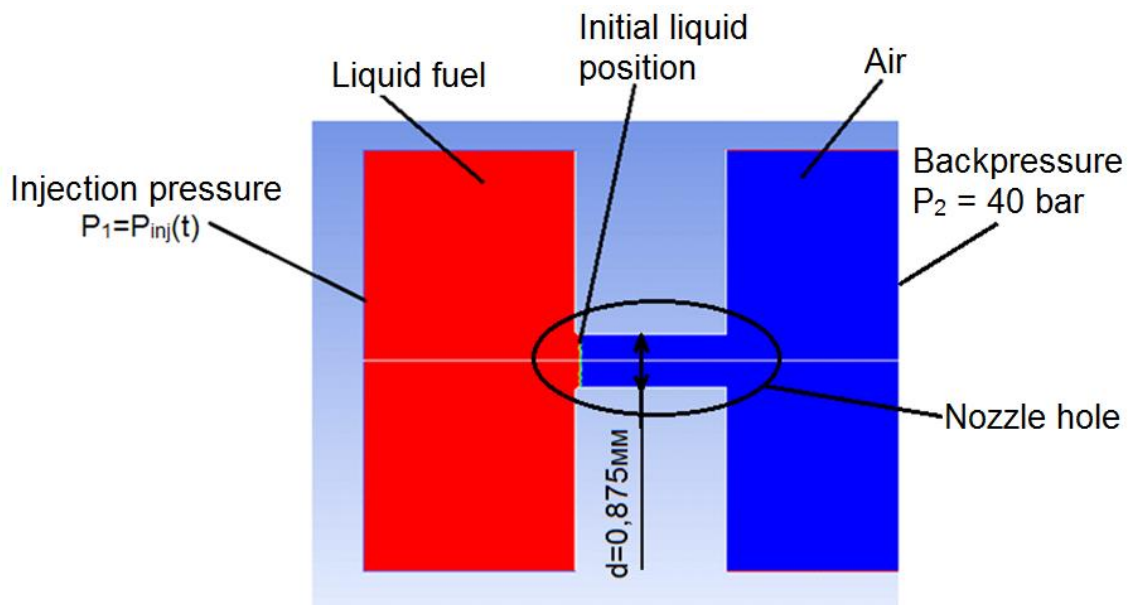


Fig. 2.27. Initial and boundary conditions of estimating simulation of nozzle hole filling by a fuel

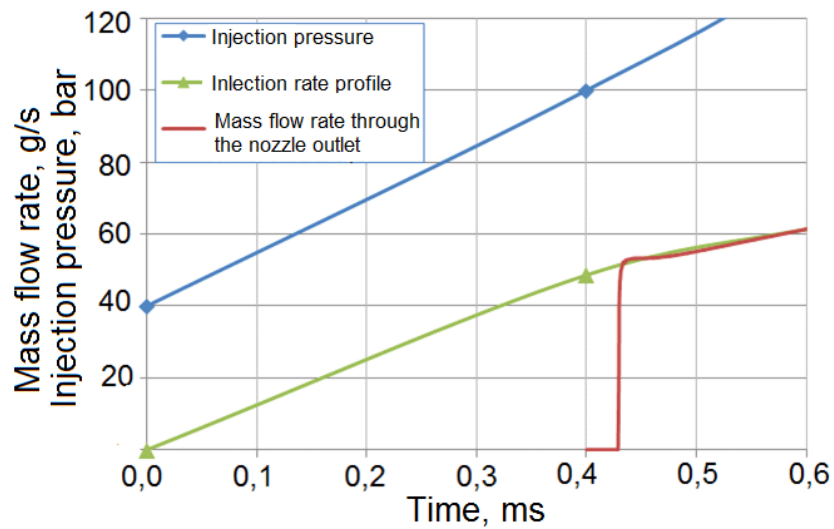


Fig. 2.28. Comparison of conventional injection rate profile and flow rate through the nozzle hole outlet

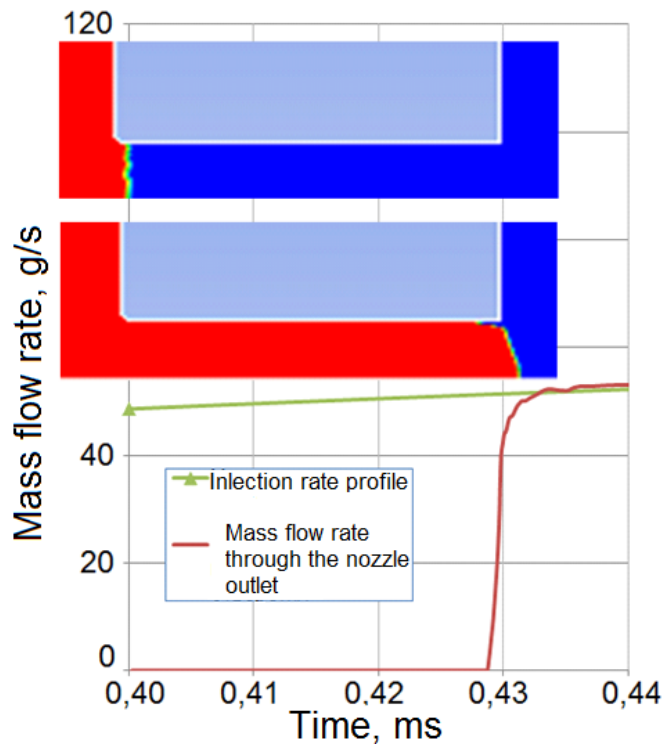


Fig. 2.29. Results of estimating simulation of nozzle hole filling

For correct statement of problem of in-cylinder spray behavior simulation it was performed modeling of injections under pressure of 60 and 160 MPa corresponding described in work [175]. The main conditions of experiments are given in Table 2.4. During adjustment of statement and validation of models it was made investigations of influence of computational grid size, the time step size, the used turbulent model and other parameters and settings.

Basic parameters of problem statement of simulation in different approaches

are specified in Table 2.5 (the options possessing the best qualities for these simulations highlighted in bold type).

Table 2.4.

Conditions of the experiments according to [175]

№	Injector	Quantity of nozzle holes	$P_{inj, max}$, MPa	Backpressure p_c , MPa	Gas temp., K	Gas-fuel density ratio	d , mm	L , mm	r , mm	Fuel temperature, K	Evaporation
1	<i>Delphi DF11.3 VCO</i>	7	60	2	410	0,0227	0,135	1	-	410	no
2	<i>Bosch VCO</i>	1	160	4	580	0,0360	0,200	1	-	490	insignificant

Note: "-" - data are absent

Table 2.5.

Features of problem statement and used models

Parameter of statement	Value
Dimension of statement	1. 2D (axisymmetric) 2. 3D
Time dependence	Transient
Dimensions of a computational domain	350 mm in the axial direction, 60 mm in radial
Energy equation	Enabled
Description of density of continuous medium	Ideal gas law
Properties of substances	Dependence on temperatures at value of cylinder pressure
Turbulent model	1. <i>RNG $k-\epsilon$</i> 2. Realizable $k-\epsilon$ 3. <i>Reynolds Stress model</i> 4. <i>Large Eddy Simulation (LES)</i>
Mass transfer	<i>Species transport model</i>
Model of the dispersion medium of droplets	<i>Discrete Phase model (DPM)</i>
Type of dispersion particles	Evaporating droplets
Evaporation model	1. <i>Diffusion controlled</i> 2. Convection/Diffusion controlled
Model of collision/coalescence of droplets	1. Enabled 2. Disabled
Model of jet primary break-up	1. Plain orifice atomizer 2. Initial droplets with a specified size
Inlet edge radius for <i>Plain orifice atomizer</i> model	1. $r=30\text{micron}$ (single-phase flow) 2. $r=10\text{micron}$ (cavitating flow) 3. $r=1\text{micron}$ (hydraulic flip)
Model of a droplets secondary break-up	1. Kelvin-Helmholtz - Rayleigh-Taylor (KH-RT) 2. <i>Wave</i> 3. Disabled
Drag of droplets	<i>Dynamic drag model</i>
Turbulent dispersion of droplets	<i>Stochastic tracking</i>
Size of computational grid cells, mm	0,4 0,2 0,1 For LES: 0,3 0,15
Time step size / particle Time step, microsecond	Collision/coalescence model disabled 0,5 (0,5) 0,25 (0,25) Collision/coalescence model enabled 0,5 (0,1) 0,5 (0,05)

In work [175] it is mentioned that the injection velocity profile $U_{inj}(t)$ obtained by use of injection rate $Q(t)$ as follows:

$$U_{inj}(t) = \frac{Q(t)}{\rho_l A_0 i_c}, \quad (2.64)$$

where A_0 - the geometrical sectional area of a nozzle hole; i_c - number of holes; ρ_l - density of a liquid DF; $Q(t)$ - injection rate profile. In [175] it is noted that for evaluation of U_{inj} jet contraction due to cavitation was not considered. Proceeding from these data, the injection rate profile has been recovered (Fig. 2.30) for a case №.1 of Table 2.4. It was also obtained the curve of mass flow rate through a nozzle hole outlet at an assumption that fuel reaches an outlet when injection pressure (before nozzle holes) is about 15 MPa.

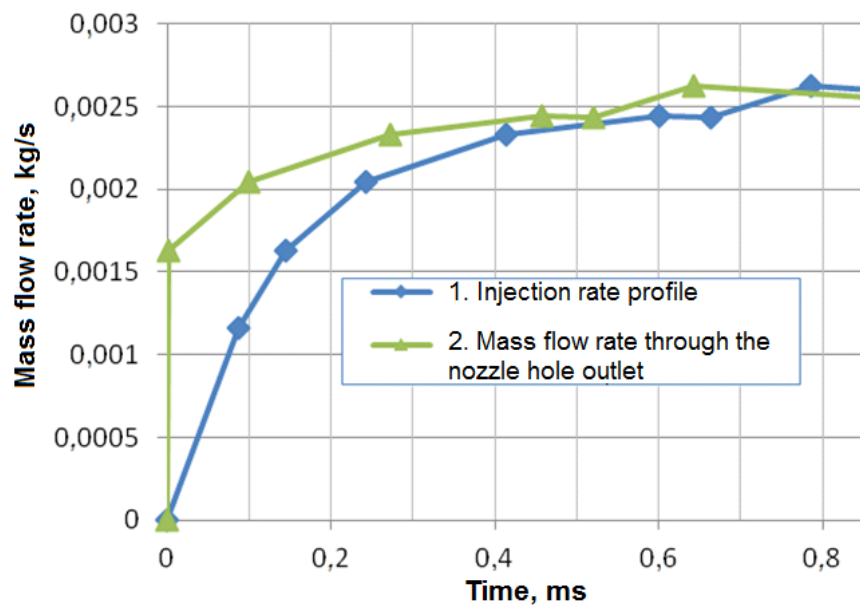


Fig. 2.30. An injection rate profile and mass flow rate through a nozzle hole outlet for injector No. 1 of Table 2.4

On Fig. 2.31 comparison of the experimental data and results obtained using of a different type of profiles from Fig. 2.30 as boundary condition is presented. Fig. 2.31 contains also results of simulation without use of droplets secondary break-up model. Experimental results on Fig. 2.31 are presented with the $\pm 10\%$ error of measurements according to [175]. From Fig. 2.31 it is visible that use of an injection rate profile as boundary conditions causes delay of dynamics of jet penetration at the initial stage, and refusal of use of droplets secondary break-up

model from some instant makes overestimation of a spray tip penetration. The second fact may be explained by insufficient droplets break-up and, as a result, preservation of the greater part of a jet impulse.

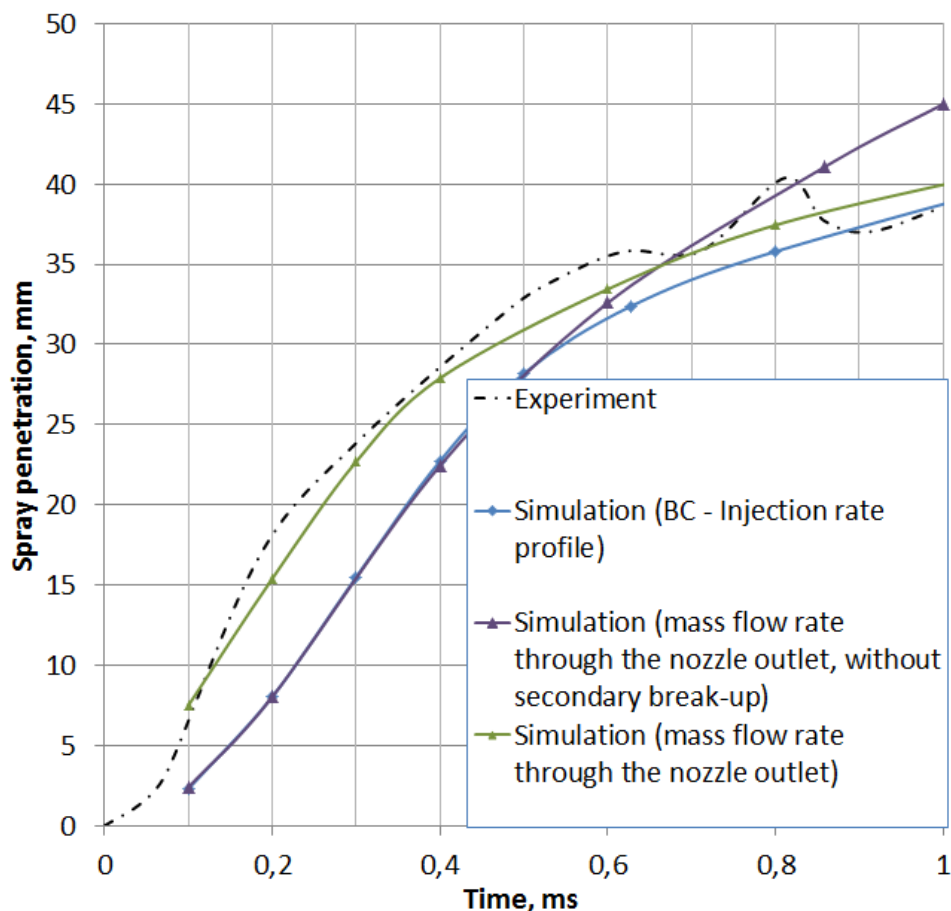


Fig. 2.31. Results of computation of a spray tip penetration at different input data for injector No. 1 of Table 2.4

Let's note that the results obtained with specification for boundary condition of injection rate profile have the nature close to results of numerical simulation of work [175]. Fig. 2.32,*a* shows a comparison of visualizations of a spray in an instant of 0,5 ms after start of injection with an experimental photo and with a result of simulation in work [175]. Fig. 2.32,*b* shows visualization of results of *3D LES*. The results obtained by *3D LES* can be considered as the most precision that is explained by smaller quantity of assumptions (in particular, about an axisymmetric) and more detailed simulation of turbulence. But also the results obtained in two-dimensional axisymmetric statement too rather exact (in particular on characteristics of spray tip penetration and Sauter mean diameter) and can be

obtained with considerable economy of computational and time resources. Therefore mainly axisymmetric statement was applied to further researches.

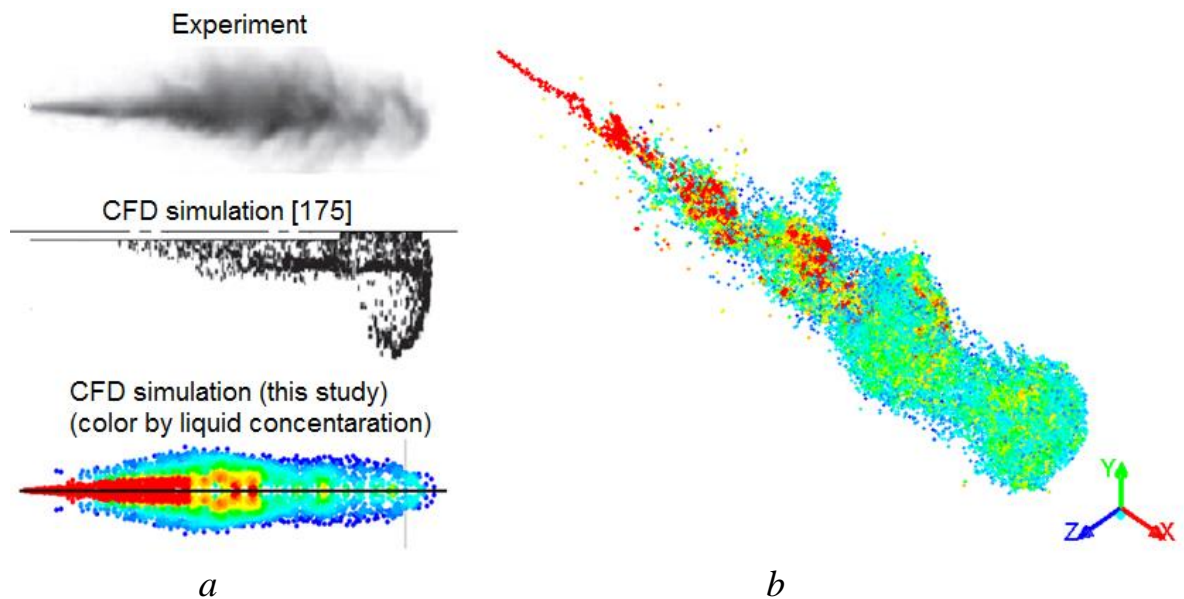


Fig. 2.32. Visualization of a spray at 0,5 ms after SOI for injector No. 1 of Table 2.4: *a* - comparison with experiment and simulation of [175]; *b* - visualization of 3D LES results

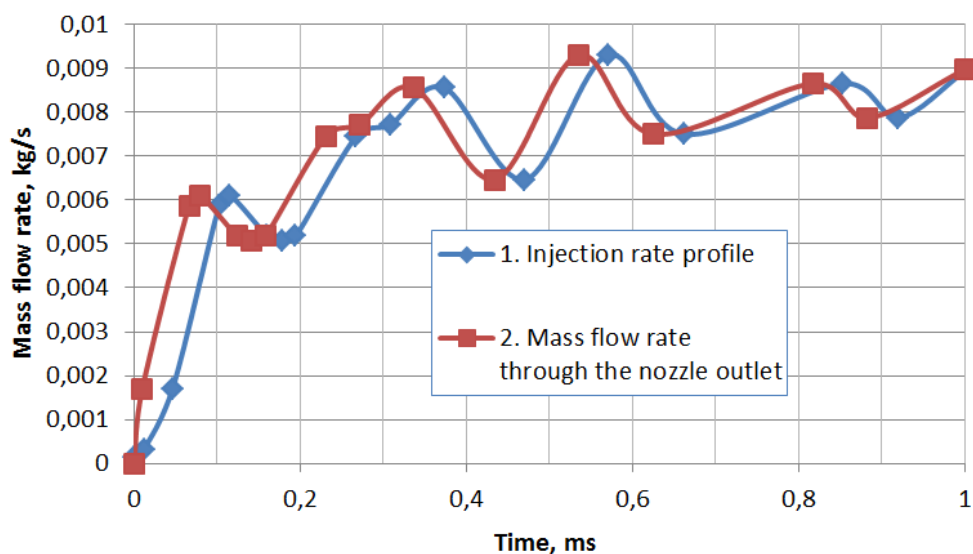


Fig. 2.33. An injection rate profile and mass flow rate through a nozzle hole outlet for an injector No. 2 of Table 2.4

Similar approach with nozzle outlet flow rate specification as boundary condition has been applied also to the second case (No. 2, Table 2.4). The injection rate profiles corresponding to work [175] and mass flow rate through a nozzle hole outlet are presented on Fig. 2.33.

Results of simulation of spray tip penetration dynamics at assumptions that the flow through a nozzle hole could be cavitating or flipped are presented on Fig. 2.34. It has been noted above that the flow regime in *plain orifice atomizer* model is defined proceeding from the current value of Reynolds numbers Re and cavitation number K for given geometry parameters. Therefore to influence a flow in a nozzle hole and force a different regime, value of an inlet edge radius of a nozzle hole varied (Table 2.5). From Fig. 2.34 it is visible that for the cavitating flow penetration of spray is lower and for hydraulic flip is larger. In case of cavitating flow the results may be explained by the fact that vapor bubbles intensify a jet break-up, cone angle of a spray become wider and droplets become smaller, therefore the axial component of an momentum is lost quicker. In case of hydraulic flip the contraction of a jet in the nozzle hole becomes maximal. As a result mass of fuel arrives through narrower cross-section, but with higher velocities. At the same time a flow much more smooth in comparison with cavitating flow because fluctuating vapor bubbles completely were substituted with air from the cylinder and a jet has the steady form.

It should be noted that the inlet edge radius predetermines also the moment on the mass flow rate profile (exact value of injection rate) when the flow transformed from single-phase into cavitating. Proceeding from an experimental curve on Fig. 2.34 it may be assumed that cavitation occurs an instant of 0,3 ms and by the time of 0,5 ms it has already significant influence on a jet break-up.

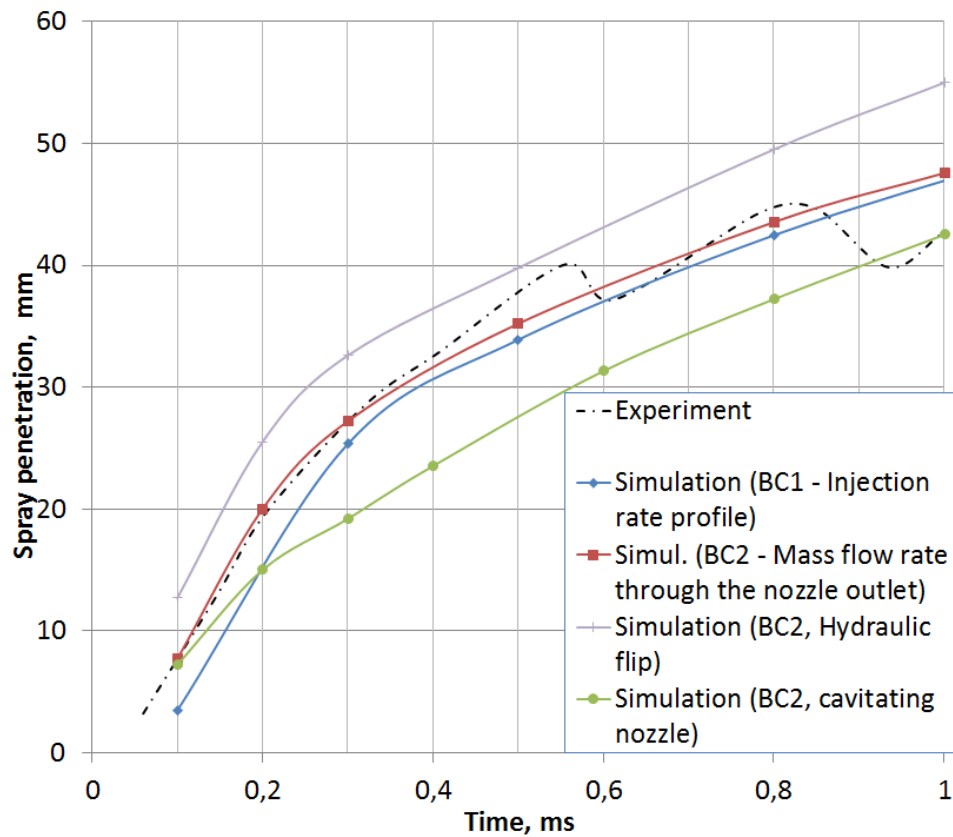


Fig. 2.34. Results of computation of a spray tip penetration at different input data for injector No. 2 of Table 2.4

The experiments considered in Table 2.4 are carried out in the absence of evaporation therefore results are given for a short time interval (1 ms). Simulation of long-range jets for a bigger time interval and accounting of evaporation impact on a spray tip penetration is also interesting. For this purpose, simulation of behavior of the spray produced by a marine diesel coaxial injector with single nozzle hole, corresponding to conditions in work [177] has been made. The main conditions of carrying out experiments are given in Table 2.6. Results of simulation of spray tip penetration for conditions No. 1 of Table 2.6 at different input data are shown on Fig. 2.35. On this figure time is represented in coordinates of a crank angle of a marine diesel with rotating speed $n=114$ rpm. It is visible that at an assumption about a single-phase flow regime in a nozzle hole (without cavitation) and with use as boundary condition of an injection rate profile results of simulation much more underestimate spray tip penetration in comparison with experiment.

Table 2.6.

Conditions of the experiments [177]

N_0	Number of nozzle holes i_c	$P_{inj\ max}$, MPa	Ambient gas	Gas temperature, K	Gas density, kg/m^3	Swirl	d, mm	L, mm	r, mm	Evaporation
1	1	100	Air	400	33.7	1. Yes 2. No	0,875	3,55	no design rounding	no
2			Nitrogen	900		Yes				Yes

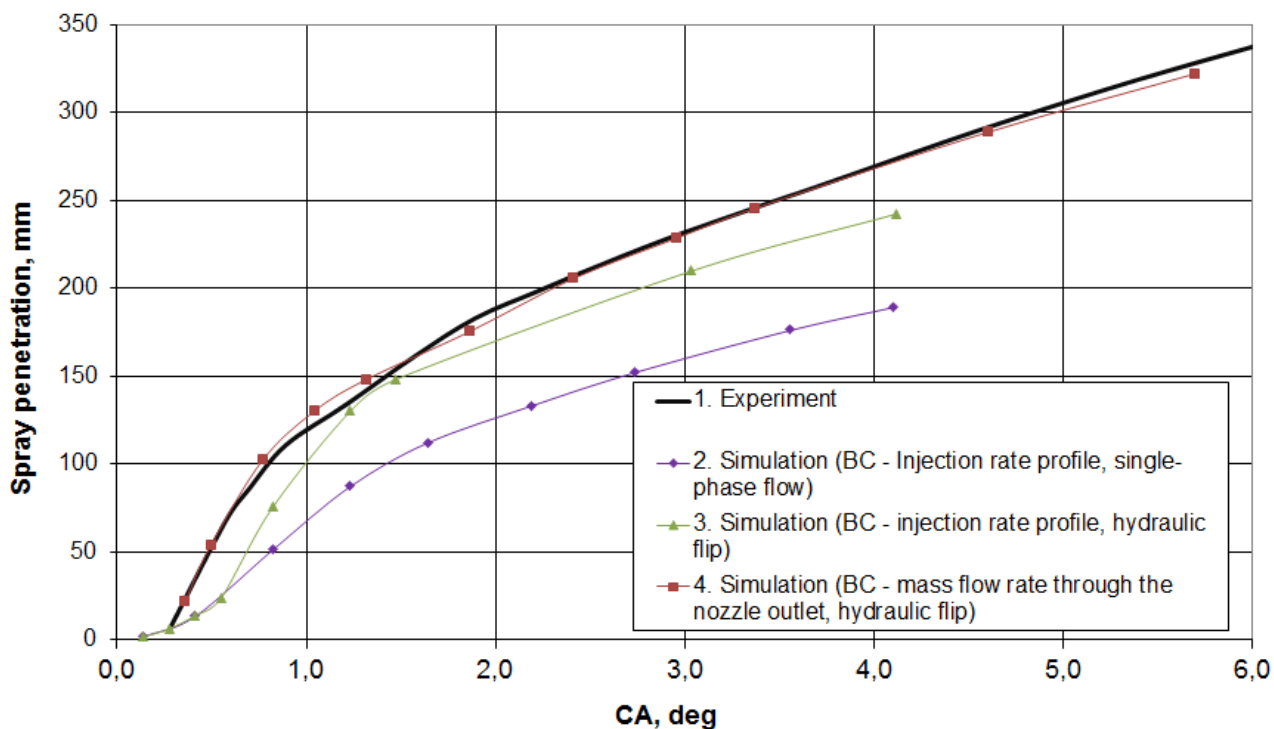


Fig. 2.35. Results of computation of spray tip penetration at different input data for conditions No. 1 of Table 2.6

Continuation of nozzle hole filling simulation (see Fig. 2.27-2.29) shows the cavitation development and substitution of vapor zone by surrounding gas soon. In chapter 1 it has been noted that total hydraulic flip is typical of coaxial nozzles with single nozzle hole. Result of simulation for a hole with inlet edge radius $r=20$ microns are presented on Fig. 2.36. In this case flow regime in the nozzle hole transforms to the hydraulic flip at pressure value of 330 bars. For much smaller or absent of rounding radius hydraulic flip occurs at much smaller pressure. At $r=1$ micron this "critical" pressure becomes about 140 bars (such value of r is accepted for the further calculations of spray behavior corresponding to Table 2.6 conditions).

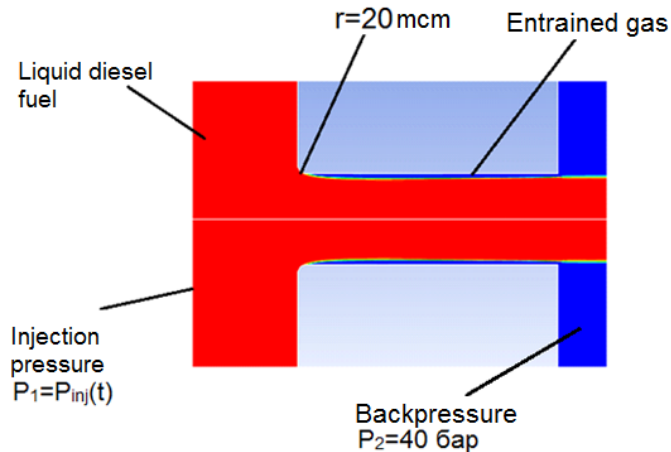


Fig. 2.36. Total hydraulic flip in a hole with diameter $d=0,875\text{mm}$ of a coaxial nozzle

Curve on 3 Fig. 2.35 shows that after transition of a flow to hydraulic flip (time corresponds 0,5 CA deg.) slope angle of this curve is close to slope angle of an experimental curve. Experimental curve 1 on Fig. 2.35 has such slope angle from the outset because while fuel has reached the nozzle hole outlet (0,43 ms after the beginning of a needle lift [177]) injection pressure has increased up to "critical" level and the flow has almost instantly separated from walls. The curve 4 is obtained by setting inlet edge radius of $r=1$ micron and the nozzle hole outlet flow rate profile at an assumption that fuel reaches a nozzle hole outlet when injection pressure becomes 140 bars at time of 0,43 ms (0,3 CA deg.).

In work [177] the explanation is given that sensors which were used for spray measurements have limited sensitivity to concentration of particles in a cloud (spray transparency), that is concentration below a certain level were not caught by sensors. Fig. 2.37 shows comparison of experimental picture of a spray with visualizations of simulation results at different concentration threshold (particles in zones with concentration of fluid below the threshold level were not displayed). It may be seen that the greatest correspondence with experimental picture have a visualization with concentration of fluid higher than 2 kg per 1 cubic meter of gas. In this case there is a good coincidence to experimental data on a spray angle at distance $75d$ from an injector. In work [177] such part of a spray that may be distinguished by sensors is called dense core. It is noted that for experimental

Fig. 2.38. In work [177] results are obtained only up to 2,2 CA deg. Obviously it is connected with the fact that sensitivity of sensors did not allow to distinguish areas with lower concentration of droplets. At the same time numerical simulation allows to track the position even of a single droplet. So Fig. 2.38 shows the maximum axial coordinate of such droplet which completely evaporates only at distance of 319 mm from an injector. It is often important to determine areas which cannot be reached by droplets in the conditions of evaporation or to provide absence of cylinder wall hitting by droplets. In such cases the numerical simulation can be more convenient and even more precision tool, than experiment.

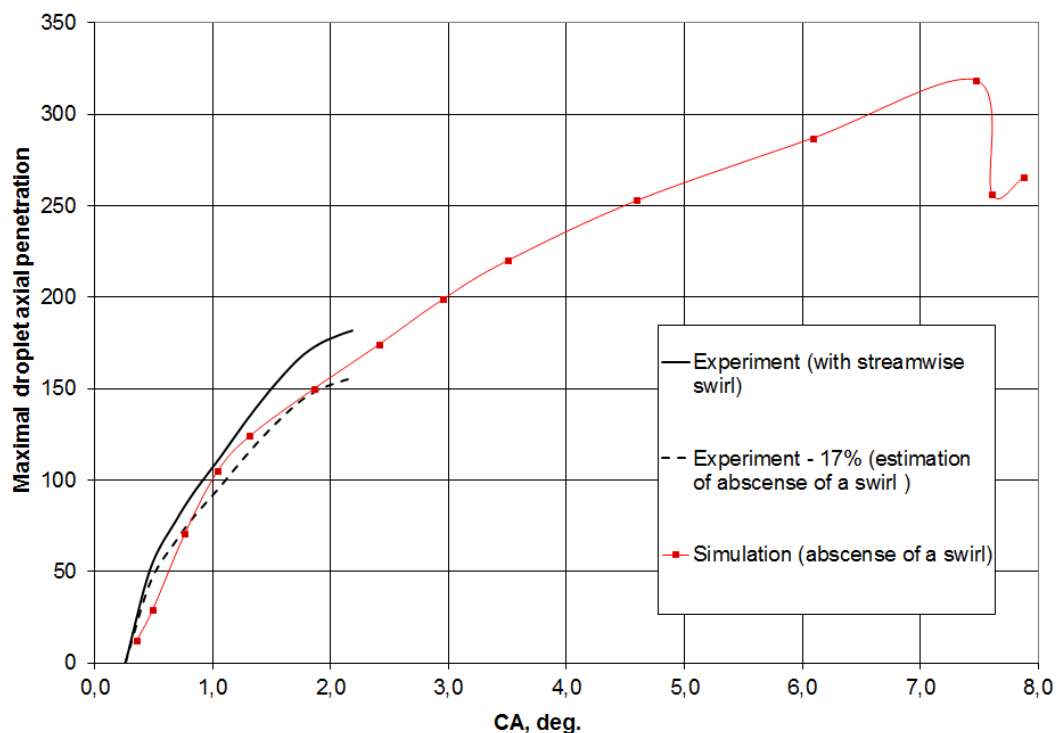


Fig. 2.38. The maximal penetration of droplets in the conditions of evaporation (case No. 2, Table 2.6)

Results of a spray dense core penetration are presented on Fig. 2.39. It has been noted above that dense core at simulation according to experiment is the cloud of droplets with concentration of fluid more than 2 kg per cubic meter of gas.

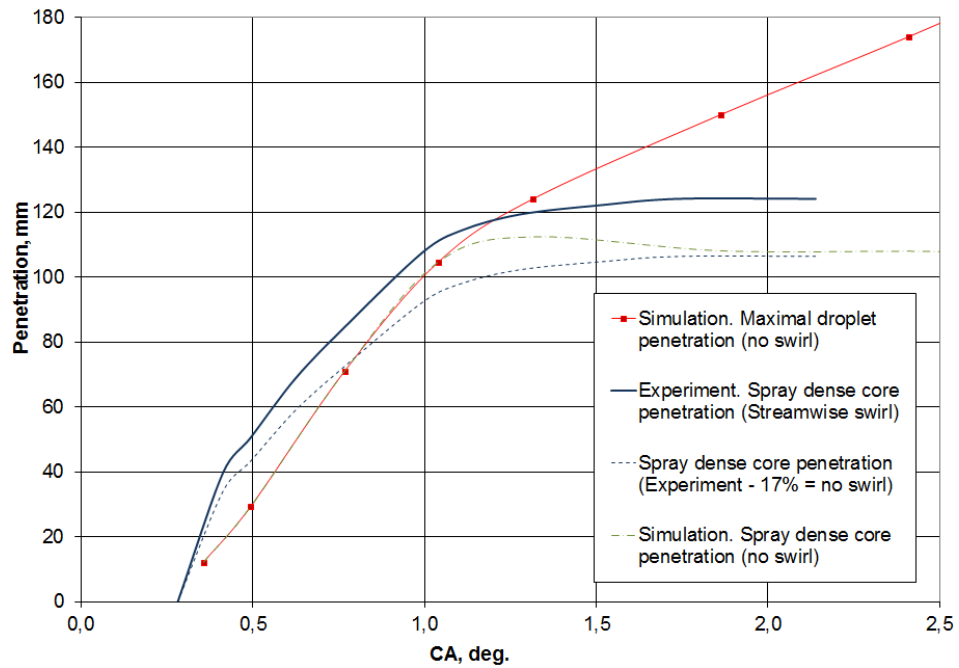


Fig. 2.39. Spray and droplet penetration in the conditions of evaporation (case No. 2 of Table 2.6)

Calculation of the droplets size is also important task. On Fig. 2.40 it is presented the dependence of SMD on the spray axis at distance of 30 mm from an injector obtained with use and without use of droplets collision/coalescence model for conditions No. 1 of Table 2.4. In work [175] it is shown that in the specified spray point SMD is established about value of 10 microns at 0,8 ms after SOI. Thus including of collision/coalescence model allows to obtain more exact results. On the other hand, use of this model has considerable limitations in *the ANSYS FLUENT* and it cannot be used for simulation of injections under high pressure [117]. So it was succeeded to use this model for injection with pressure 60 MPa (case No. 1 of Table 2.4) with significant increase of simulation time and for case No. 2 of Table 2.4 use of model was impossible.

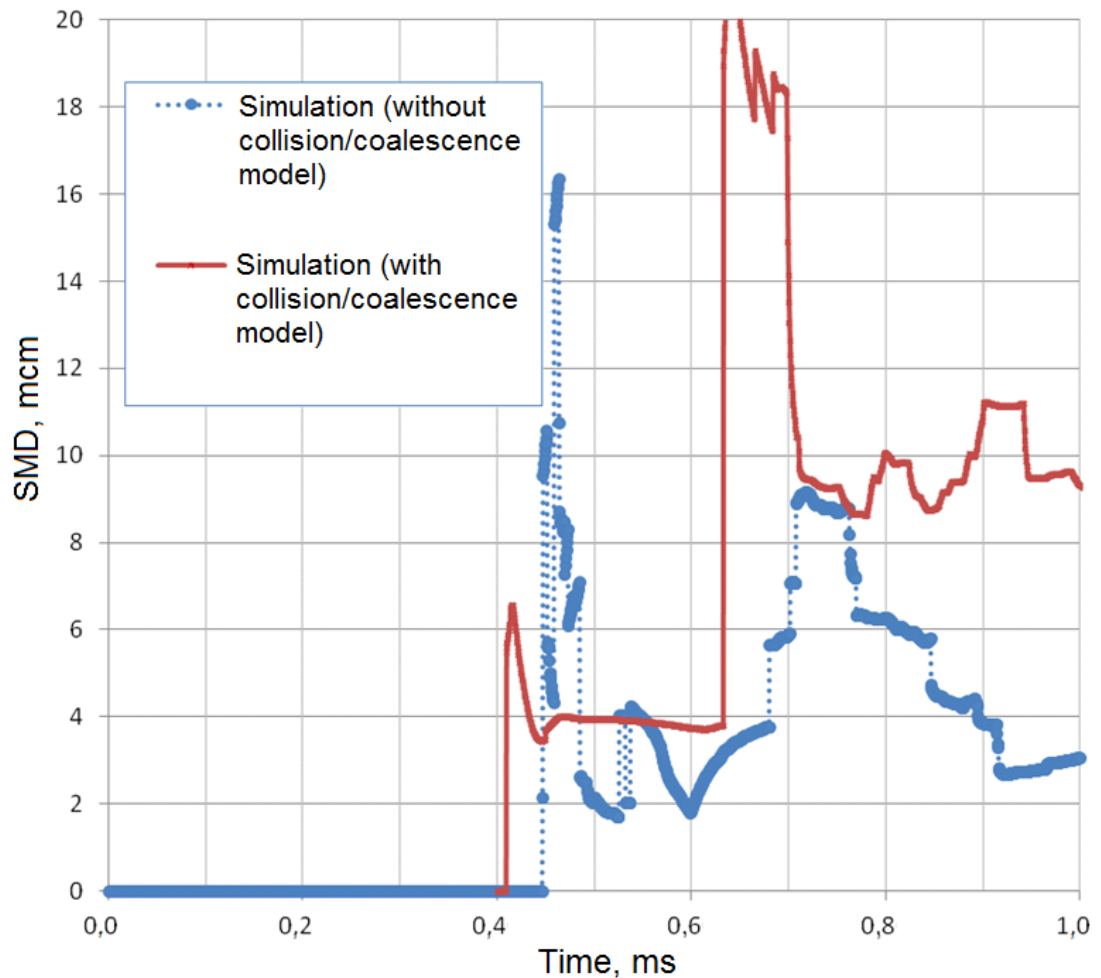


Fig. 2.40. SMD on spray axis at distance of 30 mm from an injector obtained by use of different models

2.6. Simulation of a fuel flow in a pintle nozzle

For simulation of a flow in a pintle nozzle it was created the computational model similar to presented in work *Ming Jia et.al.* [140]. In this work the steady-state simulation of fuel injection into liquid at the maximum pintle lift has been conducted. Inlet pressure in a computational domain was set equal 500 bars, outlet pressure - 1 bar. On Fig. 2.41 the sketch of a nozzle and a computational domain are shown, on Fig. 2.42 comparison of results of simulations is given. Results of simulation of a fuel injection into gas are also presented on Fig. 2.42.

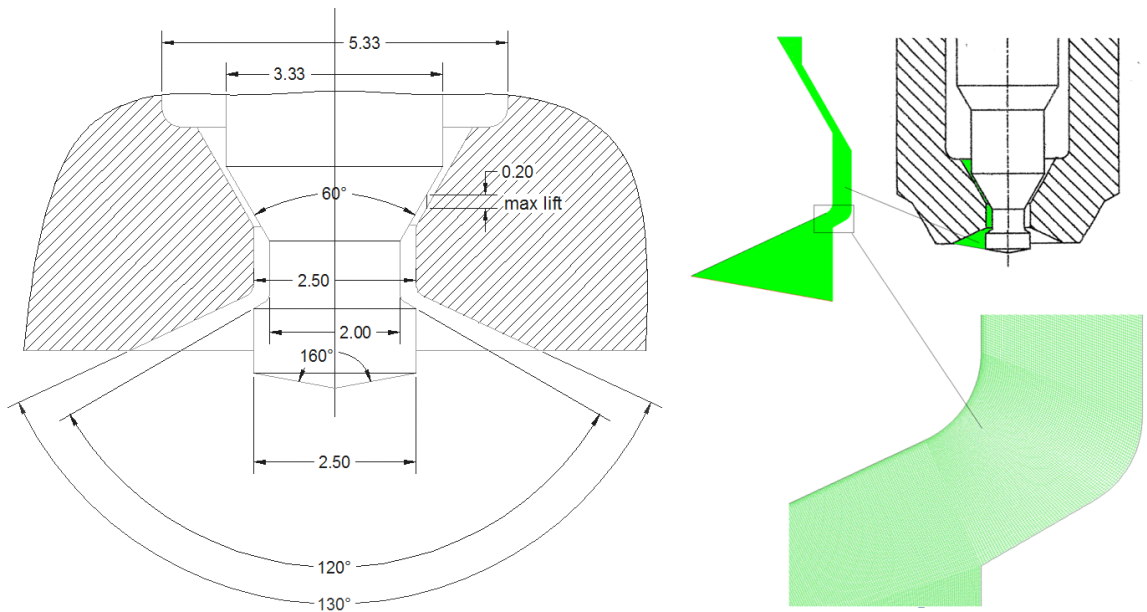


Fig. 2.41. Sketch of a nozzle and computational domain

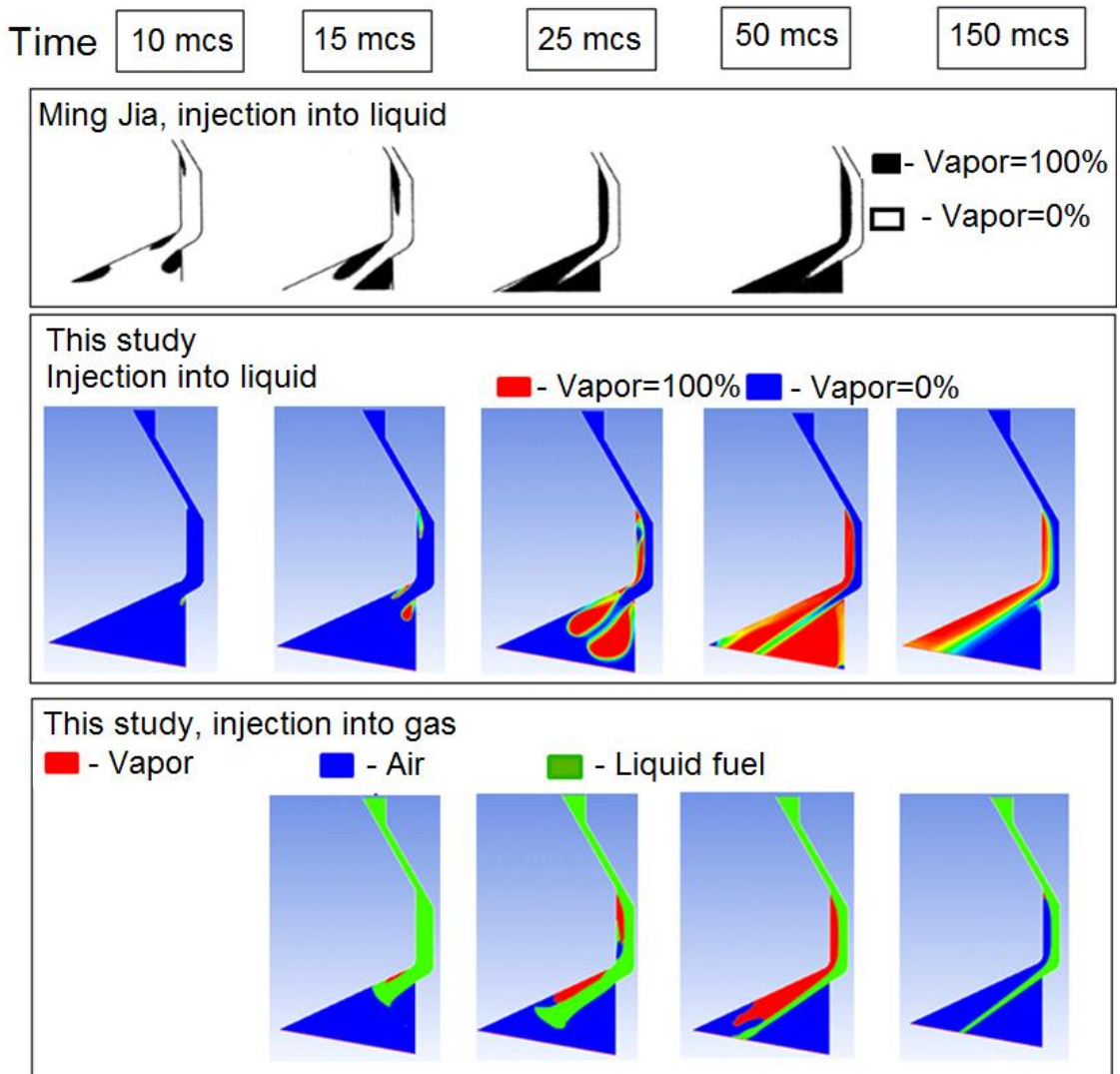


Fig. 2.42. The results of computational phases distribution obtained at simulation of Ming Jia [140] and in this work

From Fig. 2.42 it may be seen a good correspondence of simulation results of injection into liquid obtained in this work and in work [140] until the time of 50 microseconds. In work [140] the assumption is made that to this instant the flow was established. Really, if as criterion of a steady flow to consider a flow rate (Fig. 2.43) then a similar conclusion is justified. However forming of a flow by this moment is not finished yet and the field of vapor volume fraction distribution is established only by the time of 150 microseconds (Fig. 2.42). It is also possible to note that when accounting air environment (injection in gas) the flow pattern considerably differs. The main difference is that by the time of forming of a steady flow the vapor area is completely substituted with air and the flow with a partial hydraulic flip is produced.

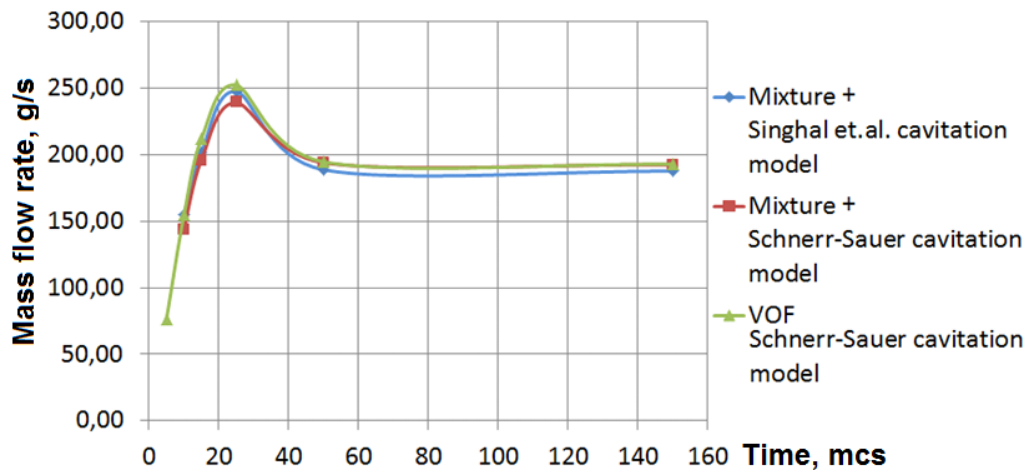


Fig. 2.43. Comparison of simulations results obtained by use of different models

In section 2.3 it has been noted that the fullest model of the cavitation considering surface tension and the gases dissolved in liquid is the *Singhal et.al full cavitation model*, but also are noted its shortcomings and limitations on application. In particular, this model may be combined only with *Mixture* model of multiphase medium and cannot be used for simulation of moving objects. For the exact description of interphase boundaries, simulation of the pintle movement and an analysis of jet primary break-up it is necessary to use *Volume of fluid (VOF)* model of a multiphase medium (see section 2.3). Fig. 2.43 presents the comparison of results on nozzle outlet flow rate obtained by use of combinations of these models. From these data it is visible that results differ slightly and for further

researches *VOF* + *Schnerr-Sauer* combination can be used. This set possesses the best combination of qualities for the solution of the considered tasks.

Results of Fig. 2.42 are obtained when using *RANS* approach of turbulence simulation with *Realizable-k-ε* model. Above in section 2.3 it has been noted that for describing of jets break-up it is necessary to use more global approach, such as the hybrid *DES* method. Fig. 2.44 presents comparison of visualizations of liquid volume fraction distributions at time of 50 microseconds obtained by use of different approaches to the turbulence modeling. It is visible that generally flow pattern is identical. It will be shown below that integral characteristics such as flow rate differ slightly. However use of *RANS* method does not allow to describe the actual shape of interphase boundaries due to the approach of averaging put in this method.

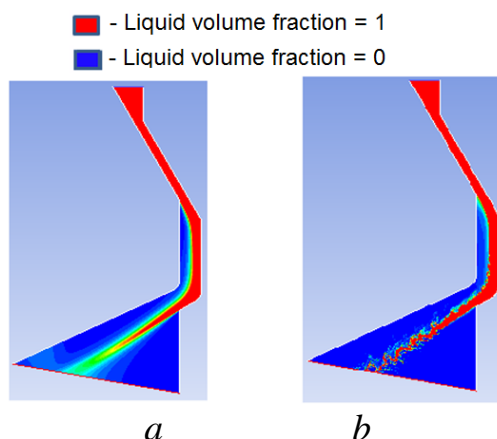


Fig. 2.44. Distribution of liquid volume fraction: *a* - *RANS* method; *b* - *DES* method (*LES+RANS*)

Injection of fuel is non-steady process therefore transient analysis is more demonstrative than results of quasi-steady simulations. Fuel supply process taking into account the pintle movement has been thereby simulated. The pintle lift profile has been obtained in the SP INJECT at an assumption of an invariance of section of the pintle channel (section *exit*, Fig. 2.47). Total pressure on inlet P_{in} is accepted equal to an average for supply duration pressure in a nozzle pocket (1050 bars). The scheme of set of initial and boundary conditions of this model is shown on Fig. 2.45.

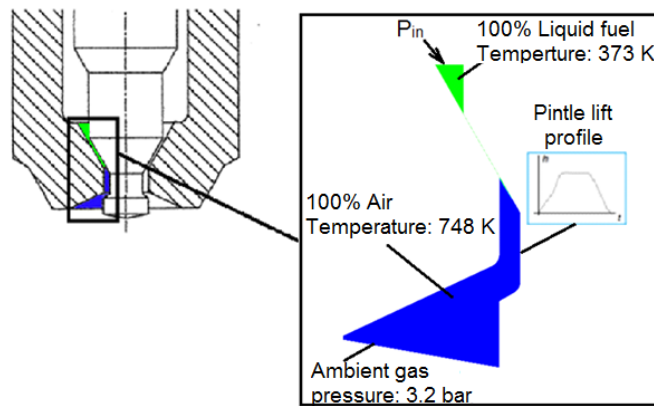


Fig. 2.45. Setting of initial and boundary conditions for simulation of a fuel flow inside the nozzle taking into account the pintle movement

Fig. 2.46 shows computational phases distribution at a stage of pintle lifting up. It demonstrates that dynamics of this distribution has rather difficult character and exerts significant influence on a final shape of a jet. Quasi-steady flow regime is formed in some time after full lift of a pintle - by the time of 150 microseconds. The flow pattern at this moment corresponds well with the results on Fig. 2.42 obtained in steady-state statement with the fixed most lifted pintle. Thus, for obtaining flow parameters in some time after full open of the needle (pintle) the method of steady simulation may be employed. However transient calculation with a dynamic computational mesh is necessary for obtaining of flow dynamics and instant values of velocities and a coefficient of discharge. From Fig. 2.46 it is also visible that jet break-up occurs more intensively in the presence of vapor in a cavity than after its full substitution by air.

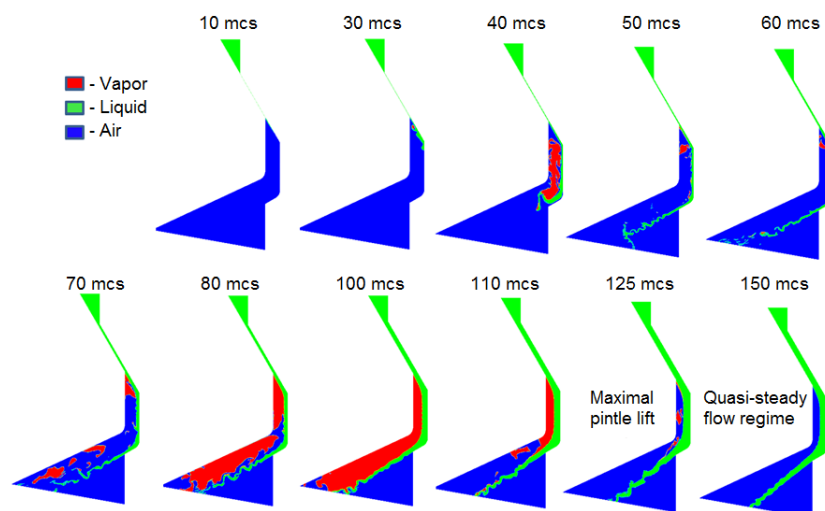


Fig. 2.46. Distribution of computational phases during lifting a pintle up

The typical dimensions for picture of fuel outflow from a pintle nozzle are presented on Fig. 2.47. For the *exit* section the mass flow rate and mass-weighted average velocity histories were recorded. In conventional approach of a fuel supply process computation pressure are defined in the sections located upstream from a clamping cone (in a nozzle pocket) and downstream from a clamping cone in a nozzle sac or before nozzle holes (injection pressure). In this work as the section downstream from a clamping cone was chosen the section *mid* in which mass-weighted average static pressure was recorded.

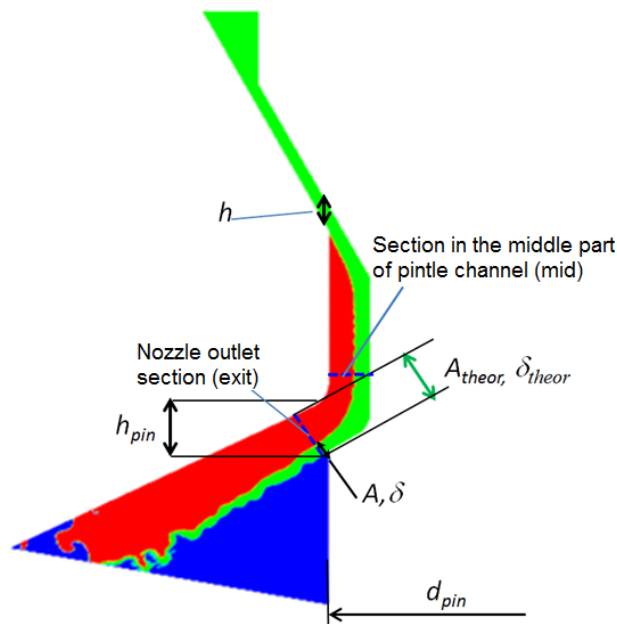


Fig. 2.47. The typical dimensions for process of fuel outflow from a pintle nozzle

The mass flow rate profile through the nozzle outlet (in *exit* section) obtained at different settings of turbulent modeling are presented on Fig. 2.48. It should be noted that accounting of the member of viscous dissipation (heating on friction) in the energy equation does not influence flow rate characteristics. However it can matter for the description of a liquid thermal condition and sound speed at higher injection pressure (more than 200 MPa).

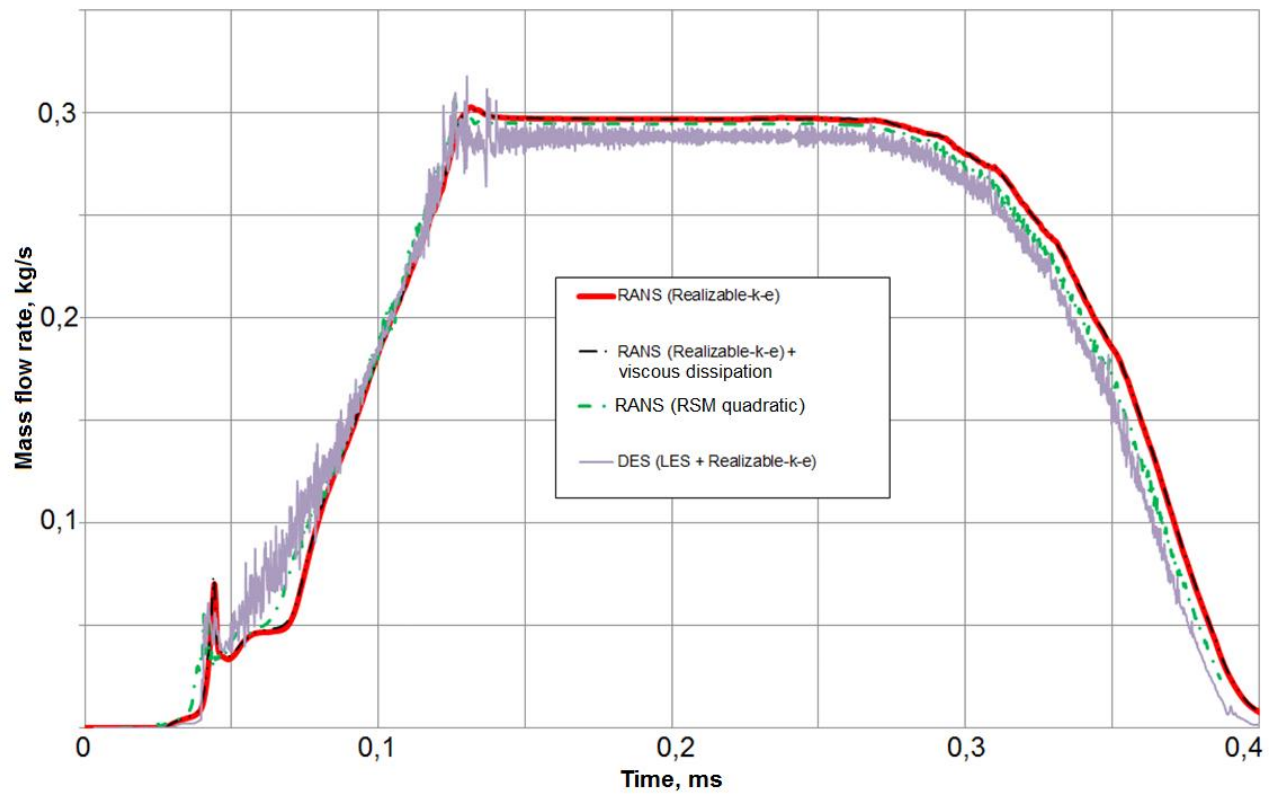


Fig. 2.48. Mass flow rate profiles through the nozzle *exit* section at different settings of turbulence modeling

Fig 2.49 presents comparison of results for pressure in section downstream from a clamping cone (*mid* section) obtained by use of SP INJECT and *CFD* simulation. It may be seen a distinction of these results at a stage of lifting up and lowering of a pintle. They are explained, first of all, by the assumption accepted for calculation in the SP INJECT about invariance of section of the pintle channel (section *exit*, Fig. 2.47). It should be noted that considerable part of section *mid* is occupied by gaseous medium with the low pressure therefore area-weighted average pressure in section is much lower, than mass-weighted. On the other hand, unlike a section in a sac volume of a multi-hole injector, total pressure in section *mid* of the pintle nozzle is much higher than static.

Characteristics of a flow in *exit* section versus time are presented on Fig. 2.50. The coefficient of usage of section *exit* can be defined as follows:

$$C_{exit} = \frac{Q}{\rho_l \cdot A_{theor} \cdot u_{theor}} \quad u_{theor} = \sqrt{\frac{2(p_{in} - p_c)}{\rho_l}} \quad (2.65)$$

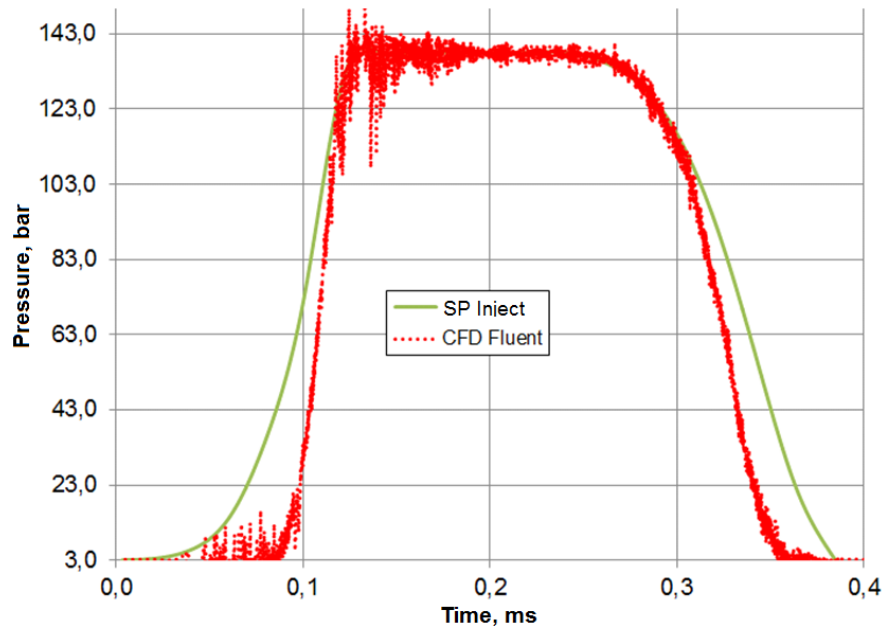


Fig. 2.49. Pressure in a middle part of the pintle channel of a nozzle (in *mid* section)

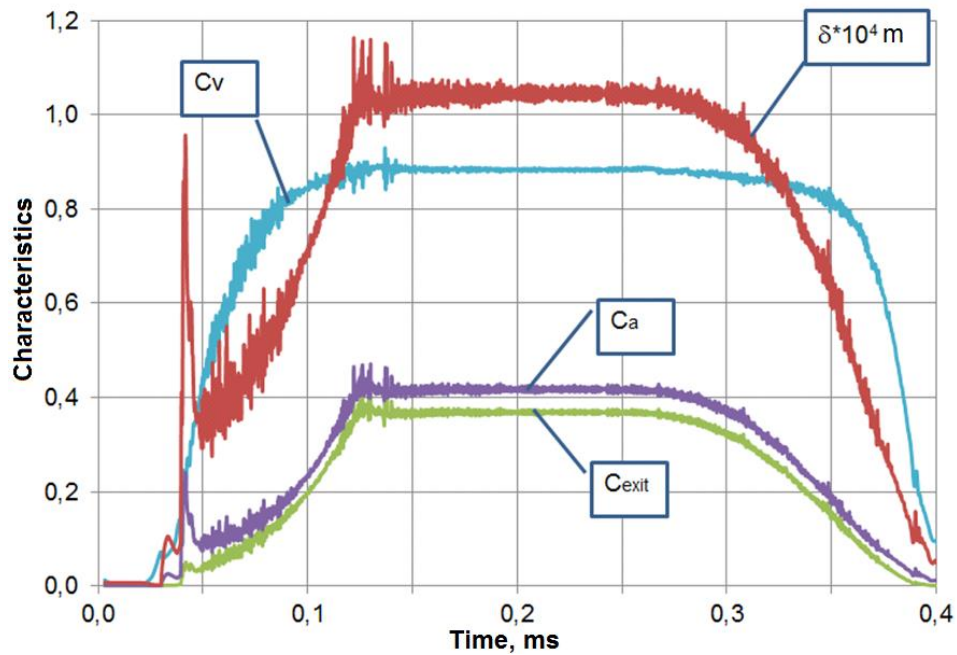


Fig. 2.50. Geometrical and velocity characteristics in *exit* section versus time

Contraction coefficient assumed equal area coefficient C_a , coefficient of velocity C_v and thickness of a jet δ in the section *exit* can be defined as follows:

$$C_a = \frac{A}{A_{theor}} \approx \frac{\delta}{\delta_{theor}} \quad C_v = \frac{u_{eff}}{u_{theor}} \quad \delta = \frac{C_{exit} \cdot \delta_{theor} \cdot u_{theor}}{u_{eff}} \quad (2.66)$$

where flow velocity u_{eff} can be calculated numerically as mass-weighted average velocity in *exit* section. Besides, the coefficient C_{exit} can be used for determination of effective hydraulic diameter:

$$d_{eff} = C_{exit} \cdot d_h = C_{exit} \cdot 2\delta_{theor} \quad (2.67)$$

where $d_h=2\delta_{theor}$ - hydraulic diameter for the nozzles producing a hollow cone spray.

2.7. Simulation of the hollow cone spray

For adjustment of model of spray formation by injectors producing a hollow cone (pintle-type, outward-opening, swirl etc.) there were conducted the simulations of injections under conditions according to the experimental studies. So in work [181] it have been carried out the experimental studies of injection by the pintle nozzle into air with a temperature of 298 K with different backpressures and injection rate profiles. A computational scheme and grid are shown on Fig. 2.51.

At simulation of the spray produced by a nozzle hole (section 2.5) to get data about initial droplets velocities and size distributions it was enough to set the hole outlet mass flow rate profile (because the semi-empirical *plain orifice atomizer* model described in Table 2.2 was used). For the spray produced by nozzles of nonconventional geometry, such as pintle nozzle more general approach is used - in addition to a flow rate through the outlet of a nozzle there were set velocities and the sizes of initial droplets.

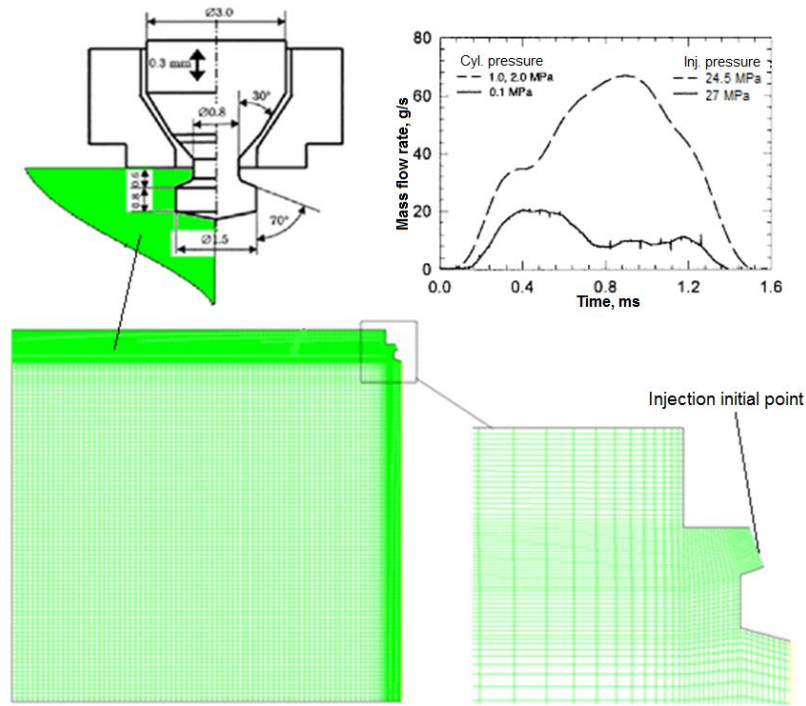


Fig. 2.51. Sketch of a nozzle, injection rate profiles (work [181]) and computational grid

In work [181] the injection velocity (velocity of initial droplets) was defined from equation:

$$u_{eff} = C_d \sqrt{\frac{2\Delta P}{\rho_l}} - C_1, \quad (2.68)$$

where $C_d=0,665$, $C_1=25$ m/s. Both coefficients are obtained experimentally for this nozzle. The initial size of droplets has been accepted equal to jet thickness on outlet of an injector:

$$d_{mit} = \delta = \frac{Q}{\pi \cdot d_{pin} \cdot \rho_l \cdot u_{eff}}, \quad (2.69)$$

where d_{pin} - diameter of a pintle on outlet of an injector (see Fig. 2.47.). Let's note that (2.69) can be obtained also when sharing (2.65) and (2.66). Similar approach to setting of velocities and diameters of initial droplets has been applied to statement of this simulation. Fig. 2.52 presents the comparison of simulations results of this work with experimental data and simulations results of *Obokata et.al.* [181] at backpressure of 0,1 MPa and Fig. 2.53 shows the comparison of visualizations of spray in different instants at backpressure of 1 MPa.

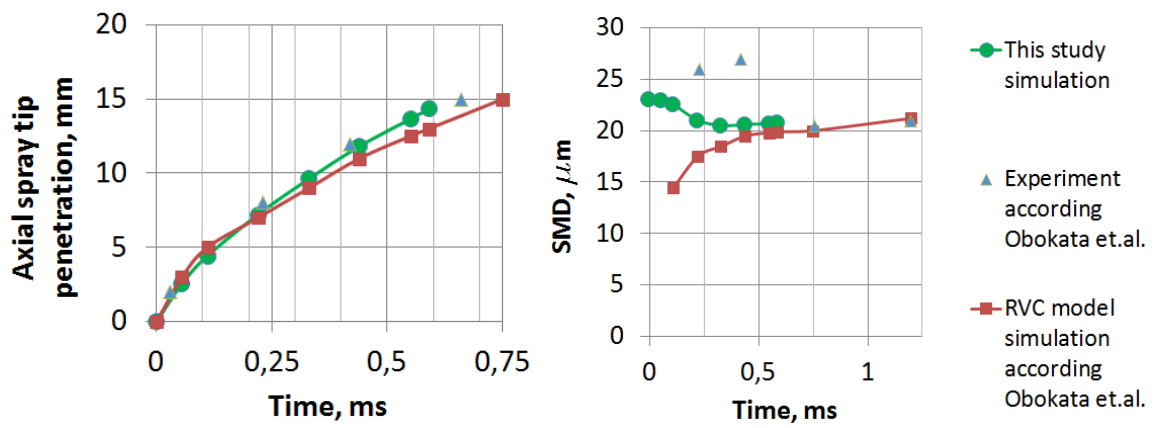


Fig. 2.52. Axial spray penetration and Sauter mean diameter (backpressure 0,1 MPa)

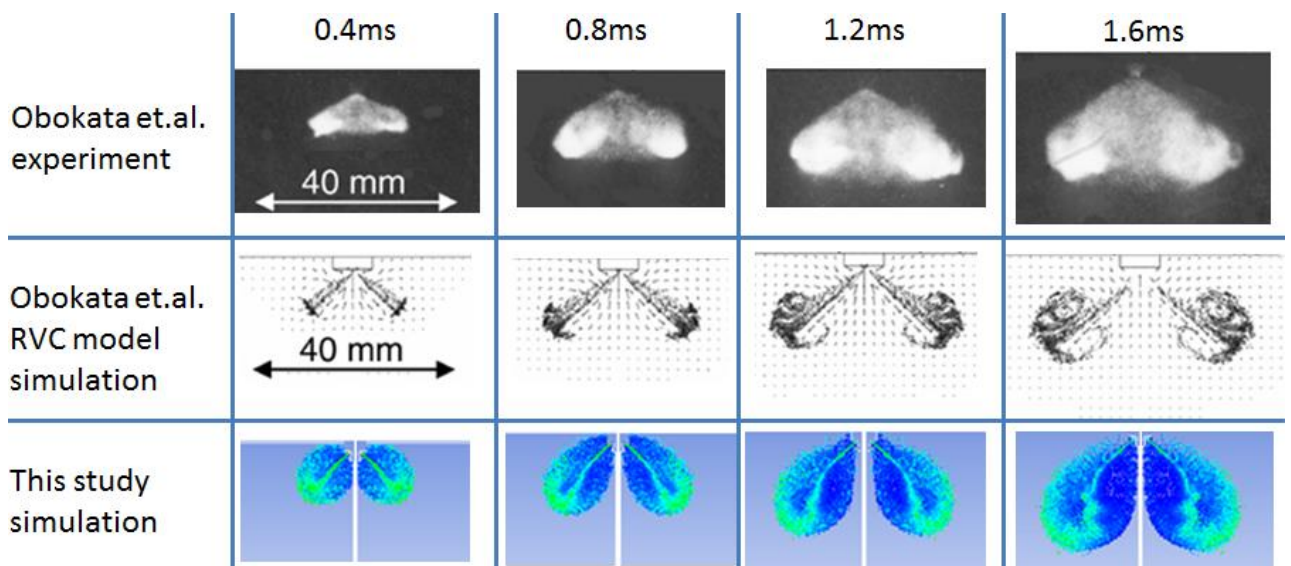


Fig. 2.53. Comparison of visualizations of spray in different time after SOI (backpressure is 1 MPa)

For limitation of spray tip penetration in downsized diesels are used small-size injectors. In work [171] such outward-opening injector (valve lift is $h=23$ microns) is considered. The jets produced by it intensively breaking up to droplets even in the conditions of the low injection pressure and density of gases in the cylinder. Simulation has been carried out of such injector under the conditions similar to experiments [171]. The obtained results and visualizations of spray in a medium with a density of 2,2 and 6,6 kg/m³ are given on Fig. 2.54.

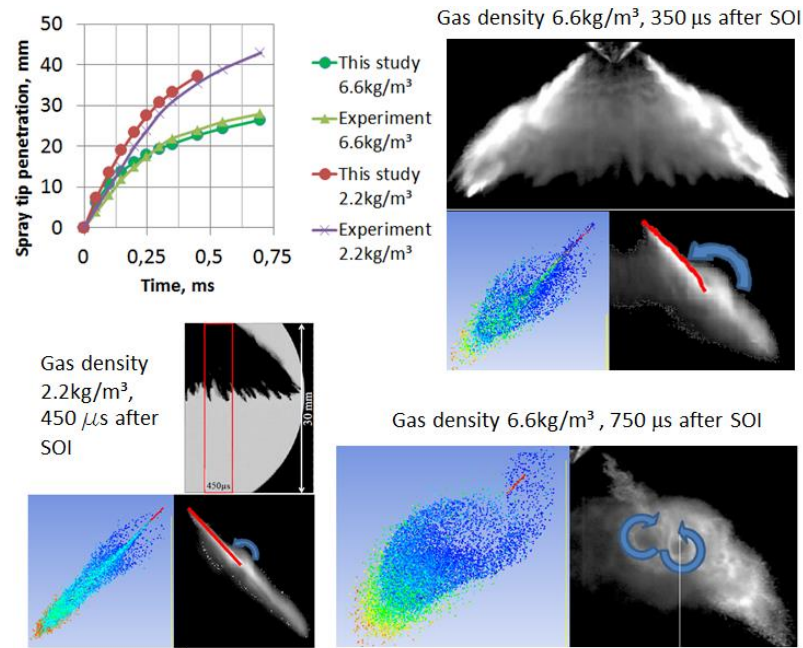


Fig. 2.54. Comparison of characteristics of a spray produced by outward-opening injector obtained in experiment [171] and in simulation

2.8. Simulation of evaporation of single droplet

In section 2.5 simulation of a spray penetration in the conditions of evaporation is carried out, however details of evaporation process have not been mentioned. The most convenient and demonstrative is simulation of single droplet evaporation. In this work the convective-diffusion evaporation model is implemented which is based on works of S.S. Sazhin [169,170]. For adjustment of evaporation model in this work the article [169] has been used. In this paper comparative analysis and validation of different evaporation models is carried out. According to one of the tests in work [169] injection of a single droplet of n-dodecane with a diameter of 20 microns with initial velocity of 1 m/s and with the temperature of 300 K performed into air with temperature of 880 K and pressure of 3 MPa. Comparison of results on the rate of heating and evaporation rate is presented on Fig. 2.55. Comparison is given with experimental data and with the results obtained by widely used law of evaporation of B.I. Sreznevsky:

$$d_p^2 = d_{p0}^2 - K\tau \quad K = 4 \cdot 10^6 Nu_D D_p P_S / \rho_l \quad (2.70)$$

where $Nu_d = Sh$ - a diffusion Nusselt number (Sherwood number (2.48)); D_p - baro-

diffusion coefficient. Proceeding from Fig. 2.55 heating time of a small slow droplet up to the temperature of equilibrium vaporization takes a quarter of the total evaporation time. By this reason it is desirable to consider heating period of a droplet. Distinctions on the level of equilibrium vaporization temperatures on Fig. 2.55,*a* are connected, first of all, with not accounting of fuel density dependence from temperature. These results are obtained in the *Ansys Fluent* version 14 which did not have a possibility to set such dependence (in version 15 such opportunity is implemented). At the same time it is important to set correctly dependences of substances properties on temperature under current pressure in a computational domain (see Table 2.3). Fig. 2.56. presents the simulation results for conditions in the cylinder of the HCCI engine which will be considered below (*HCCI* realization in the *Z-engine*).

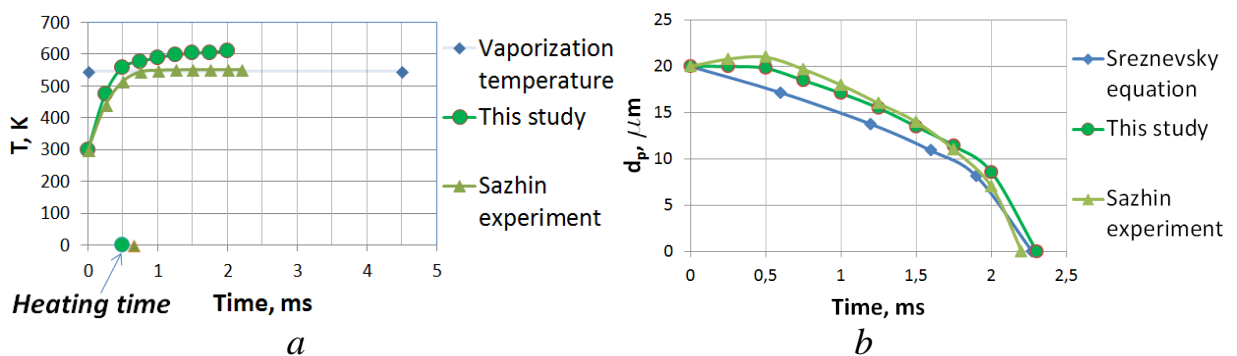


Fig. 2.55. Comparison of results on droplet heating and evaporation history, obtained by different methods: *a* - droplet temperature; *b* - diameter of a droplet (particle)

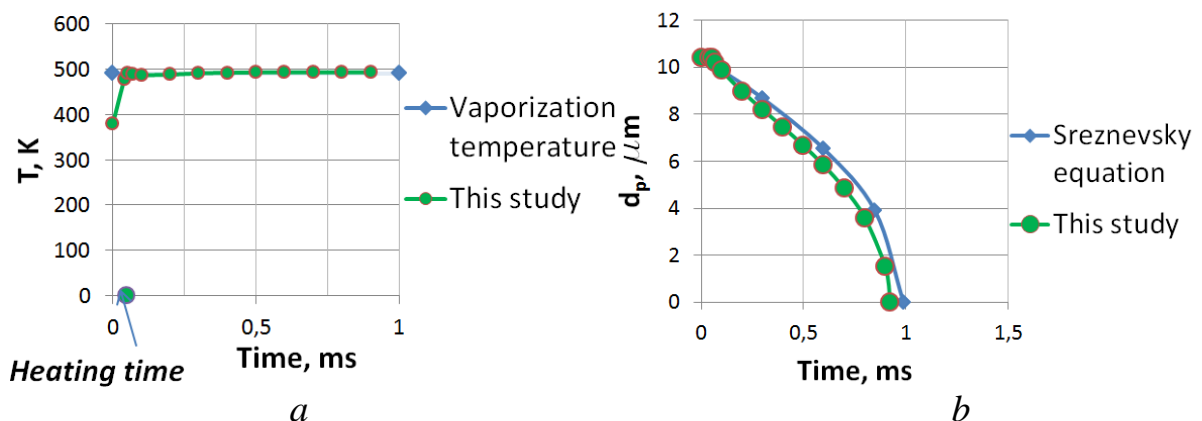


Fig. 2.56. The history of droplet heating (*a*) and evaporation (*b*) obtained by different methods at conditions of *HCCI* realization in the *Z-engine* (gas temperature - 748 K, gas pressure - 3,2 bars, droplet velocity - 30 m/s)

2.9. Two-stage method of analysis of fuel injection atomization and evaporation by a nozzle with nonconventional geometry

After adjustment of all models necessary for the description of fuel outflow, atomization and evaporation, it is possible to start simulation of injection process on the whole. In this work the methodology consisting in division of this process into two stages is offered: on the first stage the internal nozzle fuel flow is modeled, on the second - development of fuel spray and droplets evaporation in the cylinder (in-cylinder spray behavior). Implementation of this methodology is described in work [8], it's schematically representation on the example of a pintle nozzle is given in Fig. 2.57.

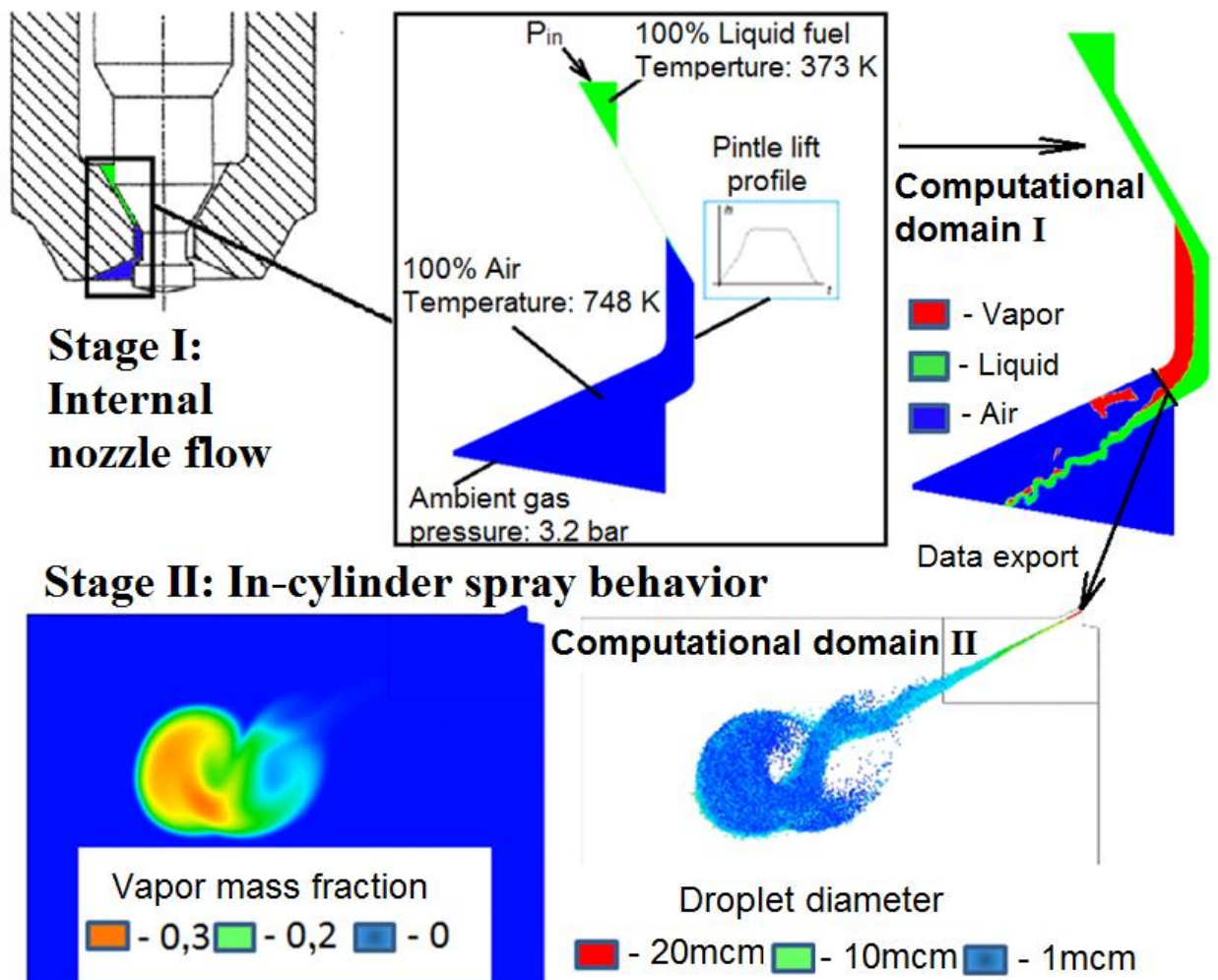


Fig. 2.57. The scheme of a two-stage method of analysis of fuel injection, atomization and evaporation on the example of a pintle nozzle

Computation of a flow in internal channels of a nozzle (a computational domain of I) at the first stage is similar to the simulation given in section 2.6. As a result of this calculation the typical dimensions and velocities at nozzle outlet are determined. These data are used as boundary conditions for calculation of formation and evaporation of a spray in the cylinder (a computational domain of II) similar to described in section 2.7. Among these data: mass flow rate and mass-weighted average velocity in the nozzle outlet section and jet thickness in the same section. The size of initial droplets within this methodology for a pintle nozzle can be accepted equal to jet thickness, similar to a hypothesis (2.69) of work [181]. More difficult dependence considering in-cylinder medium parameters is obtained in work [171]:

$$d_{init} = h_{pin} \cdot 10^6 \left(\frac{\rho_{amb}}{\rho_{liq}} \right)^{0.378} \cdot \left(\frac{P_o}{P_{inj}} \right)^{0.6} \cdot \left(\frac{16000 \cdot d_{eff}}{5 \cdot 10^{-11}} \right)^{0.25} ; d_{eff} = C_{exit} \cdot d_h = C_{exit} \cdot 2\delta_{theor}. \quad (2.71)$$

It has been noted above that for *CFD* simulation of behavior of a spray produced by nozzles with standard geometry (such as hole nozzles) there are approaches helping set of BCs and describing of primary break-up results. This approaches such as *plain orifice atomizer* model (Table 2.2.) based on use of semi-empirical formulas. Besides, for an estimation spray tip penetration, spray angle and average droplets diameter engineers often use semi-empirical or criteria dependences of Lyshevsky [69], Hiroyasu [137] and others [48]. Calculation by these dependences does not demand considerable computational resources, however they are not universal. In particular, in work [171] it is shown that any of the considered dependences for spray tip penetration is inapplicable for the outward-opening injector described in work.

The offered methodology (Fig. 2.57) can be used for calculation of nozzles with any geometry. For the solution of a question of transition from jet thickness on a nozzle outlet to the sizes of initial droplets the dependences similar given above (Fig. 2.69, 2.71), experimental data or result of direct simulation of jet primary break-up can be used. Calculation by such methodology has been made for the nozzle and conditions corresponding Fig. 2.57. Maximum pressure on inlet of

computational domain was 1050 bars. Visualization of results of in-cylinder spray behavior is given on Fig. 2.58. It is visible that considerable fuel fraction reaches a cylinder wall, without having managed to evaporate. It occurs because the impulse of a spray is too large for conditions of so low gases backpressure and density.

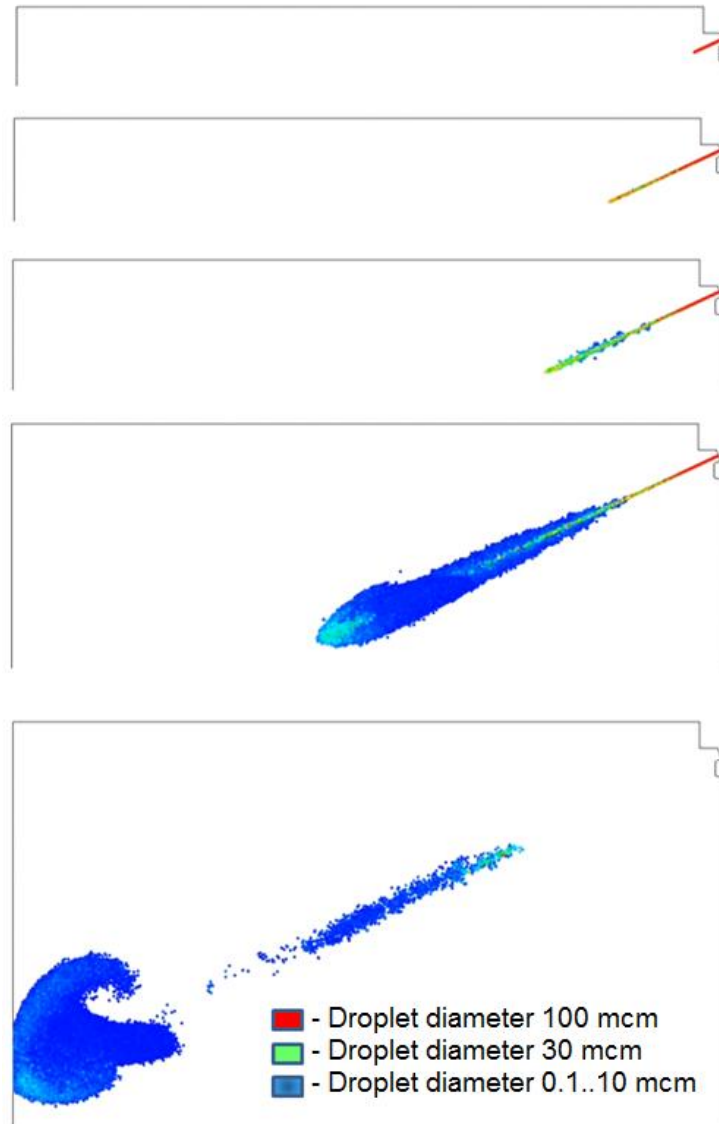


Fig. 2.58. In-cylinder spray behavior visualization

2.10. Search of methods for limiting of spray tip penetration

Limitation of spray tip penetration can be reached by the methods reducing a total pulse of a jet. Extensive methods are decrease of fuel mass flow rate due to reduction of the geometrical dimensions of a nozzle, extension of injection duration or division of fuel supply into several stages. Intensive methods consist in

strengthening of jet break-up due to increase of injection velocity with reduction of a jet cross-section at the outlet, cavitation and turbulization of a flow. As has been shown above the simultaneous jet contraction, increase of its velocity and turbulization is possible due to cavitation, especially at a choked flow and at partial hydraulic flip. The equation (2.66) can be rewritten as:

$$C_{exit} = \left(\frac{\delta}{\delta_{theor}} \right) \left(\frac{u_{eff}}{u_{theor}} \right) = C_a \cdot C_v \quad (2.72)$$

In work [140] it was performed the simulation of fuel outflow from a submerged pintle nozzle. Results of this work (Fig. 2.59) indicate that at the developed cavitation the coefficient of velocity C_v increases due to decrease of contraction coefficient C_a .

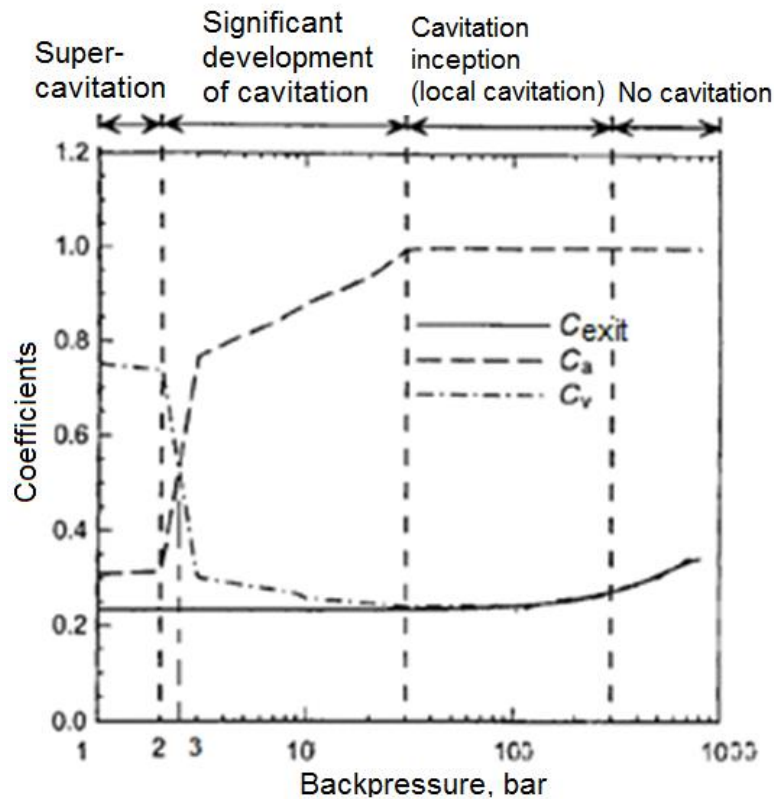


Fig. 2.59. Coefficients for outlet (exit) section of a submerged pintle nozzle obtained by simulation in work [140] (inlet pressure - 1000 bars)

For investigation of influence of different factors on a spray parameters and rate of its evaporation it was conducted analyses of in-cylinder spray behavior and evaporation at different values of the influencing factors (their most demonstrative combination is given in Table 2.7). For all analyses No. 1-5 of Table 2.7 initial

conditions in the cylinder corresponded to Fig. 2.57. At the same time the movement of the piston was considered and computation of internal nozzle fuel flow (stage I, Fig. 2.57) was not carried out.

Table 2.7.

The factors influencing spray parameters and rate of evaporation

№	Maximum pintle lift $h_{pin.max}$, mcm	$p_{in.max}$, bar	C_a	Injection duration τ_{inj} , ms	Cyclic delivery, mg
1	200	1050	0,42	0,33	70
2	40	1050	0,8	0,22	11
3	40	1550	0,8	0,25	16,5
4	40	1550	0,5	0,23	11
5	40	1550	0,5	0,32	19,6

On Fig. 2.60 results on spray tip penetration and mass of the evaporated fuel for conditions No. 1-5 of Table 2.7 are presented, on Fig. 2.61 - the SMD history. During search of the best combination of parameters the injection of maximum fuel without hit of fuel on cylinder walls was considered as optimum.

Decrease of geometrical cross-section of a jet due to reduction of the maximum pintle lift looks more effective method in comparison with reduction of a pintle diameter. At the same time with decrease of injected fuel mass the jet thickness δ on nozzle outlet decreases as well, that leads to more intensive break-up and smaller diameters of initial droplets.

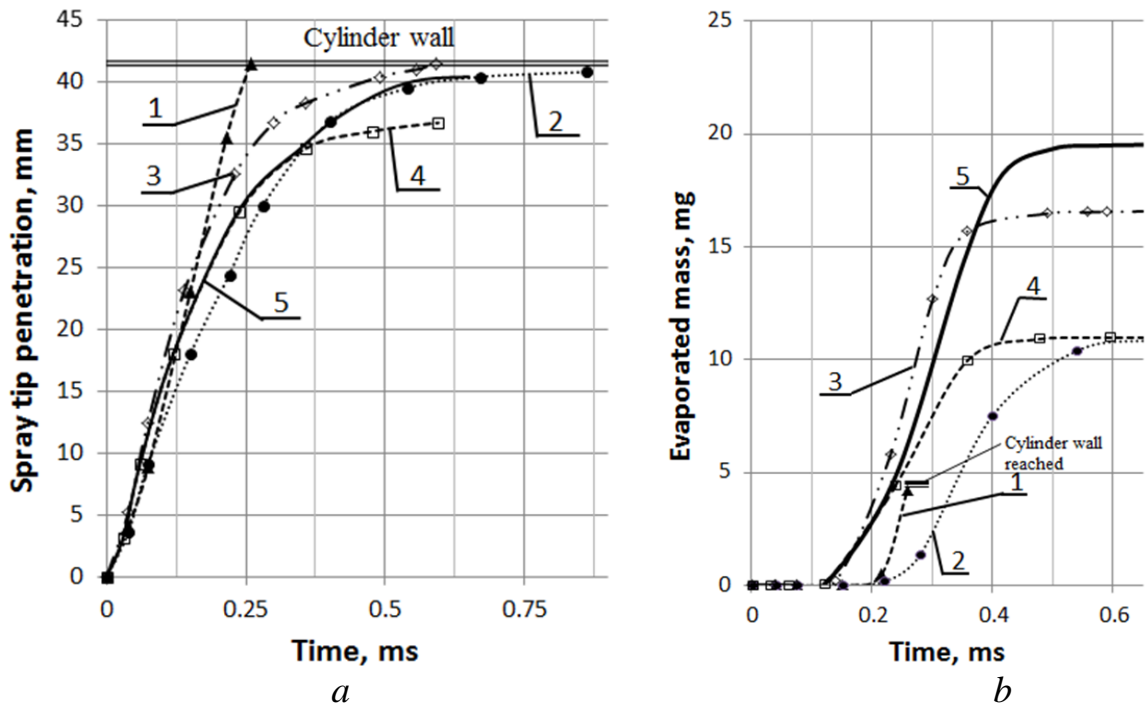


Fig. 2.60. Spray tip penetration (a) and the mass of the evaporated fuel (b) for conditions No. 1-5, Table 2.7

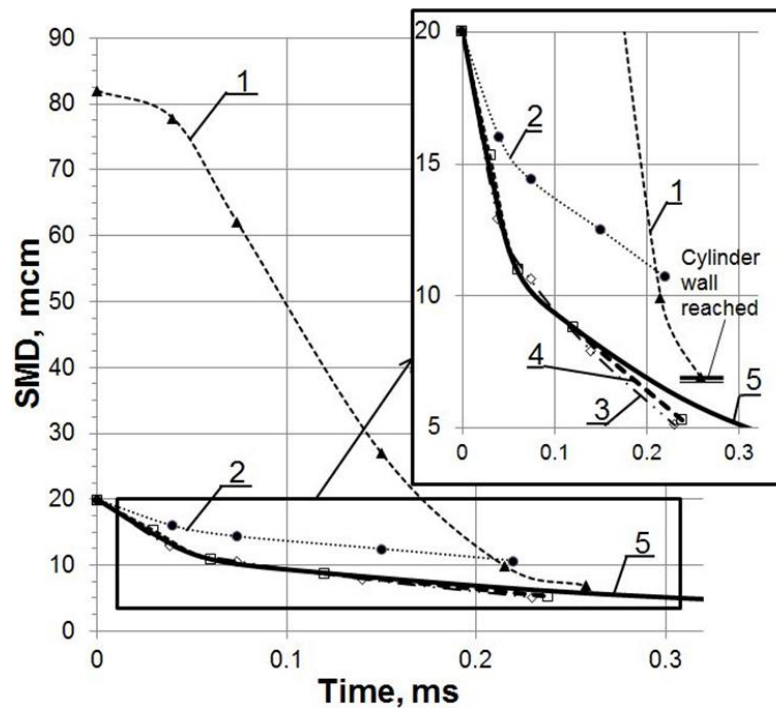


Fig. 2.61. SMD time history for conditions No. 1-5, Table 2.7

Comparison of a curve 1 (conditions No. 1 of Table 2.7) with other curve Fig. 2.60a shows that spray tip penetration considerably decreases with decrease of a maximal pintle lift. Conditions No. 3 of Table 2.7, differ from No. 2 by higher injection pressure at an assumption that value of coefficient C_a is unchanged.

Increase of injection velocities due to higher pressure leads to more intensive break-up (curve 3, Fig. 2.61) and, as a result, to faster evaporation (curve 3, Fig. 2.60, *b*). But at the same time increase of mass flow rate leads to hit of fuel on a wall (curve of 3 Fig. 2.60, *a*). If pressure rise leads to additional contraction of a jet section due to cavitation (No. 4, Table 2.7), then injection happens with higher velocities at almost unchanged mass flow rate. As a result, break-up of droplets occurs with the same intensity (curve 4, Fig. 2.61) and spray does not reach a cylinder wall because spray total pulse became lower (curve 4 on Fig. 2.60, *a*). These positive factors give the possibility to increase injection duration almost twice (No. 5, Table 2.7) that does not lead to hit of fuel on a wall (curve 5, Fig. 2.60, *a*).

Thus, it is possible to draw a conclusion that in these conditions it is necessary to carry out injection by a small-sized high-speed injector with the small pintle lift at the maximum contraction of jet section due to cavitation and gas entrainment from the cylinder. However Table 2.7 shows impossibility to provide injection of all necessary fuel mass (70 mg) without hit of fuel on cylinder walls. For the solution of this problem it is necessary to use a multistage injection strategy. This approach has been also simulated in this work. On Fig. 2.62. two of four stages of such injection are presented.

As may be seen described multistage strategy of injection by the pintle nozzle with small effective flow section provides full droplets evaporation and prevents hit of fuel on cylinder walls in the conditions of low gas density. Therefore such mixture formation concept can be used for *HCCI* realization.

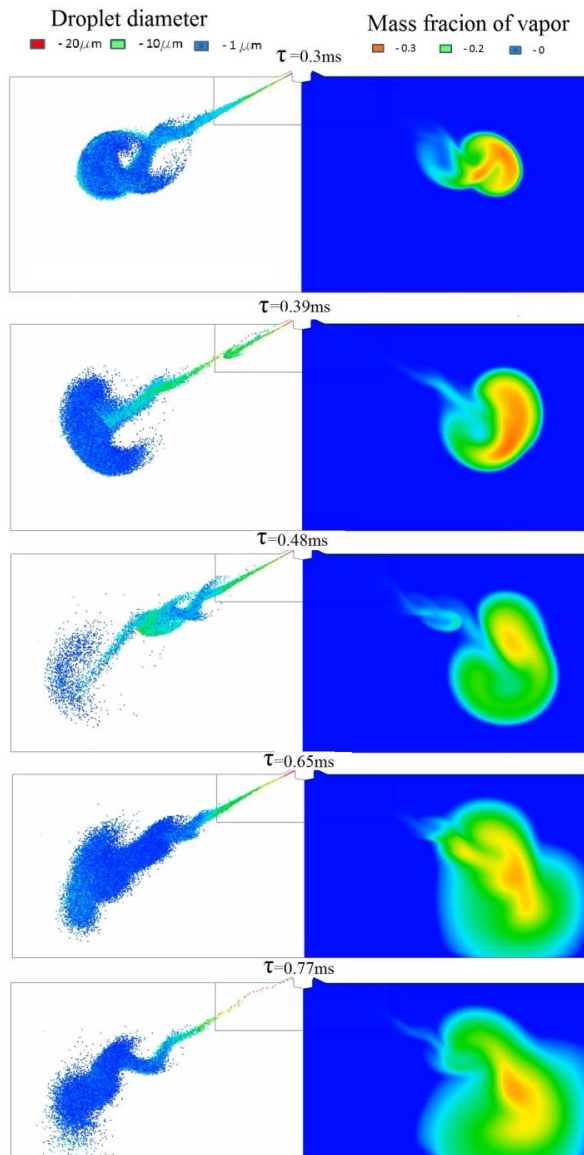


Fig. 2.62. Visualization of multistage injection by a pintle nozzle

2.11. Problems of simulation of jet primary break-up

Some of problems of mixture formation simulation are determination of sizes of the initial droplets which are formed as a result of a jet primary break-up and providing of a coupling of solutions of jet primary break-up with further secondary break-up, spray penetration and evaporation. For conventional geometries researchers offer different empirical approaches (see, for example, Table 2.2 for a nozzle hole, a formula (2.69) and (2.71) - for hollow cone sprays). But, usually it remains a question of a serious experimental study. An alternative method is direct

simulation of a jet primary break-up. Direct simulation of a jet break-up assumes resolution by a computational grid of whole range of droplets sizes which are in interest. Even the most modern and precision model of interphase boundary tracking requires use of about 4-9 cells (finite elements) of a computational grid for the approximate description of a droplet surface in 2D (Fig. 2.65), 8-27 cells in 3D. The computational grid with the cells size about 2 microns is necessary for the accurate description of a droplet with a diameter of 10 microns. Besides the size of a computational time step also has small values because it is necessary to maintain values of Courant number $Cu=u\Delta\tau/\Delta x$ about unit. The necessity of use of more detailed turbulence simulation than *RANS* method has been also noted above. For solution of these problems considerable computational and time resources are required. For example, in work [155] the picture of primary break-up (Fig. 2.63) of a jet with initial velocity of 100 m/s obtained at *CFD* simulation using the computational grid containing 15 million elements. Later authors have carried out refinement of this calculation - the resulting grid contained 130 million elements, a calculation was carried out on 128 processors.



Fig. 2.63. The visualization of jet primary break-up obtained at *CFD* simulation in work [155]

Other problem of direct jet primary break-up simulation in the *Ansys Fluent* is that for the accurate description of interphase boundaries it is necessary to use the explicit scheme of *VOF* model with the most precision scheme of interface reconstruction *Geo-Reconstruct*. But this type of *VOF* model in the *Ansys Fluent* is inapplicable together with cavitation models because the assumption about interpenetration of continuous mediums implemented within the cavitation models do not corresponds with the sharp interface description by *Geo-Reconstruct* [117]. Application of the implicit *VOF* scheme together with cavitation model is possible,

but more detailed computational grid is necessary for the adequate accuracy of the interphase boundaries description in comparison with the explicit scheme with *Geo-Reconstruct*. Such approach (implicit *VOF* scheme) together with a *DES* turbulence are employed in this work. Approach with the explicit *VOF* scheme with *Geo-Reconstruct* can be applied for simulation of a flow without cavitation or after hydraulic flip development, when there is no phase transition.

Fig. 2.64 shows the visualization of jet primary break-up obtained in this work using *Geo-Reconstruct* in axisymmetric statement for an outward-opening injector and conditions according to Fig. 2.54 [171]. The obtained results corresponds well with theory of V. G. Levich (2.56). The diameter of initial droplets in simulation is overestimated by 10% in comparison with the data obtained in experiments of work [171] and by a formula (2.71). It is due to not accounting in model of a real velocity profile and cavitation.

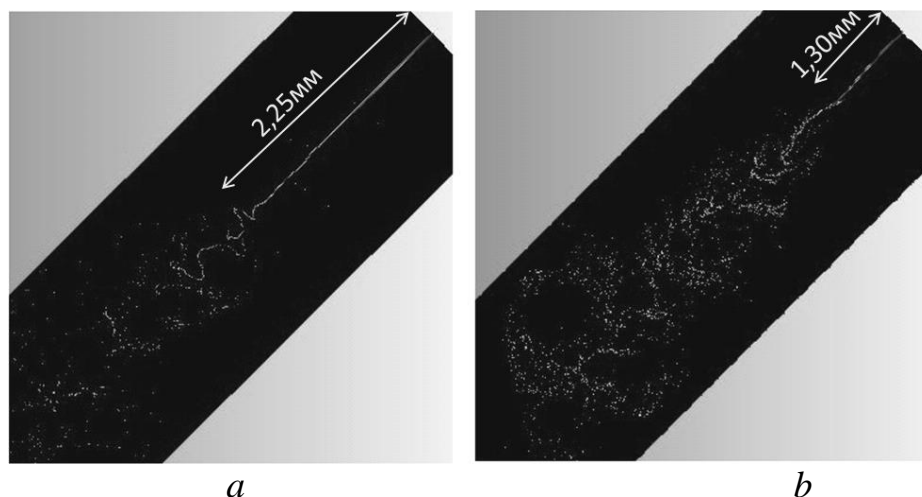


Fig. 2.64. Simulation of primary break-up of a jet produced by outward-opening injector under injection pressure of 12 MPa and different density of a medium: *a* - gas density $\rho_{gas}=2,2 \text{ kg/m}^3$; *b* - $\rho_{gas}=6,6 \text{ kg/m}^3$

Thus, simulation of whole spray produced by an injector by method of direct simulation is extremely resource-intensive task. Therefore there is a necessity of transition from the results obtained in direct simulation of jet primary break-up to further computation using Euler-Lagrange approach and models of dispersion medium (stage II, Fig. 2.57). It should be noted that such transition requires creating of two computational domains (Fig. 2.57) and use of great number of

submodels. Besides, collecting of data about results of primary break-up is necessary (statistics on the droplets sizes and velocities, evaluation of the most probable diameter in the Rosin-Rammler distribution).

For the purpose of creation of more universal model for spray simulations it was initiated the development of an alternative implementation of *VOF* model within the Russian *CFD* tool *FlowVision* [127]. Feature of this implementation is that at the solution there are as the droplets resolved by a computational grid (overgrid) and subgrid droplets(Fig. 2.65). Unlike implementations in other *CFD* codes where subgrid droplets are just cut (or the interphase boundary in areas with such droplets is smeared) in the offered approach these droplets are not lost, they continue keep computational variables and the characteristic dimensions, interact with surrounding gas (drag) and can merge in overgrid structures. It provides better mass conservation and does possible convert these droplets in Lagrangian coordinates for further computation (secondary break-up and evaporation) using disperse phase relationships without change of a computational domain.

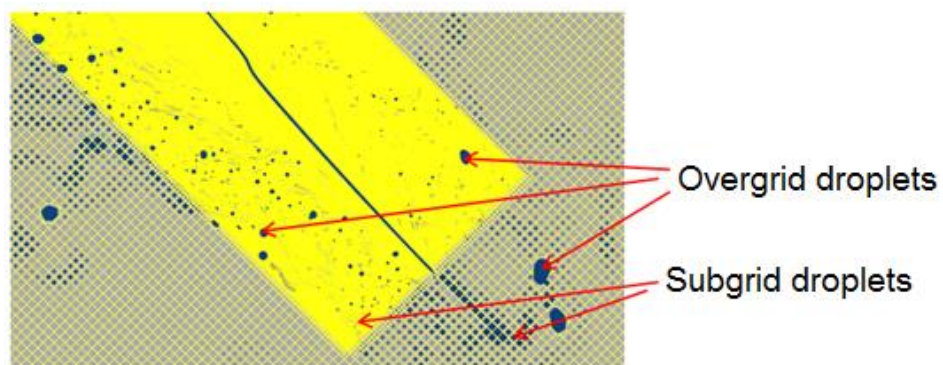


Fig. 2.65. Overgrid and subgrid droplets

Fig. 2.66 presents comparison of jet visualizations obtained in experiment [171] and at simulation in the *FlowVision* and Fig. 2.67 shows a curve of jet penetration. According to experiment [171] of fuel injection under pressure 0,7 MPa in an atmospheric air at distance about 4,1 mm from an injector liquid surface begin to produce the waves. The flow regime in experiment is close to laminar ($Re=1900$), and cavitation is absent therefore the parabolic injection velocity profile is set. The distance from the initial point of injection prior to place where waves appear results about 4,2 mm.

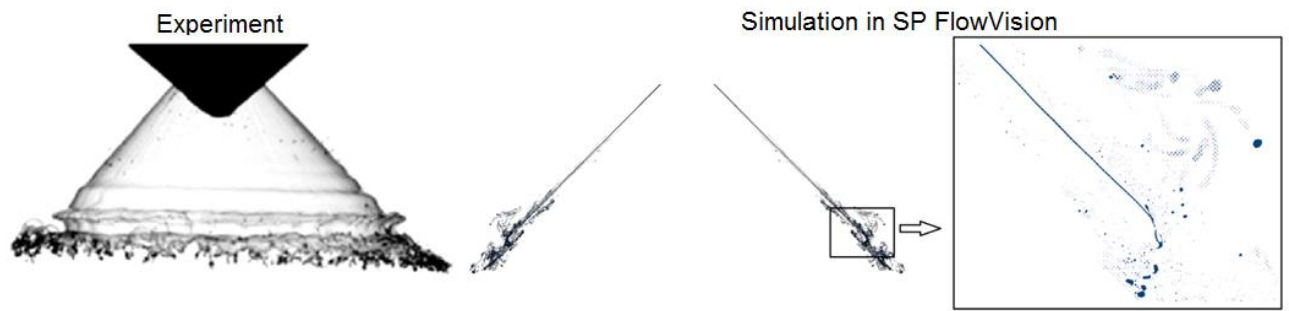


Fig. 2.66. Visualization of a jet in experiment and at simulation in SP *FlowVision* (injection under pressure 0,7 MPa in an atmospheric air)

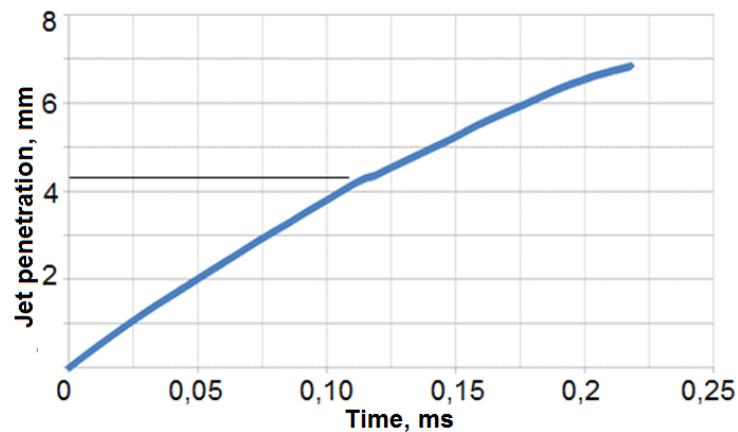


Fig. 2.67. Jet penetration obtained at simulation in SP *FlowVision*

In general using developed approach a two-stage methodology (Fig. 2.57) can reduce a to single analysis where primary break-up is simulated in the direct way and subgrid droplets submit to the equations of dispersion medium and models of secondary break-up. Fine grid resolution will necessary only in region where initial droplets are formed and other spray zones may have much coarser mesh according to requirements of Euler-Lagrange approach.

2.12. Chapter 2 summary

By results of the researches conducted in a chapter, for the description of the different processes related with injection, atomization and fuel evaporation in an ICE within *CFD* the set of the most suitable models is defined. The list of the phenomena which are subject to simulation and the most reasonable models for their description is presented in Table 2.8.

Table 2.8.

The phenomena characterizing fuel injection, atomization, evaporation and reasonable models for their description

Stage	I: Internal nozzle flow				II: In-cylinder spray behavior			
Zone	Internal channels of the injector nozzle		Transition zone from the injector nozzle to the cylinder		In-cylinder zone			
Process	Flow in internal channels		Primary break-up		Spray penetration, secondary break-up, evaporation, mixture formation			
	Phenomena	Model in ANSYS Fluent	Phenomena	Model in ANSYS Fluent	Phenomena	Model in ANSYS Fluent	Phenomena (continuation)	Model in ANSYS Fluent
	Turbulence	<i>Realizable k-ε</i>	Turbulence	<i>DES (LES + Realizable k-ε)</i>	Turbulence	<i>Realizable k-ε</i> or <i>RSM</i>	Heat exchange between droplets and gas	<i>Ranz-Marshall</i>
	Near-wall flow	<i>Scalable wall function</i>	Near-wall flow	<i>Enhanced wall treatment</i>	Near-wall flow	<i>Scalable wall function</i>	Mass exchange	<i>Species transport model</i>
	Cavitation	<i>Schnerr-Sauer cavitation model</i>	Cavitation	<i>Schnerr-Sauer cavitation model</i>	Movement of dispersion medium	<i>Discrete phase model</i>	Evaporation	<i>Convection / Diffusion controlled</i>
	Compressibility of fuel	<i>Tait equation</i>	Compressibility of fuel	<i>Tait equation</i>	Aerodynamic interaction	<i>Dynamic drag model</i>	Turbulent dispersion of droplets	<i>Stochastic tracking</i>
	Multiphase flow, air entrainment	<i>Volume of fluid model</i>	Multiphase flow, air entrainment	<i>Volume of fluid model</i>	Droplets secondary break-up	<i>Kelvin-Helmholtz Rayleigh-Taylor model</i>		
	Surface tension	<i>Continuum surface force</i>	Surface tension	<i>Continuum surface force</i>	Collision / Coalescence of droplets	<i>Collision/coalescence model</i> or disabled		
	Needle movement	<i>Dynamic mesh (Smoothing/ Remeshing)</i>	Needle movement	<i>Dynamic mesh (Smoothing/ Remeshing)</i>	Piston movement	<i>Dynamic mesh (Layering)</i>		

The following conclusions for the chapter 2 can be made:

1. It have been performed the overview and analysis of the software packages for simulations of a fluid flow inside difficult geometry in the conditions of cavitation for performing numerical investigations of internal nozzle fuel flow of an ICE injectors.

2. For simulation of internal nozzle fuel flow, in-cylinder spray formation, penetration and evaporation the software package *Ansys Fluent* was chosen.

3. As a result of numerical investigations it was shown the influence of cavitation and air entrainment on characteristics of a fuel flow in nozzles with different geometry and on characteristics of a spray.

4. By use of experimental data it was carried out the choice and adjustment of

mathematical models of fuel injection, atomization and evaporation for nozzles with nonconventional geometry of a flowing channel in the conditions of cavitation. The analysis and comparison of the computational results obtained using different models have been performed. For *CFD* simulations it has been determined the set of the most reasonable models describing processes of injection, atomization and fuel evaporation in ICE.

5. The two-stage method of analysis of fuel injection, atomization and evaporation has been developed. By use of this method it can be obtained characteristics of a fuel flow, fuel spray and mixture formation, quality metrics of atomization and evaporation for any nonconventional geometry of a nozzle.

6. Influence of different factors on characteristics of a fuel spray, its atomization and evaporation was investigated. Ways of limitation of spray tip penetration and improvement of quality metrics of atomization in the conditions of low gas density in the cylinder were offered. The mixture formation concept for the HCCI engine which provides full droplets evaporation and prevents hit of fuel on cylinder walls was developed.

7. There was offered the concept of model for spray simulations within the Russian *CFD* tool *FlowVision* allowing to combine calculation of jet primary and secondary break-up without division of the solution on separate stages and computational domains.

CHAPTER 3. NUMERICAL INVESTIGATIONS OF OPERATION CHARACTERISTICS OF THE DIESEL AND *HCCI* ENGINE. *Z-ENGINE*

3.1. Substantiation of necessity of development and deployment of new types of internal combustion engines. *Z-engine*

As shown in chapter 1, the present stage of development of engine building is characterized by continuous toughening of requirements to an EG toxicity. At the same time internal combustion engines play a significant role in pollution of the atmosphere. Therefore, with improvement of economic characteristics of the ICE, a minimization of pollutant emissions becomes first-priority task. Improvement of ecological characteristics of ICE requires implementation in engine building of different methods decreasing EG toxicity. Cardinal improvement of the specified characteristics can be reached by development of essentially new types of engines [20, 66, 75].

Now the great part of the world motor transport is equipped by ICE working on a four-stroke cycle. Two-stroke engines continue to be used, generally to motorcycles, boats, vessels, and also in stationary energetics. The reasons of limited use of these engines are following drawbacks: poor quality of gas exchange, release of a fresh charge to exhaust manifold, hit of oil in the cylinder and its combustion. It leads to increase of fuel consumption, high noisiness of engine operation, deterioration in characteristics of EG toxicity and smoke. But two-stroke ICEs possess also a number of advantages such as relative compactness and lower specific weight. They have potentially higher power density and efficiency due to the fact that useful work is made at each crankshaft revolution. Marine low-speed two-stroke diesel engines have the highest values of efficiency. A number of advantages, including listed, are not completely disclosed in two-stroke engines and have perspectives to improvement.

The most widespread schemes of gas exchange (scavenging) of two-stroke engines are presented on Fig. 3.1. The loop scheme (port scavenging) is basically used in small-sized engines (Fig. 3.1,*a*). The uniflow scavenging is applied in

engines with large diameters of the cylinder and provides the best quality of gas exchange and best efficiency. It should be noted that presence of inlet and exhaust ports in these schemes complicates the management of gas distribution phases depending on operation modes.

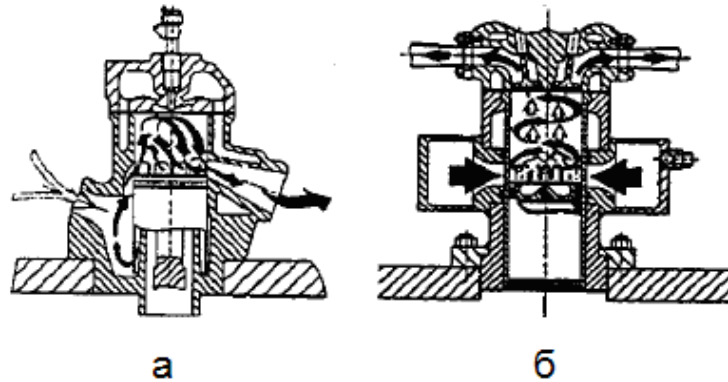


Fig. 3.1. Schemes of gas exchange in two-stroke engines: Loop (port) scavenging (a) and uniflow scavenging (b)

The new principle of engine operation called *Z-engine* is offered by the *Aumet Oy* company (Finland) [1, 8, 35, 36, 42, 141] and patented in 11 countries of the world. This principle combines the main advantages of two-stroke and four-stroke schemes. As well as in a two-stroke engine, useful work is made at each crankshaft revolution. At the same time the engine has inlet and outlet valves, exhaust occurs almost as well as in the conventional four-stroke engine - due to gas displacement from the cylinder by the piston and not due to scavenging forced by the fresh air coming to the cylinder. Thus, there are no losses of a fresh charge which in conventional two-stroke engines is thrown out to exhaust manifold. Absence of ports and crankcase scavenging allows to prevent hit of oil in the cylinder and installation of additional piston rings is not required. Air intake occurs very intensively due to essentially new valve train and considerable compression of air prior intake to the cylinder by means of the piston compressor. The scheme of the *Z-engine* operation is presented on Fig. 3.2.

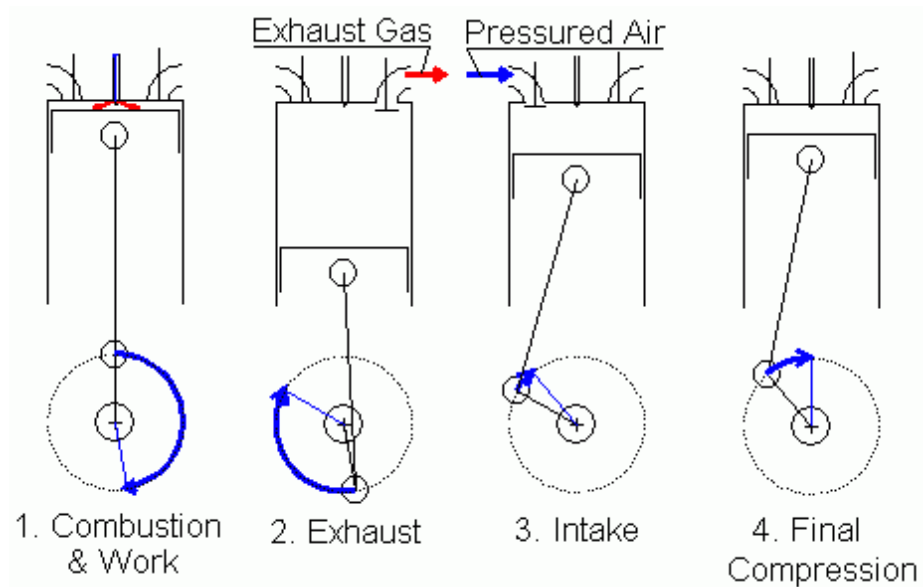


Fig. 3.2. The scheme of the *Z-engine* operation

In the *Z-engine* combustion and working stroke have almost same duration as in conventional four-stroke engines. Gas exchange begins with opening of an exhaust valve prior the bottom dead center (BDC), exhaust of gas from the cylinder starts and then EG is forced out from the cylinder at the upward piston movement. Duration of exhaust is sufficient for high-quality cleaning of the cylinder, but at the same time pumping losses are rather small. The intake valves opens about the time when exhaust valve closing (Fig. 3.3) or several degrees later, but intake duration is no longer than 22 CA deg. on maximum power mode. It is enough for intake because air significantly compressed in the piston compressor.

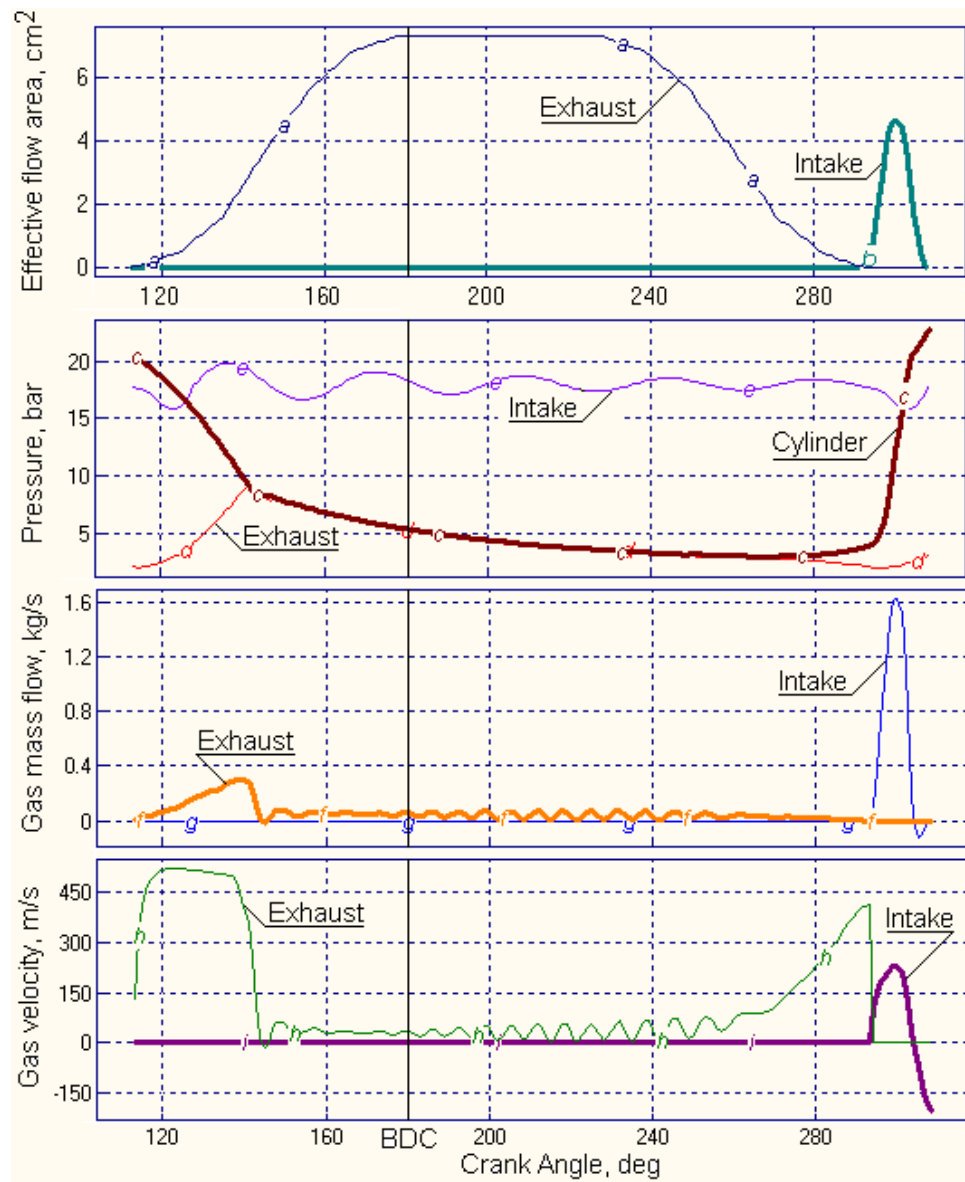


Fig. 3.3. Characteristics of gas exchange of the *Z-engine*

Final compression in the cylinder occupies about 40 CA deg. The geometrical compression ratio $\epsilon=15,5$ is provided as a result. It should be noted that such scheme of gas exchange lead to the fact that considerable fraction of EG remains in the cylinder, i.e. the internal EGR is implemented. This factor can be used for HCCI organization in the absence of uncontrollable self-ignition. Such operation provides considerable decrease in maximum combustion temperatures and therefore cardinal reduction of nitrogen oxides emission with EG. High pressure of intake air allows to organize intensive swirling of gases in the cylinder that promotes improvement of quality of mixture formation and decreases emissions of

soot and other unburnt combustibles.

The specified concept of *Z-engine* gas exchange considerably alters a usual indicator diagram. On Fig. 3.4 comparison of indicator diagrams of the four-stroke diesel engine and *Z-engine* with the same cylinder dimensions is presented. It shows that the indicator work in the *Z-engine* cylinder exceeds an indicator work in the cylinder of the four-stroke engine. It occurs because the part of compression work is performed out of the engine cylinder - in the piston compressor.

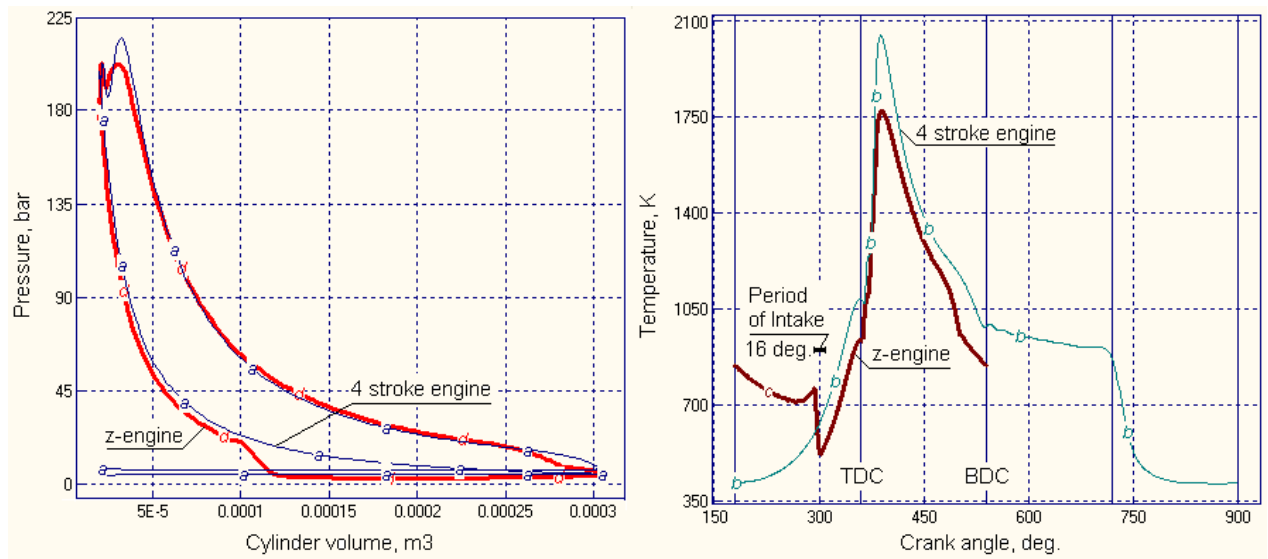


Fig. 3.4. Comparison of indicator diagrams of the four-stroke diesel engine and *Z-engine* at peak load conditions ($p_e=26,2$ bar, $n=1500$ rpm)

Numerical investigations have also shown that two-cylinder *Z-engine* with the boost scheme presented on Fig. 3.5 is capable to produce the same effective power as the four-cylinder four-stroke diesel engine with the same dimensions of cylinders [1, 36]. Thus, downsizing and lower cost can become competitive advantages of the *Z-engine* in the market of transport engines. Undoubted advantage of the *Z-engine* is the possibility of *HCCI* implementation allowing to reach extremely low emissions of the main regulated toxic components - nitrogen oxides and soot. These factors promote widespread introduction of such engines.

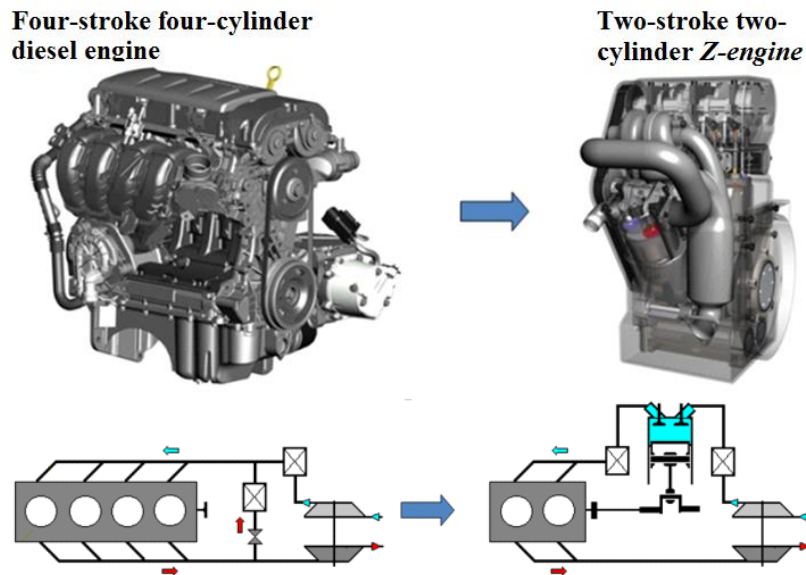


Fig. 3.5. General view and boost scheme of the compared four-stroke four-cylinder diesel engine and two-stroke two-cylinder *Z-engine* with the same cylinder dimensions. Approach to decrease of mass-dimensional characteristics at preservation of the power output

In chapter 2 numerical investigations of injection, atomization and mixture formation in the diesel and the HCCI engine are conducted. At the same time essential differences of the specified processes in these two types of engines are revealed. These differences in characteristics of injection, atomization and mixture formation undoubtedly impact on operation behavior of the studied engines. Experimental and numerical researches of the Diesel and *the HCCI engines* operation in works [7, 27, 33, 48, 53, 89, 103, 106, 157, 165, 161, 166] confirm this fact.

But, it should be noted that experimental studies of operation of different types of internal combustion engines are labor-consuming and demand the expensive experimental equipment, including high-precision metering equipment for determination of characteristics of fuel efficiency and EG toxicity. Thereby at a stage of comparison of different options of ICE operation it is more reasonable use of the computational research methods which are based on modern numerical, analytical and thermodynamical models. Use of modern software packages for simulation of diesel and *the HCCI engines* operation allows with the smallest material and time cost to evaluate influence of features of injection, atomization

and mixture formation on operation of the studied engines. And also to determine characteristics of fuel efficiency and toxicity of exhaust gases [20, 22, 146]. Besides there is a possibility of a numerical investigation of considerable number of different variations of features of injection, atomization and mixture formation that it is basically not possible when using experimental research techniques. Let's consider modern software packages for simulation of operation of internal combustion engines.

3.2. Software packages for simulation of internal combustion engines operation

The choice of software package for simulation of engine operation is caused both by design features of the studied engine and by those tasks which need to be solved at numerical investigations. Also time that necessary for engine operation calculation and accuracy of the obtained calculation data are important. Besides the determining factor is availability of the required computational resources for use of SP.

The modern software for simulation and optimization of engine operation very variously. Considerable efforts of the advanced scientific centers are concentrated on development *CFD* software implementing three-dimensional simulation of a gas flow and injected fuel in cylinders and manifolds of ICE. For the considered elements of the engine creates a decomposition into a great number of computational grid cells, in which the system of equations of conservation of mass, energy and momentum is solved. At simulation processes of evaporation, combustion and formation of pollutant emissions are modeled. The most widely used software are: *KIVA (Los Alamos)*, *FIRE (AVL)*, *VECTIS (Ricardo)*, *STAR-CD (CD-adapco)* [22, 61]. Considerable efforts are made for calculation of emission of soot, NO_x and CO in them using chemical reactions modeling. However it is premature to claim that *CFD* is the best way. Besides *CFD* simulation requires expensive computational resources, high experience of engineer and reliability of

simulation results that can be obtained in adequate time appears insufficient for practical needs. The existing *CFD* solutions for ICE are basically used for carrying out the labor-consuming and scientific calculations providing the high accuracy of the obtained results.

Other widely used approach exists and develops - the thermodynamic or phenomenological, using 0- and 1-dimensional representations. World leaders in such methods are the software packages *BOOST (AVL)*, *WAVE (Ricardo)*, *GT-Power (Gamma Technologies)*. The Russian developments available for commercial use are the software packages *IMPULSE* and *VOLNA* developed in *CNIDI* and *DIZEL-RK* developed in *BMSTU*. Competing among themselves *BOOST*, *WAVE* and *GT-Power* represent very perfect developments, in particular, for simulation of engine intake and exhaust manifolds and selection of boost-producing devices. For calculation in such program the modern personal computer is enough. For combustion calculation this SPs use the method which are based on the equations offered in 1962 by I.I. Vibe or later similar approaches. The users subroutine for calculation of combustion or another process may be implemented to SP. But simulation of mixture formation and combustion represents the main problem when developing such programs. At best, the computational methods somehow considering the injection rate profile and a fineness of atomization, average distance from the nozzle hole to a wall and gas swirl motion in the cylinder. In particular, the latest version of the SP *IMPULSE (CNIDI)* and early versions of the SP *DIESEL (BMSTU)* has implemented the method of combustion simulation published by professor N. F. Razleytsev in 1980 which was at that time the most advanced of the existing methodologies [89]. The American *GT-Power* in addition to the Vibe model has implemented combustion model of professor H. Hiroyasu which considers a free jet development.

For simulation of diesel engine operation with different fuel supply systems the SP *DIESEL-RK* developed in *BMSTU* and intended for numerical computations, investigations and optimizations of two-stroke and four-stroke aspirated, supercharged and turbocharged ICEs [20, 60, 61, 62, 146, 148].

DIESEL-RK has included the module of visualization of mixture formation which displays results of calculation of fuel spray development and the near-wall flows formed by fuel jets. The analysis of the visualization of spray behavior is very important when carrying out simulations and optimization of mixture formation. It allows to control fuel quantity, getting to typical zones of the cylinder and to obtain the most favorable fuel distribution on volume of cylinder and CC.

DIESEL-RK has passed a validation testing on engines with different dimensions, speed and assignment and has shown good compliance of calculation and experimental data. In particular, some results of the experimental and numerical investigations of the diesel SMD-60 (6 cylinder four-stroke, bore/stroke=130mm/115mm) conducted by use of DIESEL-RK are presented on Fig. 3.6.

DIESEL-RK allows to conduct numerical investigations of operation of almost any ICE. Use of the mathematical models describing essence of the physical processes in the engine allows to obtain the high accuracy simulation results. Experience of use of a software package DIESEL-RK for simulation of operation of engines of the different dimensions and assignments has shown that the program allows to carry out calculations basically without labor-consuming preliminary adjustment of the model constants for specific engine. Correctly adjusted mathematical model of forced induction engine allows to make using identical empirical coefficients the exact calculations of different load modes, including the low load modes.

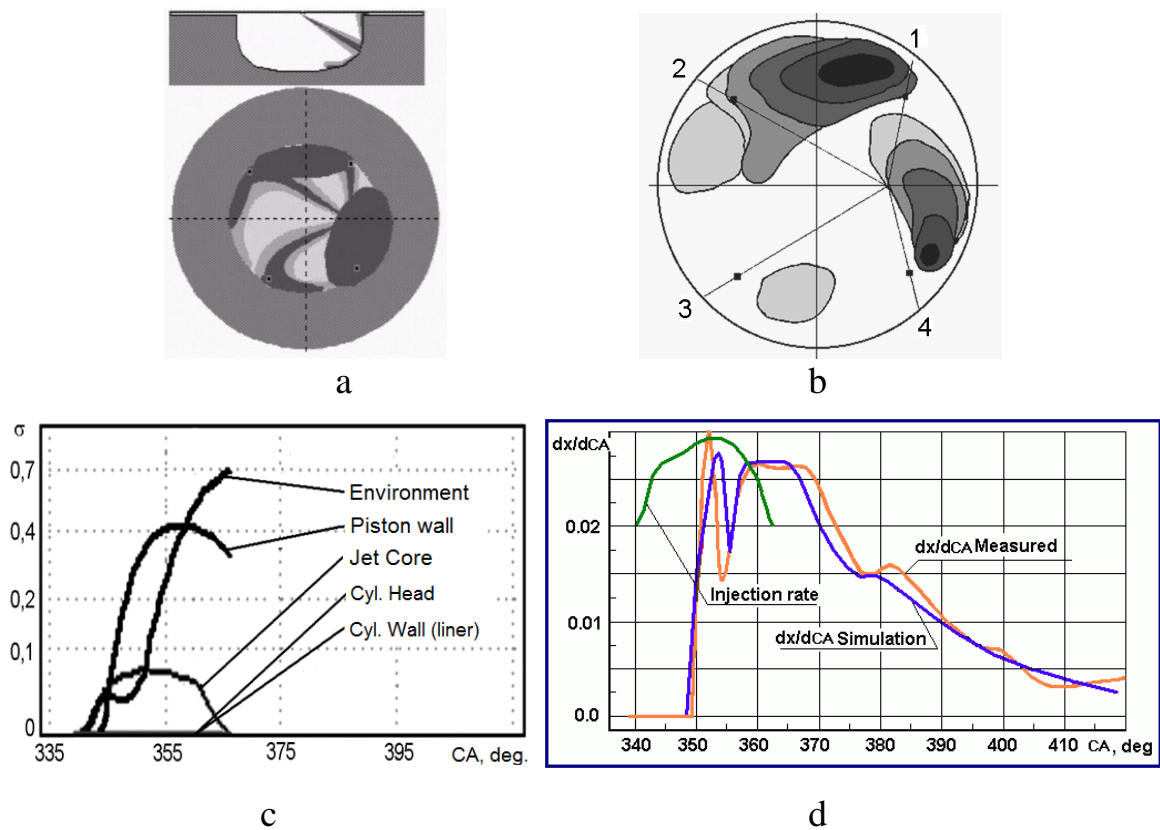


Fig. 3.6. Results of experimental and numerical investigations of mixture formation and heat release of the diesel SMD-60: *a* – visualization of the simulation results; *b* - experimental picture; *c* - numerical results of injected fuel distribution over typical spray zones (for jet No. 1); *d* - heat release rate dx/dCA and injection rate profile; 1-4 numbers of jets

In DIESEL-RK is used a wide set of computational methods for simulation of the complex physical processes in the engine. For better universality basically implemented not empirical, but fuller methods describing the processes in ICE. Gas parameters in cylinders and manifolds of the engine are evaluated in step-by-step solution of system of finite difference equations of conservation of energy, mass and equation of state which is written down for open thermodynamic systems. At the same time working medium properties dependence on composition and temperature is considered.

For analysis of mixture formation and combustion in diesels the RK-model is used which based on the computational method offered in the early nineties by professor N. F. Razleytsev and improved by professor A.S. Kuleshov. The RK-model considers features of injection rate profile, including multiphase injection,

fuel atomization fineness, orientation of jets, dynamics of fuel spray development, interaction of jets with swirling air and walls. Model considers the conditions of each fuel jet development and near-wall flows formed by jets and also jets interactions among themselves. Main idea of the RK-model is close to model of professor H. Hiroyasu but it has the essential differences mainly related with more detailed consideration of interaction of fuel jets with walls and among themselves. For the correct description of a fuel injection by nozzle with nonconventional geometry DIESEL-RK has a possibility of flexible correction of values of empirical constants in relationships for evaluation of spray tip penetration and SMD. These values can be specified by means of experimental data or by a result of *CFD* simulation.

When simulating of fuel atomization and the subsequent mixture formation two sites of spray development are distinguished: an initial site of the pulsing spray development and main site of cumulative development. During the spray movement it is performed evaluations of fuel fractions which have got to typical zones with different evaporation and burning conditions. Among them there are also near-wall zones of CC, piston crown, cylinder wall and head (Fig. 3.7). Trajectories of free jets and movement of the near-wall flow formed by them are calculated taking into account influence of a swirl which set by swirling number H and also considering the angles between spray axis and wall surface normal.

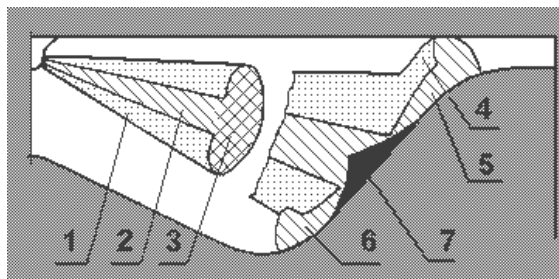


Fig. 3.7. Computational scheme of a diesel spray: 1 - dilute outer sleeve of free spray; 2 - dense core of free spray; 3 - dense spray front; 4 - dilute outer surrounding of a near-wall flow; 5 - dense core of a near-wall flow; 6 - spray front of a near-wall flow (wall); 7 - axial conical core of a near-wall flow

During fuel supply and fuel spray development the combustion rate is limited, mainly, by fuel evaporation rate in the in-cylinder conditions. Inside free spray the

zones with intensive heat exchange and evaporation of atomized fuel are the front and spray sleeve (Fig. 3.8). In a high-speed and dense axial flow fuel heating and droplets evaporation are insignificant. When hitting of a spray on a wall evaporation rate of the fuel which allocated in the spray front sharply decreases to a minimum. It is caused by the wall temperature which is lower in comparison with a gas temperature, by reduction of heat exchange between gas and droplets, by densification of disperse mixture on a wall, coalescence and mixing of liquid on wall with colder droplets which are flying up to a wall. After laying of the spray front on a wall the two-phase mixture begins to spread on a wall out of spray cone borders. Fuel evaporation rate in a near-wall zone increases, but stays smaller than in volume. When spreading on a piston crest the part of fuel can get in top clearance between piston and cylinder heads and get on cylinder liner and head walls.

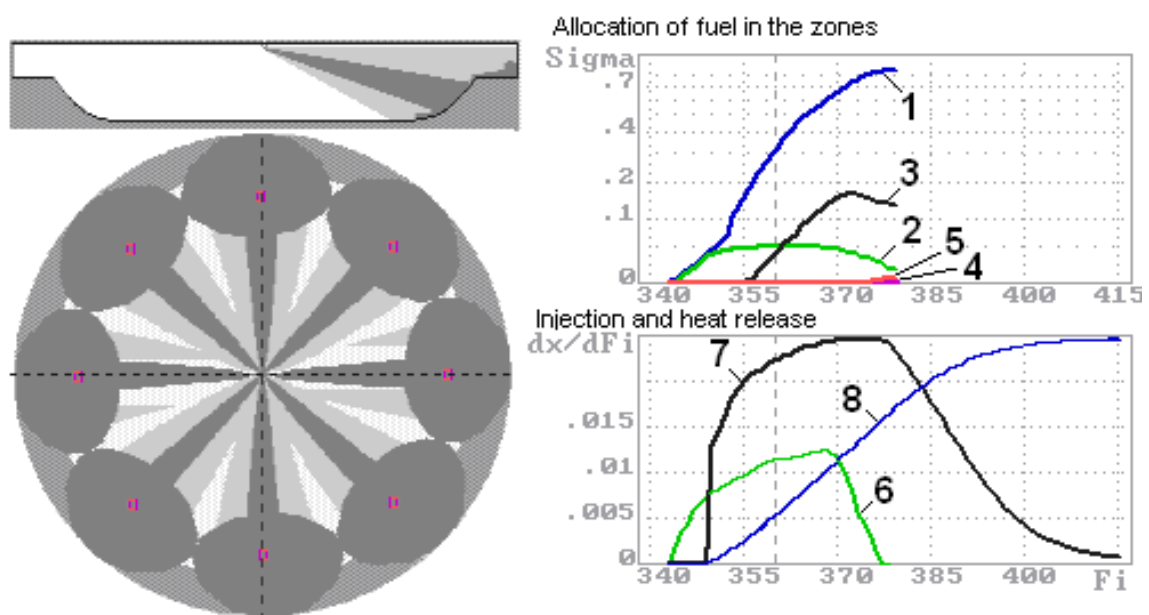


Fig. 3.8. Visualization of mixture formation in a diesel CC: 1 - dilute outer sleeve of free spray and near-wall flow; 2 - dense core of free spray; 3 – core of near wall flow on a piston surfaces; 4 - fuel fraction allocated on a cylinder head; 5 - fuel fraction allocated on a cylinder liner; 6 - injection rate profile; 7 - heat release rate $dx/d\varphi$; 8 - integral heat release

Evaporation rate of the fuel which has come to each of the called zones of intensive heat exchange is equal to the sum of evaporation rates of separate droplets. Evaporation of each droplet before fuel ignition submits to the law of B.

I. Sreznevsky (2.70). The fuel equipment of the forced diesels provides quite uniform atomization of fuel, especially on main stage of injection. Therefore calculation of fuel evaporation can be performed by Sauter mean diameter d_{32} .

For calculation of fuel evaporation rate the constants in different zones of a jet are defined (2.70). Estimations of evaporation constants values are made taking into account a number of parameters. Among these parameters there are a Nusselt number for diffusion processes (Sherwood number); baro-diffusion coefficient; saturated vapor pressure; density of liquid fuel; characteristic pressure and temperatures, including temperatures of walls on which fuel has got. During this work some adjustments in the evaporation models are made. These corrections directed to improvement of universality and an opportunity to consider features of HCCI.

In a computational model of heat release it is distinguished four periods differing in the physicochemical features and factors limiting process rate: an ignition delay period, the period of initial flare, the period of the controlled combustion during injection after flare, the period of diffusion combustion after end of injection. After of the ignition delay period (IDP) there is explosive flame propagation through the activated mixture in spray outer zones. The first maximum of a heat release rate depends, generally on a part of fuel which has evaporated during IDP, degree of vapor activation, fuel evaporation rate during flare, i.e. depends on the mass of injected fuel, quality of its atomization and distribution, evaporation time, physicochemical, thermo - and gas dynamical characteristics of combustible mixture.

After initial flare and burning out of the fuel vapors formed during IDP, the heat release rate is defined, generally by fuel evaporation rate and rate of afterburning of unburnt combustibles in the cylinder which, in turn, depends on average oxygen concentration (see Fig. 3.8). In the period of diffusion combustion, after the end of injection and completion of spray development, occurs reduction in the combustion rate which sharp at first and then the slowed-down. It is related with reduction of mass of unburned fuel and with the limiting role of diffusion

during this period: the flame decomposes to a set of the centers around local fuel accumulations in sprays cores. If considerable fuel fraction is allocated on the piston walls, especially on walls near a cylinder head, then in the range of 15-30 CA deg. after a TDC on heat release curve one smaller peak is observed. It is related with perturbation and destruction of a quasi-laminar near-wall layer at sharp lengthening of a gas column over the corresponding surface.

Development of a reliable methodology for calculation of the ignition delay period is necessary for accurate numerical modeling of combustion in the HCCI engine. Traditional equations for the calculation of the ignition delay period are valid for the conditions in which zones with the stoichiometric fuel/air ratio are present within the fuel-air mixture. Usually, in diesel engines there are always zones with stoichiometric air/fuel composition inside the cylinder around of evaporating droplets. In these zones pre-ignition chemical reactions occur with a maximum rate. The existing empirical equations for the ignition delay predictions are derived for such the stoichiometric conditions, so these do not describe accurately physical processes in engines with HCCI. Moreover, the above empirical equations, as a rule, do not take into account the presence of a significant fraction of the exhaust gases in the fuel/air mixture, which considerably slows down the pre-ignition reactions. Equations which account for recirculation of the exhaust gases have been recently proposed. For simulation of HCCI with changing in time pressure, temperature and mixture composition in the SP DIESEL-RK is implemented an approach based on calculation of Livengood-Wu integral:

$$\int_0^{\tau_i} \frac{d\tau}{\tau_{ign}} \quad (3.1)$$

where $d\tau$ - time step; τ_{ign} - the theoretical ignition delay period at each time step. In this approach the τ_{ign} in each instant is function of four variables: pressure, temperatures, EG fraction in cylinder, and an air-fuel equivalence ratio. For calculations of τ_{ign} the kinetic mechanism proposed by Lawrence Livermore National Laboratory is used. The mechanism includes 1540 chemical reactions

between 160 species. It is assumed that the self-ignition occurs when the integral (3.1) equal 1. In the case of the integral is less than 1 during the compression and expansion processes, the self-ignition process does not take place, and an additional source for the initiating the ignition is required. As such source may be an additional fuel portion or spark.

The mathematical model of gas exchange considers a non-steady gas flow in channels, influence of the neighboring cylinders and the pulse converters. All air-gas manifold of the boosted ICE consisting of an intake manifold, inlet valve channels, the cylinder, exhaust valve channels and an exhaust manifold is decomposed into the fragments exchanging among themselves by the mass and energy. For each of fragments the system of equations of conservation of mass, energy, momentum and an equation of state are solved with the assumptions, typical of this fragment. In each fragment, except pulse converter heat exchange with walls is considered. In lengthy fragments with high pressure gradients the flow is considered as one-dimensional transient flow. For calculation of parameters in lengthy fragments it is used the method offered by professor A.S. Orlin.

For calculation of gas parameters of exhaust manifold the boundary conditions from the turbine are set by the equation approximating its performance characteristic. For calculation of mixing of flows from two collectors in the pulse converter located before the turbine or directly in turbine volute the equations of an ejector are used. Pressure and temperature of EG in the first exhaust manifold are evaluated from a system of conservation equations, written down for one exhaust manifold. This system of equations is solved together with systems of equations for cylinder and intake manifold. Parameters in the second exhaust manifold are accepted proceeding from the first collector with shift on a crank angle value

$$\Delta\varphi = 360/i_{\text{cyl}}, \quad (3.2)$$

where i_{cyl} - number of the cylinders connected with common exhaust manifold (collector). Velocity of the gas coming from collectors to the mixing zone is evaluated from Bernoulli relation for an incompressible fluid.

Total pressure of EG and their temperature in the mixing zone is determined

by different methodologies, depending on a design of the pulse converters. Then using turbine performance characteristic the gas flow rate is evaluated for obtained stagnation parameters. During cylinder scavenging of four-stroke ICE it is used an assumption about full mixing and instantaneous disturbance propagation. Whole cylinder volume represents a uniform thermodynamic system in which gas parameters are evaluated.

Parameters of turbines and compressors are considered in the different ways: are set in an explicit form, are calculated from turbine-compressor balance, are defined by coupling of turbine and compressor characteristics. The methodology of combined calculation of a piston ICE with boost devices allows to predict speed, load, altitude and other operation characteristics of supercharged and turbocharged engines on different modes. It is possible to perform selection of boost devices providing required characteristics of a boosted engine.

Heat exchange is modeled separately for different surfaces which temperatures are determined by a solution of heat conductivity task. The heat-transfer coefficient from gases to a wall of the cylinder is determined by a formula of professor G. Woschni which first forms have been published in 1965-1968. Critical dependence for heat exchange in the presence of a turbulent boundary layer is basis of this formula:

$$h_{\Sigma} = 110 \frac{P_{ft}^{0.8} \omega^{0.8}}{T^{0.53} D^{0.2}}, \quad (3.3)$$

where T - temperature, [K]; P_{ft} - pressure at the crankshaft free turning (without combustion), [bar]; D - diameter of the cylinder, [m], ω - a speed factor: $\omega = 6,18 C_m$ - for a scavenging and admission, $\omega = 2,28 C_m$ - for compression,

$$\omega = 2,28 \cdot C_m + 3,24 \cdot 10^{-3} \frac{V_h \cdot T_a}{P_a \cdot V_a} (P - P_{ft}) \quad (3.4)$$

- for combustion and expansion, i.e. $\omega = c_1 C_m + c_2 \Delta P$. Here: P - current pressure, V_h - cylinder capacity; V_a - cylinder volume at the beginning of compression; P_a and T_a - gas parameters at the beginning of compression, C_m - average piston velocity, c_1 and c_2 - constants. The speed factor has different influence on separate

sites of an operating cycle, the loading and forcing of the engine is considered through initial parameters of compression and an increment of pressure ΔP comparing to free compression. The actual size of the cylinder is considered and temperature has negative power that is typical for the criterial equations. Woschni's formula considers also radiation heat exchange, i.e. it is constructed for difficult radiation-convective heat exchange.

DIESEL-RK also performs calculation of nitrogen oxides formation in the ICE cylinder based on the thermal mechanism of the academician Y.B. Zeldovich. Definition of composition of combustion products is carried out on 18 components. For determination of temperatures the zonal model is used (a methodology of professor B.A. Zvonov). At mathematical modeling of combustion and formation of nitrogen oxides in the engine the combustion process has been conditionally separated into two zones: zone of fresh mixture and zone of combustion products. The zone of fresh mixture represents mixture of residual gases with the air which has come to the cylinder during admission. Before combustion this zone occupies all cylinder volume. During combustion the volume of a combustion products zone increases. A two-zone mathematical model of combustion has the following assumption: burning of fuel in the cylinder occurs under a local value of air-fuel equivalence ratio in the burning zone. This value during combustion changes from its initial $\alpha_{burn} < 1$ to $\alpha_{burn} = 1$.

The current value of cylinder air-fuel equivalence ratio α during combustion is defined by linear relation:

$$\alpha = \alpha_{burn} + \frac{1 - \alpha_{burn}}{\varphi_z} \varphi, \quad (3.5)$$

where φ_z - combustion duration, CA deg.; φ - the current value of a crank angle from the beginning of combustion, CA deg. The developed methodology have following features: calculation on each time step of equilibrium composition in a zone of combustion products for eighteen components and computation of kinetics of thermal nitrogen oxides formation using the Zeldovich's chain mechanism.

Evaluation of combustion products temperature in a combustion zone is carried out by a formula:

$$T_{cp} = \frac{\sqrt{B - 4A \left\{ \frac{1 - r_{cp}}{r_{cp}} [H_{mix}(T_{mix}) - H_{mix}(T_{mean})] - AT_{mean}^2 - BT_{mean} \right\} - B}}{2A}, \quad (3.6)$$

where A and B - coefficients in combustion products enthalpy equation, which can be expressed in a view:

$$H_{cp}(T_{cp}) = A \cdot T_{cp}^2 + B \cdot T_{cp} + C, \text{ kJ / kmol.} \quad (3.7)$$

Coefficients A , B , C are determined as a result of special calculations, for example, for combustion products of diesel fuel: $A=0,000966$; $B=35,4882 + 0,47283 P$; r_{cp} - combustion products fraction in a cylinder gases; P - cylinder pressure at the end of a computational step, MPa; T_{mix} - temperature of fresh mixture at the end of a computational step, K; T_{mean} - the mean temperature of a charge at the end of a computational step, K; H_{mix} - the enthalpy of fresh mixture, kJ / kmol.

The enthalpy of fresh mixture is evaluated by expression:

$$H_{mix}(T_{mix}) = [a_{mix} + 8,314 + b_{mix} T_{mix} / 2 + c_{mix} T_{mix}^2 / 3] \cdot T_{mix}, \quad (3.8)$$

where a_{mix} , b_{mix} , c_{mix} - coefficients in the expression of true molar heat capacity at constant volume of the compressed charge. For conditions of fuels combustion in internal combustion engines the formation of "thermal" nitrogen oxides is determinative. Therefore in the model all calculations are made on the thermal mechanism.

Oxidation of nitrogen in a diesel cylinder occurs by Zeldovich's chain mechanism which main reactions are:



The last reaction is determinative and its rate depends on concentration of elemental oxygen. Calculation of NO formation is performed by chain mechanism for a combustion zone, then average NO concentration on whole cylinder volume

is evaluated. Volume fraction of nitrogen oxide r_{NO} in the combustion products formed in a combustion zone on this step of calculation is evaluated by following relation:

$$\frac{dr_{NO}}{d\varphi} = \frac{P \cdot 2,333 \cdot 10^7 \cdot e^{\frac{38020}{T_{cp}}} \cdot r_{N2eq} \cdot r_{Oeq} \cdot [1 - (\frac{r_{NO}}{r_{NOeq}})^2]}{RT_{cp} (1 + \frac{2346}{T_{cp}} e^{\frac{3365}{T_{cp}}} \cdot \frac{r_{NO}}{r_{O2eq}})} \cdot \frac{1}{\omega}, \quad (3.10)$$

where P - cylinder pressure, Pa; T_{cp} - temperature in a zone of combustion products, K; R - universal gas constant, J / (mol · K); ω - the angular speed of the crankshaft, is rad/s; r_{NOeq} , r_{N2eq} , r_{Oeq} , r_{O2eq} - equilibrium concentrations of nitrogen oxide, molecular nitrogen, elemental and molecular oxygen respectively.

Equilibrium concentrations of components are evaluated on each step of calculation. Calculation is conducted for 18 components of EG: O, O₂, O₃, H, H₂, OH, H₂O, C, CO, CO₂, CH₄, N, N₂, NO, NO₂, NH₃, HNO₃, HCN. For this purpose it is performed the solution of the system consisting of 14 equilibrium equations, three material balance equations and Dalton law relations. The nitrogen oxide fraction over whole cylinder r_{NOc} is determined as equilibrium concentration of monoxide r_{NO} multiplied by equilibrium concentration of combustion products r_{cp} :

$$r_{NOc} = r_{NO} \cdot r_{cp}. \quad (3.11)$$

Specific emission (g/kW·h) of nitrogen monoxide NO is calculated by a formula:

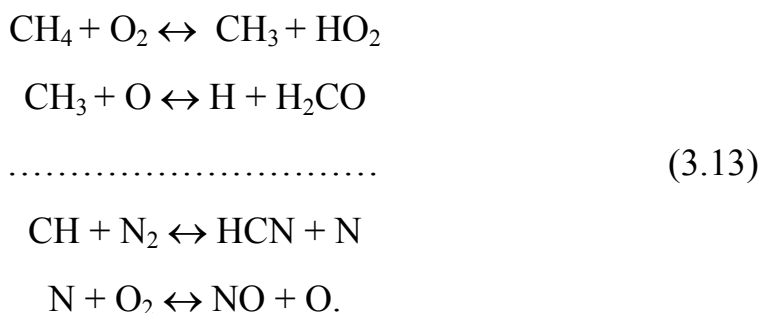
$$e_{NOx} = \frac{30 \cdot r_{NO} \cdot M_{cp}}{L \cdot \eta_m} \cdot 3600000, \quad (3.12)$$

where M_{cp} - amount of combustion products at the end of combustion, kmol; L - cycle work, kJ; η_m - mechanical efficiency of the engine.

For calculation of NOx formation in processes, considerably different from conventional diesel combustion, such as *HCCI*, in DIESEL-RK is used the mechanism of detailed chemical kinetics. According to this mechanism combustion of complex hydrocarbons occurs by stages: very fast disintegration of a fuel molecule on radicals and molecules with smaller number of atoms and

further considerably slower process of delayed burning in which particles with one - two atoms of carbon participate. For simplification of the description of the first stage of combustion for more complex, than methane, hydrocarbons (components of diesel fuel, biofuel, DME) gross-reactions which describe disintegration of the higher hydrocarbons and their derivatives up to simple molecules and radicals are implemented. Initial disintegration kinetic of a fuel molecule is described by 40 reactions with participation of 10 species. It is supposed, that regardless of initial composition of hydrocarbon at its combustion in the second phase participate the same simple hydrocarbons. Therefore for the description of delayed burning process non-empirical detail kinetic mechanism of combustion of the elementary hydrocarbon – methane is used.

The kinetic scheme of NO formation at combustion of the methane is compiled on the basis of the kinetic scheme by prof. Basevich V.J.:



This mechanism consists of 199 reactions between 33 species. The material balance of the species participating in chemical reactions, is described by system of the kinetic equations:

$$\left. \begin{aligned}
 \frac{dC_1}{d\tau} &= \pm k_1 C_j C_k \pm k_2 C_l C_m \dots \pm k_{199} C_p C_r \\
 \frac{dC_2}{d\tau} &= \pm k_1 C_a C_b \pm k_2 C_c C_d \dots \pm k_{199} C_e C_f \\
 \dots\dots\dots \\
 \frac{dC_{33}}{d\tau} &= \pm k_1 C_\alpha C_\beta \pm k_2 C_\gamma C_\delta \dots \pm k_{199} C_\epsilon C_\zeta
 \end{aligned} \right\}
 \tag{3.14}$$

where C_j, C_k, \dots, C_ζ - are mole fraction of the appropriate substances, τ - time, k_i - are the constant of chemical reaction rate which is defined from the Arrhenius equation:

$$k_i = A \cdot T^n \cdot e^{-\frac{E_A}{RT}}, \quad (3.15)$$

where A - pre-exponential factor, n - exponent, E_A - activation energy, R - universal gas constant, T - temperature. The numerical solution of the differential equations system is carried out by Gear's method with variable order of accuracy..

DIESEL-RK performs calculation of soot emission based on a methodology of professor N. F. Razleytsev. This method considers influence of features of atomized fuel burning on formation and burning out of soot particles. It is assumed, the soot is formed mainly by two ways: as a result of chain destructive transformation of molecules of fuel diffusing from the surface of drops to the front of a flame, and owing to high-temperature thermal polymerization and dehydrogenization of a vapor-liquid core of evaporating drops. In parallel to this, the process of burning of soot particles and reduction of their volumetric concentration owing to expansion occurs.

Within the offered methodology soot formation rate in a burning zone is:

$$\left(\frac{d[C]}{d\tau}\right)_K = 0,004 \cdot \frac{q_c}{V} \frac{dx}{d\tau}, \quad (3.16)$$

where V - current cylinder volume; q_c - cyclic fuel delivery; $dx/d\tau$ - heat release rate.

Soot formation rate due to high-temperature thermal polymerization of drops nucleuses is proportionate to rate of disappearance of drops because of full evaporation. In different processes one is calculated with different equations. During injection:

$$\left(\frac{d[C]}{d\tau}\right)_\Pi = 1,7 \cdot \frac{q_c}{V} \frac{1 - \exp\left[-\left(\frac{\sqrt{K\tau}}{d_{32}}\right)^{n'}\right]}{\tau_{inj}}, \quad (3.17)$$

where τ - the current time from SOI; τ_{inj} - injection duration; n' - spreading parameter (for diesel injectors $n' = 2..4$); K - evaporation constant; d_{32} - Sauter mean diameter.

For the period after injection termination the following equation is used:

$$\left(\frac{d[C]}{d\tau}\right)_{\Pi} = 0,0028(1 - x_{EOI}) \frac{n' \cdot q_c}{2V\tau_2} \left(\frac{\sqrt{K\tau}}{d_{32}}\right)^{n'} \exp\left(-\frac{\sqrt{K\tau}}{d_{32}}\right)^{n'}, \quad (3.18)$$

where τ_2 - the current time from the end of injection (EOI); χ_{EOI} - is a fraction of heat released at the end of injection.

Rate of soot burning out is determined by expression:

$$\left(\frac{d[C]}{d\tau}\right)_B = 3,1 \cdot 10^{-6} \cdot n^{0,5} \cdot p[C] \quad (3.19)$$

where p - current cylinder pressure, MPa; $[C] = \dot{C} / V$ - the current concentration of soot in cylinder volume.

Rate of soot concentration decrease due to expansion:

$$\left(\frac{d[C]}{d\tau}\right)_V = 0,75 \frac{6n}{V} \frac{dV}{d\varphi} [C] \quad (3.20)$$

Then the resulting rate of soot concentration change in the cylinder is determined as the sum:

$$\left(\frac{d[C]}{d\tau}\right) = B \left(\frac{d[C]}{d\tau}\right)_K + B \left(\frac{d[C]}{d\tau}\right)_{\Pi} - \frac{1}{B} \left(\frac{d[C]}{d\tau}\right)_B - \left(\frac{d[C]}{d\tau}\right)_V, \quad (3.21)$$

where $B = A (n_{nom}/n)^m$ is an empiric factor; n - engine speed; n_{nom} - nominal speed; A and m - empirical coefficients.

The concentration of soot in EG related to standard conditions is:

$$[C] = \int_{\varphi_B}^{480} \frac{d[C]}{d\tau} \frac{d\varphi}{6n} \left(\frac{0,1}{p_{480}}\right)^{\frac{1}{k}}, \quad (3.22)$$

where p_{480} - cylinder pressure at 60 CA deg. before BDC; k - adiabatic exponent of EG (it is accepted equal 1,33).

Conversion of the obtained value of soot concentration C [g/m^3] to Hartridge smoke level is carried out by the equation:

$$\text{Hartridge} = 100[1 - 0,9545 \exp(-2,4226[C])]. \quad (3.23)$$

Alike equations are used to calculate Bosch smoke number and Factor of Absolute Light Absorption K , m^{-1} . Particulate Matter emission is calculated by equation of Alkidas as a function of Bosch smoke number:

$$[PM] = 565 \left(\ln \frac{10}{10 - \text{Bosch}}\right)^{1,206} \quad (3.24)$$

The provided description of the SP DIESEL-RK and examples of computations for engines of different assignments confirm a possibility of usage of this software for simulations of operation of diesels and *the HCCI engines*.

3.3. Numerical investigations of operation of the diesel and *Z-engine*

At the first stage of numerical investigations by use of software package DIESEL-RK it have been performed the simulation of operation of two-cylinder *Z-engine* with dimension $D/S = 72\text{mm}/70\text{mm}$ with conventional combustion and its comparison with operation of the four-cylinder four-stroke diesel engine with the same dimensions ($4L72/70$). The general view of these engines with the boost schemes are given above on Fig. 3.5. In Table 3.1 basic characteristics of the studied engines are given, in Table 3.2 - characteristics of the *Z-engine* on the peak load conditions.

Table 3.1.

Basic characteristics of the studied engines

Characteristics	Four-cylinder four-stroke diesel	<i>Z-engine</i>
Bore, mm	72	72
Stroke, mm	70	70
Compression ratio	16,5	15,5
Boost	TC	TC + piston compressor
BMEP at peak load conditions	26,5 bars at 1500 rpm	26,2 bars at 1500 rpm

Table 3.2.

Characteristics of the *Z-engine* at peak load conditions

Characteristics	Values
BMEP	26,2 bars at 1500 rpm
Cyclic fuel delivery	53 mg
TC Pressure ratio /efficiency	4,3 / 0,47
Piston compressor pressure ratio /efficiency	4,25 / 0,85
Fraction of residual gases (EGR)	0,163
Maximum cycle pressure	202 bar
Nozzle	$8 \times 0,131$ mm
Fuel supply	2 stage:15% and 85%
Injection timing	0 CA deg. before TDC
Maximum injection pressure	1400 bar
BSFC	255 g/(kW·h)
NO _x specific emission	1,1 g/(kW·h)

Comparison of indicator diagrams of the studied engines (Fig.3.4) shows that the indicator work in the cylinder of the *Z-engine* exceeds an indicator work in the cylinder of the four-cycle diesel engine with the same dimensions. This results from the fact that the part of compression work is performed outside of the engine cylinder - in the piston compressor. It is also shown that *Z-engine* with the boost scheme presented on Fig. 3.5 produces the same effective power, as four-cylinder four-stroke diesel with the same dimension.

Precompressed and cooled air considerably reduces temperature in the cylinder in final compression process. It leads to reduce of temperature of combustion and expansion (Fig. 3.9). At the same time considerable fraction of EG remains in the cylinder (internal EGR). As a result of numerical investigations it has been found that temperature in the cylinder by the end of compression decreases with increase in loading (see Fig. 3.9). It is can be explained by a higher ratio of the fresh charge and residual gases in the volume of dead space which is formed after the short intake phase over at 60 degrees of CA before TDC (Fig. 3.10). These two factors (high recirculation and low temperature in combustion zone T_{burn}) promote considerable decrease in nitrogen oxide emissions, even at the organization of conventional diesel combustion in the engine (see Fig. 3.10).

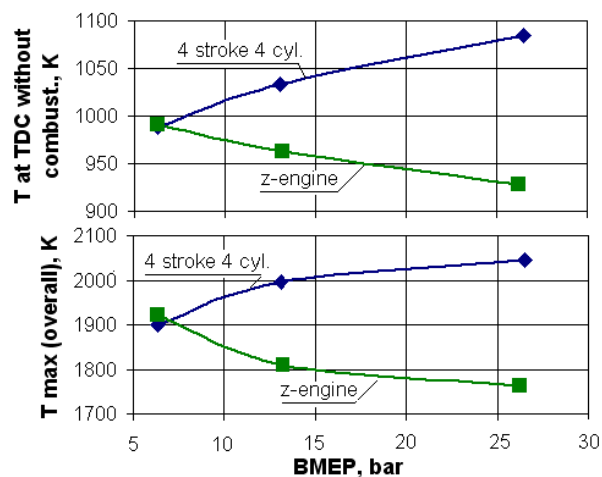


Fig. 3.9. Temperature in the cylinder at the end of compression (without combustion) and the maximum cycle temperature as function of load for the *Z-engine* and for the four-cylinder four-stroke diesel ($n=1500$ rpm)

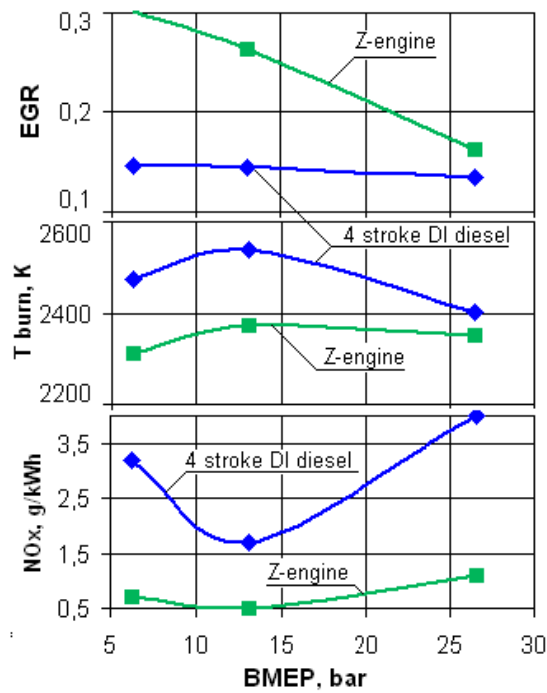


Fig. 3.10. Characteristics of the *Z-engine* and four-cylinder four-stroke diesel as function of load ($n=1500$ rpm)

Fig. 3.11 represents the comparison of the computational results of NO_x emission obtained at simulation of operation of the *Z-engine* and four-cylinder four-stroke diesel *4L72/70* with *EGR* on a different modes and Fig. 3.12 shows the comparison of BSFC of these engines.

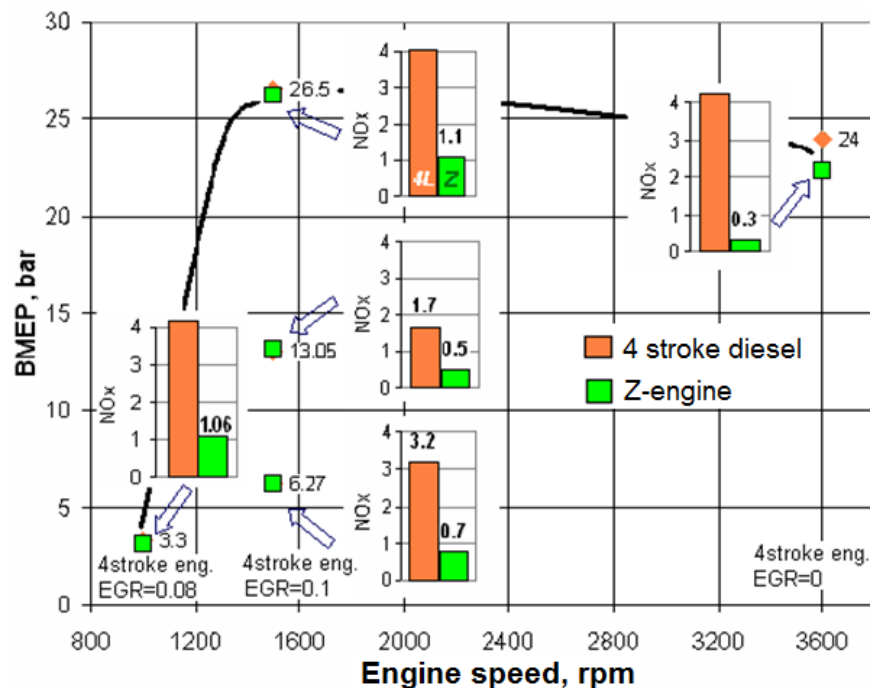


Fig. 3.11. Comparison of specific NO_x emissions in g/(kW·h) of the *Z-engine* and four-cylinder four-stroke diesel with *EGR*

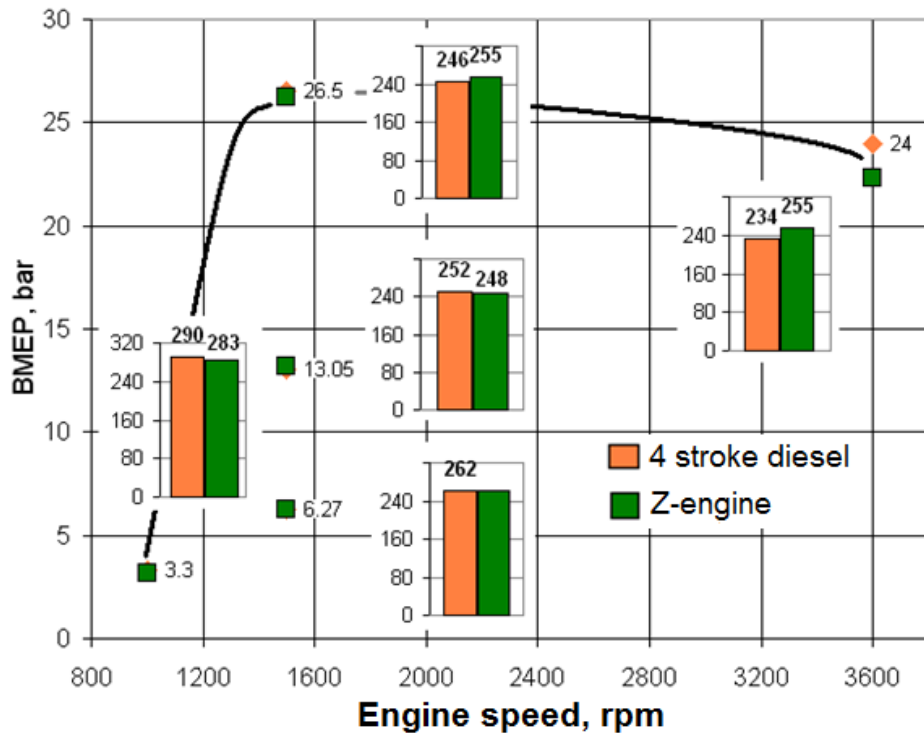


Fig. 3.12. Comparison of BSFC in $\text{g}/(\text{kW}\cdot\text{h})$ of the *Z-engine* and four-cylinder four-stroke diesel with *EGR*

The results presented on Fig. 3.11 and 3.12 show that *Z-engine* differs from the conventional diesel engine by considerably smaller nitrogen oxide emission, smaller mass-dimensional characteristics (see Fig. 3.5) at approximately identical fuel consumption.

The presented results have been obtained at simulation of conventional diesel combustion in the *Z-engine*. However the best characteristics of this engine are reached at implementation of *HCCI* in it. Therefore at the second stage of numerical investigations it has been performed the comparison of characteristics of two-cylinder *Z-engine* with dimensions $D/S = 80\text{mm}/80\text{mm}$ at realization of a conventional diesel combustion and at implementation of *SA HCCI* (*Spark Assisted Homogeneous Charge Compression Ignition*) - with ignition of a fuel-air mixture from a spark plug. It should be noted once again that implementation of combustion of a homogeneous air-fuel mixture (*HCCI*) allows to improve the main operational and technical characteristics. Reduction of combustion duration in the case of *HCCI* leads to decrease of a BSFC, decrease of local temperatures in a

combustion zone - to sharp reduction of nitrogen oxides emission, full droplets evaporation and a high air-fuel equivalence ratio - to great decrease of PM emission. For this reason further numerical investigations have been devoted to *HCCI*. Simulation, calculation and optimization of *HCCI* operation implemented in the *Z-engine* have been conducted using SP DIESEL-RK. The main results of these calculations are given below. Listings of the obtained results of simulation of the *Z-engine* with conventional diesel combustion and with *HCCI* are presented in appendices A1 and A2.

Let's consider the basic preconditions for *HCCI* organization in the cylinder of the *Z-engine*. The characteristics of cylinder pressure and temperature obtained at preliminary simulation of *HCCI* in the *Z-engine* using DIESEL-RK are presented on Fig. 3.13. It can be seen that in *Z-engine* injection of fuel occurs in a hot gas (about 800K) with the low pressure (about 3 bars). These conditions lead to much better fuel droplets evaporation (curve "a" Fig. 3.14) than in the cylinder of the conventional diesel. Besides, injection of fuel happens in a medium with large fraction of EG therefore pre-ignition reactions considerably slow down. As it has been noted above, the intake of cold fresh air occurs very intensively. It promotes, on the one hand, a mixture formation intensification (results in the increased turbulence of mixture in the cylinder, the fuel spray breaks up by airflow), on the other hand - leads to temperature decrease (curve "o" of Fig. 3.14) and to additional delay of pre-ignition reactions.

At numerical investigations it have been performed calculations of an ignition delay period using jointly software packages *CHEMKIN PRO* and DIESEL-RK. For an assessment of readiness of mixture for self-ignition it was used the Livengood-Wu integral calculated according to (3.1). Parameter τ_{ign} is calculated by kinetic mechanism proposed by *Lawrence Livermore National Laboratory (LLNL)* (1540 reactions between 160 species) in SP *CHEMKIN PRO*. As a result the function τ_{ign} from four parameters is formed: temperature, pressure, air-fuel equivalence ratio and fraction of combustion products (*EGR*). Afterwards the

obtained function is implemented to DIESEL-RK and it is employed during the calculation and optimization of engine operation. It is shown that Livengood-Wu integral does not reach value 1 (curve "j" of Fig. 3.14) owing to delay of pre-ignition reactions and uncontrollable ignition does not occur. On the other hand, because the intake produces shortly before TDC (about 60 CA deg. in comparison with 220 CA deg. at conventional two-stroke engines) and the amount of active radicals remains sufficient to initiate ignition by means of additional source. In the considered way of a homogeneous mixture ignition called *SA HCCI* combustion initiates by means of a spark plug. Preparation of mixture for ignition in a required moment on whole range of modes is carried out by means of the following ways: control by mixture temperature, pressure and mixture composition, an air-fuel equivalence ratio and percentage of EG in the cylinder using variable valve actuation system. With the same purpose it is necessary to implement control by the compressor power and efficiency of intake air intercooling, by the injection timing and duration, by the spark timing.

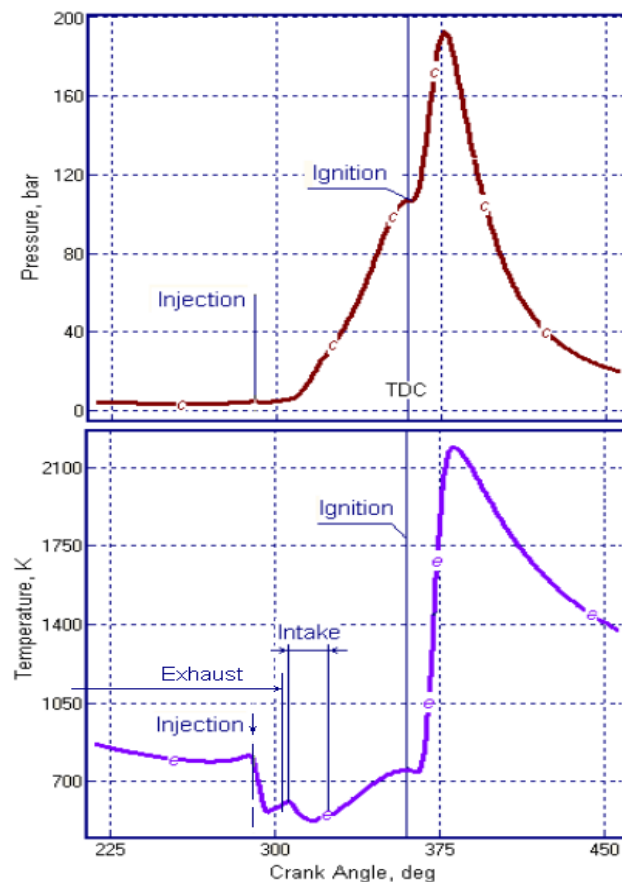


Fig. 3.13. Cylinder pressure and temperature of the *Z-engine* with *HCCI*

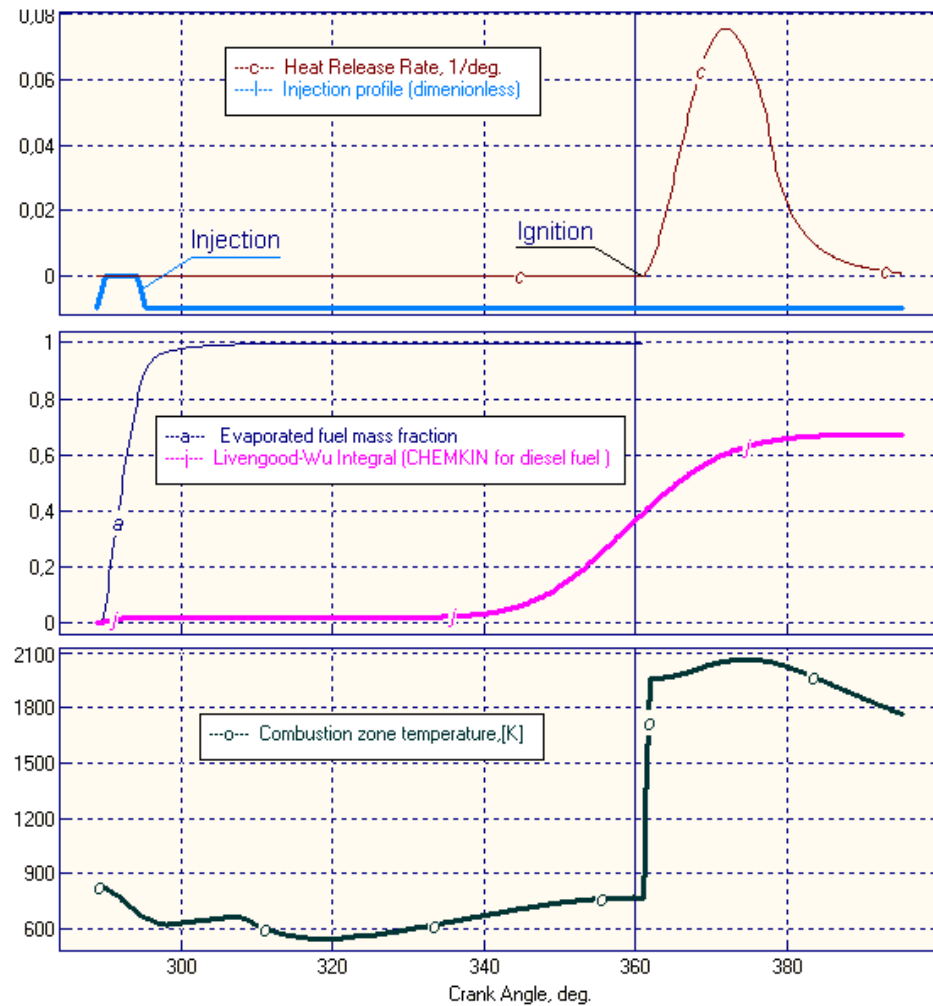


Fig. 3.14. Characteristics of injection and heat release of the Z-engine with HCCI

At numerical investigations it have been performed calculations of an ignition delay period using jointly software packages *CHEMKIN PRO* and *DIESEL-RK*. For an assessment of readiness of mixture for self-ignition it was used the Livengood-Wu integral calculated according to (3.1). Parameter τ_{ign} is calculated by kinetic mechanism proposed by *Lawrence Livermore National Laboratory (LLNL)* (1540 reactions between 160 species) in SP *CHEMKIN PRO*. As a result the function τ_{ign} from four parameters is formed: temperature, pressure, air-fuel equivalence ratio and fraction of combustion products (*EGR*). Afterwards the obtained function is implemented to *DIESEL-RK* and it is employed during the calculation and optimization of engine operation. It is shown that Livengood-Wu integral does not reach value 1 (curve "j" of Fig. 3.14) owing to delay of pre-

ignition reactions and uncontrollable ignition does not occur. On the other hand, because the intake produces shortly before TDC (about 60 CA deg. in comparison with 220 CA deg. at conventional two-stroke engines) and the amount of active radicals remains sufficient to initiate ignition by means of additional source. In the considered way of a homogeneous mixture ignition called *SA HCCI* combustion initiates by means of a spark plug. Preparation of mixture for ignition in a required moment on whole range of modes is carried out by means of the following ways: control by mixture temperature, pressure and mixture composition, an air-fuel equivalence ratio and percentage of EG in the cylinder using variable valve actuation system. With the same purpose it is necessary to implement control by the compressor power and efficiency of intake air intercooling, by the injection timing and duration, by the spark timing.

For implementation of *HCCI* in the cylinder of the engine it is necessary to carry out atomization of fuel with required uniformity and a fineness of droplets, to prevent hit of fuel on cylinder walls. At the same time it must be kept in mind that backpressure in the cylinder of the *Z-engine* is only 2,5-3,5 bars and gas density is only 1,2-1,5 kg/m³ that is much less, than in the cylinder of the conventional diesel engine. Results of researches of chapter 2 of the thesis have shown that necessary quality of a fuel atomization in conditions of so low cylinder gas density can be provided by means of multistage injection with a pintle nozzle with the small effective jet cross-section (Table 2.7 and Fig. 2.60-2.62 of chapter 2). Results of investigations have shown that for prevention of fuel hitting on cylinder walls in this case it is necessary to provide the main part of each injection stage with mass flow rate not exceeded 60 mg/s and with mass-weighted average fuel velocity on nozzle outlet (injection velocity) of 380 m/s and higher.

Proceeding from these reasons, for the case similar to the case No. 5 of Table 2.7 it have been performed simulation using method of Fig.2.57 from chapter 2. The three-dimensional computational domain of internal nozzle channel has been created, flow rate and velocity characteristics have been obtained. Also at direct simulation of jet primary break-up there was obtained the typical sizes of initial

droplets. At the second stage of simulation these obtained characteristics have been used for specification of a mass flow rate and actual injection velocity and for correction of constants of jet break-up model. At simulation of in-cylinder spray behavior (Stage II of method from Fig.2.57) for reduction of radial spray penetration there was assumed that nozzle have swirling passages producing tangential component of velocity which equal 10% of total velocity value. It was accounted by injection velocity vector direction.

As a result of *CFD* simulation in the *Ansys Fluent* there was obtained the characteristics of spray tip penetration and evaporation rate. These characteristics were used for adjusting of constants in mixture formation model of SP DIESEL-RK for simulation of spray produced by a pintle nozzle. Then were performed calculation and optimization of the *Z-engine* operation with *SA HCCI* and four stages of injection by pintle nozzle. The scheme of simulation of operation of this engine by use of the described methodology is shown on Fig. 3.15.

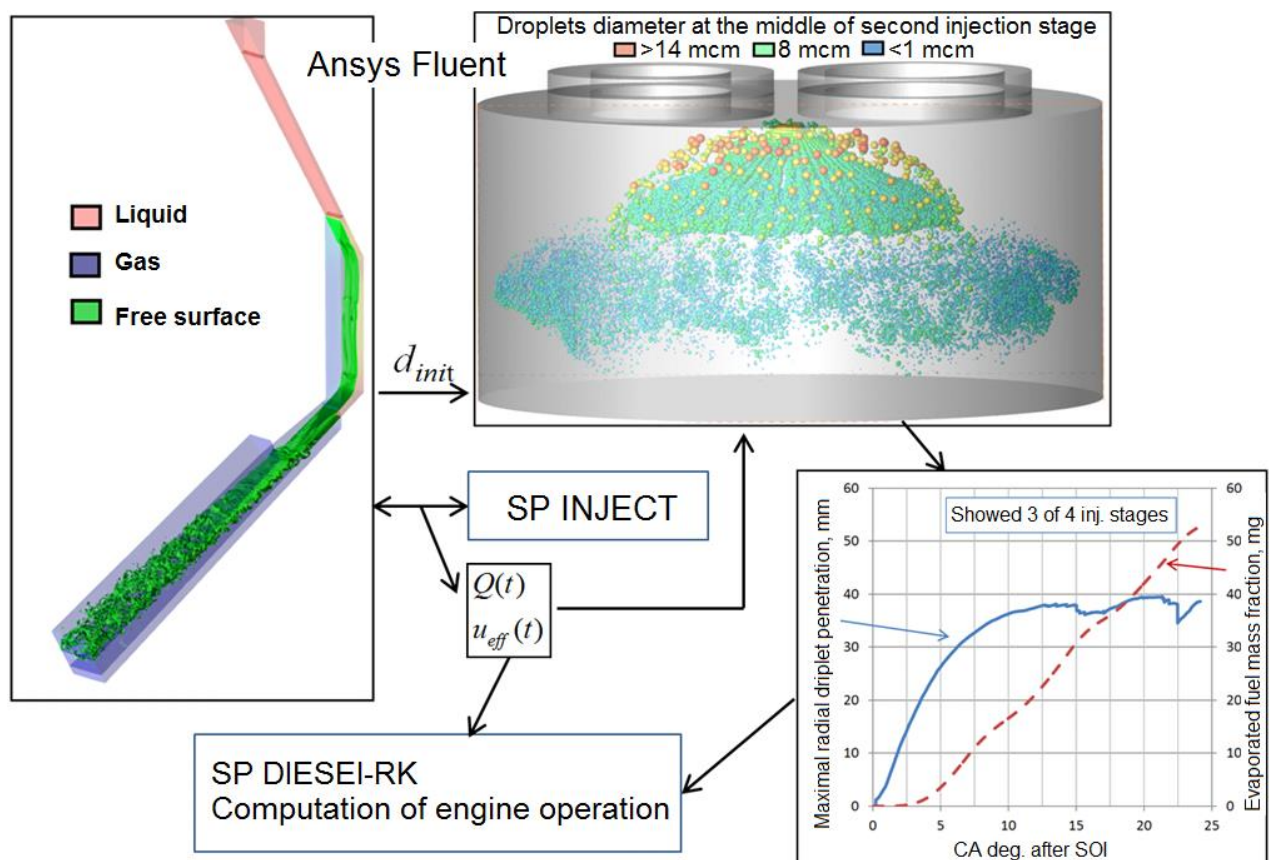


Fig. 3.15. Method of sharing the software packages *Ansys Fluent*, *INJECT* and *DIESEL-RK* for simulation of *HCCI* with multistage fuel injection by a nozzle with nonconventional geometry

The obtained results on mixture formation and combustion are presented on Fig. 3.16. History of fuel evaporation rate and Livengood-Wu integral are showed for the first and last injection portion (stage). For the first portion it is given the comparison of the evaporation rates obtained in the *CFD* simulation and by the thermodynamic RK-model (RKM) in DIESEL-RK. Their difference on initial stage (shift of curve) is explained by the fact that the thermodynamic modeling does not account of droplet heating period (accepts that heating of droplets to temperature of equilibrium vaporization occurs instantly).

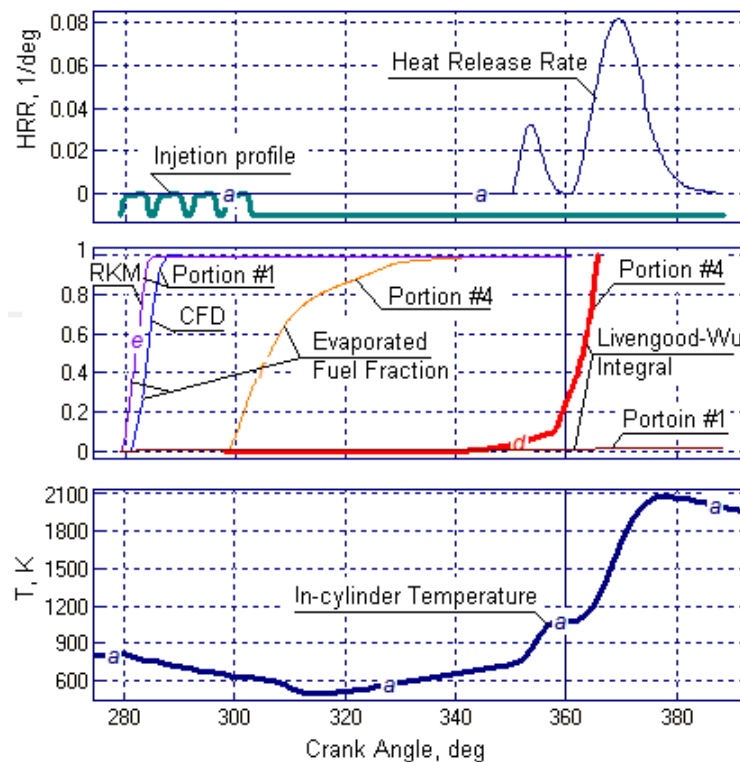


Fig. 3.16. Characteristics of mixture formation and combustion in the cylinder of the *Z-engine* with *SA HCCI* at peak load conditions (BMEP $p_e=31,1$ bars at $n=2800$ rpm)

As it has been noted above, *SA HCCI* presupposes that ignition is initiated by means of spark plug in the moment close to a TDC. Value of Livengood-Wu integral is used as criterion of suitability of an instant for producing of a spark (up to this moment value of integral have to remain less 1). If before required instant value of this integral reaches 1, it means that mixture can prematurely self-ignite. Therefore it is necessary to improve mixture formation and to reduce temperature of an air-fuel mixture. The most effective method of decrease of temperature in the

cylinder - increase the pressure ratio in the piston compressor delivering air to the cylinder. Fig. 3.16 shows that the specified integral in a TDC has not reached 1 yet therefore ignition can be successfully initiated by means of a spark plug.

Numerical investigations have also shown that implementation of *SA HCCI* in the *Z-engine* requires considerable cooling of charging air, especially after a second stage of compression. It is desirable to organize heat insulation of inlet pipelines. Results of simulations of the *Z-engine* operation performed in DIESEL-RK on the different modes of the full-load curve (FLC), including the modes of the peak load (at $n=2800$ rpm) and maximum capacity (at $n=3600$ rpm) are presented in Table 3.3. The full-load curve of the studied *Z-engine* is shown on Fig. 3.17.

It should be noted that characteristics presented in Table 3.3 have been got taking into account expenses of a work on the drive of the piston compressor. The data on a diesel combustion at peak load conditions (at $n=2800$ rpm) presented in Table 3.3 demonstrate that implementation of diesel combustion leads to smaller nitrogen oxide emission due to much expanded duration of combustion. However at the same time the BSFC is nearly 10% higher and smoke level is extremely higher. It demonstrates that the organization of diesel combustion in this engine on the specified mode is inexpedient.

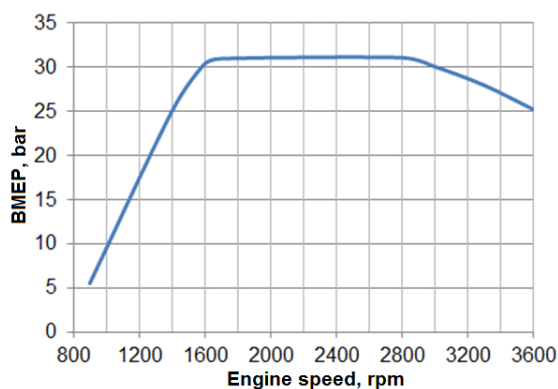


Fig. 3.17. The full-load BMEP curve of the studied *Z-engine*

In general, the conducted numerical investigations have confirmed efficiency of the *Z-engine* for improvement of characteristics of EG toxicity. There was shown the expediency of implementation of *HCCI* and its kind *SA HCCI* in the *Z-engine* for the purpose of decrease emissions of nitrogen oxides and smoke.

Table 3.3.

Characteristics of the *Z-engine* with implementation of *SA HCCI* and conventional diesel combustion

Engine speed, rpm (process type)	1600 (SA HCCI)	2800 (SA HCCI)	3600 (SA HCCI)	2800 (Diesel combustion)
Number of cylinders	2			
Bore / stroke, mm/mm	80/80			
BMEP, bar	30,44	31,11	26,21	28,42
Engine power, kW	65,28	116,8	126,5	106,7
Power of the piston compressor, KW	15,26	25,7	30,5	21,3
Cyclic delivery, g	0,069	0,070	0,059	0,070
Number of injection stages (portions)	3	4	4	1
Pressure ratio in TC / efficiency	4,0/0,75	4,3/0,76	4,5/0,75	4,3/0,75
Pressure ratio in the piston compressor / efficiency	4,5/0,85	4,5/0,85	4,8/0,85	4,5/0,85
Boost pressure, bar	17,71	18,74	20,88	18,84
Intake air temperature, K	315,1	316,4	321,4	313,3
Residual gas mass fraction	0,177	0,196	0,245	0,157
Intake duration, CA deg.	16	20	20	20
Air-fuel equivalence ratio	1,498	1,340	1,485	1,160
Injection pressure, bar	832	836	841	1435
Injection duration, CA deg.	12,4	22,2	24,0	33,8
Injection timing, CA deg. before TDC	70	80	80	20
Start of combustion, CA deg. before TDC	-1	-1	1	11,7
Maximum cylinder pressure, bar	236,0	238,7	223,0	220,0
Rate of pressure rise $dp/d\phi$, bar/deg.	6,14	6,60	6,47	10,20
Duration of 95% of combustion, CA deg.	31,2	29,4	29,0	71,6
BSFC, g/(kW·h)	202,9	201,4	201,5	220,0
Specific NO _x emission, g/(kW·h)	0,323	0,821	1,005	0,190
Smoke, <i>Bosch</i> unit	0,089	0,093	0,068	1,325
Compression ratio	13			
Exhaust valve opening, CA deg. before BDC	56			
Exhaust valve closing, CA deg. before TDC	72			
Intake valve opening, CA deg. before TDC	55			

3.4. Chapter 3 summary

1. The performed analysis of requirements imposed to EG toxicity characteristics of ICE has confirmed necessity of development and deployment of new types of engines for the purpose of decrease emissions of nitrogen oxides and smoke.

2. It was proposed the concept of the *Z-engine* representing the two-stroke diesel engine with the valve-controlled gas exchange and compression separated into two parts - preliminary in external units and final in the engine cylinder. The separated compression process and an intensive intake allow to leave sufficient time for exhaust which duration is about 180 CA deg.

3. In the *Z-engine* the preliminary stage of compression is separated into two steps - in a turbocharger and a driven piston compressor with the pressure ratio equal 4,5-5,5. After the piston compressor air is considerably cooled therefore the work spent for compression decreases and air comes to the cylinder with smaller temperature in comparison with conventional diesels.

4. There was shown the expediency of implementation of *HCCI* and its kind *SA HCCI* in the *Z-engine* for the purpose of decrease emissions of nitrogen oxides and smoke.

5. It was confirmed the necessity of numerical investigations of characteristics of the conventional diesel and the engine with implementation of *HCCI* and its kind *SA HCCI* by use of the modern software packages modeling operation of internal combustion engines.

6. The overview and the analysis of the software packages used for simulation of operation of internal combustion engines have allowed to choose for numerical investigations the SP DIESEL-RK developed in BMSTU.

7. It have been conducted the simulation and optimization of operation of the two-cylinder *Z-engine* with conventional diesel combustion and its comparative analysis with operation of the four-stroke four-cylinder diesel engine with the same dimensions.

8. There was shown that implementation of the *Z-engine* concept allows to considerably decrease mass-dimensional characteristics and nitrogen oxide emissions due to low temperature in the cylinder and high EGR. The *Z-engine* concept allows to achieve it keeping maximum capacity and fuel consumption on the same level.

9. It is presented the possibility of *SA HCCI* implementation in the *Z-engine* allowing to considerably reduce smoke and BSFC. For prevention of hit of fuel on cylinder walls the multistage injection strategy by the pintle nozzle with small effective flow section was offered.

10. The method of sharing the software packages *Ansys Fluent*, INJECT and DIESEL-RK for simulation of *HCCI* with multistage fuel injection by a nozzle with nonconventional geometry was implemented.

11. Results of computations show that on the peak load conditions implementation of *SA HCCI* in the *Z-engine* allows to reduce BSFC almost by 10%, and smoke more than by 10 times in comparison with implementation of conventional diesel combustion in this engine. Besides, the nitrogen oxide emission decreases in comparison with conventional diesels.

CHAPTER 4. EXPERIMENTAL STUDIES OF OPERATION CHARACTERISTICS OF THE Z-ENGINE

4.1. Substantiation of necessity of experimental studies of the *Z-engine*

In a chapter 3 it was shown that among the methods of improvement of toxicity indicators of ICE and achievement of modern level of their fuel efficiency the very important method is related with development and deployment of new types of internal combustion engines. Besides there was offered the new concept of engine operation - the *Z-engine*. It was shown that use of the *Z-engine* with *SA HCCI* allows to reduce BSFC almost by 10% and smoke more than by 10 times in comparison with implementation of conventional diesel combustion in this engine. At the same time nitrogen oxide emissions decrease in comparison with conventional diesels.

Researches of operation of internal combustion engines are conducted by use of different computational and experimental methods. For comparative analysis of several types of the operation behavior implemented in ICE the most reasonable method is to use the computational researches allowing to analyze a large number of calculations with different variants of operation features. Experimental studies are usually more labor-consuming and demand presence of the motor test stand equipped with the corresponding metering equipment including a gas-analyzing devices. At the same time, generally, usage of modern high-precision metering equipment ensure gaining of the reliable results and, as a rule, do not demand additional check. Therefore at limited number of experiments this approach is preferable. Besides, experimentally obtained data allow to carry out verification of the computational results of ICE operation obtained earlier and to determine the adequacy of the used mathematical models. Thereby, there were conducted the experimental studies of the *Z-engine*.

4.2. Experimental studies of the *Z-engine*

In a chapter 3 it was shown that implementation of the *Z-engine* concept is impossible without improvement of air supply system and use of the new principles of gas exchange. For the organization of high-quality gas exchange in the *Z-engine* it is necessary to provide an intensive intake of enough air amount in a whole range of modes. The mechanism providing variable valves timing is necessary for this purpose. Optimization of intake duration depending on crankshaft speed is also necessary. The result of the optimization of intake duration performed by use of DIESEL-RK is presented on Fig. 4.1.

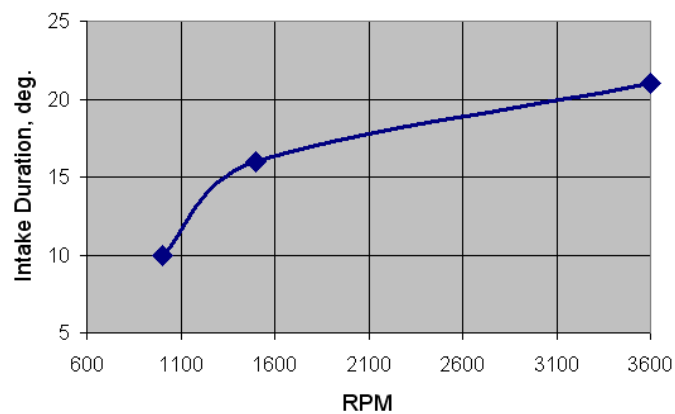


Fig. 4.1. Optimal duration of the intake of the *Z-engine* as function of engine speed

Essentially new valve train is necessary for the organization of the scheme of gas exchange for the *Z-engine*. For providing short intensive air intake this mechanism should have the high-speed drive of inlet valves. At the same time for management of intake duration and quantity of EG remaining in the cylinder the specified mechanism should change valves timing. For achievement of the best characteristics the *Z-engine* should also be supplied by the efficient piston compressor with a variable compression ratio and intercoolers with high efficiency. Temperature of inlet air should not exceed 320 K at maximum capacity.

The prototype of a valve train has been developed and made by efforts of ICE laboratory of the Helsinki university of technology [1, 36]. The 3D model and the photo of this prototype are presented on Fig. 4.2. The prototype of a valve train has

been tested at the experimental stand with the drive from an electric motor (Fig. 4.3).

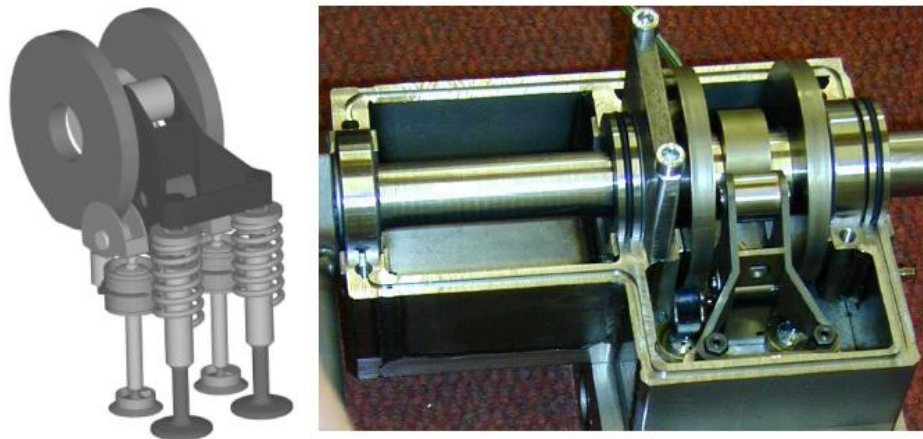


Fig. 4.2. 3D model and photo of a valve train prototype

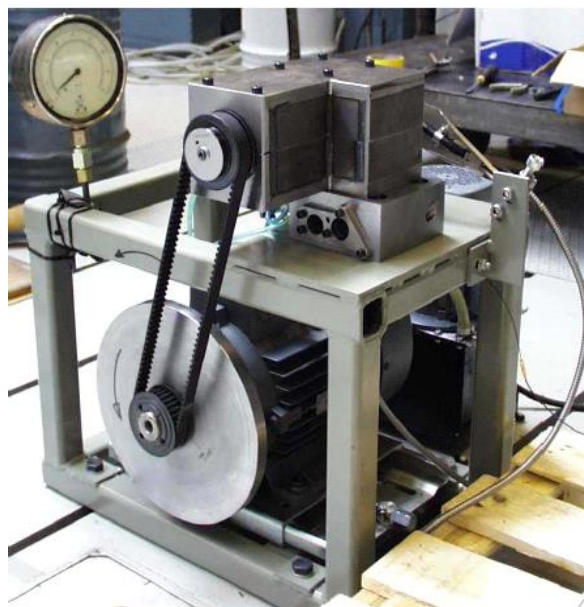


Fig. 4.3. Test stand of a valve train

During tests of a valve train there were measured accelerations of the intake valve by the accelerometer (Fig. 4.4), the amplitude-frequency characteristics (AFC) at different speeds of camshaft. The results obtained using the test stand were compared to the results obtained by simulation of the studied mechanism. Fig. 4.5 shows the dependences of the inlet valve acceleration versus camshaft angle obtained experimentally and numerically at rotating speed of $n=2000$ rpm and Fig. 4.6 presents AFCs obtained at the same rotating speed[36].



Fig. 4.4. The accelerometer mounted on the inlet valve

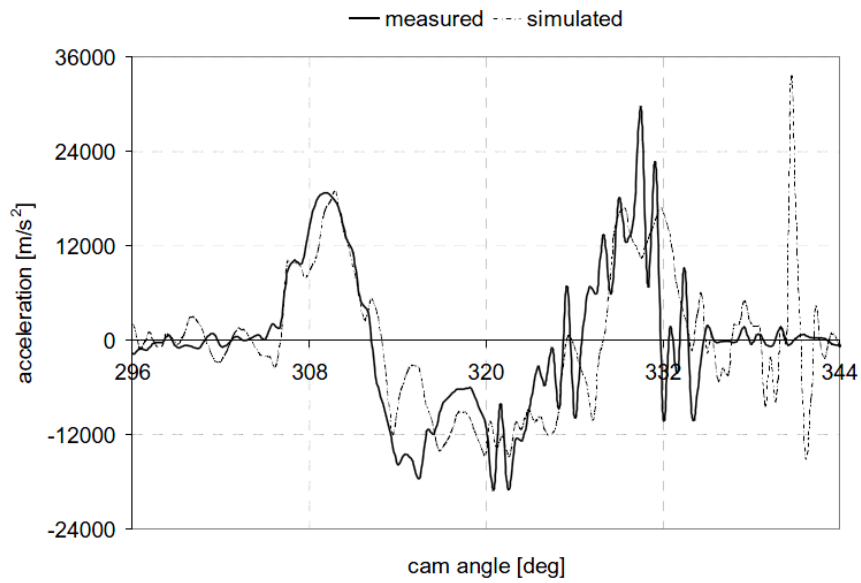


Fig. 4.5. Acceleration of the inlet valve versus camshaft angle at its rotating speed $n=2000$ rpm

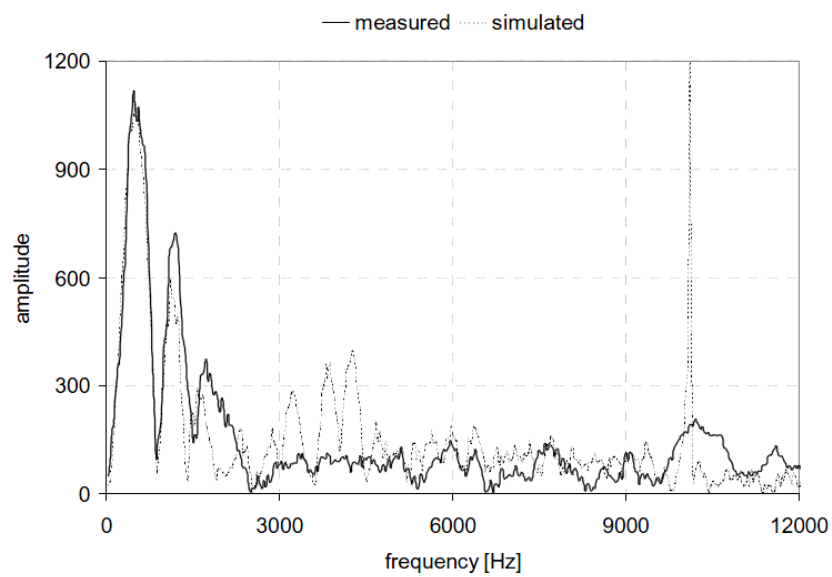


Fig. 4.6. AFC of measured and simulated inlet valve acceleration at camshaft speed $n=2000$ rpm

For assessment of efficiency of the *Z-engine* and determination of characteristics of its operation there were conducted the experimental studies. The prototype of the engine has been developed by the company *Aumet Oy* (Finland) with the participation of the Technical Research center of Finland (*VTT*). The author of the thesis participated in improvement and operational development of a fuel supply system of the engine.

The prototype of the engine has been made on the basis of the air-cooled single-cylinder four-stroke diesel engine (Fig. 4.7). For transformation of a standard operation cycle of the four-stroke engine to the *Z-engine* cycle the new cylinder head with the described valve train has been installed on the engine. In the *Z-engine* prototype the piston has been also substituted and the fuel supply system has been modified for supply of fuel in a two-stroke cycle. The piston has been developed especially for this prototype (Fig. 4.8). The Combustion Chamber (CC) is fixed in a piston head by a threaded connection and the edge of CC is made of copper alloy. For supplying of necessary amount of air the detached piston compressor has been used.



Fig. 4.7. The *Z-engine* prototype



Fig. 4.8. Piston of the *Z-engine* prototype

Experimental studies of the developed *Z-engine* prototype have been conducted on the basis of the Technical Research center of Finland (*VTT*). Experiments were made at the dynamometer test stand (Fig. 4.9).

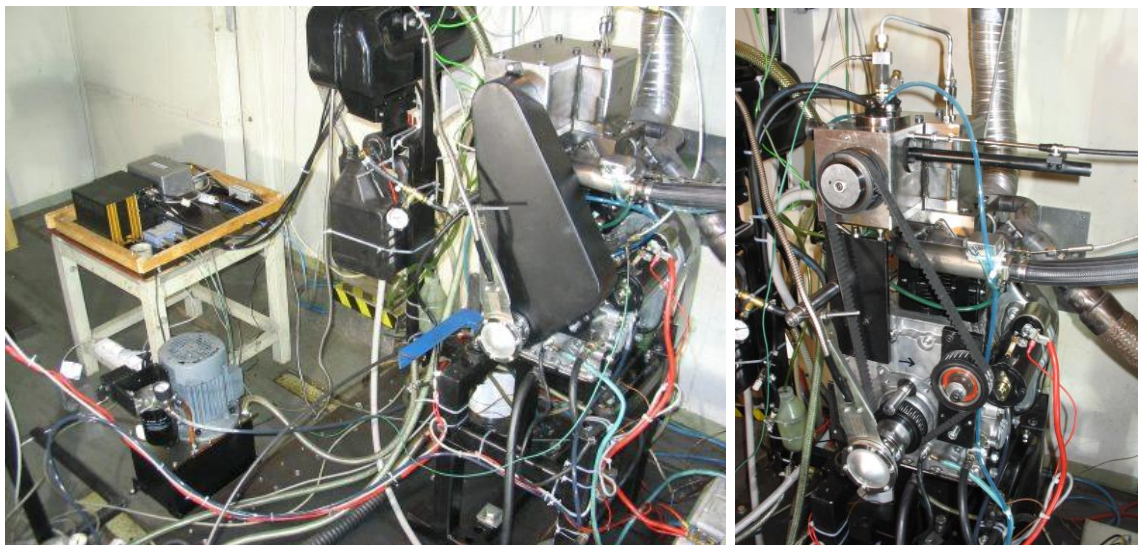


Fig. 4.9. The test stand at experimental studies of the *Z-engine*

At experimental studies of the *Z-engine* the following parameters were controlled: intake air temperature and pressure, intake air flow rate, temperature and composition of EG, temperature of the liquid cooling a cylinder head, fuel consumption, moment of resistance, the engine speed, pressure in the cylinder, the fuel injection pressure and a crank angle. By means of the module of fast data acquisition the cylinder pressure and injection pressures curves were displayed on

the laptop (Fig. 4.10) other experimental data were processed by means of the systems mounted in the laboratory. In particular, for gaining nitrogen oxide emissions data laboratory provided by gas analyzer *CLD 700 REht* manufactured by Swiss company *ECO Physics*.

At motor tests of the *Z-engine* it were investigated the dependences of different parameters from valve timing, from injection timing and its duration, from intake air pressure. In the course of tests some improvements were performed, in particular, in a fuel supply system, but the greatest changes have affected a piston design. The first variant of the piston was made using alloys of aluminum and copper, in the second variant the CC was heat-insulated and made of heat-resistant steel (Fig. 4.11). The design of CC with a ribbed surface for increase of the evaporation area and the turbulence intensity (Fig. 4.12) was the most successful.

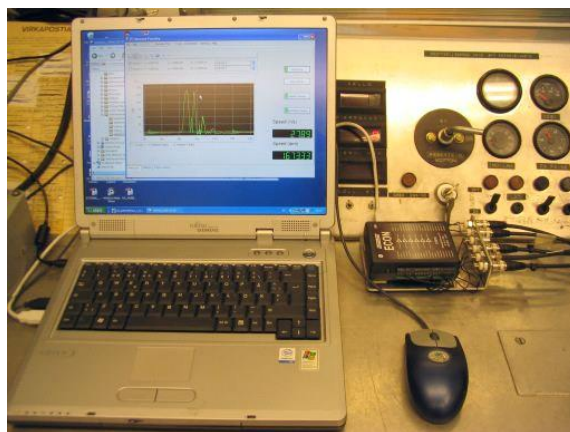


Fig. 4.10. Data acquisition



Fig. 4.11. The piston with the heat-insulated CC of the *Z-engine*

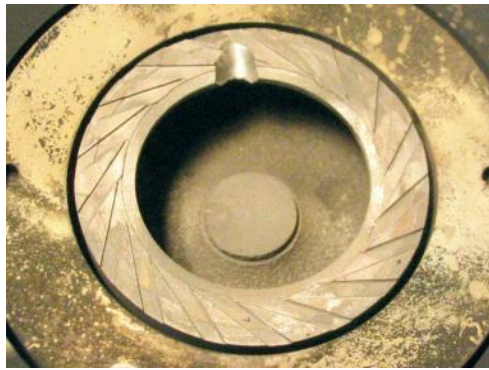


Fig. 4.12. The piston with a ribbed surface of CC of the *Z-engine*

High pressure of intake air has allowed to use energy of a fresh charge for mixture formation intensification. The shapes of CC and intake channel also promote to swirl motion of a charge with high intensity. At tests it has been used as the scheme of mixture formation with a displacer in a cylinder head (Fig. 4.13, a), and without displacer and the central placement of CAV microinjector (Fig. 4.13, b). At the same time the different ways of intake air direction to the combustion chamber have been used (Fig. 4.14, 4.15).

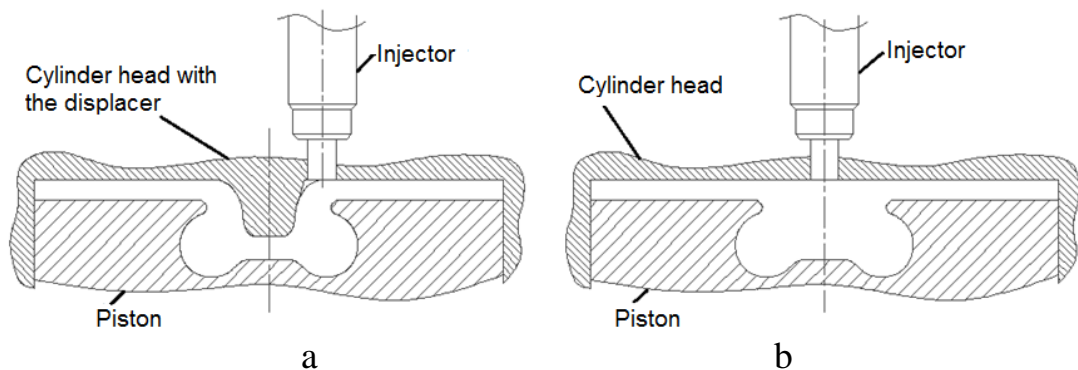


Fig. 4.13. Scheme of mixture formation of the *Z-engine*

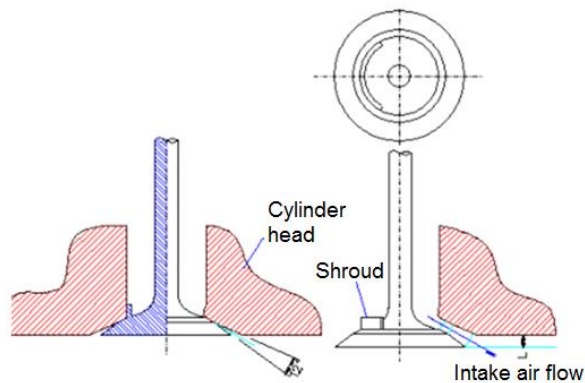


Fig. 4.14. The scheme of intake air direction by means of the valve with a shroud

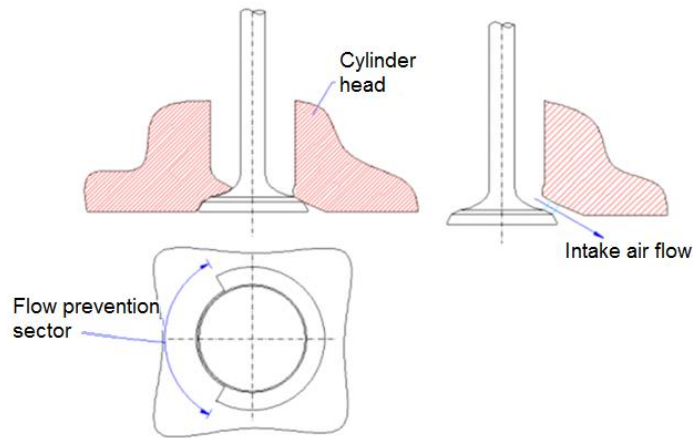


Fig. 4.15. The scheme of intake air direction using partially flow prevention by a shoulder in intake channel

The described scheme of mixture formation in the *Z-engine* prototype is a combination of a swirl chamber and the *Perkins "Squish Lip"*. According to results of numerical researches, in the *Z-engine* CC airflow velocity is so considerable that the swirl number reaches the level of swirl-chamber diesel engines [36]. Using software *NSF* [42] it has been calculated the characteristics of turbulence in the cylinder of the studied engine. As can be seen from Fig. 4.16, after opening of inlet valves the level of turbulent kinetic energy of a charge in the cylinder is very high. It promotes implementation of high quality mixture formation: the high-turbulent flow of inlet air breaks a jet of the injected fuel and uniformly distributes droplets on cylinder volume. The high level of turbulence in the cylinder remains during 20-25 CA deg. and at the time of arrival of the piston to a TDC does not exceed the level of four-stroke diesel analogs. Therefore there are not additional heat losses at combustion.

After operational development of the engine on the basis of the Technical Research center of Finland (*VTT*) it has been conducted the next engine tests of the *Z-engine* with conventional diesel combustion (not *HCCI*) at partial load conditions. At these tests the injection pump *Bosch PFE* was used and the outward-opening injector was located on a cylinder axis (Fig. 4.13, b). In Table 4.1 some characteristics of the *Z-engine* obtained at these tests on the mentioned mode are presented.

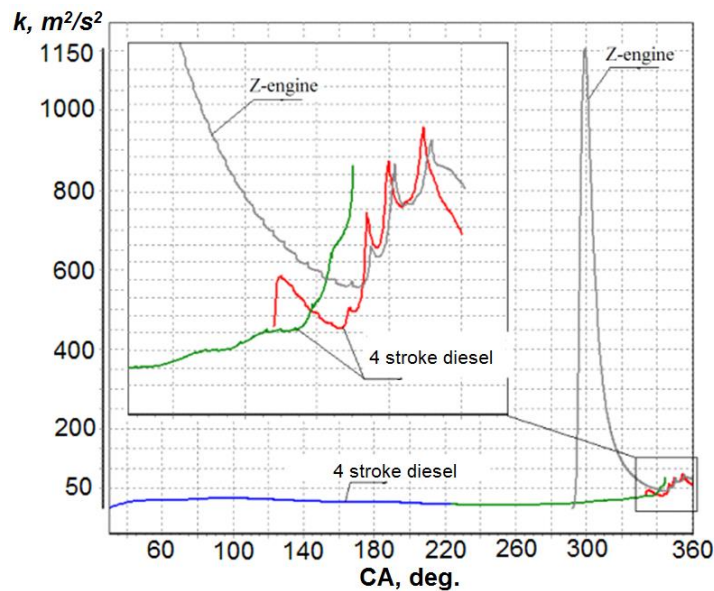


Fig. 4.16. History of turbulent kinetic energy k versus crank angle of the *Z-engine* and four-stroke diesel engine

Table 4.1.

The *Z-engine* characteristics obtained at engine test at partial load condition

Characteristic		Value
Engine speed, rpm		1600
BMEP, bar		4,1
Valves timing	Exhaust valve opening, CA deg. before BDC	60
	Exhaust valve closing, CA deg. after BDC	120
	Intake valve opening, CA deg. after BDC	120
	Intake valve closing, CA deg. after BDC	136
Cyclic fuel delivery, mg		18,3
Boost pressure (after the piston compressor), bar		7,8
Air-fuel equivalence ratio		1,65
Efficiency		0,35
Specific nitrogen oxide emission, g/(kW·h)		0,8

Data in Table 4.1 demonstrate that on a mode with engine speed $n=1600$ rpm and the load corresponding to BMEP $p_e=4,1$ bar, the efficiency was $\eta_e=0,35$ that corresponds to a BSFC $g_e=242,0$ g/(kW·h). At the same time specific nitrogen oxide emission was equal to $e_{NOx}=0,8$ g/(kW·h).

Fig. 4.17 shows the indicator diagram of the studied engine in p - V coordinates and Fig. 4.18 presents the characteristics of cylinder pressure and injection pressure versus crank angle. Fig. 4.19 shows the cylinder pressure history in the course of gas exchange.

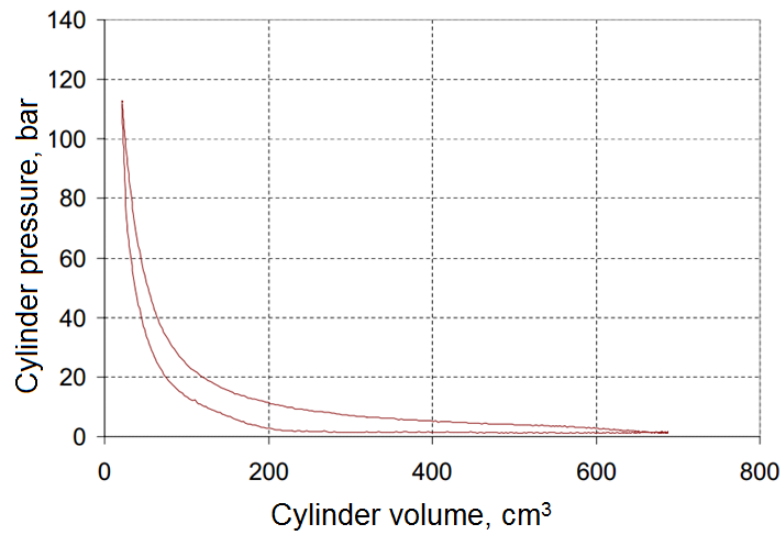


Fig. 4.17. An indicator diagram of the studied *Z-engine*

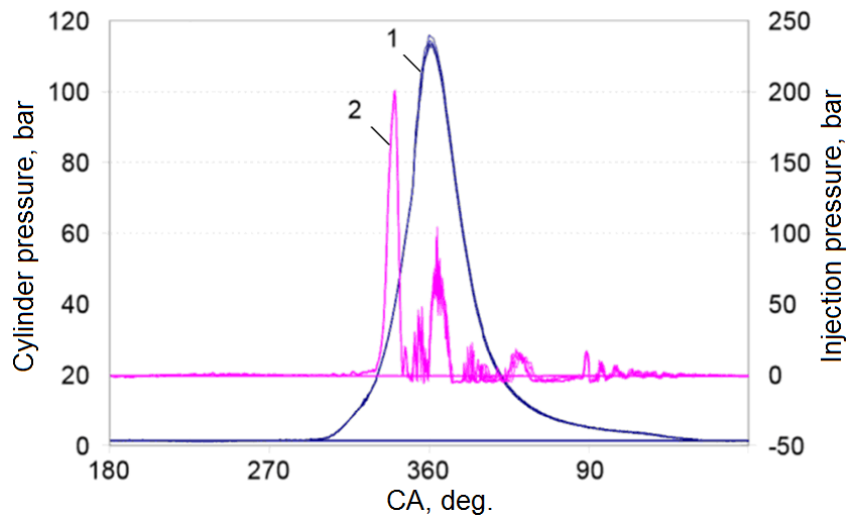


Fig. 4.18. Characteristics of the *Z-engine* cylinder pressure (1) and injection pressure (2)

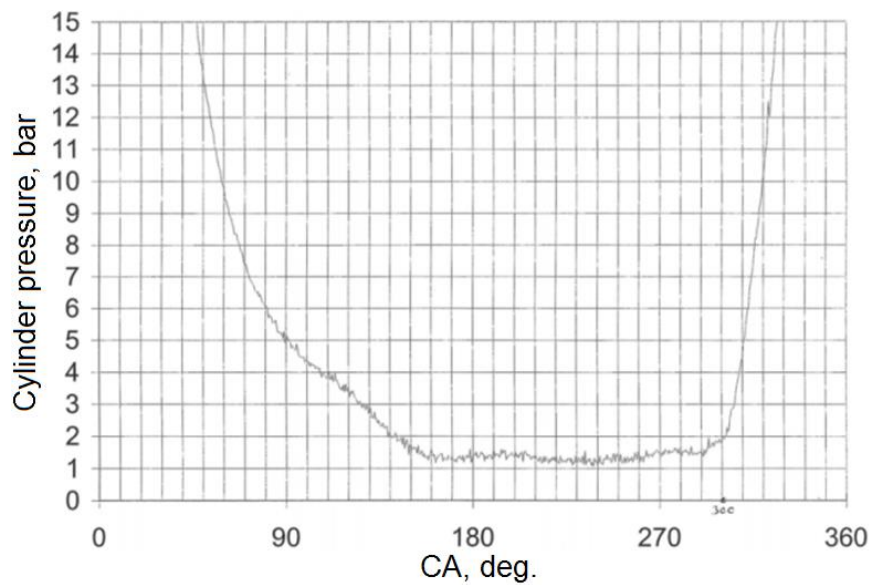


Fig. 4.19. The *Z-engine* cylinder pressure history in the course of gas exchange

The obtained experimental data confirm a possibility of creation of the *Z-engine* with the EG toxicity characteristics improved in comparison with the conventional diesel engine. Besides, as it is noted above, these experimental data allow to carry out verification of the results of numerical investigations of operation of the *Z-engine* obtained earlier and to evaluate adequacy of the used mathematical models.

4.3. Comparative analysis of experimental and calculation data of the *Z-engine*

For an assessment of adequacy of the results obtained at calculations by use of SP DIESEL-RK it has been performed a comparison with the experimental data obtained on the basis of the Technical Research center of Finland (VTT). The comparison performed for the *Z-engine* operation with conventional diesel combustion (not a *HCCI*) at partial load condition. Table 4.2 presents the characteristics of the *Z-engine* obtained at tests and by simulation.

Table 4.2.

The *Z-engine* prototype characteristics at partial load condition obtained at experiment and by simulation in DIESEL-RK

Characteristic		Experiment	Simulation
Number of cylinders		1	
Bore / Stroke, mm/mm		96/92	
Engine speed		1600	
BMEP, bar		4,1	4,1
Engine power, kW		7,25	7,29
Valve timings	Exhaust valve opening, CA deg. before BDC	60	
	Exhaust valve closing, CA deg. before TDC	60	
	Intake valve opening, CA deg. before TDC	60	
	Intake valve closing, CA deg. before TDC	44	
Cyclic delivery, mg		18,3	
Boost pressure (after the piston compressor), bar		7,8	7,7
BSFC, g/(kW·h)		242	241
Specific nitrogen oxide emission, g/(kW·h)		0,80	0,79

Fig. 4.20 shows the comparison of charts of the *Z-engine* cylinder pressure obtained in experiment and by simulation, and Fig. 4.21 presents comparison of cylinder pressure curves in the course of gas exchange. The analysis of these data confirms good coincidence of results of computational and experimental characteristics. In particular, comparison of maximum cycle pressure shows that the difference between experimentally obtained value ($p_z=117$ bar) and a calculated value ($p_z=118$ of bars) does not exceed 1%.

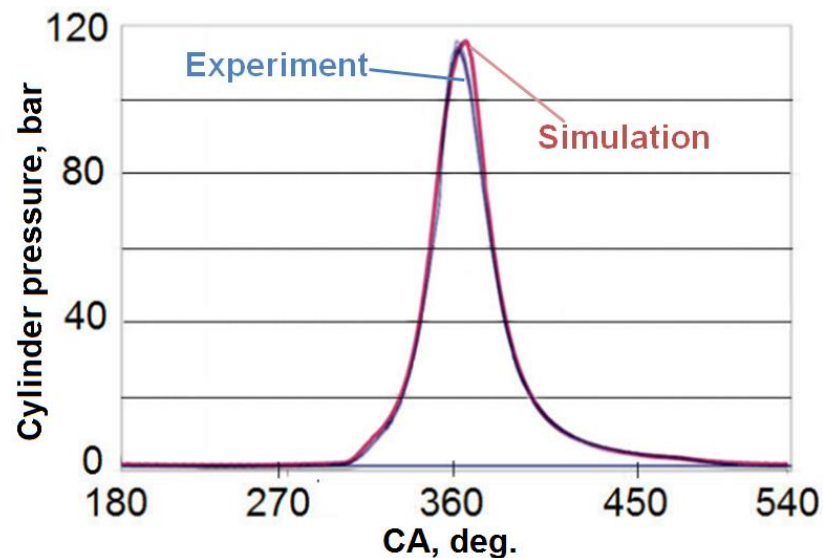


Fig. 4.20. Comparison of the *Z-engine* cylinder pressure obtained in experiment and by simulation

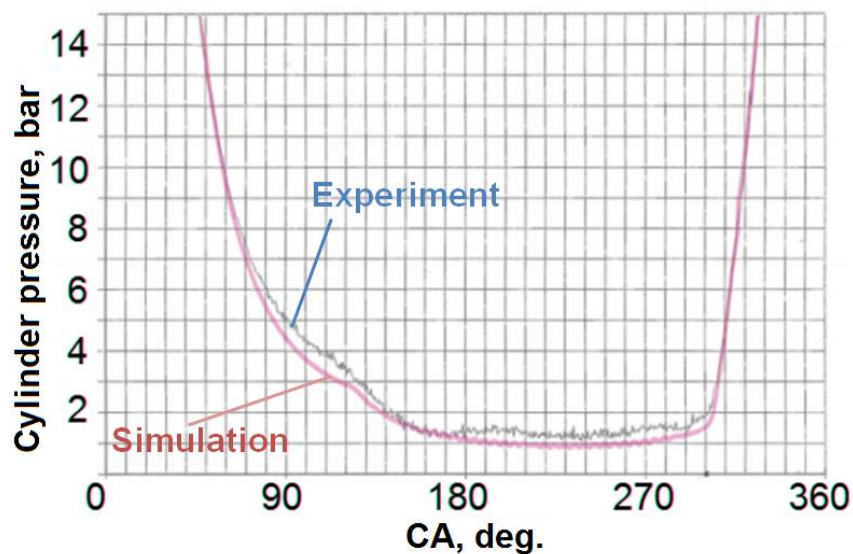


Fig. 4.21. Cylinder pressure in the course of gas exchange of the *Z-engine* obtained in experiment and by simulation

4.4. Chapter 4 summary

1. It was substantiated the necessity of carrying out the experimental studies of characteristics of fuel efficiency and EG toxicity of the engine.

2. For achievement of the best characteristics, the *Z-engine* should be supplied with the valve train with variable timings for management of intake duration. It is necessary to use the efficient piston compressor with a variable compression ratio and intercoolers with high efficiency. Temperature of inlet air should not exceed 320 K on maximum capacity mode.

3. It have been conducted the experimental studies on a single-cylinder prototype of the *Z-engine* at partial load conditions. The indicator diagram and other characteristics of the studied engine have been obtained.

4. The obtained experimental data demonstrate that on a mode with engine speed $n=1600$ rpm and the load corresponding to BMEP $p_e=4,1$ bar, the efficiency is $\eta_e=0,35$ that corresponds to a BSFC $g_e=242,0$ g/(kW·h). At the same time specific nitrogen oxide emission is equal to $e_{\text{NOx}}=0,8$ g/(kW·h).

5. It have been performed the comparative analysis of experimental data of the studied *Z-engine* at partial load condition with calculation data obtained by use of software package DIESEL-RK.

6. Comparative analysis of these data confirms good coincidence of results of computational and experimental characteristics. In particular, comparison of maximum cycle pressure shows that the difference between experimentally obtained value ($p_z=117$ bar) and a calculated value ($p_z=118$ of bars) does not exceed 1%.

7. Results of the conducted experimental studies have confirmed operability of the developed *Z-engine* and its efficiency for decreasing emissions of nitrogen oxides and smoke of EG.

THE MAIN RESULTS AND CONCLUSIONS OF THE THESIS

The conducted numerical and experimental investigations have shown that by improvement of fuels injection and atomization in the HCCI engine it is possible to provide considerable improvement of characteristics of fuel efficiency and EG toxicity of an internal combustion engine. The results obtained at investigations can be summarized by the following main conclusions:

1. The two-stage method of analysis of fuel injection, atomization and evaporation has been developed. By use of this method it can be obtained characteristics of a fuel flow, fuel spray and mixture formation, quality metrics of atomization and evaporation for any nonconventional geometry of a nozzle. The method of sharing the software packages *Ansys Fluent*, INJECT and DIESEL-RK for simulation of *HCCI* with multistage fuel injection by a nozzle with nonconventional geometry was implemented.

2. At numerical investigations of internal nozzle fuel flow and in-cylinder spray behavior it was shown the influence of cavitation and air entrainment on characteristics of a fuel flow in nozzles with different geometry and on characteristics of a spray.

3. By use of experimental data it was carried out the choice and adjustment of mathematical models of fuel injection, atomization and evaporation for nozzles with nonconventional geometry of a flowing channel in the conditions of cavitation. The analysis and comparison of the computational results obtained using different models have been performed. For *CFD* simulations it has been determined the set of the most reasonable models describing processes of injection, atomization and fuel evaporation in ICE.

4. Influence of different factors on characteristics of a fuel spray, its atomization and evaporation was investigated. Ways of limitation of spray tip penetration and improvement of quality metrics of atomization in the conditions of low gas density in the cylinder were offered. The mixture formation concept for the HCCI engine which provides full droplets evaporation and prevents hit of fuel

on cylinder walls was developed.

5. It was proposed the concept of the *Z-engine* representing the two-stroke diesel engine with the valve-controlled gas exchange and compression separated into two parts - preliminary in external units and final in the engine cylinder. The separated compression process and an intensive intake allow to leave sufficient time for exhaust which duration is about 180 CA deg. In the *Z-engine* the preliminary stage of compression is separated into two steps - in a turbocharger and a driven piston compressor with the pressure ratio equal 4,5-5,5. After the piston compressor air is considerably cooled therefore the work spent for compression decreases and air comes to the cylinder with smaller temperature in comparison with conventional diesels.

6. There was shown the expediency of implementation of *HCCI* and its kind *SA HCCI* in the *Z-engine* for the purpose of decrease emissions of nitrogen oxides and smoke.

7. There was shown that implementation of the *Z-engine* concept allows to considerably decrease mass-dimensional characteristics and nitrogen oxide emissions due to low temperature in the cylinder and high EGR. The *Z-engine* concept allows to achieve it keeping maximum capacity and fuel consumption on the same level.

8. Results of computations show that on the peak load conditions implementation of *SA HCCI* in the *Z-engine* allows to reduce BSFC almost by 10%, and smoke more than by 10 times in comparison with implementation of conventional diesel combustion in this engine. Besides, the nitrogen oxide emission decreases in comparison with conventional diesels.

9. It have been conducted the experimental studies on a single-cylinder prototype of the *Z-engine* at partial load conditions. The indicator diagram and other characteristics of the studied engine have been obtained. The obtained experimental data demonstrate that on a mode with engine speed $n=1600$ rpm and the load corresponding to BMEP $p_e=4,1$ bar, the efficiency is $\eta_e=0,35$ that corresponds to a BSFC $g_e=242,0$ g/(kW·h). At the same time specific nitrogen

oxide emission is equal to $e_{\text{NO}_x}=0,8 \text{ g}/(\text{kW}\cdot\text{h})$.

10. It have been performed the comparative analysis of experimental data of the studied *Z-engine* at partial load condition with calculation data obtained by use of software package DIESEL-RK. Comparative analysis of these data confirms good coincidence of results of computational and experimental characteristics. In particular, comparison of maximum cycle pressure shows that the difference between experimentally obtained value ($p_z=117 \text{ bar}$) and a calculated value ($p_z=118 \text{ of bars}$) does not exceed 1%.

11. Results of the conducted experimental studies have confirmed operability of the developed *Z-engine* and its efficiency for decreasing emissions of nitrogen oxides and smoke of EG.

REFERENCES

1. Kuleshov A.S., Akimov V.S., Janhunen T. Numerical investigation of cavitation development in pintle-type injector of the HCCI engine // Problems of gas dynamics, heat and mass transfer in power plants. Proceedings of school-seminar of young scientists and specialists under supervision of professor A.I. Leontiev, academician of the Russian academy of sciences. Moscow: MPEI publishing house, 2013, pp. 125-126 (in Russian).
2. Alekseev V.P., Vyubov D.N. A principal physics of processes in combustion chambers of ICE. Moscow: publishing house of MVTU named after N.E. Bauman, 1977. 34 p. (in Russian).
3. Belov I.A., Isaev S.A., Korobkov V.A. Tasks and methods of computation of separated flows of an incompressible fluid. Leningrad.: Shipbuilding, 1989. 256 p. (in Russian).
4. Markov V.A., Devyanin S.N., Nagornov S.A., Akimov V.S. Fuels produced from various raw material sources // Transport na alternativnom toplive [Alternative Fuel Transport], No. 3 (21), 2011, pp. 25-31 (in Russian).
5. Boldyrev I.V. A simple model of a fuel spray taking into account changes of mixture composition // Engine building. 1982. No. 12. pp. 16-20 (in Russian).
6. Markov V.A., Akimov V.S., Shumovskiy V.A., Markova V.V. Influence of mixed biofuel composition on the parameters of fuel injection process in diesel engine // Traktory i selhozmashiny [TRACTORS AND AGRICULTURAL MACHINERY], № 12, 2014, pp. 3-9 (in Russian).
7. Voinov A.N. Combustion in high-speed diesels. Moscow: Mechanical engineering, 1977. 277 p. (in Russian).
8. Akimov V.S., Kuleshov A.S., Markov V.A., Yakovchuk A.Yu, Janhunen T.T. Fuel Injection and Spray Processes in a Z-Engine // Gruzovik [Truck], № 2, 2015, pp. 14-20 (in Russian).
9. Vyubov D.N., 1954, "Method of calculation of fuel evaporation," // Publications of BMSTU, Vol. 25, pp. 20-34 (in Russian).
10. Vyubov D.N. About mixture formation calculation // Proceedings of

Higher Educational Institutions. Machine Building. 1973. No. 11. pp. 86-90 (in Russian).

11. Vyubov D.N. Mixture formation problems in the diesels // Increase of power and economy of internal combustion engines: higher education institutions collection Moscow: Mashgiz, 1957. 280 p. (in Russian).

12. Vyubov D.N. Mixture formation in Diesel engines// Operations of internal combustion engines and their units:higher education institutions collection. Moscow: Mashgiz, 1946. pp. 5-54 (in Russian).

13. Gavrilov V.V., Zakharenko B.A. Experimental research technique of structure of a jet of a diesel injector // Engine building. 1979. No. 9. pp. 34-37 (in Russian).

14. Golubkov L.N. Hydrodynamic processes in fuel systems of diesels at a two-phase state of fuel//Engine building. 1987. No. 1. pp. 32-35 (in Russian).

15. Golubkov L.N. Generalization of the theory, development of computational methods and improvement of fuel systems of automobile and tractor diesels: Doctoral Diss.: 05.04.02. Moscow: BMGTU, 1990. 410 p. (in Russian).

16. Golubkov L.N., Perepelin A.P. Metod of hydrodynamic calculation of a fuel system of the diesel taking into account a two-phase state of fuel // Operations in ICE and their units: Collection of scientific works of MADI. Moscow: MADI publishing house, 1987. pp. 80-87 (in Russian).

17. Golubkov L.N. A numerical investigation of ways of an increase of fuel injection pressure in diesels// Automobile and tractor internal combustion engines: Collection of scientific works of MADI. Moscow: MADI publishing house, 1986. pp.71-76 (in Russian).

18. Gorbunov V.V., Patrakhaltsev N. N. Toxicity of internal combustion engines. Moscow: Publishing house of the RUDN University, 1998. 216 p. (in Russian).

19. Grekhov L.V., Gabitov I.I., Negovora A.V. Design, calculation and technical service of fuel supply systems of diesels: Manual for higher education institutions. Moscow: Legion-Avtodata publishing house, 2013. 292 p. (in

Russian).

20. Grekhov L.V., Ivaschenko N.A., Markov V.A. Fuel systems and diesel control. Moscow: Legion-Autodata, 2005. 344 p. (in Russian).

21. Grekhov L.V. Use of the linearized Godunov method for calculation of a fuel supply in diesels // Automobile and tractor engines: higher education institutions collection of MAMI. 1999. Issue 16. pp. 81-87 (in Russian).

22. Kuleshov A.S., Grekhov L.V. Matematicheskoe modelirovanie i komp'yuternaia optimizatsiia toplivopodachi i rabochikh protsessov dvigatelei vnutrennego sgoraniia [Mathematical modeling and computer-optimized fuel and work processes of internal combustion engines]. Moscow, Bauman Press, 2000. 64 p. (in Russian).

23. Grekhov L.V. Scientific bases of development of systems of a fuel supply in the cylinder of internal combustion engines: Doctor Diss: 05.04.02. Moscow: BMGTU, 1999. 390 p. (in Russian).

24. Grekhov L.V. The refined mathematical model of process of fuel supply in the diesel//Proceedings of Higher Educational Institutions. Machine Building. 1997. No. 10-12. pp. 47-51 (in Russian).

25. Grinshman A.Z., Romanov S.A., Sviridov Y.B. Analytical model of development of a spray of atomized liquid fuel in a motionless gaseous fluid // Research and designing of the fuel equipment of diesel engines: Collections of articles. Leningrad: TsNITA, 1975. Issue 64. pp. 17-23 (in Russian).

26. Gusakov S.V., Afanasyeva I.V., Murad H. The analysis of a feasibility of application of fuels with the low specific heat of combustion in ICE//Alternative Fuel Transport. 2011. No. 2. pp. 34-37 (in Russian).

27. Gusakov S.V., Yepifanov I.V. Investigation of *HCCI* by use single-zone chemical-kinetic model of combustion//RUDN Bulletin. Engineering Researches series. 2008. No. 2. pp. 67-73 (in Russian).

28. Gusakov S.V., Makhmoud Mohamed El-Gobashi El-Hagar. Simulation of operation of the piston engine with self-ignition of a homogeneous charge//News of the Tula state university. Motor transport series. 2003. pp. 173-179 (in Russian).

29. Gusakov S.V., Makhmoud Mohamed El-Gobashi El-Hagar. Experience of simulation of ICE operation with ignition of a homogeneous charge from compression // RUDN Bulletin. Engineering Researches series. 2004. No. 2. pp. 25-28 (in Russian).

30. Gusakov S.V. Development of methods of improvement of processes of mixture formation and combustion in piston engines: Doctor Diss.: 05.04.02. Moscow: BMSTU, 2002. 344 p. (in Russian).

31. Gusakov S.V., Savastenko A.A. Physicochemical bases of processes of mixture formation and combustion in ICE. Moscow: RUDN publishing house, 2001. 134 p. (in Russian).

32. Orlin A.S., Kruglov M.G., Yefimov S.I., Ivashchenko N.A., Ivin V.I. et.al. Internal combustion engines: Systems of piston and hybrid engines: Textbook for higher education institutions. Moscow: Machine building. 1985. 456 p. (in Russian).

33. Orlin A.S., Kruglov M.G., Vyubov D.N., Ivashchenko N.A., Ivin V.I. et.al. Internal combustion engines. The theory of piston and composite engines: Textbook for higher education institutions. Moscow: Machine building. 1983. 372 p. (in Russian).

34. Orlin A.S., Kruglov M.G., Alekseev V.P., Voronin V.F., Grekhov L.V. et. al. Internal combustion engines: Structure and operation of piston and hybrid engines: Textbook for higher education institutions. Moscow: Machine building, 1990. 288 p. (in Russian).

35. Akimov V.S., Kuleshov A.S., Markov V.A., Yakovchuk A.Yu, Janhunen T.T. Z-engine: optimization of fuel injection and spray processes // Avtomobilnaya promyshlennost [Automotive industry], No. 3, 2015, pp. 17-21 (in Russian).

36. Janhunen T.T, Akimov V.S., Kuleshov A.S., Markov V.A. Diesel Engine with HCCI-Process // Gruzovik [Truck], No. 10, 2014, pp. 33-43 (in Russian).

37. Devyanin S. N., Markov V.A., Semenov V. G. Vegetable oils and fuels on their basis for diesel engines. Moscow: MGAU named after Goryachkin publishing house, 2008. 340 p. (in Russian).

38. Devyanin S. N. Improvement of operational and technical characteristics of the high-speed diesel by improvement of a fuel injection and atomization: Doctor Diss.: 05.04.02. Moscow: BMSTU, 2005. 390 p. (in Russian).

39. Dobrodeyev V.P., Mochalova N.A. Calculation of thermodynamic processes in fuel supply systems in the engine // Proceedings of Higher Educational Institutions. Aeronautics. 1995. No. 3. pp. 49-52 (in Russian).

40. Yepifanov I.V. Increase of economic and ecological parameters of ICE by organization of process with self-ignition of a homogeneous charge: Ph.D. thesis: 05.04.02. Moscow: RUDN, 2008. 141 p. (in Russian).

41. Zaitsev D.K., Smirnov E.M., Yakubov S.A. Parallelization of hydrodynamic calculations on the block-structured grids // Software products and systems. 2009. No. 3. pp. 148-150 (in Russian).

42. Zenkin V.A., Kuleshov A. S. Shaping of inlet ports of a diesel for conditions of high pressure charging and high pressure differentials between a collector and a cylinder // Science and education: Scientific edition of BMSTU. 2013. No. 10. pp. 43-84. URL: <http://technomag.bmstu.ru/en/doc/617277.html> (in Russian).

43. Zienkiewicz O.C. The finite element method in technics: Translation from English under the editorship of B. E. Pobedri. Moscow: World, 1975. 541 p. (in Russian).

44. Use of vegetable oils and fuels on their basis in diesel engines / V.A. Markov, S. N. Devyanin, V. G. Semenov, et.al. Moscow: LLC Research Center "Inzhener", LLC "Oniko-M", 2011. 536 p. (in Russian).

45. Markov V.A., Stremyakov A.V., Akimov V.S., Shumovsky V.A. Computational analysis for fuel supply process in a diesel engine equipped with sprayers with different shapes of fuel channels // Herald of the BMSTU. Mechanical engineering. 2011. No. 4. pp. 113. (Theses of the report on All-Russian Scientific and Technical Seminar named after Prof. V.I. Krutov on Automatic Control and Regulation of Thermal Power Engineering Plants). (in Russian).

46. Akimov V.S., Kuleshov A.S., Markov V.A., Yakovchuk A.Yu., Janhunen T.T. Investigations of operation processes of the Z-engine // "Solution of energy-ecological problems in a motor transportation complex": theses of reports of the international scientific and technical conference "The 7th Lukanin's readings". Moscow: MADI, 2015. pp. 3-5 (in Russian).

47. Kavtaradze R.Z. Local heat transfer in internal combustion engines: Manual for HIGHER EDUCATION INSTITUTIONS. Moscow: BMSTU publishing house, 2001. 592 p. (in Russian).

48. Kavtaradze R.Z. Theory piston engines. Special chapters: Manual for HIGHER EDUCATION INSTITUTIONS. Moscow: BMSTU publishing house, 2008. 720 p. (in Russian).

49. Kaluzhin S.A., Romanov S.A., Sviridov Y.B. Distribution of liquid fuel in volume of a diesel spray//Engine building. 1980. No. 8. pp. 6-8 (in Russian).

50. Kaluzhin S.A., Romanov S.A., Sviridov Y.B. An experimental study of motion velocity of liquid and gaseous phases in a diesel fuel spray//Engine building. 1980. No. 7. pp. 5-8 (in Russian).

51. Kamaltdinov V.G., Dragunov G.D., Markov V.A. Prediction of characteristics of an operating cycle of HCCI boosted engine at different load and speed modes // Engine building. 2013. No. 3. pp. 9-15 (in Russian).

52. Kamaltdinov V.G., Markov V.A., Dragunov G.D. Assessment of characteristics of an operating cycle of HCCI boosted engine at different load and speed modes // Proceedings of Higher Educational Institutions. Machine Building. 2014. No. 6. pp. 25-34 (in Russian).

53. Kamaltdinov V. G. New model of fuel combustion in ICE // Engine building. 2008. No. 3. pp. 17-20 (in Russian).

54. Kamaltdinov V. G. Organization of effective fuel combustion for the perspective internal combustion engine: Doctor Diss.: 05.04.02. Chelyabinsk: SOUTH URAL STATE UNIVERSITY, 2009. 298 p. (in Russian).

55. Kamfer G. M. Processes of a heat-mass transfer and evaporation at mixture formation in diesels: Manual. Moscow: The higher school, 1974. 143 p.

(in Russian).

56. Korotnev of A.G., Kulchitsky A.R., Chestnov Y.I. Design of a flowing channel of a nozzle and diesel parameters//Automotive industry. 2002. No. 2. pp. 15-17 (in Russian).

57. Krokhotin Y.M. Fuel supply systems of diesels: Manual for HIGHER EDUCATION INSTITUTIONS. Voronezh: VGLTA, 1999. 333 p. (in Russian).

58. Krokhotin Y.M. Improvement of economy of diesel locomotive engines by refinement of their fuel equipment: Ph.D. Thesis: 05.04.02. Moscow: BMSTU, 2007. 177 p. (in Russian).

59. Krupsky M. G., Rudakov V. Y. Calculation of geometrical characteristics of a fuel spray at injection in the diesel combustion chamber // Engine building. 2008. No. 1. pp. 24-25 (in Russian).

60. Kuleshov A.S., Grekhov L.V. Raschetnoe formirovanie optimal'nykh zakonov upravleniia dizeliami na traditsionnykh i al'ternativnykh toplivakh [Calculated formation of optimal control laws for diesels on conventional and alternative fuels]. Bezopasnost'v tekhnosfere [Safety in Technosphere]. 2007, no. 5, pp. 30-32 (in Russian).

61. Kuleshov A.S. Multi-zone diesel combustion model. Calculation of fuel distribution in a spray // Herald of the BMSTU. Mechanical engineering. 2007. Special release "Internal combustion engines". pp. 18-31 (in Russian).

62. Kuleshov A. S. Development of computational methods of calculation and optimization of internal combustion engines operation: Doctor Diss.: 05.04.02. Moscow: BMSTU, 2011. 236 p. (in Russian).

63. Kulchitsky A.R. Toxicity of automobile and tractor engines. Vladimir city: Publishing house of the Vladimir state university, 2000. 256 p. (in Russian).

64. Kutovoy V.A. Fuel injection in diesels. Moscow: Mechanical engineering, 1981. 119 p. (in Russian).

65. Lebedev O.N., Marchenko V.N. A computational method of calculation of dynamics of fuel droplets evaporation in the conditions of combustion chambers of diesels // Engine building. 1981. No. 6. pp. 54-56 (in Russian).

66. Likhanov V.A., Saykin A.M. Decrease in toxicity of autotractor diesels. Moscow: Kolos, 1994. 224 p. (in Russian).

67. Loytsyansky L.G. Liquid and gas mechanics . Moscow: Science, 1973. 848 p. (in Russian).

68. Lukanin V.N., Malchuk V.I. Correction of fuel supply and atomization in the diesel combustion chamber // TRACTORS AND AGRICULTURAL MACHINERY. 2000. No. 3. pp. 27-30 (in Russian).

69. Lyshevsky A.S. Processes of a fuel atomization by diesel injectors. Moscow: Mashgiz, 1963. 180 p. (in Russian).

70. Lyshevsky A.S. Fuel atomization in marine diesels. Leningrad: Shipbuilding, 1971. 248 p. (in Russian).

71. Lyshevsky A. S. Fuel supply systems of diesels. Moscow: Mechanical engineering, 1981. 216 p. (in Russian).

72. Malchuk V.I. Fuel supply and zonal mixture formation in diesels. Moscow: MADI publishing house, 2009. 176 p. (in Russian).

73. Markov V.A., Akimov V.S., Shumovsky V.A. Analysis of characteristics of gasoline engine running on propane-butane mixture // AvtoGazoZapravochnyj Kompleks + Alternativnoe toplivo [AutoGas Filling Complex + Alternative Fuel], № 2., 2010, pp. 3-9 (in Russian).

74. Markov V.A., Akimov V.S., Shumovsky V.A. Analysis of characteristics of gasoline running on propane-butane mixture// Avtomobilnaya promyshlennost [Automotive industry], No. 3, 2011, pp. 6-9 (in Russian).

75. Markov V.A., Bashirov R.M., Gabitov I.I. Toxicity of exhaust gases of diesels. Moscow: BMSTU publishing house, 2002. 376 p. (in Russian).

76. Markov V.A., Devyanin S.N., Malchuk V.I. Fuel injection and atomization in diesels. Moscow: BMSTU publishing house, 2007. 360 p. (in Russian).

77. Markov V.A., Furman V.V., Akimov V.S.. Fuel Supply system with electronically control of diesel locomotive engine // Izvestiya vysshih uchebnyh zavedenij. Mashinostroenie [Proceedings of Higher Educational Institutions.

Machine Building], No. 7, 2013, pp. 60-65 (in Russian).

78. Markov V.A., Shumovsky V.A., Akimov V.S. Investigation of fuel injection process in a diesel engine running on water-fuel emulsion // "Solution of energy-ecological problems in a motor transportation complex": theses of reports of the international scientific and technical conference "The 7th Lukanin's readings". Moscow: MADI, 2015. pp. 41-43 (in Russian).

79. Markov V.A., Shumovsky V.A., Akimov V.S. Computational analysis of fuel injection process in a diesel engine running on water-fuel emulsion // Transport na alternativnom toplive [Alternative Fuel Transport], No. 1 (43), 2015, pp. 56-65 (in Russian).

80. Makhmoud Mohamed El-Gobashi El-Hagar. Development of methods of management of operation of the engine with self-ignition of a homogeneous charge: Ph.D. Thesis: 05.04.02. Moscow: RUDN, 2004. 155 p. (in Russian).

81. Markov V.A., Stremyakov A.V., Akimov V.S., Shumovsky V.A. A Method of Improving Fuel Spray Process Quality in a Diesel Engine Running on Mixture Biofuel. // Transport na alternativnom toplive [Alternative Fuel Transport], No. 2 (43), 2011, pp. 24-29 (in Russian).

82. Mizev K.S. Refinement of characteristics of the transport diesel by improvement of process of a fuel supply of oil-based and alternative fuels. Ph.D.: 05.04.02. Moscow: BMSTU, 2012. 160 p. (in Russian).

83. Markov V.A., Devyanin S.N., Akimov V.S., Shumovsky V.A., Bykovskaya L.I., Markova V.V. Optimization of composition of multicomponent mixed biofuel for agricultural machinery // Herald of the BMSTU. Mechanical engineering. 2014. No. 1. pp. 123-124. (Theses of the report on All-Russian Scientific and Technical Seminar named after Prof. V.I. Krutov on Automatic Control and Regulation of Thermal Power Engineering Plants). (in Russian).

84. Patankar S. Numerical methods of solution of problems of heat exchange and fluid dynamics: Translation from English by V.D. Vilensky. Moscow: Energoatomizdat, 1984. 152 p. (in Russian).

85. Petrichenko R. M., Rusinov R. V. Theoretical analysis of structure and

ejection ability of a atomized fuel jet//Engine building. 1982. No. 11. pp. 15-18.

86. Pobyarzhin P.I. Research of influence of internal swirl formation in an injector on quality of atomization and a spray of atomized fuel//Internal combustion engines: Collection of higher education institution. Edited by A.S. Orlin. Moscow: Mashgiz, 1958. pp. 84-103 (in Russian).

87. Supplying and atomization of fuel in diesels / I.V. Astakhov, V.I. Trusov, A.C. Hachiyani, et.al. Edited by I.V. Astakhov. Moscow: Mechanical engineering, 1971. 359 p. (in Russian).

88. Markov V.A., Akimov V.S., Shumovsky V.A., Tarantin S.A. Operation of diesel running on water-fuel emulsion // "Solution of energy-ecological problems in a motor transportation complex": theses of reports of the international scientific and technical conference "The 6th Lukanin's readings". Moscow: MADI, 2013. pp. 3-5 (in Russian).

89. Razleytsev N. F. Simulation and optimization of a combustion in diesels. Kharkiv: Higher School publishing house, 1980. 169 p. (in Russian).

90. The distributed informational-computational system of simulation by methods of computational fluid dynamics / V.D. Goryachev et.al. // Software products and systems. 2004. No. 3. pp. 2-7 (in Russian).

91. Markov V.A., Akimov V.S., Shumovsky V.A., Stremyakov A.V. Calculation Research of the Influence of Mixed Biofuel Composition on Fuel Injection Parameters and Diesel Engine // AvtoGazoZapravochnyj Kompleks + Alternativnoe toplivo [AutoGas Filling Complex + Alternative Fuel], № 11., 2014, pp. 19-32 (in Russian).

92. Markov V.A., Akimov V.S., Shumovsky V.A., Stremyakov A.V. Calculation analysis of characteristics of vehicle diesel engine running on mixtures of diesel fuel and rapeseed oil methyl ester // Gruzovik [Truck], No. 4, 2011, pp. 35-43 (in Russian).

93. Markov V.A., Stremyakov A.V., Akimov V.S., Shumovsky V.A. Computational analysis for fuel supply process in a diesel engine equipped with sprayers with different shapes of fuel channels // Gruzovik [Truck], No. 3, 2011,

pp. 13-17 (in Russian).

94. Grekhov L.V., Markov V.A., Akimov V.S., Furman V.V. Calculation Analysis of Electronic System for Controlling Fuel Supply in Diesel Engine // Herald of the BMSTU. Mechanical engineering. 2012. No. 3. pp. 118. (Theses of the report on All-Russian Scientific and Technical Seminar named after Prof. V.I. Krutov on Automatic Control and Regulation of Thermal Power Engineering Plants). (in Russian).

95. Grekhov L.V., Markov V.A., Akimov V.S., Chzhao J., Furman V.V. Calculation Analysis of Electronic System for Controlling Fuel Supply in Diesel Engine // Gruzovik [Truck], No. 11, 2012, pp. 21-27 (in Russian).

96. Roache P. Computational fluid dynamics. Moscow: World, 1980. 616 p. (in Russian).

97. Rusinov R.V. Designing and calculation of the diesel fuel equipment. Moscow: Mechanical engineering, 1965. 240 p. (in Russian).

98. Rusinov R.V. Determination of length of a atomized fuel jet in relation to conditions of its movement in the combustion chamber of the high-speed forced diesel // Engine building. 1981. No. 11. C. 15-17 (in Russian).

99. Segerlind L.Zh. Application of the finite-element method: Translation from English by A.A. Shestakova, edited by B. E. Pobedri. Moscow: World, 1979. 392 p. (in Russian).

100. Sergeev S. S. Decrease of concentration of nitrogen oxides and soot in exhaust gases of the diesel by improvement of operation process : Ph.D thesis: 05.04.02. Moscow: MGTU of N.E. Bauman, 2011. 134 p. (in Russian).

101. Sviridov Yu.B., Malyavinsky L.V., Vikhert M.M. Fuel and fuel supply of automobile and tractor diesels. L.: Mechanical engineering, 1979. 248 p. (in Russian).

102. Sviridov Yu.B. Mixture formation and combustion in diesels. Leningrad: Mechanical engineering, 1972. 224 p. (in Russian).

103. Semenov B.N., Pavlov E.P., Koptsev V.P. Operation of high-speed diesels of low power. Leningrad: Mechanical engineering, 1990. 240 p. (in

Russian).

104. Smirnov E.M., Zaytsev D.K. A finite volume method in the application to problems of a fluid dynamics and heat exchange in the regions of difficult geometry // St. Petersburg State Polytechnical University Journal. 2004. No. 2. pp. 70-81 (in Russian).

105. Stremyakov A. V. Improvement of characteristics of the transport diesel running on diesel fuel and mixed biofuels by refinement of injector nozzles design: Ph.D.: 05.04.02. Moscow: BMSTU, 2011. 191 p. (in Russian).

106. Theory of internal combustion engines / N.H. Dyachenko, A. K. Kostin, B.P. Pugachev et.al. Edited by N. H. Dyachenko. Leningrad: Mechanical engineering, 1974. 552 p. (in Russian).

107. Fuel systems and economy of diesels / I.V. Astakhov, L.N. Golubkov, V.I. Trusov, et.al. Moscow: Mechanical engineering, 1990. 288 p. (in Russian).

108. Trusov V.I., Mladenov M.B. Influence of cavitation and swirl formation in a nozzle hole on a fuel atomization fineness // Proceedings of MADI. 1976. Issue 126. pp. 46-53 (in Russian).

109. Improvement of economic and ecological characteristics of diesels by an intensification of fuel supply / L.V. Grekhov, V.A. Markov, V.A. Pavlov, et.al. // Gruzovik [Truck]. 2002. No. 8. pp. 36-37, No. 9. pp. 33-35, No. 10. pp. 32-36 (in Russian).

110. Faynleyb B.N. Fuel equipment of automobile and tractor diesels: Handbook. Leningrad: Mechanical engineering, 1990. 352 p. (in Russian).

111. Fedyanov E.A., Itkis E.M., Kuzmin V.N. Features of heat transfer to the cylinder walls of the engine with self-ignition of a homogeneous air-fuel mixture // News of VolgGTU. Processes of energy transformation and power plant. Issue 2. 2009. No. 7. pp. 72-74 (in Russian).

112. Markov V.A., Akimov V.S., Devyanin S.N., Markova V.V. Physical and chemical properties of biofuels and fuel supply process characteristics // Gruzovik [Truck], No. 3, 2012, pp. 40-46 (in Russian).

113. Fletcher K. Computational methods in a fluid dynamics. Moscow:

World, 1991. Volume 1. 502 p. Volume 2. 552 p. (in Russian).

114. Akimov V.S., Kuleshov A.S., Markov V.A., Yakovchuk A.Yu., Janhunen T.T. Computational analysis of fuel injection and atomization by pintle-type injector in the HCCI engine // Herald of the BMSTU. Mechanical engineering. 2014. No. 5. pp. 136-137. (Theses of the report on All-Russian Scientific and Technical Seminar named after Prof. V.I. Krutov on Automatic Control and Regulation of Thermal Power Engineering Plants). (in Russian).

115. Aceves S.M., Flowers D., Marti-nez-Frias J. et al. *HCCI* combustion: analysis and experiments // SAE Technical Paper Series. 2001. № 2001-01-2077. P. 1-13.

116. ANSYS CFX, Release 12.1, HELP & Tutorials. Canonsburg (USA): ANSYS Inc., 2009. 1458 p.

117. ANSYS Fluent, Release 15.0, Theory Guide. Canonsburg (USA): ANSYS Inc., 2015. 2620 p.

118. Bae C., Kang J. The Structure of a Break-up Zone in the Transient Diesel Spray of a Valve-Covered Orifice Nozzle // International Journal of Engine Research. 2006. Vol. 7. P. 12-25.

119. Bae C., Yu J., Kang J. Effect on Nozzle Geometry on the Common-Rail Diesel Spray // SAE Technical Paper Series. 2002. №2002-01-1625. P. 1-13.

120. Befrui B., Corbinelli G., Hoffmann G., Andrews R. et al. Cavitation and Hydraulic Flip in the Outward-Opening GDI Injector Valve-Group // SAE Technical Paper Series. 2009. № 2009-01-1483. P. 1-14.

121. Bergwerk, W. Flow Pattern in Diesel Nozzle Spray Holes // Proceedings of the Institution of Mechanical Engineers. 1959. Vol. 173. P. 655-660.

122. Brennen C.E. Cavitation and bubble dynamics. Oxford: University Press. 1995. 254 p.

123. Chen, Z., Konno M., Oguma M. et al. Experimental study of CI natural-gas/DME homogeneous charge engine // SAE Technical Paper Series. 2000. № 2000-01-0329. P. 1-10.

124. Dent J.C. A Basis for the Comparison of Various Experimental Methods for Studying Spray Penetration // SAE Technical Paper Series. 1971. № 710571. P. 1-6.
125. Faeth G.M., Hsiang L.P., Wu P.K. Structure and breakup properties of sprays // International Journal of Multiphase Flow. 1995. Vol. 21. P. 99-127.
126. Fath A., Fettes C., Leipetz A. Investigation of the Diesel Break-up Close to the Nozzle at Different Injection Conditions // The Fourth International Symposium. Kyoto (Japan): COMODIA, 1998. P. 429-434.
127. FlowVision User's Guide 3.09.05 // Official FlowVision web-site. URL: https://flowvision.ru/webhelp/fven_30905/.
128. Ganipa L.C. Andersson S., Chomiak J. Combustion Characteristics of Diesel Sprays from Equivalent Nozzles with Sharp and Rounded Inlet Geometries // Combustion Science Technologies. 2003. Vol. 175. P. 1015-1032.
129. Gavaises M., Tonini S., Marchi A. et al. Modelling of Internal and Near-Nozzle Flow of a Pintle-Type Outwards-Opening Gasoline Piezo-Injector // International Journal of Engine Research. 2006. № 7. P. 381-397.
130. Goney K.H. Corradini M.L. Isolated Effects of Ambient Pressure, Nozzle Cavitation and Hole Inlet Geometry on Diesel Injector Spray Characteristics // SAE Technical Paper Series. 2000. № 2000-01-2043. P. 1-14.
131. Gray A.W., Ryan III T.W. Homogeneous Charge Compression Ignition of Diesel Fuel // SAE Technical Paper Series. 1997. № 971676. P. 1-10.
132. Han J., Lu P., Xie X. et al. Investigation of Diesel Spray Primary Break-up and Development for Different Nozzle Geometries // SAE Technical Paper Series. 2002. № 2002-01-2775. P. 1-15.
133. Harada A., Shimazaki N., Sasaki S. et al. The Effects of Mixture Formation on Premixed Lean Diesel Combustion Engine // SAE Technical Paper Series. 1998. № 980533. P. 1-8
134. He D., Wang M. Contribution Feedstock and Fuel Transportation to Total Fuel-Cycle Energy Use and Emissions // SAE Technical Paper Series. 2000. № 2000-01-2976. P. 1-15.

135. Helmantel A., Gustavsson J., Denbratt I. Operation of a DI Diesel Engine With Variable Effective Compression Ratio in HCCI and Conventional Diesel Mode // SAE Technical Paper Series. 2005. № 2005-01-0177. P. 1-9.
136. Higgins B.S., Mueller C.J., Siebers D.L. Measurements of Fuel Effects on Liquid-Phase Penetration in DI Sprays // SAE Technical Paper Series. 1999. № 1999-01-0519. P. 1-14.
137. Hiroyasu H., Arai M. Structure of Fuel Sprays in Diesel Engines // SAE Technical Paper Series. 1990. № 900475. P. 1-10.
138. Hou D., Huang Y., Huo M. et al. Spray and Atomization Characterization of a Micro-Variable Circular-Orifice (MVCO) Fuel Injector // SAE Technical Paper Series. 2011. № 2011-01-0679. P. 1-10.
139. Hou D., Zhang H., Kalish Y. et al. Adaptive PCCI Combustion Using Micro-Variable Circular-Orifice (MVCO) Fuel Injector – Key Enabling Technologies for High Efficiency Clean Diesel Engines // SAE Technical Paper Series. 2009. № 2009-01-1528. P. 1-9.
140. Jia M., Hou D., Li J. et al. A Micro-Variable Circular Orifice Fuel Injector for *HCCI*-Conventional Engine Combustion - Part I. Numerical Simulation of Cavitation // SAE Technical Paper Series. 2007. № 2007-01-0249. P. 1-12.
141. Janhunen T. *HCCI*-Combustion in the Z Engine // SAE Technical Paper Series. 2012. № 2012-01-1132. P. 1-10.
142. Kampmann S., Dittus B., Mattes P. et al. The Influence of Hydro Grinding at VCO Nozzles on Mixture Preparation in a DI Diesel Engine // SAE Technical Paper Series. 1996. № 9608676. P. 1-13.
143. Kimura S., Aoki O., Kitahara, Y. et al. Ultra-Clean Combustion Technology Combining a Low-Temperature and Premixed Combustion Concept for Meeting Future Emission Standards // SAE Technical Paper Series. 2001. № 2001-01-0200. P. 1-12.
144. Knapp R.T., Daily J.W., Hammitt F.G. Cavitation. New York: McGraw-Hill Book Company, 1970. 578 p.

145. Kong, S.C. A study of natural gas/DME combustion in *the HCCI engines* using CFD with detailed chemical kinetics // *Fuel*. 2007. Vol. 86. P. 1483-1489.
146. Kuleshov A.S., Kozlov A.V., Mahkamov K. Self-Ignition delay Prediction in PCCI direct injection diesel engines using multi-zone spray combustion model and detailed chemistry // *SAE Technical Paper Series*. 2010. № 2010-01-1960. P. 1-12.
147. Kuleshov, A., Mahkamov, K., Janhunen, T., Akimov, V. et al., "New Downsized Diesel Engine Concept with HCCI Combustion at High Load Conditions," *SAE Technical Paper* 2015-01-1791, 2015, doi:10.4271/2015-01-1791.
148. Kuleshov A.S. Multi-Zone DI Diesel Spray Combustion Model and its Application for Matching the Injector Design with Piston Bowl Shape // *SAE Technical Paper Series*. 2007. № 2007-01-1908. P. 1-10.
149. Lagumbay R.S. Modeling and Simulation of Multiphase/Multicomponent Flows: PhD Thesis. Colorado (CIHA): University of Colorado at Boulder, 2006. 150 p.
150. Levich V. G. *Physicochemical Hydrodynamics*. Englewood Cliffs, NJ: Prentice-Hall Inc., 1962. 700 p.
151. Lim O.T., Ketadani S., Kumano et al. The effects of inhomogeneity in DME/n-butane–air mixture in combustion chamber on homogeneous charge compression ignition combustion // *ISAF XV International Symposia on Alcohol Fuels*. 2005. P. 230-236.
152. Marchi A., Nouri J., Yan, Y. et al. Internal Flow and Spray Characteristics of Pintle-Type Outwards Opening Piezo Injectors for Gasoline Direct-Injection Engines // *SAE Technical Paper Series*. 2007. № 2007-01-1406. P. 1-14.
153. Markov V.A., Gladyshev S.P., Devyanin S.N. et al. Perfection of the Processes of the Fuel Spraying and the Fuel-Air Mixture Creating in a High-Speed Diesel Engine, Working on the Bio-Fuel Mixture // *SAE Technical Paper Series*. 2009. № 2009-01-0845. P. 1-7.

154. Martynov S. Numerical Simulation of the Cavitation Process in Diesel Fuel Injectors: PhD Thesis. Brighton (Великобритания): University of Brighton, 2005. 150 p.
155. Ménard T., Tanguy S., Berlemont A. Coupling level set/VOF/ghost fluid methods: Validation and application to 3D simulation of the primary break-up of a liquid jet // International Journal of Multiphase Flow. 2007. Vol. 33. № 5. P. 510-534.
156. Menter F.R. Two-Equation Eddy-Viscosity Turbulence Models for Engineering Applications // AIAA Journal. 1994. Vol. 32. № 8. P. 1598-1605.
157. Najt P., Foster D.E. Compression Ignited Homogeneous Charge Combustion // SAE Technical Paper Series. 1983. № 830264. P. 1-9.
158. Nordgren H., Hultqvist A., Johansson B. Start of Injection Strategies for HCCI-combustion // SAE Technical Paper Series. 2004. № 2004-01-2990. P. 1-8.
159. Nurick W.H. Orifice Cavitation and its Effect on Spray Mixing // Transactions ASME. Journal of Fluids Engineering. 1976. Vol. 98. P. 681-687.
160. Ohnesorge V.W. Anwendung eines kinematographischen Hochfrequenzapparates mit mechanischer Regelung der Belichtung zur Aufnahme der Tropfenbildung und des Zerfalls flüssiger Strahlen: Dissertation Techn. Hochschule. Berlin: Univ.Techn., 1937. 569 p.
161. Onishi S., Jo S.H., Shoda K. et al. Active Thermo Atmospheric Combustion (ATAC) – A New Combustion process for Internal Combustion Engines // SAE Technical Paper Series. 1979. № 790501. P. 1-7.
162. Payri R., Salvador F.J. Gimeno J. Effects of Nozzle Geometry on Direct Injection Diesel Engine Combustion Process // Applied Thermal Engineering. 2009. Vol. 29. P. 2051-2060.
163. Perry R.H., Green D.W., Maloney J.O. Perry's Chemical Engineers' Handbook: 6th edition. New York: McGraw-Hill, 1984. 2728 p.
164. Pilch M., Erdman C.A. Use of breakup time data and velocity history data to predict the maximum size of stable fragments for acceleration-induced

breakup of liquid drop // International Journal of Multiphase Flow. 1987. Vol. 13. № 6. P. 741-757.

165. Ramos J.I. Internal combustion engine modeling. New York: HPB, 1984. 422 p.

166. Ranzi E., Faravelli T., Gaffuri P. et al. A wide-range modeling study of iso-octane oxidation // Combustion and Flame. 1997. Vol. 108. P. 24-42.

167. Reitz R.D. Atomization and other Breakup Regimes of a liquid jet: Ph.D. Thesis. Princeton (CША), Princeton University, 1978. 150 p.

168. Reitz R.D. Mechanisms of Atomization Processes in High-Pressure Vaporizing Sprays // Atomization and Spray Technology. 1987. Vol. 3. P. 309–337.

169. Sazhin S.S. Advanced Models of Fuel Droplet Heating and Evaporation // Progress in Energy and Combustion Science. Elsevier Science. 2006. Vol. 32. P. 162-214.

170. Sazhin S.S., Kristyadi T., Abdelghaffar W.A. et al. Models for fuel droplet heating and evaporation: Comparative analysis // Fuel. 2006. Vol. 85. P. 1613–1630.

171. Schmid A. Experimental characterization of the two phase flow of a modern, piezo activated hollow cone injector. Dr .Dissertation (Diss. ETH № 20852). Zürich (Швейцария): Swiss Federal Institute of Technology, 2012. 275 p.

172. Schmidt D., Rutland C., Corradini M. et al. Cavitation in Two-Dimensional Asymmetric Nozzles // SAE Technical Papers Series. 1999. № 1999-01-0518. P. 1-12.

173. Soteriou C., Andrews R., Smith M. Direct Injection Diesel Sprays and the Effect of Cavitation and Hydraulic Flip on Atomization // SAE Technical Papers Series. 1995. № 950080. P. 1-10.

174. Sun Y., Reitz R. Adaptive Injection Strategies (AIS) for Ultra-Low Emissions Diesel Engines // SAE Technical Paper Series. 2008. № 2008-01-0058. P. 1-12.

175. Turner M.R., Sazhin S.S., Healey J.J. et al. A Breakup Model for Transient Diesel Fuel sprays // Fuel: The Science and Technology of Fuel and Energy. 2012. Vol. 97. P. 288-305.

176. Vanegas A., Won H., Peters N. Influence of the Nozzle Spray Angle on Pollutant Formation and Combustion Efficiency for a PCCI Diesel Engine // SAE Technical Papers Series. 2009. № 2009-01-1445. P. 1-12.

177. Von Rotz B., Herrmann K., Weisser G. et al. Impact of Evaporation, Swirl and Fuel Quality on the Characteristics of Sprays typical of Large 2-Stroke Marine Diesel Engine Combustion Systems // Proceedings of the 24 th ILASS-Europe Conference. Estoril. 2011. P. 27-29.

178. Wilcox D.C. Turbulence Modeling for CFD. California: DCW Industries, Inc. La Canada. 1998. 460 p.

179. Winklhofer E., Kull E., Kelz E. et al. Comprehensive hydraulic and flow field documentation in modl throttle experiments under cavitation conditions // Proceedings of the ILASS-Europe Conference. Zurich: 2-6 September, 2001. P. 574-579.

180. Wu P.K., Tseng L.K., Faeth G.M. Primary Breakup in Gas/Liquid Mixing Layers for Turbulent Liquids // Atomization and Sprays. 1995. Vol. 2. P. 295-317.

181. Yang X., Takamoto Y., Okajima A. et al. Comparison of Computed and Measured High-Pressure Conical Diesel Sprays // SAE Technical Paper Series. 2000. № 2000-01-0951. P. 1-10.

APPENDIX

A.1. Listing of results of computation of the *Z-engine* operation with conventional diesel combustion at peak load conditions (at $n=2800$ rpm) obtained using DIESEL-RK

```
RESULT OF COMPUTATION AT 2800 RPM
---- PARAMETERS OF ENGINE WITH TURBOCOMPANDING OR SUPERCHARGING ----
106.68 - P_ovrl - Overall Power with account of geared units, kW
-21.334 - dP_add - Power added by geared Turb/Comp/TC/EGR_compr., kW
363.84 - Torq_ovrl- Overall Torque in view of geared/units, N m
28.423 - BMEP_ovrl- Overall BMEP, bar
0.21954 - SFC_ovrl - Overall Specific Fuel Consumption, kg/kWh
0.21888 - SFC_o.ISO- Same Specific Fuel Consumption but in ISO, kg/kWh
0.38584 - Eta_ovrl - Overall Engine Efficiency
10.000 - R_gear - Gear ratio of TK speed reducer
0.95000 - Eta_mC.hp- Mechanical Efficiency of HPC
-23.047 - dPdrv_hp - Power added by geared Unit of HP stage, kW
10.000 - R_gear.lp- Gear Ratio of LP Units and drive shaft coupling
0.95000 - Eta_mC.lp- Mechanical Efficiency of LP Compressor
1.7129 - dPdrv_lp - Power added by geared Unit of LP stage, kW

----- PARAMETERS OF EFFICIENCY AND POWER -----
2800.0 - RPM - Engine Speed, rev/min
128.01 - P_eng - Piston Engine Power, kW
34.107 - BMEP - Brake Mean Effective Pressure, bar
436.60 - Torque - Brake Torque, N m
0.06970 - m_f - Mass of Fuel Supplied per cycle, g
0.18295 - SFC - Specific Fuel Consumption, kg/kWh
0.18240 - SFC_ISO - Specific Fuel Consumption in ISO, kg/kWh
0.46300 - Eta_f - Efficiency of piston engine
35.387 - IMEP - Indicated Mean Effective Pressure, bar
0.48038 - Eta_i - Indicated Efficiency
7.4667 - Sp - Mean Piston Speed, m/s
1.2799 - FMEP - Friction Mean Effective Pressure, bar (VW ex.data)
0.96383 - Eta_m - Mechanical Efficiency of Piston Engine

----- ENVIRONMENTAL PARAMETERS -----
1.0000 - p_sea - Static Atmospheric Pressure on sea level, bar
298.00 - T_sea - Static Atmospheric Temperature on sea level, K
0.0000 - A_ab.sea - Altitude Above Sea Level, km
0.0000 - v_flight - Velocity of Flight, km/h (for aircraft engine)
1.0000 - p_amb - Static Ambient Pressure, bar
298.00 - T_amb - Static Ambient Temperature, K
1.0000 - po_amb - Total Ambient Pressure, bar
298.00 - To_amb - Total Ambient Temperature, K
1.0400 - p_Te - Exhaust Back Pressure, bar (after turbine)
0.98000 - po_afltr - Total Pressure after Induction Air Filter, bar

----- TURBOCHARGING AND GAS EXCHANGE -----
18.843 - p_C - Pressure before Inlet Manifold, bar
313.34 - T_C - Temperature before Inlet Manifold, K
0.10294 - m_air - Total Mass Airflow (+EGR) of Piston Engine, kg/s
0.76769 - Eta_TC - Turbocharger Efficiency
3.1172 - po_T - Average Total Turbine Inlet Pressure, bar
1116.9 - To_T - Average Total Turbine Inlet Temperature, K
0.11243 - m_gas - Mass Exhaust Gasflow of Pison Engine, kg/s
1.0918 - A/F_eq.t - Total Air Fuel Equivalence Ratio (Lambda)
0.91589 - F/A_eq.t - Total Fuel Air Equivalence Ratio
0.13499 - Eta_v - Volumetric Efficiency
0.15719 - x_r - Residual Gas Mass Fraction
0.97040 - Phi - Coeff. of Scavenging (Delivery Ratio / Eta_v)
0.0000 - BF_int - Burnt Gas Fraction Backflowed into the Intake, %
0.45564 - %Blow-by - % of Blow-by through piston rings
```

```

----- INTAKE SYSTEM -----
18.830 - p_int - Average Intake Manifold Pressure, bar
318.52 - T_int - Average Intake Manifold Temperature, K
2.0990 - v_int - Average Gas Velocity in intake manifold, m/s
321.38 - Tw_int - Average Intake Manifold Wall Temperature, K
197.96 - hc_int - Heat Transfer Coeff. in Intake Manifold, W/(m2*K)
164.82 - hc_int.p - Heat Transfer Coeff. in Intake Port, W/(m2*K)
7.1004 - A_v.thrt - Total Effective Valve Port Throat Area, cm2
Valve Dim. Estim.: Num=2 Dv= 29.0 Dt= 26.0 Ds= 5.5 Lv= 6.2 Lv_max= 7.2 mm

```

```

----- EXHAUST SYSTEM -----
3.0690 - p_exh - Average Exhaust Manifold Gas Pressure, bar
1124.4 - T_exh - Average Exhaust Manifold Gas Temperature, K
50.773 - v_exh - Average Gas Velocity in exhaust manifold, m/s
54.282 - Sh - Strouhal number: Sh=a*Tau/L (has to be: Sh > 8)
943.95 - Tw_exh - Average Exhaust Manifold Wall Temperature, K
205.63 - hc_exh - Heat Transfer Coeff. in Exhaust Manifold, W/(m2*K)
287.98 - hc_exh.p - Heat Transfer Coeff. in Exhaust Port, W/(m2*K)
8.7808 - A_v.thrt - Total Effective Valve Port Throat Area, cm2
Valve Dim. Estim.: Num=2 Dv= 30.0 Dt= 27.0 Ds= 5.5 Lv= 7.6 Lv_max= 7.5 mm

```

```

----- COMBUSTION -----
1.1604 - A/F_eq - Air Fiel Equival. Ratio (Lambda) in the Cylinder
0.86180 - F/A_eq - Fuel Air Equivalence Ratio in the Cylinder
219.59 - p_max - Maximum Cylinder Pressure, bar
2108.5 - T_max - Maximum Cylinder Temperature, K
7.0000 - CA_p.max - Angle of Max. Cylinder Pressure, deg. A.TDC
20.000 - CA_t.max - Angle of Max. Cylinder Temperature, deg. A.TDC
10.175 - dp/dTheta- Max. Rate of Pressure Rise, bar/deg.
11.053 - Ring_Intn- Ringing / Knock Intensity, MW/m2
11181. - F_max - Max. Gas Force acting on the piston, kg
1434.5 - p_inj.max- Max. Sac Injection Pres. (before nozzles), bar
1287.4 - p_inj.avr- Mean Sac Press. for Total Fuel Portion, bar
8.1051 - d_32 - Sauter Mean Diameter of Drops, microns
20.000 - SOI - Start Of Injection or Ignition Timing, deg. B.TDC
33.800 - Phi_inj - Duration of Injection, CA deg.
1.0000 - Phi_d1 - Durat. of first phase of inj. flow rise, CA deg.
3.0000 - Phi_d2 - Durat. of second phase of inj. flow rise, CA deg.
0.50000 - C_inflex - Rated highness of fuel flow rise curve inflexion
8.3118 - Phi_ign - Ignition Delay Period, deg.
- ... - calculated by modified Tolstov method : 8.3
11.688 - SOC - Start of Combustion, deg. B.TDC
0.12484 - x_e.id - Fuel Mass Fraction Evaporated during Ignit. Delay
149.80 - Phi_z - Combustion duration, deg.
Phi_z 5%= 5.4; Phi_z 50%= 20.2; Phi_z 95%= 71.6
2.1085 - Rs_tdc - Swirl Ratio in the Combustion Chamber at TDC
1.6000 - Rs_ivc - Swirl Ratio in the Cylinder at IVC
18.375 - W_swirl - Max. Air Swirl Velocity, m/s at cylinder R= 30

```

```

----- ECOLOGICAL PARAMETERS -----
12.267 - Hartridge- Hartridge Smoke Level
1.3246 - Bosch - Bosch Smoke Number
0.30472 - K,m-1 - Factor of Absolute Light Absorption, 1/m
0.18766 - PM - Specific Particulate Matter emission, g/kWh
707.40 - CO2 - Specific Carbon dioxide emission, g/kWh
0.19032 - NO - Specif. NOx emiss. reduc. to NO, g/kWh(DKM)
0.65271 - SE - Summary emission of PM and NOx
0.0000 - SO2 - Specific SO2 emission, g/kWh

```

```

----- CYLINDER PARAMETERS -----
31.285 - p_ivc - Pressure at IVC, bar
647.84 - T_ivc - Temperature at IVC, K
102.21 - p_tdc - Compression Pressure (at TDC), bar
882.41 - T_tdc - Compression Temperature (at TDC), K
15.750 - p_evo - Pressure at EVO, bar
1416.6 - T_evo - Temperaure at EVO, K

```

```

----- HEAT EXCHANGE IN THE CYLINDER -----
1447.8 - T_eq - Average Equivalent Temperature of Cycle, K

```

```

834.93 - hc_c - Aver. Factor of Heat Transfer in Cyl., W/m2/K
836.15 - Tw_pist - Average Piston Crown Temperature, K
420.00 - Tw_liner - Average Cylinder Liner Temperature, K
774.39 - Tw_head - Average Head Wall Temperature, K
404.71 - Tw_cool - Average Temperature of Cooled Surface
head of Cylinder Head, K
398.16 - Tboil - Boiling Temp. in Liquid Cooling System, K
12519. - hc_cool - Average Factor of Heat Transfer, W/(m2*K)
from head cooled surface to coolant
2826.2 - q_head - Heat Flow in a Cylinder Head, J/s
2566.9 - q_pist - Heat Flow in a Piston Crown, J/s
4172.9 - q_liner - Heat Flow in a Cylinder Liner, J/s

----- MAIN ENGINE CONSTRUCTION PARAMETERS -----
13.000 - CR - Compression Ratio
2.4009 - CR_opn.h - CR in view of losses due to open height of porting
8.0000 - n_inj - Number of Injector Nozzles
0.13000 - d_inj - Injector Nozzles Bore, mm
33.800 - Phi_inj - Injection Duration for specif. Inj. Profile, deg.
0.0000 - m_f_ip - Fuel Mass for specified Injection Profile, g
-125.00 - IVO - Intake Valve Opening, deg. before DC
145.00 - IVC - Intake Valve Closing, deg. after BDC
56.000 - EVO - Exhaust Valve Opening, deg. before BDC
108.00 - EVC - Exhaust Valve Closing, deg. after DC

----- COMPRESSOR PARAMETERS LP stage -----
28000. - RPM_C.lp - Rotor Speed of LPC, rev/min
21.252 - P_C.lp - Power of LP Compressor, kW
0.75000 - Eta_C.lp - Adiabatic Efficiency of LP Compressor
0.10294 - m_C.lp - Mass Airflow of LP Compressor, kg/sec
1.8133 - m*_C.lp - Mass Airflow Parameter, kg SQRT(K)/(s bar)
0.10504 - m.cor_Clp - Corrected Mass Airflow of LPC, kg/s
1622.0 - RPM*_C.lp - Rotor Speed Parameter, rev/min SQRT(K)
28000. - RPMcor_lp - Corrected Rotor Speed, rev/min
4.3000 - PR_C.lp - Pressure Ratio of LP Compressor
0.0000 - Kpi_C.lp - Factor Kpi of LP Compressor
0.98000 - po_iC.lp - Inlet Total Pressure of LPC, bar
298.00 - To_iC.lp - Inlet Total Temperature of LPC, K
4.2140 - po_"C.lp - Total Discharge Press.(before LP cooler), bar
503.43 - To_"C.lp - Total Discharge Temp. (before LP cooler), K
0.80000 - Ecool.lp - Thermal Efficiency of LP Air Inter-cooler
293.00 - Tcool.lp - LP Inter-cooler Refrigerant Temperature, K
4.1940 - po_C.lp - Total Pressure after LP Inter-cooler, bar
335.09 - To_C.lp - Total Temperature after LP Inter-cooler, K

----- COMPRESSOR PARAMETERS HP stage -----
28000. - RPM_C.hp - Rotor Speed of HPC, rev/min
21.894 - P_C.hp - Power of HPC, kW
0.85000 - Eta_C.hp - Adiabatic Efficiency of HPC
0.10294 - m_C.hp - Mass Airflow of HP Compressor, kg/s
0.44930 - m*_C.hp - Mass Airflow Parameter, kg SQRT(K)/(s bar)
0.02603 - m.cor_Chp - Corrected Mass Airflow of HPC, kg/s
1529.6 - RPM*_C.hp - Rotor Speed Parameter, rev/min SQRT(K)
26405. - RPMcor_hp - Corrected Rotor Speed, rev/min
4.5000 - PR_C.hp - Pressure Ratio of HP Compressor
0.0000 - Kpi_C.hp - Factor Kpi of HP Compressor
4.1940 - po_iC.hp - Inlet Total Pressure of HPC, bar
335.09 - To_iC.hp - Inlet Total Temperature of HPC, K
18.873 - po_"C.hp - Total Discharge Press. (before HP cooler), bar
546.72 - To_"C.hp - Total Discharge Temp. (before HP cooler), K
0.80000 - Ecool.hp - Thermal Efficiency of HP Air Inter-cooler
255.00 - Tcool.hp - HP Inter-cooler Refrigerant Temperature, K
18.843 - po_C.hp - Total Pressure after Inter-cooler, bar
313.34 - To_C.hp - Total Temperature after Inter-cooler, K

----- TURBINE PARAMETERS HP stage -----
28000. - RPM_T.hp - HP Turbine Rotor Speed, rev/min
0.0000 - P_T.hp - Effective Power of HPT, kW
1.0000 - Eta_T.hp - Internal turbine Efficiency of HPT
0.90900 - Eta_mT.hp - Mechanical Efficiency of HPT

```

```

0.11243 - m_T.hp - Mass Gasflow of HPT, kg/s
0.01205 - m*_T.hp - Mass Gasflow Parameter, (kg SQRT(K))/(s kPa)
837.81 - RPM*_T.hp- Rotor Speed Parameter, rev/min SQRT(K)
1.0000 - PR_T.hp - Expansion Pressure Ratio of HPT
0.0000 - B_T.hp - Relative Work B=118.34 {1-PR**[(1-k)/k]} Eta_T
3.1172 - po_T.hp - Inlet Total Pressure of HPT, bar
1116.9 - To_T.hp - Inlet Total Temperature of HPT, K
3.1172 - po_eT.hp - HP Turbine Exhaust Back Pressure, bar
1116.9 - To_eT.hp - HP Turbine Exhaust Back Temperature, K

```

----- TURBINE PARAMETERS LP stage -----

```

28000. - RPM_T.lp - LP Turbine Rotor Speed, rev/min
23.055 - P_T.lp - Effective Power of LPT, kW
0.75000 - Eta_T.lp - Adiabatic Efficiency of LPT
0.90900 - Eta_mT.lp- Mechanical Efficiency of LPT
0.11243 - m_T.lp - Mass Gasflow of LPT, kg/s
0.01205 - m*_T.lp - Mass Gasflow Parameter, (kg SQRT(K))/(s kPa)
837.81 - RPM*_T.lp- Rotor Speed Parameter, rev/min SQRT(K)
3.0000 - PR_T.lp - Expansion Pressure Ratio of LPT
21.176 - B_T.lp - Relative Work B=118.34 {1-PR**[(1-k)/k]} Eta_T
3.1172 - po_T.lp - Inlet Total Pressure of LPT, bar
1116.9 - To_T.lp - Inlet Total Temperature of LPT, K
1.0391 - po_eT.lp - LP Turbine Exhaust Back Pressure, bar
910.41 - To_eT.lp - LP Turbine Exhaust Back Temperature, K

```

THE ALLOCATION OF FUEL IN THE ZONES AT THE END OF INJECTION

```

=====
N|In plan| Spray|Impingment|_____Fractions of fuel in the zones %_____
s| Angle | Angle| Surface | Dilut. S.Core Piston Inters. Head Liner
=====

```

```

1| 0.0 | 75.0 |pist. bowl| 98.75 0.30 0.95 0.00 0.00 0.00
=====

```

```

Sum of all sprays % 100.| 98.17 0.66 1.17 0.00 0.00 0.00
=====

```

```

Evaporation constants bi | 17402 1496 17370 14678 13092 54
=====

```

```

The note: "Inters." is column with fraction of fuel in a zone of
intersection of Near-Wall Flows formed by adjacents sprays.
Rs:Swirl; (Piston clearance,mm 2.50) |Optimal|-Geometric formula: 1.33
Ratio; Rs of piston bowl 2.11 | Rs |-by Razleytsev : 1.20

```

```

Versions: Kernel 04.01.13; RK-model 06.01.13; NOx-model 22.02.13

```

A.2. Listing of results of computations of the Z-engine operation with SA HCCI on the different modes of full-load curve obtained using DIESEL-RK

```

RESULT OF COMPUTATION AT 2800 RPM
----- PARAMETERS OF ENGINE WITH TURBOCOMPAUNDING OR SUPERCHARGING -----
116.75 - P_ovrl - Overall Power with account of geared units, kW
-25.688 - dP_add - Power added by geared Turb/Comp/TC/EGR_compr., kW
398.21 - Torq_ovrl- Overall Torque in view of geared units, N m
31.108 - BMEP_ovrl- Overall BMEP, bar
0.20145 - SFC_ovrl - Overall Specific Fuel Consumption, kg/kWh
0.19741 - SFC_o.ISO- Same Specific Fuel Consumption but in ISO, kg/kWh
0.42048 - Eta_ovrl - Overall Engine Efficiency
10.000 - R_gear - Gear ratio of TK speed reducer
0.95000 - Eta_mC.hp- Mechanical Efficiency of HPC
-24.559 - dPdrv_hp - Power added by geared Unit of HP stage, kW
10.000 - R_gear.lp- Gear Ratio of LP Units and drive shaft coupling
0.97000 - Eta_mC.lp- Mechanical Efficiency of LP Compressor
-1.1295 - dPdrv_lp - Power added by geared Unit of LP stage, kW

----- PARAMETERS OF EFFICIENCY AND POWER -----
2800.0 - RPM - Engine Speed, rev/min
142.44 - P_eng - Piston Engine Power, kW
37.953 - BMEP - Brake Mean Effective Pressure, bar
485.83 - Torque - Brake Torque, N m
0.07000 - m_f - Mass of Fuel Supplied per cycle, g
0.16512 - SFC - Specific Fuel Consumption, kg/kWh
0.16181 - SFC_ISO - Specific Fuel Consumption in ISO, kg/kWh
0.51300 - Eta_f - Efficiency of piston engine
39.311 - IMEP - Indicated Mean Effective Pressure, bar
0.53136 - Eta_i - Indicated Efficiency
7.4667 - Sp - Mean Piston Speed, m/s
1.3583 - FMEP - Friction Mean Effective Pressure, bar (VW data)
0.96545 - Eta_m - Mechanical Efficiency of Piston Engine

----- ENVIRONMENTAL PARAMETERS -----
1.0000 - p_sea - Static Atmospheric Pressure on sea level, bar
298.00 - T_sea - Static Atmospheric Temperature on sea level, K
0.0000 - A_ab.sea - Altitude Above Sea Level, km
0.0000 - v_flight - Velocity of Flight, km/h (for aircraft engine)
1.0000 - p_amb - Static Ambient Pressure, bar
298.00 - T_amb - Static Ambient Temperature, K
1.0000 - po_amb - Total Ambient Pressure, bar
298.00 - To_amb - Total Ambient Temperature, K
1.0400 - p_Te - Exhaust Back Pressure, bar (after turbine)
0.98000 - po_afltr - Total Pressure after Induction Air Filter, bar

----- TURBOCHARGING AND GAS EXCHANGE -----
18.743 - p_C - Pressure before Inlet Manifold, bar
316.39 - T_C - Temperature before Inlet Manifold, K
0.11660 - m_air - Total Mass Airflow (+EGR) of Piston Engine, kg/s
0.80303 - Eta_TC - Turbocharger Efficiency
3.1149 - po_T - Average Total Turbine Inlet Pressure, bar
977.20 - To_T - Average Total Turbine Inlet Temperature, K
0.12631 - m_gas - Mass Exhaust Gasflow of Pison Engine, kg/s
1.2314 - A/F_eq.t - Total Air Fuel Equivalence Ratio (Lambda)
0.81206 - F/A_eq.t - Total Fuel Air Equivalence Ratio
0.15862 - Eta_v - Volumetric Efficiency
0.19641 - x_r - Residual Gas Mass Fraction
0.94938 - Phi - Coeff. of Scavenging (Delivery Ratio / Eta_v)
0.0000 - BF_int - Burnt Gas Fraction Backflowed into the Intake, %
0.42824 - %Blow-by - % of Blow-by through piston rings

----- INTAKE SYSTEM -----
18.725 - p_int - Average Intake Manifold Pressure, bar
313.58 - T_int - Average Intake Manifold Temperature, K
2.3588 - v_int - Average Gas Velocity in intake manifold, m/s

```

316.57 - Tw_int - Average Intake Manifold Wall Temperature, K
 199.86 - hc_int - Heat Transfer Coeff. in Intake Manifold, W/(m2*K)
 166.83 - hc_int.p - Heat Transfer Coeff. in Intake Port, W/(m2*K)
 7.1004 - A_v.thrt - Total Effective Valve Port Throat Area, cm2
 Dim. Estim.: Num=2 Dv= 29.0 Dt= 26.0 Ds= 5.5 Lv= 6.2 Lv_max= 7.2 mm Valve

----- EXHAUST SYSTEM -----

3.0638 - p_exh - Average Exhaust Manifold Gas Pressure, bar
 975.82 - T_exh - Average Exhaust Manifold Gas Temperature, K
 50.954 - v_exh - Average Gas Velocity in exhaust manifold, m/s
 50.569 - Sh - Strouhal number: Sh=a*Tau/L (has to be: Sh > 8)
 832.77 - Tw_exh - Average Exhaust Manifold Wall Temperature, K
 208.11 - hc_exh - Heat Transfer Coeff. in Exhaust Manifold, W/(m2*K)
 287.58 - hc_exh.p - Heat Transfer Coeff. in Exhaust Port, W/(m2*K)
 8.7808 - A_v.thrt - Total Effective Valve Port Throat Area, cm2
 Valve Dim. Estim.: Num=2 Dv= 30.0 Dt= 27.0 Ds= 5.5 Lv= 7.6 Lv_max= 7.5 mm

----- COMBUSTION -----

1.3387 - A/F_eq - Air Fuel Equival. Ratio (Lambda) in the Cylinder
 0.74697 - F/A_eq - Fuel Air Equivalence Ratio in the Cylinder
 238.66 - p_max - Maximum Cylinder Pressure, bar
 2218.7 - T_max - Maximum Cylinder Temperature, K
 14.000 - CA_p.max - Angle of Max. Cylinder Pressure, deg. A.TDC
 18.000 - CA_t.max - Angle of Max. Cylinder Temperature, deg. A.TDC
 6.5990 - dp/dTheta - Max. Rate of Pressure Rise, bar/deg.
 4.3882 - Ring_Intn - Ringing / Knock Intensity, MW/m2
 12152. - F_max - Max. Gas Force acting on the piston, kg
 836.46 - p_inj.max - Max. Sac Injection Pres. (before nozzles), bar
 620.78 - p_inj.avr - Mean Sac Press. for Total Fuel Portion, bar
 7.3160 - d_32 - Sauter Mean Diameter of Drops, microns
 80.000 - SOI - Start Of Injection or Ignition Timing, deg. B.TDC
 22.180 - Phi_inj - Duration of Injection, CA deg.
 81.000 - Phi_ign - Ignition Delay Period, deg.
 - ... - Calculation with user Model : 81.0
 -1.0000 - SOC - Start of Combustion, deg. B.TDC
 0.25326 - x_e.id - Fuel Mass Fract. Evaporated during Ignit. Delay
 109.70 - Phi_z - Combustion duration, deg.
 Phi_z 5%= 3.6; Phi_z 50%= 20.2; Phi_z 95%= 29.4
 2.0405 - Rs_tdc - Swirl Ratio in the Combustion Chamber at TDC
 1.6000 - Rs_ivc - Swirl Ratio in the Cylinder at IVC
 17.783 - W_swirl - Max. Air Swirl Velocity, m/s at cylinder R= 30

----- ECOLOGICAL PARAMETERS -----

0.84948 - Hartridge - Hartridge Smoke Level
 0.09304 - Bosch - Bosch Smoke Number
 0.02023 - K,m-1 - Factor of Absolute Light Absorption, 1/m
 0.00723 - PM - Specific Particulate Matter emission, g/kWh
 649.12 - CO2 - Specific Carbon dioxide emission, g/kWh
 0.8210 - NO - Specif. NOx emiss. reduc. to NO, g/kWh(DKM)
 0.46778 - SE - Summary emission of PM and NOx
 0.0000 - SO2 - Specific SO2 emission, g/kWh

----- CYLINDER PARAMETERS -----

30.984 - p_ivc - Pressure at IVC, bar
 539.54 - T_ivc - Temperature at IVC, K
 102.71 - p_tdc - Compression Pressure (at TDC), bar
 745.61 - T_tdc - Compression Temperature (at TDC), K
 15.666 - p_evo - Pressure at EVO, bar
 1243.7 - T_evo - Temperature at EVO, K

----- HEAT EXCHANGE IN THE CYLINDER -----

1273.9 - T_eq - Average Equivalent Temperature of Cycle, K
 857.06 - hc_c - Aver. Factor of Heat Transfer in Cyl., W/m2/K
 771.02 - Tw_pist - Average Piston Crown Temperature, K
 420.00 - Tw_liner - Average Cylinder Liner Temperature, K
 713.81 - Tw_head - Average Head Wall Temperature, K
 398.48 - Tw_cool - Average Temperature of Cooled Surface
 head of Cylinder Head, K
 398.16 - Tboil - Boiling Temp. in Liquid Cooling System, K
 12519. - hc_cool - Average Factor of Heat Transfer, W/(m2*K)

```

                from head cooled surface to coolant
2413.0 - q_head - Heat Flow in a Cylinder Head, J/s
2166.5 - q_pist - Heat Flow in a Piston Crown, J/s
3633.3 - q_liner - Heat Flow in a Cylinder Liner, J/s

----- MAIN ENGINE CONSTRUCTION PARAMETERS -----
13.000 - CR - Compression Ratio
2.4009 - CR_opn.h - CR in view of loss. due to open height of porting
49.000 - n_inj - Number of Injector Nozzles
0.07700 - d_inj - Injector Nozzles Bore, mm
22.180 - Phi_inj - Injection Duration for specif. Inj. Profile, deg.
0.0000 - m_f_ip - Fuel Mass for specified Injection Profile, g
-125.00 - IVO - Intake Valve Opening, deg. before DC
145.00 - IVC - Intake Valve Closing, deg. after BDC
56.000 - EVO - Exhaust Valve Opening, deg. before BDC
108.00 - EVC - Exhaust Valve Closing, deg. after DC

----- COMPRESSOR PARAMETERS LP stage -----
28000. - RPM_C.lp - Rotor Speed of LPC, rev/min
23.756 - P_C.lp - Power of LP Compressor, kW
0.76000 - Eta_C.lp - Adiabatic Efficiency of LP Compressor
0.11660 - m_C.lp - Mass Airflow of LP Compressor, kg/sec
2.0540 - m*_C.lp - Mass Airflow Parameter, kg SQRT(K)/(s bar)
0.11898 - m.cor_Clp - Corrected Mass Airflow of LPC, kg/s
1622.0 - RPM*_C.lp - Rotor Speed Parameter, rev/min SQRT(K)
28000. - RPMcor_lp - Corrected Rotor Speed, rev/min
4.3000 - PR_C.lp - Pressure Ratio of LP Compressor
0.0000 - Kpi_C.lp - Factor Kpi of LP Compressor
0.98000 - po_iC.lp - Inlet Total Pressure of LPC, bar
298.00 - To_iC.lp - Inlet Total Temperature of LPC, K
4.2140 - po_"C.lp - Total Discharge Press.(before LP cooler), bar
500.72 - To_"C.lp - Total Discharge Temp. (before LP cooler), K
0.91500 - Ecool.lp - Thermal Efficiency of LP Air Inter-cooler
298.00 - Tcool.lp - LP Inter-cooler Refrigerant Temperature, K
4.1740 - po_C.lp - Total Pressure after LP Inter-cooler, bar
315.23 - To_C.lp - Total Temperature after LP Inter-cooler, K

----- COMPRESSOR PARAMETERS HP stage -----
28000. - RPM_C.hp - Rotor Speed of HPC, rev/min
23.331 - P_C.hp - Power of HPC, kW
0.85000 - Eta_C.hp - Adiabatic Efficiency of HPC
0.11660 - m_C.hp - Mass Airflow of HP Compressor, kg/s
0.49599 - m*_C.hp - Mass Airflow Parameter, kg SQRT(K)/(s bar)
0.02873 - m.cor_Chp - Corrected Mass Airflow of HPC, kg/s
1577.0 - RPM*_C.hp - Rotor Speed Parameter, rev/min SQRT(K)
27224. - RPMcor_hp - Corrected Rotor Speed, rev/min
4.5000 - PR_C.hp - Pressure Ratio of HP Compressor
0.0000 - Kpi_C.hp - Factor Kpi of HP Compressor
4.1740 - po_iC.hp - Inlet Total Pressure of HPC, bar
315.23 - To_iC.hp - Inlet Total Temperature of HPC, K
18.783 - po_"C.hp - Total Discharge Press. (before HP cooler), bar
514.33 - To_"C.hp - Total Discharge Temp. (before HP cooler), K
0.91500 - Ecool.hp - Thermal Efficiency of HP Air Inter-cooler
298.00 - Tcool.hp - HP Inter-cooler Refrigerant Temperature, K
18.743 - po_C.hp - Total Pressure after Inter-cooler, bar
316.39 - To_C.hp - Total Temperature after Inter-cooler, K

----- TURBINE PARAMETERS HP stage -----
28000. - RPM_T.hp - HP Turbine Rotor Speed, rev/min
0.0000 - P_T.hp - Effective Power of HPT, kW
1.0000 - Eta_T.hp - Internal turbine Efficiency of HPT
0.90900 - Eta_mT.hp - Mechanical Efficiency of HPT
0.12631 - m_T.hp - Mass Gasflow of HPT, kg/s
0.01268 - m*_T.hp - Mass Gasflow Parameter, (kg SQRT(K))/(s kPa)
895.71 - RPM*_T.hp - Rotor Speed Parameter, rev/min SQRT(K)
1.0000 - PR_T.hp - Expansion Pressure Ratio of HPT
0.0000 - B_T.hp - Relative Work B=118.34 {1-PR**[(1-k)/k]} Eta_T
3.1149 - po_T.hp - Inlet Total Pressure of HPT, bar
977.20 - To_T.hp - Inlet Total Temperature of HPT, K

```

```

3.1149 - po_eT.hp - HP Turbine Exhaust Back Pressure, bar
977.20 - To_eT.hp - HP Turbine Exhaust Back Temperature, K

----- TURBINE PARAMETERS LP stage -----
28000. - RPM_T.lp - LP Turbine Rotor Speed, rev/min
22.660 - P_T.lp - Effective Power of LPT, kW
0.75000 - Eta_T.lp - Adiabatic Efficiency of LPT
0.90900 - Eta_mT.lp- Mechanical Efficiency of LPT
0.12631 - m_T.lp - Mass Gasflow of LPT, kg/s
0.01268 - m*_T.lp - Mass Gasflow Parameter, (kg SQRT(K))/(s kPa)
895.71 - RPM*_T.lp- Rotor Speed Parameter, rev/min SQRT(K)
3.0000 - PR_T.lp - Expansion Pressure Ratio of LPT
21.176 - B_T.lp - Relative Work B=118.34 {1-PR**[(1-k)/k]} Eta_T
3.1149 - po_T.lp - Inlet Total Pressure of LPT, bar
977.20 - To_T.lp - Inlet Total Temperature of LPT, K
1.0383 - po_eT.lp - LP Turbine Exhaust Back Pressure, bar
796.52 - To_eT.lp - LP Turbine Exhaust Back Temperature, K

----- MULTIPLE INJECTION PARAMETERS -----
      SOI Fraction Mass Separ. Duration d32 Ign.Delay Burst
      [CA BTDC] [g] [CA] [CA] [micron] [CA] [CA]
Pilot 1 80.0 0.253 0.0177 ---- 5.281 7.47 81.00 361.0
Pilot 2 74.4 0.265 0.0185 0.35 5.633 7.42 75.37 361.0
Pilot 3 68.4 0.232 0.0163 0.35 4.929 7.27 69.38 361.0
Main 63.1 0.249 0.0175 0.35 5.281 7.10 64.10 361.0

      THE ALLOCATION OF FUEL IN THE ZONES AT THE END OF INJECTION
=====
N|In plan| Spray|Impingment|_____Fractions of fuel in the zones %_____
s| Angle | Angle| Surface | Dilut. S.Core Piston Inters. Head Liner
-----
1| 0.0 | 50.0 |not imping| 68.49 14.48 0.00 0.00 0.00 0.00
-----
Sum of all sprays % 83.| 57.50 25.64 0.00 0.00 0.00 0.00
=====
Evaporation constants bi | 2632 150 2722 2300 2225 9
=====
The note: "Inters." is column with fraction of fuel in a zone of
intersection of Near-Wall Flows formed by adjacents sprays.
Rs:Swirl| (Piston clearance,mm 2.50) |Optimal|-Geometric formula: 0.33
Ratio| Rs of piston bowl 2.04 | Rs |-by Razleytsev : 0.33

-----
Versions: Kernel 04.01.13; RK-model 06.01.13; NOx-model 22.02.13

```

RESULT OF COMPUTATION AT 3600 RPM

----- PARAMETERS OF ENGINE WITH TURBOCOMPAUNDING OR SUPERCHARGING -----
 126.50 - P_ovrl - Overall Power with account of geared units, kW
 -30.487 - dP_add - Power added by geared Turb/Comp/TC/EGR_compr., kW
 335.57 - Torq_ovrl- Overall Torque in view of geared units, N m
 26.214 - BMEP_ovrl- Overall BMEP, bar
 0.20149 - SFC_ovrl - Overall Specific Fuel Consumption, kg/kWh
 0.19740 - SFC_o.ISO- Same Specific Fuel Consumption but in ISO, kg/kWh
 0.42040 - Eta_ovrl - Overall Engine Efficiency
 10.000 - R_gear - Gear ratio of TK speed reducer
 0.95000 - Eta_mC.hp- Mechanical Efficiency of HPC
 -30.487 - dPdrv_hp - Power added by geared Unit of HP stage, kW

----- PARAMETERS OF EFFICIENCY AND POWER -----
 3600.0 - RPM - Engine Speed, rev/min
 156.98 - P_eng - Piston Engine Power, kW
 32.532 - BMEP - Brake Mean Effective Pressure, bar
 416.44 - Torque - Brake Torque, N m
 0.05900 - m_f - Mass of Fuel Supplied per cycle, g
 0.16236 - SFC - Specific Fuel Consumption, kg/kWh
 0.15907 - SFC_ISO - Specific Fuel Consumption in ISO, kg/kWh
 0.52172 - Eta_f - Efficiency of piston engine
 33.905 - IMEP - Indicated Mean Effective Pressure, bar
 0.54372 - Eta_i - Indicated Efficiency
 9.6000 - Sp - Mean Piston Speed, m/s
 1.3722 - FMEP - Friction Mean Effective Pressure, bar (VW data)
 0.95953 - Eta_m - Mechanical Efficiency of Piston Engine

----- ENVIRONMENTAL PARAMETERS -----
 1.0000 - p_sea - Static Atmospheric Pressure on sea level, bar
 298.00 - T_sea - Static Atmospheric Temperature on sea level, K
 0.0000 - A_ab.sea - Altitude Above Sea Level, km
 0.0000 - v_flight - Velocity of Flight, km/h (for aircraft engine)
 1.0000 - p_amb - Static Ambient Pressure, bar
 298.00 - T_amb - Static Ambient Temperature, K
 1.0000 - po_amb - Total Ambient Pressure, bar
 298.00 - To_amb - Total Ambient Temperature, K
 1.0400 - p_Te - Exhaust Back Pressure, bar (after turbine)
 0.98000 - po_afltr - Total Pressure after Induction Air Filter, bar

----- TURBOCHARGING AND GAS EXCHANGE -----
 20.878 - p_C - Pressure before Inlet Manifold, bar
 321.38 - T_C - Temperature before Inlet Manifold, K
 0.13566 - m_air - Total Mass Airflow (+EGR) of Piston Engine, kg/s
 0.86900 - Eta_TC - Turbocharger Efficiency
 3.1251 - po_T - Average Total Turbine Inlet Pressure, bar
 908.04 - To_T - Average Total Turbine Inlet Temperature, K
 0.14866 - m_gas - Mass Exhaust Gasflow of Pison Engine, kg/s
 1.3221 - A/F_eq.t - Total Air Fuel Equivalence Ratio (Lambda)
 0.75637 - F/A_eq.t - Total Fuel Air Equivalence Ratio
 0.13521 - Eta_v - Volumetric Efficiency
 0.24528 - x_r - Residual Gas Mass Fraction
 0.91890 - Phi - Coeff. of Scavenging (Delivery Ratio / Eta_v)
 0.0000 - BF_int - Burnt Gas Fraction Backflowed into the Intake, %
 0.35084 - %Blow-by - % of Blow-by through piston rings

----- INTAKE SYSTEM -----
 20.835 - p_int - Average Intake Manifold Pressure, bar
 317.23 - T_int - Average Intake Manifold Temperature, K
 2.4961 - v_int - Average Gas Velocity in intake manifold, m/s
 320.23 - Tw_int - Average Intake Manifold Wall Temperature, K
 212.40 - hc_int - Heat Transfer Coeff. in Intake Manifold, W/(m2*K)
 165.08 - hc_int.p - Heat Transfer Coeff. in Intake Port, W/(m2*K)
 7.1004 - A_v.thrt - Total Effective Valve Port Throat Area, cm2
 Valve Dim. Estim.: Num=2 Dv= 29.0 Dt= 26.0 Ds= 5.5 Lv= 6.2 Lv_max= 7.2 mm

----- EXHAUST SYSTEM -----
 3.0643 - p_exh - Average Exhaust Manifold Gas Pressure, bar
 903.47 - T_exh - Average Exhaust Manifold Gas Temperature, K
 55.132 - v_exh - Average Gas Velocity in exhaust manifold, m/s

37.845 - Sh - Strouhal number: $Sh = a \cdot \tau / L$ (has to be: $Sh > 8$)
787.95 - Tw_exh - Average Exhaust Manifold Wall Temperature, K
223.66 - hc_exh - Heat Transfer Coef. in Exhaust Manifold, W/(m²*K)
304.90 - hc_exh.p - Heat Transfer Coeff. in Exhaust Port, W/(m²*K)
8.7808 - A_v.thrt - Total Effective Valve Port Throat Area, cm²
Valve Dim. Estim.: Num=2 Dv= 30.0 Dt= 27.0 Ds= 5.5 Lv= 7.6 Lv_max= 7.5 mm

----- COMBUSTION -----
1.4852 - A/F_eq - Air Fuel Equival. Ratio (Lambda) in the Cylinder
0.67333 - F/A_eq - Fuel Air Equivalence Ratio in the Cylinder
222.84 - p_max - Maximum Cylinder Pressure, bar
2062.4 - T_max - Maximum Cylinder Temperature, K
12.000 - CA_p.max - Angle of Max. Cylinder Pressure, deg. A.TDC
17.000 - CA_t.max - Angle of Max. Cylinder Temperature, deg. A.TDC
6.4707 - dp/dTheta- Max. Rate of Pressure Rise, bar/deg.
7.2021 - Ring_Intn- Ringing / Knock Intensity, MW/m²
11347. - F_max - Max. Gas Force acting on the piston, kg
841.00 - p_inj.max- Max. Sac Injection Pres. (before nozzles), bar
621.08 - p_inj.avr- Mean Sac Press. for Total Fuel Portion, bar
7.1211 - d_32 - Sauter Mean Diameter of Drops, microns
80.000 - SOI - Start Of Injection or Ignition Timing, deg. B.TDC
24.000 - Phi_inj - Duration of Injection, CA deg.
79.000 - Phi_ign - Ignition Delay Period, deg.
- ... - Calculation with user Model : 79.0
1.0000 - SOC - Start of Combustion, deg. B.TDC
0.25309 - x_e.id - Fuel Mass Fraction Evaporated during Ignit. Delay
107.49 - Phi_z - Combustion duration, deg.
Phi_z 5%= 3.2; Phi_z 50%= 18.6; Phi_z 95%= 29.0
1.7409 - Rs_tdc - Swirl Ratio in the Combustion Chamber at TDC
1.4361 - Rs_ivc - Swirl Ratio in the Cylinder at IVC
19.506 - W_swirl - Max. Air Swirl Velocity, m/s at cylinder R= 30

----- ECOLOGICAL PARAMETERS -----
0.62077 - Hartridge- Hartridge Smoke Level
0.06799 - Bosch - Bosch Smoke Number
0.01478 - K,m-1 - Factor of Absolute Light Absorption, 1/m
0.00537 - PM - Specific Particulate Matter emission, g/kWh
649.25 - CO2 - Specific Carbon dioxide emission, g/kWh
1.00454 - NO - Specif. NOx emiss. reduc. to NO, g/kWh(DKM)
0.08290 - SE - Summary emission of PM and NOx
0.0000 - SO2 - Specific SO2 emission, g/kWh

----- CYLINDER PARAMETERS -----
30.783 - p_ivc - Pressure at IVC, bar
556.03 - T_ivc - Temperature at IVC, K
101.71 - p_tdc - Compression Pressure (at TDC), bar
765.77 - T_tdc - Compression Temperature (at TDC), K
13.834 - p_evo - Pressure at EVO, bar
1139.7 - T_evo - Temperature at EVO, K

----- HEAT EXCHANGE IN THE CYLINDER -----
1200.0 - T_eq - Average Equivalent Temperature of Cycle, K
1012.9 - hc_c - Aver. Factor of Heat Transfer in Cyl., W/m²/K
777.86 - Tw_pist - Average Piston Crown Temperature, K
420.00 - Tw_liner - Average Cylinder Liner Temperature, K
718.55 - Tw_head - Average Head Wall Temperature, K
397.69 - Tw_cool - Average Temperature of Cooled Surface
head_of Cylinder Head, K
398.16 - Tboil - Boiling Temp. in Liquid Cooling System, K
12803. - hc_cool - Average Factor of Heat Transfer, W/(m²*K)
from head cooled surface to coolant
2451.3 - q_head - Heat Flow in a Cylinder Head, J/s
2149.3 - q_pist - Heat Flow in a Piston Crown, J/s
3882.9 - q_liner - Heat Flow in a Cylinder Liner, J/s

----- MAIN ENGINE CONSTRUCTION PARAMETERS -----
13.000 - CR - Compression Ratio
2.4009 - CR_opn.h - CR in view of loss. due to open height of porting
49.000 - n_inj - Number of Injector Nozzles
0.07700 - d_inj - Injector Nozzles Bore, mm

24.000 - Phi_inj - Injection Duration for specif. Inj. Profile, deg.
0.0000 - m_f_ip - Fuel Mass for specified Injection Profile, g
-125.00 - IVO - Intake Valve Opening, deg. before DC
145.00 - IVC - Intake Valve Closing, deg. after BDC
56.000 - EVO - Exhaust Valve Opening, deg. before BDC
108.00 - EVC - Exhaust Valve Closing, deg. after DC

----- COMPRESSOR PARAMETERS LP stage -----
102361 - RPM_C.lp - Rotor Speed of LPC, rev/min
29.082 - P_C.lp - Power of LP Compressor, kW
0.75000 - Eta_C.lp - Adiabatic Efficiency of LP Compressor
0.13566 - m_C.lp - Mass Airflow of LP Compressor, kg/sec
2.3897 - m*_C.lp - Mass Airflow Parameter, kg SQRT(K)/(s bar)
0.13843 - m.cor_Clp - Corrected Mass Airflow of LPC, kg/s
5929.7 - RPM*_C.lp - Rotor Speed Parameter, rev/min SQRT(K)
102361 - RPMcor_lp - Corrected Rotor Speed, rev/min
4.5000 - PR_C.lp - Pressure Ratio of LP Compressor
0.0000 - Kpi_C.lp - Factor Kpi of LP Compressor
0.98000 - po_iC.lp - Inlet Total Pressure of LPC, bar
298.00 - To_iC.lp - Inlet Total Temperature of LPC, K
4.4100 - po_"C.lp - Total Discharge Press.(before LP cooler), bar
511.31 - To_"C.lp - Total Discharge Temp. (before LP cooler), K
0.90000 - Ecool.lp - Thermal Efficiency of LP Air Inter-cooler
298.00 - Tcool.lp - LP Inter-cooler Refrigerant Temperature, K
4.3600 - po_C.lp - Total Pressure after LP Inter-cooler, bar
319.33 - To_C.lp - Total Temperature after LP Inter-cooler, K

----- COMPRESSOR PARAMETERS HP stage -----
36000. - RPM_C.hp - Rotor Speed of HPC, rev/min
28.963 - P_C.hp - Power of HPC, kW
0.85000 - Eta_C.hp - Adiabatic Efficiency of HPC
0.13566 - m_C.hp - Mass Airflow of HP Compressor, kg/s
0.55603 - m*_C.hp - Mass Airflow Parameter, kg SQRT(K)/(s bar)
0.03221 - m.cor_Chp - Corrected Mass Airflow of HPC, kg/s
2014.6 - RPM*_C.hp - Rotor Speed Parameter, rev/min SQRT(K)
34777. - RPMcor_hp - Corrected Rotor Speed, rev/min
4.8000 - PR_C.hp - Pressure Ratio of HP Compressor
0.0000 - Kpi_C.hp - Factor Kpi of HP Compressor
4.3600 - po_iC.hp - Inlet Total Pressure of HPC, bar
319.33 - To_iC.hp - Inlet Total Temperature of HPC, K
20.928 - po_"C.hp - Total Discharge Press. (before HP cooler), bar
531.76 - To_"C.hp - Total Discharge Temp. (before HP cooler), K
0.90000 - Ecool.hp - Thermal Efficiency of HP Air Inter-cooler
298.00 - Tcool.hp - HP Inter-cooler Refrigerant Temperature, K
20.878 - po_C.hp - Total Pressure after Inter-cooler, bar
321.38 - To_C.hp - Total Temperature after Inter-cooler, K

----- TURBINE PARAMETERS HP stage -----
36000. - RPM_T.hp - HP Turbine Rotor Speed, rev/min
0.0000 - P_T.hp - Effective Power of HPT, kW
1.0000 - Eta_T.hp - Internal turbine Efficiency of HPT
0.90900 - Eta_mT.hp - Mechanical Efficiency of HPT
0.14866 - m_T.hp - Mass Gasflow of HPT, kg/s
0.01433 - m*_T.hp - Mass Gasflow Parameter, (kg SQRT(K))/(s kPa)
1194.7 - RPM*_T.hp - Rotor Speed Parameter, rev/min SQRT(K)
1.0000 - PR_T.hp - Expansion Pressure Ratio of HPT
0.0000 - B_T.hp - Relative Work $B=118.34 \{1-PR^{**}[(1-k)/k]\}$ Eta_T
3.1251 - po_T.hp - Inlet Total Pressure of HPT, bar
908.04 - To_T.hp - Inlet Total Temperature of HPT, K
3.1251 - po_eT.hp - HP Turbine Exhaust Back Pressure, bar
908.04 - To_eT.hp - HP Turbine Exhaust Back Temperature, K

----- TURBINE PARAMETERS LP stage -----
102361 - RPM_T.lp - LP Turbine Rotor Speed, rev/min
24.784 - P_T.lp - Effective Power of LPT, kW
0.75000 - Eta_T.lp - Adiabatic Efficiency of LPT
0.90900 - Eta_mT.lp - Mechanical Efficiency of LPT
0.14866 - m_T.lp - Mass Gasflow of LPT, kg/s
0.01433 - m*_T.lp - Mass Gasflow Parameter, (kg SQRT(K))/(s kPa)
3396.9 - RPM*_T.lp - Rotor Speed Parameter, rev/min SQRT(K)

3.0000 - PR_T.lp - Expansion Pressure Ratio of LPT
 21.176 - B_T.lp - Relative Work B=118.34 {1-PR**[(1-k)/k]} Eta_T
 3.1251 - po_T.lp - Inlet Total Pressure of LPT, bar
 908.04 - To_T.lp - Inlet Total Temperature of LPT, K
 1.0417 - po_eT.lp - LP Turbine Exhaust Back Pressure, bar
 740.14 - To_eT.lp - LP Turbine Exhaust Back Temperature, K

----- MULTIPLE INJECTION PARAMETERS -----

	SOI	Fraction	Mass	Separ.	Duration	d32	Ign.Delay	Burst
	[CA	BTDC]	[g]	[CA]	[CA]	[micron]	[CA]	[CA]
Pilot 1	80.0	0.253	0.0150	----	5.714	7.28	79.00	359.0
Pilot 2	73.9	0.265	0.0156	0.38	6.095	7.23	72.90	359.0
Pilot 3	67.4	0.232	0.0137	0.38	5.333	7.06	66.43	359.0
Main	61.7	0.249	0.0147	0.38	5.714	6.90	60.71	359.0

THE ALLOCATION OF FUEL IN THE ZONES AT THE END OF INJECTION

N In plan	Spray	Impingment	Fractions of fuel in the zones %							
s	Angle	Angle	Surface	Dilut.	S.Core	Piston	Inters.	Head	Liner	
1	0.0	50.0	not imping	80.57	5.68	0.00	0.00	0.00	0.00	
Sum of all sprays				% 94.	69.99	24.14	0.00	0.00	0.00	0.00
Evaporation constants bi				8995	564	9142	7725	7406	30	

The note: "Inters." is column with fraction of fuel in a zone of intersection of Near-Wall Flows formed by adjacents sprays.
 Rs:Swirl| (Piston clearance,mm 2.50) |Optimal|-Geometric formula: 0.31
 Ratio| Rs of piston bowl 1.74 | Rs |-by Razleytsev : 0.31

Versions: Kernel 04.01.13; RK-model 06.01.13; NOx-model 22.02.13

RESULT OF COMPUTATION AT 1600 RPM

----- PARAMETERS OF ENGINE WITH TURBOCOMPAUNDING OR SUPERCHARGING -----
 65.281 - P_ovrl - Overall Power with account of geared units, kW
 -15.260 - dP_add - Power added by geared Turb/Comp/TC/EGR_compr., kW
 389.65 - Torq_ovrl- Overall Torque in view of geared units, N m
 30.439 - BMEP_ovrl- Overall BMEP, bar
 0.20294 - SFC_ovrl - Overall Specific Fuel Consumption, kg/kWh
 0.20043 - SFC_o.ISO- Same Specific Fuel Consumption but in ISO, kg/kWh
 0.41740 - Eta_ovrl - Overall Engine Efficiency
 10.000 - R_gear - Gear ratio of TK speed reducer
 0.95000 - Eta_mC.hp- Mechanical Efficiency of HPC
 -15.260 - dPdrv_hp - Power added by geared Unit of HP stage, kW

----- PARAMETERS OF EFFICIENCY AND POWER -----
 1600.0 - RPM - Engine Speed, rev/min
 80.541 - P_eng - Piston Engine Power, kW
 37.554 - BMEP - Brake Mean Effective Pressure, bar
 480.73 - Torque - Brake Torque, N m
 0.06900 - m_f - Mass of Fuel Supplied per cycle, g
 0.16449 - SFC - Specific Fuel Consumption, kg/kWh
 0.16246 - SFC_ISO - Specific Fuel Consumption in ISO, kg/kWh
 0.51497 - Eta_f - Efficiency of piston engine
 38.718 - IMEP - Indicated Mean Effective Pressure, bar
 0.53093 - Eta_i - Indicated Efficiency
 4.2667 - Sp - Mean Piston Speed, m/s
 1.1637 - FMEP - Friction Mean Effective Pressure, bar (VW data)
 0.96995 - Eta_m - Mechanical Efficiency of Piston Engine

----- ENVIRONMENTAL PARAMETERS -----
 1.0000 - p_sea - Static Atmospheric Pressure on sea level, bar
 298.00 - T_sea - Static Atmospheric Temperature on sea level, K
 0.0000 - A_ab.sea - Altitude Above Sea Level, km
 0.0000 - v_flight - Velocity of Flight, km/h (for aircraft engine)
 1.0000 - p_amb - Static Ambient Pressure, bar
 298.00 - T_amb - Static Ambient Temperature, K
 1.0000 - po_amb - Total Ambient Pressure, bar
 298.00 - To_amb - Total Ambient Temperature, K
 1.0200 - p_Te - Exhaust Back Pressure, bar (after turbine)
 0.99000 - po_afltr - Total Pressure after Induction Air Filter, bar

----- TURBOCHARGING AND GAS EXCHANGE -----
 17.710 - p_C - Pressure before Inlet Manifold, bar
 315.07 - T_C - Temperature before Inlet Manifold, K
 0.07287 - m_air - Total Mass Airflow (+EGR) of Piston Engine, kg/s
 0.84596 - Eta_TC - Turbocharger Efficiency
 3.0547 - po_T - Average Total Turbine Inlet Pressure, bar
 877.57 - To_T - Average Total Turbine Inlet Temperature, K
 0.07853 - m_gas - Mass Exhaust Gasflow of Pison Engine, kg/s
 1.3662 - A/F_eq.t - Total Air Fuel Equivalence Ratio (Lambda)
 0.73194 - F/A_eq.t - Total Fuel Air Equivalence Ratio
 0.18453 - Eta_v - Volumetric Efficiency
 0.17668 - x_r - Residual Gas Mass Fraction
 0.94024 - Phi - Coeff. of Scavenging (Delivery Ratio / Eta_v)
 0.0000 - BF_int - Burnt Gas Fraction Backflowed into the Intake, %
 0.71775 - %Blow-by - % of Blow-by through piston rings

----- INTAKE SYSTEM -----
 17.694 - p_int - Average Intake Manifold Pressure, bar
 308.28 - T_int - Average Intake Manifold Temperature, K
 1.5519 - v_int - Average Gas Velocity in intake manifold, m/s
 311.30 - Tw_int - Average Intake Manifold Wall Temperature, K
 195.79 - hc_int - Heat Transfer Coeff. in Intake Manifold, W/(m2*K)
 169.60 - hc_int.p - Heat Transfer Coeff. in Intake Port, W/(m2*K)
 7.1004 - A_v.thrt - Total Effective Valve Port Throat Area, cm2
 Valve Dim. Estim.: Num=2 Dv= 29.0 Dt= 26.0 Ds= 5.5 Lv= 6.2 Lv_max= 7.2 mm

----- EXHAUST SYSTEM -----
 2.9573 - p_exh - Average Exhaust Manifold Gas Pressure, bar
 838.42 - T_exh - Average Exhaust Manifold Gas Temperature, K
 36.468 - v_exh - Average Gas Velocity in exhaust manifold, m/s

82.029 - Sh - Strouhal number: $Sh = a \cdot \tau / L$ (has to be: $Sh > 8$)
 695.81 - Tw_exh - Average Exhaust Manifold Wall Temperature, K
 146.99 - hc_exh - Heat Transfer Coef. in Exhaust Manifold, $W/(m^2 \cdot K)$
 207.99 - hc_exh.p - Heat Transfer Coeff. in Exhaust Port, $W/(m^2 \cdot K)$
 8.7808 - A_v.thrt - Total Effective Valve Port Throat Area, cm^2
 Valve Dim. Estim.: Num=2 Dv= 30.0 Dt= 27.0 Ds= 5.5 Lv= 7.6 Lv_max= 7.5 mm

----- COMBUSTION -----
 1.4979 - A/F_eq - Air Fuel Equival. Ratio (Lambda) in the Cylinder
 0.66761 - F/A_eq - Fuel Air Equivalence Ratio in the Cylinder
 235.99 - p_max - Maximum Cylinder Pressure, bar
 2082.0 - T_max - Maximum Cylinder Temperature, K
 14.000 - CA_p.max - Angle of Max. Cylinder Pressure, deg. A.TDC
 19.000 - CA_t.max - Angle of Max. Cylinder Temperature, deg. A.TDC
 6.1362 - dp/dTheta- Max. Rate of Pressure Rise, bar/deg.
 1.2137 - Ring_Intn- Ringing / Knock Intensity, MW/m2
 12017. - F_max - Max. Gas Force acting on the piston, kg
 831.75 - p_inj.max- Max. Sac Injection Pres. (before nozzles), bar
 630.00 - p_inj.avr- Mean Sac Press. for Total Fuel Portion, bar
 7.3006 - d_32 - Sauter Mean Diameter of Drops, microns
 70.000 - SOI - Start Of Injection or Ignition Timing, deg. B.TDC
 12.400 - Phi_inj - Duration of Injection, CA deg.
 71.000 - Phi_ign - Ignition Delay Period, deg.
 - ... - Calculation with user Model : 71.0
 -1.0000 - SOC - Start of Combustion, deg. B.TDC
 0.33526 - x_e.id - Fuel Mass Fraction Evaporated during Ignit. Delay
 99.106 - Phi_z - Combustion duration, deg.
 Phi_z 5%= 3.4; Phi_z 50%= 21.8; Phi_z 95%= 31.2
 2.4136 - Rs_tdc - Swirl Ratio in the Combustion Chamber at TDC
 1.8038 - Rs_ivc - Swirl Ratio in the Cylinder at IVC
 12.020 - W_swirl - Max. Air Swirl Velocity, m/s at cylinder R= 30

----- ECOLOGICAL PARAMETERS -----
 0.80890 - Hartridge- Hartridge Smoke Level
 0.08859 - Bosch - Bosch Smoke Number
 0.01926 - K,m-1 - Factor of Absolute Light Absorption, 1/m
 0.00758 - PM - Specific Particulate Matter emission, g/kWh
 653.91 - CO2 - Specific Carbon dioxide emission, g/kWh
 0.3232 - NO - Specif. NOx emiss. reduc. to NO, g/kWh(DKM)
 0.21565 - SE - Summary emission of PM and NOx
 0.0000 - SO2 - Specific SO2 emission, g/kWh

----- CYLINDER PARAMETERS -----
 26.186 - p_ivc - Pressure at IVC, bar
 484.03 - T_ivc - Temperature at IVC, K
 103.27 - p_tdc - Compression Pressure (at TDC), bar
 703.62 - T_tdc - Compression Temperature (at TDC), K
 15.415 - p_evo - Pressure at EVO, bar
 1151.4 - T_evo - Temperature at EVO, K

----- HEAT EXCHANGE IN THE CYLINDER -----
 1218.4 - T_eq - Average Equivalent Temperature of Cycle, K
 574.77 - hc_c - Aver. Factor of Heat Transfer in Cyl., $W/m^2 \cdot K$
 666.08 - Tw_pist - Average Piston Crown Temperature, K
 420.00 - Tw_liner - Average Cylinder Liner Temperature, K
 616.49 - Tw_head - Average Head Wall Temperature, K
 389.08 - Tw_cool - Average Temperature of Cooled Surface
 head_of Cylinder Head, K
 398.16 - Tboil - Boiling Temp. in Liquid Cooling System, K
 11875. - hc_cool - Average Factor of Heat Transfer, $W/(m^2 \cdot K)$
 from head cooled surface to coolant
 1739.1 - q_head - Heat Flow in a Cylinder Head, J/s
 1595.8 - q_pist - Heat Flow in a Piston Crown, J/s
 2053.1 - q_liner - Heat Flow in a Cylinder Liner, J/s

----- MAIN ENGINE CONSTRUCTION PARAMETERS -----
 13.000 - CR - Compression Ratio
 2.7173 - CR_opn.h - CR in view of loss. due to open height of porting
 49.000 - n_inj - Number of Injector Nozzles
 0.07700 - d_inj - Injector Nozzles Bore, mm

12.400 - Phi_inj - Injection Duration for specif. Inj. Profile, deg.
0.0000 - m_f_ip - Fuel Mass for specified Injection Profile, g
-125.00 - IVO - Intake Valve Opening, deg. before DC
141.00 - IVC - Intake Valve Closing, deg. after BDC
56.000 - EVO - Exhaust Valve Opening, deg. before BDC
108.00 - EVC - Exhaust Valve Closing, deg. after DC

----- COMPRESSOR PARAMETERS LP stage -----
42830. - RPM_C.lp - Rotor Speed of LPC, rev/min
14.141 - P_C.lp - Power of LP Compressor, kW
0.75000 - Eta_C.lp - Adiabatic Efficiency of LP Compressor
0.07287 - m_C.lp - Mass Airflow of LP Compressor, kg/sec
1.2706 - m*_C.lp - Mass Airflow Parameter, kg SQRT(K)/(s bar)
0.07360 - m.cor_Clp - Corrected Mass Airflow of LPC, kg/s
2481.1 - RPM*_C.lp - Rotor Speed Parameter, rev/min SQRT(K)
42830. - RPMcor_lp - Corrected Rotor Speed, rev/min
4.0000 - PR_C.lp - Pressure Ratio of LP Compressor
0.0000 - Kpi_C.lp - Factor Kpi of LP Compressor
0.99000 - po_iC.lp - Inlet Total Pressure of LPC, bar
298.00 - To_iC.lp - Inlet Total Temperature of LPC, K
3.9600 - po_"C.lp - Total Discharge Press.(before LP cooler), bar
491.10 - To_"C.lp - Total Discharge Temp. (before LP cooler), K
0.92000 - Ecool.lp - Thermal Efficiency of LP Air Inter-cooler
298.00 - Tcool.lp - LP Inter-cooler Refrigerant Temperature, K
3.9400 - po_C.lp - Total Pressure after LP Inter-cooler, bar
313.45 - To_C.lp - Total Temperature after LP Inter-cooler, K

----- COMPRESSOR PARAMETERS HP stage -----
16000. - RPM_C.hp - Rotor Speed of HPC, rev/min
14.497 - P_C.hp - Power of HPC, kW
0.85000 - Eta_C.hp - Adiabatic Efficiency of HPC
0.07287 - m_C.hp - Mass Airflow of HP Compressor, kg/s
0.32743 - m*_C.hp - Mass Airflow Parameter, kg SQRT(K)/(s bar)
0.01897 - m.cor_Chp - Corrected Mass Airflow of HPC, kg/s
903.73 - RPM*_C.hp - Rotor Speed Parameter, rev/min SQRT(K)
15601. - RPMcor_hp - Corrected Rotor Speed, rev/min
4.5000 - PR_C.hp - Pressure Ratio of HP Compressor
0.0000 - Kpi_C.hp - Factor Kpi of HP Compressor
3.9400 - po_iC.hp - Inlet Total Pressure of HPC, bar
313.45 - To_iC.hp - Inlet Total Temperature of HPC, K
17.730 - po_"C.hp - Total Discharge Press. (before HP cooler), bar
511.42 - To_"C.hp - Total Discharge Temp. (before HP cooler), K
0.92000 - Ecool.hp - Thermal Efficiency of HP Air Inter-cooler
298.00 - Tcool.hp - HP Inter-cooler Refrigerant Temperature, K
17.710 - po_C.hp - Total Pressure after Inter-cooler, bar
315.07 - To_C.hp - Total Temperature after Inter-cooler, K

----- TURBINE PARAMETERS HP stage -----
16000. - RPM_T.hp - HP Turbine Rotor Speed, rev/min
0.0000 - P_T.hp - Effective Power of HPT, kW
1.0000 - Eta_T.hp - Internal turbine Efficiency of HPT
0.90900 - Eta_mT.hp - Mechanical Efficiency of HPT
0.07853 - m_T.hp - Mass Gasflow of HPT, kg/s
0.00762 - m*_T.hp - Mass Gasflow Parameter, (kg SQRT(K))/(s kPa)
540.11 - RPM*_T.hp - Rotor Speed Parameter, rev/min SQRT(K)
1.0000 - PR_T.hp - Expansion Pressure Ratio of HPT
0.0000 - B_T.hp - Relative Work $B=118.34 \{1-PR^{**}[(1-k)/k]\}$ Eta_T
3.0547 - po_T.hp - Inlet Total Pressure of HPT, bar
877.57 - To_T.hp - Inlet Total Temperature of HPT, K
3.0547 - po_eT.hp - HP Turbine Exhaust Back Pressure, bar
877.57 - To_eT.hp - HP Turbine Exhaust Back Temperature, K

----- TURBINE PARAMETERS LP stage -----
42830. - RPM_T.lp - LP Turbine Rotor Speed, rev/min
12.652 - P_T.lp - Effective Power of LPT, kW
0.75000 - Eta_T.lp - Adiabatic Efficiency of LPT
0.90900 - Eta_mT.lp - Mechanical Efficiency of LPT
0.07853 - m_T.lp - Mass Gasflow of LPT, kg/s
0.00762 - m*_T.lp - Mass Gasflow Parameter, (kg SQRT(K))/(s kPa)
1445.8 - RPM*_T.lp - Rotor Speed Parameter, rev/min SQRT(K)

3.0000 - PR_T.lp - Expansion Pressure Ratio of LPT
 21.176 - B_T.lp - Relative Work B=118.34 {1-PR**[(1-k)/k]} Eta_T
 3.0547 - po_T.lp - Inlet Total Pressure of LPT, bar
 877.57 - To_T.lp - Inlet Total Temperature of LPT, K
 1.0182 - po_eT.lp - LP Turbine Exhaust Back Pressure, bar
 715.31 - To_eT.lp - LP Turbine Exhaust Back Temperature, K

----- MULTIPLE INJECTION PARAMETERS -----

	SOI	Fraction	Mass	Separ.	Duration	d32	Ign.	Delay	Burst
	[CA	BTDC]	[g]	[CA]	[CA]	[micron]	[CA]	[CA]	[CA]
Pilot 1	70.0	0.338	0.0233	----	3.957	7.41	71.00	361.0	
Main	65.8	0.353	0.0243	0.26	4.221	7.33	66.78	361.0	
Post 1	61.3	0.310	0.0214	0.26	3.694	7.15	62.29	361.0	

THE ALLOCATION OF FUEL IN THE ZONES AT THE END OF INJECTION

N	In plan	Spray	Impingment	Fractions of fuel in the zones %				
s	Angle	Angle	Surface	Dilut.	S.Core	Piston	Inters.	Head Liner
1	0.0	50.0	not imping	62.09	23.39	0.00	0.00	0.00 0.00
Sum of all sprays				% 79.	51.07	27.67	0.00	0.00 0.00 0.00
Evaporation constants bi				57344	2900	37460	31654	20100 228

The note: "Inters." is column with fraction of fuel in a zone of intersection of Near-Wall Flows formed by adjacents sprays.
 Rs:Swirl| (Piston clearance,mm 2.50) |Optimal|-Geometric formula: 0.59
 Ratio| Rs of piston bowl 2.41 | Rs |-by Razleytsev : 0.59

 Versions: Kernel 04.01.13; RK-model 06.01.13; NOx-model 22.02.13

A.3. User-defined functions for simulations in SP ANSYS FLUENT

```
/*Dynamic viscosity of Diesel fuel*/
#include "udf.h"
DEFINE_PROPERTY(cell_viscosity, cell, thread)
{
    real T = C_T(cell, thread) ;
    real p = C_P(cell, thread) ;
    real power2 = ((0.001529*p)/(1e5))/(1+0.004423*(T-273.15)) ;
    real e_power = pow(2.718,power2) ;
    real A = 0.004881 ;
    real B = (1-0.001839*(T-273.15))/(1+0.039991*(T-273.15)) ;
    return A*B*e_power ;
}

/*Maximal radial droplet penetration and SMD*/
#include "udf.h"
#include "dpm.h"
DEFINE_EXECUTE_AT_END(MaxPX)
{
    #if !RP_NODE
        FILE *fout;
    #endif
    Injection *Ilist;
    Injection *I;
    Particle *p;
    Thread *t;
    cell_t c;
    real xc[ND_ND];
    real XMax = 0;
    real XP, SD, T, Dpow3, Dpow2, SDup = 0, SDdown = 0;
    Ilist = Get_dpm_injections();
    loop(I, Ilist) /*loop over particles from every injector - returns
values for each compute nodes*/
    {
        loop(p, I->p)
        {
            XP=P_POS(p)[2];
            if (XP>XMax)
            {
                XMax = XP;
            }
            Dpow3 = pow(P_DIAM(p), 3);
            Dpow2 = pow(P_DIAM(p), 2);
            SDup+=Dpow3;
            SDdown+=Dpow2;
        }
    }
}
```

```

        }
    }
    SDup = PRF_GRSUM1(SDup); /*global reduction summation over all compute nodes*/
    SDdown = PRF_GRSUM1(SDdown); /*global reduction summation over all compute
nodes*/
    SD = SDup/SDdown;
    XMax = PRF_GRHIGH1(XMax); /*global reduction maximum over all compute nodes*/
    T = CURRENT_TIME;
    node_to_host_real_2(XMax,SD); /*pass variable from node0 to host*/
    #if !RP_NODE
    Message("Time, Max distance, Sauter diameter %e %e %e\n ",T,XMax,SD);
    fout = fopen("param.out", "a");
    fprintf(fout, "%e %e %e\n", T,XMax,SD);
    fclose(fout);
    #endif
}

```